

Dissertation zur Erlangung des Doktorgrades
der Fakultät für Chemie und Pharmazie
der Ludwig-Maximilians-Universität München

**Novel Contributions to the
Solid-State Chemistry of Diazenides**

Sebastian Bernhard Schneider

aus

München, Deutschland

2013

Erklärung

Diese Dissertation wurde im Sinne von § 7 der Promotionsordnung vom 28. November 2011 von Herrn Prof. Dr. Wolfgang Schnick betreut.

Eidesstattliche Versicherung

Diese Dissertation wurde eigenständig und ohne unerlaubte Hilfe erarbeitet.

München, 11.11.2013

.....

(Sebastian Bernhard Schneider)

Dissertation eingereicht am 11.11.2013

1. Gutachter: Prof. Dr. Wolfgang Schnick

2. Gutachter: Prof. Dr. Dirk Johrendt

Mündliche Prüfung am 16.12.2013

To my family

ACKNOWLEDGEMENTS

First, I would like to express my gratitude to my supervisor Prof. Dr. Wolfgang Schnick for the opportunity to do my PhD under his guidance. Throughout the entire work, I appreciated his extraordinary expertise, the given freedom in research and writing and the support at any time.

For being the co-referee of my thesis, I thank Prof. Dr. Dirk Johrendt.

I am thankful to Prof. Dr. Konstantin Karaghiosoff, PD Dr. Markus Lackinger, Prof. Dr. Hans-Christian Böttcher, and Prof. Dr. Jörn Schmedt a. d. Günne for being available as examiners in my viva-voce.

In addition, I have to thank various co-workers spread all over Germany and Europe. Hereby, special thanks go to

- Volker L. Deringer, Dr. Ralf P. Stoffel as well as Prof. Dr. Richard Dronskowski (RWTH Aachen, Germany) for their long-lasting support with numerous theoretical calculations concerning novel diazenide compounds and for their ongoing enthusiasm until we found the final ground state.
- Dr. Lkhamsuren Bayarjargal, Dr. Alexandra Friedrich and Prof. Dr. Björn Winkler (all Goethe-University Frankfurt, Germany) for their support and high-level expertise in the preparation of diamond-anvil cells.
- Dr. Zuzana Konôpková, Dr. Hanns-Peter Liermann and Dr. Wolfgang Morgenroth (all Deutsches Elektronen Synchrotron *DESY*, Hamburg, Germany) as well as Dr. Sylvain Petitgirard and Dr. Ashkan Salamat (both European Synchrotron Radiation Facility *ESRF*, Grenoble, France) for their outstanding support and awesome working atmospheres during all the beam times whenever I visited the synchrotrons.
- Dr. Marcus R. Schwarz (High-Pressure Research Center Freiberg, Germany) for the hardness measurements he conducted for one of my samples.
- Prof. Dr. Gunnar Jeschke and Henryk Laqua (both ETH Zurich, Switzerland) for the various ESR experiments as well as helpful discussions.

- Dr. Rainer Frankovsky and Gina M. Friederichs (both LMU) for their patience in conductivity and magnetic measurements. Additionally I have to thank you Rainer for the numerous DFT calculations on band structures and bonding situations.
- Martin “Saubatzi” Mangstl (University of Siegen) for the persistent NMR measurements and nights at the spectrometer – whereby I wonder whether “to thank” is the right choice. Just kidding, it was fun!
- Viola Duppel (Max-Planck-Institute Stuttgart, Germany) for the TEM measurements and the phenomenal report on as-obtained data.
- Markus Seibald for his outstanding experience and support in the analysis of electron diffraction data.

For analytical measurements and help with the hardware I would like to thank the following persons (in alphabetical order): Thomas Miller, Christian Minke, Marion Sokoll and Wolfgang Wunschheim (all LMU).

I also have to thank our secretary Olga Lorenz for her helpfulness and support in all administrative concerns.

I am indebted to my bachelor and research students Tanja Holzmann, Philipp Ratza and Juliane Stahl for their excellent work and pleasant atmosphere.

Special thanks to my ex- and current lab-mates in D2.110, Florian Pucher, Dominik Baumann, Alexey “Russetsky” Marchuk, Frank Tambornino as well as Cora Hecht and Dr. Stefan Sedlmaier. Especially to Flo, Dodo, Russetky and Sedl for their support during the entire work, for various constructive discussions and a lot of gorgeous lab times.

Further, I would like to thank all my colleagues in the working groups Schnick, Johrendt, Lotsch, Oeckler, Schmedt a. d. Günne and Hoch I did not explicitly mention. I really appreciated the nice and friendly working atmosphere and the awesome events such as for example the phenomenal Sing star evenings.

Stephan Werner, Christian Ziegler and Stephan Hug...what shall I say? You guys are great! I will never forget – however unfortunately some of them I already did – our numerous, awesome, funny, excessive, outstanding, extraordinary, unexpected (I could continue like this

for hours) times, lab-hours/days, events, parties and so on and on (again I could continue listing)! In addition, besides private conversations you always had an open ear for chemical discussions and problems and made my entire PhD time unforgettable. I wish you all the best for the future and I do hope we stay in contact!

Tanja, special thanks to you for your support, patience – especially patience – and encouragement during this thesis. You are the best!

Particularly I want to thank my parents and my sister Hanna, who made my entire academic life and studies possible. Without you, I would not stand here! Thanks for everything you did!

*So eine Arbeit wird eigentlich nie fertig, man muss sie für fertig erklären,
wenn man nach der Zeit und den Umständen das Möglichste getan hat.*

(Johann Wolfgang von Goethe)

Ich habe fertig!

(Giovanni Trapattoni)

TABLE OF CONTENTS

1. INTRODUCTION.....	1
1.1 INDUSTRIAL NITROGEN FIXATION.....	1
1.2 BIOLOGICAL NITROGEN FIXATION.....	2
1.3 SYNTHETIC NITROGEN FIXATION.....	4
1.4 NITROGEN FIXATION IN SOLID-STATE CHEMISTRY.....	8
2. BINARY ALKALINE EARTH DIAZENIDES.....	27
2.1. SYNTHESIS OF ALKALINE EARTH DIAZENIDES $M_{AE}N_2$ ($M_{AE} = CA, SR, BA$) BY CONTROLLED THERMAL DECOMPOSITION OF AZIDES UNDER HIGH PRESSURE.....	28
2.1.1 <i>Introduction.....</i>	29
2.1.2 <i>Experimental Section.....</i>	30
2.1.3 <i>Results and Discussion.....</i>	34
2.1.4 <i>Conclusions.....</i>	41
2.1.5 <i>Bibliography.....</i>	41
2.2 FURTHER ALKALINE EARTH DIAZENIDES.....	45
2.2.1 <i>Experimental Section.....</i>	45
2.2.2 <i>Results, Discussion and Conclusion.....</i>	46
2.2.3 <i>Bibliography.....</i>	47
3. BINARY ALKALI DIAZENIDES.....	49
3.1. HIGH-PRESSURE SYNTHESIS AND CHARACTERIZATION OF THE ALKALI DIAZENIDE Li_2N_2.....	50
3.1.1 <i>Introduction with Results and Discussion.....</i>	51
3.1.2 <i>Bibliography.....</i>	54
3.2 FURTHER ALKALI DIAZENIDES.....	58
3.2.1 <i>Experimental Section.....</i>	58
3.2.2 <i>Results, Discussion and Conclusion.....</i>	60
3.2.3 <i>Bibliography.....</i>	63
4. MATERIALS PROPERTIES OF BINARY DIAZENIDES.....	66

4.1. ELECTRONIC AND IONIC CONDUCTIVITY IN ALKALINE EARTH DIAZENIDES $M_{AE}N_2$ ($M_{AE} = CA, SR, BA$) AND IN Li_2N_2	67
4.1.1 Introduction.....	68
4.1.2 Experimental Section.....	69
4.1.3 Results and Discussion.....	72
4.1.4 Conclusion.....	79
4.1.5 Bibliography.....	80
4.2 HIGH-PRESSURE BEHAVIOR OF BINARY DIAZENIDES.....	86
4.2.1 Introduction.....	86
4.2.2 Experimental Section.....	87
4.2.3 Results and Discussion.....	89
4.2.4 Conclusion.....	96
4.2.5 Bibliography.....	96
5. TERNARY DIAZENIDES	100
5.1. HIGH-PRESSURE SYNTHESIS AND CHARACTERIZATION OF $Li_2Ca_3[N_2]_3 - AN$ UNCOMMON METALLIC DIAZENIDE WITH $[N_2]^{2-}$ IONS	101
5.1.1 Introduction.....	102
5.1.2 Experimental Section.....	104
5.1.3 Results and Discussion.....	109
5.1.4 Conclusion.....	124
5.1.5 Bibliography.....	125
5.2 FURTHER TERNARY DIAZENIDES.....	133
5.2.1 Experimental Section.....	133
5.2.2 Results, Discussion and Conclusion.....	134
5.2.3 Bibliography.....	135
6. SUMMARY.....	136
7. CONCLUSION AND OUTLOOK	141
8. APPENDIX	146
8.1 SUPPORTING INFORMATION	146

8.1.1	<i>Supporting Information for Chapter 2.1</i>	146
8.1.2	<i>Supporting Information for Chapter 3.1</i>	147
8.1.3	<i>Supporting Information for Chapter 4.1</i>	157
8.1.4	<i>Supporting Information for Chapter 4.2</i>	161
8.1.5	<i>Supporting Information for Chapter 5.1</i>	164
8.2	LIST OF PUBLICATIONS	182
8.3	CONFERENCES AND WORKSHOPS	185
8.3.1	<i>Conferences</i>	185
8.3.2	<i>Workshops</i>	185
8.4	DEPOSITED CRYSTALLOGRAPHIC DATA	186
8.5	CURRICULUM VITAE	187

1. INTRODUCTION

1.1 INDUSTRIAL NITROGEN FIXATION

The conversion of nitrogen and hydrogen gas into ammonia is one of the world's most important chemical processes developed in 1903–1913 and named after its inventors *Fritz Haber* and *Carl Bosch*: the Haber-Bosch process.^[1] Offering rapid access to synthetic fertilizers, ammonia production has come essential for the nutrition of a large amount of the world population.^[2] On the other hand, the Haber-Bosch process also equipped diverse military armies with powerful weapons as ammonia is needed for the synthesis of oxidizing agents such as saltpeters, the main components of several explosives.^[2]

Since the first recorded data in 1946, the world's ammonia production steadily increased reaching 137 million tons of ammonia in 2012, according to the US Geological Survey (see Figure 1).^[3] Despite its global impact, the basics of the Haber-Bosch process have hardly

changed at all. It still depends on high pressures of 150 to 300 atmospheres, temperatures of about 600–800 K and an iron-ruthenium catalyst with a variety of different promoters.^[5] For

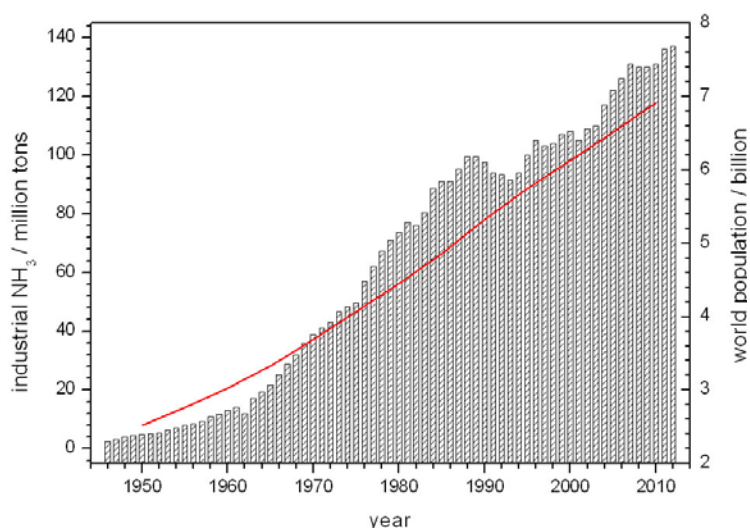


Figure 1. Worldwide ammonia production recorded from 1946 to 2012 in million tons per year referring to the bar chart and world population from 1950 to 2010 indicated as red line. The data are taken from the US Geological Survey and the United Nations, Department of Economic and Social Affairs (Population Division).^[3,4]

such an important chemical process it is surprising that it was not before the late 1970s and 1980s – the first ammonia producing industrial plant was built in 1913 in Oppau, Germany^[6] – that the catalytic process inside the autoclave was completely understood. Thereby, kinetic studies showed that the rate-limiting step is absorption and breaking the triple-bond of dinitrogen molecules as summarized in the 2007 nobel lecture *Reactions at Surfaces: From Atoms to Complexity* by Gerhard Ertl.^[7] These pioneering works however did not change the basic principle of ammonia production as its kinetics turned out to be as expected for years. It rather was and still is skillful engineering that reduces costs and raises efficiency close to the optimum. However, the Haber-Bosch process still consumes vast amounts of energy which is 1–2 % of the world’s overall energy output.^[8] Energetic savings can only be achieved if catalyst efficiency is enhanced or if a novel catalyst is tailored mimicking nature’s ability to fix and activate dinitrogen at ambient conditions. Interestingly, in a rough estimate the Haber-Bosch process produces about the same amount of ammonia as the total sum of all biological nitrogen fixation mediated by the nitrogenase enzyme.^[9]

1.2 BIOLOGICAL NITROGEN FIXATION

In nature, the enormously expensive and complex industrial process of nitrogen activation and reduction is catalyzed by the enzyme nitrogenase, whose crystal structure has been determined in high resolution by Rees et al. only very recently.^[10] The nitrogenase enzymes are able to perform the cleavage of the $\equiv\text{N}\text{N}$ triple bond already at *ambient conditions* and further transform it into ammonia according to equation 1.^[11] However, the process consumes again a huge amount of energy as turning each molecule of dinitrogen into ammonia takes at least 16 equivalents of the energy-deliverer adenosine triphosphate, ATP.^[12] Note that in addition about a quarter of the electrons involved upon N_2 -reduction are dissipated to make hydrogen gas as a by-product.



The nitrogenase enzymes fix atmospheric dinitrogen through the action of an inimitable class of metal-clusters. Nitrogenase itself consists of two major protein parts (see Figure 2).^[10,13,14] The larger iron-molybdenum (FeMo) protein ($\alpha_2\beta_2$ -tetramer) contains two iron-sulfur [4Fe-4S]-cuban-like clusters, the P-clusters ([8Fe-7S]-core) and two iron-molybdenum cofactors (FeMoCo) presenting the active site of the enzyme mediating the dinitrogen reduction. This

cofactor has been formulated as a structurally complex $[\text{MoFe}_7\text{S}_9\text{X}]$ -core, where X is a recently discovered interstitial monoatomic ligand believed to be carbon.^[15,16] Thereby, the $[\text{MoFe}_7\text{S}_9\text{X}]$ -core resembles two $[\text{4Fe-4S}]$ -cubes linked by an additional sulfur atom with one iron ion replaced by a molybdenum ion. Electrons are provided by the minor protein part, the iron (Fe) proteins by forming a complex with the FeMo-parts. Once stacked to the FeMo protein and when one electron has been transferred (energy is provided by hydrolysis of ATP), the Fe protein dissociates and recharges to reduce the FeMo protein again. After repeating this process eight times in single steps, one catalytic cycle is completed.^[17]

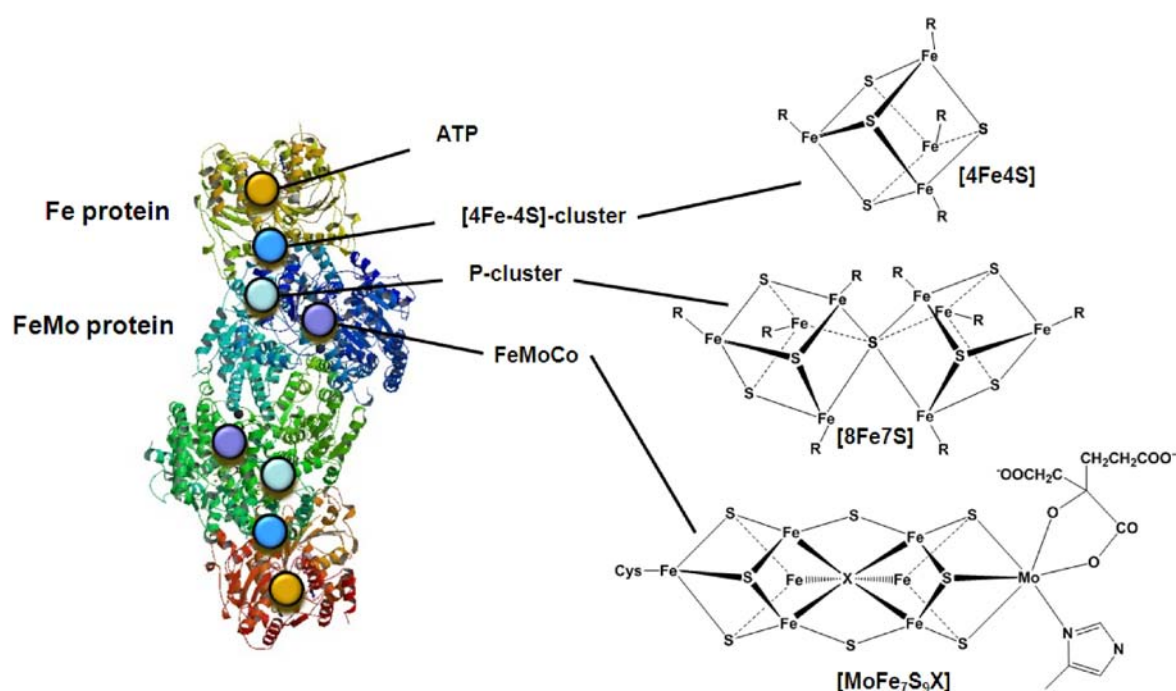


Figure 2. X-ray crystal structure of the nitrogenase enzyme with helical Fe (yellow and red) and FeMo (blue, turquoise, dark and light green) protein parts (left) obtained by extraction from *Azotobacter vinelandii* in 1997.^[10,26] Circles represent sites of located metal clusters involved in nitrogen reduction. A schematic sketch of corresponding metal clusters is given on the right.

Despite the detailed knowledge of the structural motifs in the nitrogenase enzyme, a basic mechanism for the biological reduction of nitrogen gas is not reported. Therefore, the activation and conversion of free molecular dinitrogen to ammonia including the characterization of a diversity of intermediates under ambient conditions is one of the major challenges in (bio-)inorganic and organo-metallic chemistry.^[18] Detailed spectroscopic, crystallographic and theoretical studies have been performed recently to elucidate the binding and reduction of N_2 at the FeMoCo.^[19-25] With these investigations, a few plausible mechanistic scenarios for the biological nitrogen fixation reactions have emerged, however still no definite and commonly accepted mechanism of operation exists so far as a synthetic

access to the fundamental FeMoCo protein part still lacks evidence. To inorganic chemists, the FeMoCo presents a number of longstanding challenges. The substrate binding site is unknown, the cluster charge state is uncertain, and the relationship of the cofactor structure, which derives from a resting-state enzyme, to catalytically active intermediates is unclear. In short, biological nitrogen fixation is very much a mystery at the molecular level although the structural motifs in the nitrogenase enzyme are well characterized.

1.3 SYNTHETIC NITROGEN FIXATION

Chatt and Schrock Cycles

Synthetic nitrogen fixation focuses on the binding, activation and reduction of dinitrogen on mono-, di- and polynuclear transition metal centers coordinated by capacious steric ligands. Revealing the dinitrogen fixation in such transition-metal complexes that represent structural motifs of nitrogenase could give fundamental insight in the catalytic process in nature and might help reducing costs in industrial ammonia production by tailoring corresponding catalysts. However, cubane clusters which are chemically and structurally related to the FeMoCo protein in nitrogenase exhibit only limited reactivity upon N₂ fixation.^[27,28] On the other hand, mono- and dinuclear transition metal complexes have been known to activate dinitrogen in various degrees for years, enabling protonation, reduction, functionalizing and even N–N bond cleavage steps. Besides a handful of examples of transition-metal complexes with trapped and activated N₂, up to date there are only two distinct classes of complexes that have emerged involving a full set of well-defined intermediates – such as diazenido, hydrazido, nitrido, imido, amido or amine intermediates – on the way of N₂ to NH₃. These systems form the basis of the Chatt and the Schrock cycle (see Figure 3).^[29,30] As *Schrock* et al. could show that it is most probably the molybdenum atom in the FeMoCo active site, which is responsible for dinitrogen activation, the successful synthesis of a molybdenum containing FeMoCo-analogous complex proved to catalytically reduce dinitrogen to ammonia with an efficiency of about 66 % with respect to the reducing agents.^[30–33] Thereby, the choice for the central metal in various synthetic model complexes was at hand.

Zerovalent molybdenum or tungsten (*M*) bis(dinitrogen) complexes [*M*(N₂)₂L₂] with di- up to multiphosphine (or mixed P/N) ligation (L) are the basis for the Chatt cycle, whereas the Schrock cycle is based on a trivalent molybdenum mono(dinitrogen) complex [*M*(N₂)L] with

sterically shielding ligands.^[19,23,29–38] A cyclic and catalytically active conversion of N_2 to NH_3 at ambient conditions mimicking the nitrogenase enzyme could so far only be achieved for model complexes within the Schrock system.^[30–33] Recently, *Tuczek et al.* were able to provide theoretical evidence for a possible catalytic reaction mode for Chatt model systems including enthalpy calculations for occurring intermediates upon proton-coupled electron-transfer reactions of *end-on* bound dinitrogen.^[39,40]

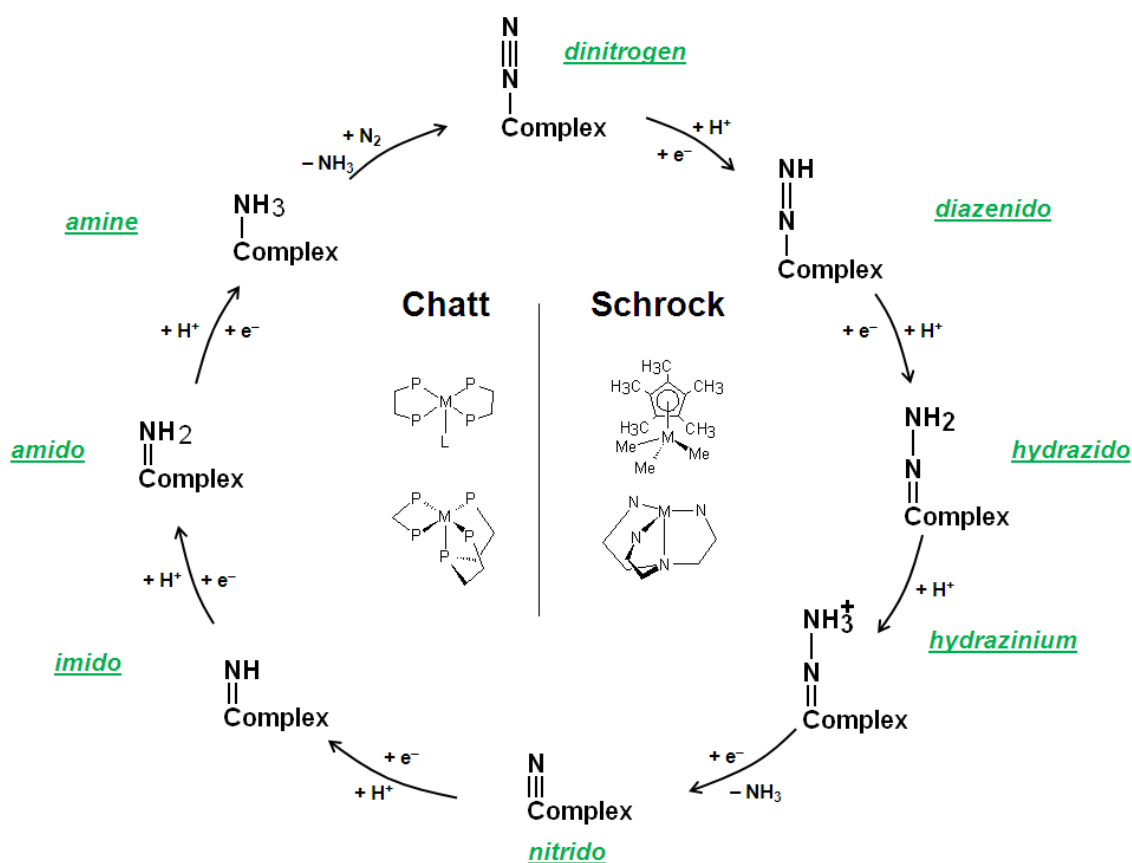


Figure 3. Schematic representation of synthetic nitrogen fixation by the Chatt or Schrock cycles.^[29,30] Upon nitrogen activation, the Chatt cycle makes use of molybdenum- or tungsten-based complexes with bidentate phosphine (top left), tetraphosphane (bottom left) or mixed multidentate phosphine/amine ligands,^[29,34–38] whereas the Schrock cycle involves molybdenum-complexes with sterically shielding ligands, for example such as methylated cyclopentadien (top right) or tetradentate triamidoamine (bottom right), the latter ligand stating the only example for a catalytically active cycle.^[30–33] The residual groups at the P- or N-ligand bridging-centers are omitted for clarity. It has to be stated, that due to separated one-electron/one-proton uptakes more intermediates are observed in detail,^[19,23,39,40] but are neglected for this schematic representation.

However, all these soluble model systems are far from replacing the Haber-Bosch process due to the fact that they consist of huge molecules to supply protons and electrons upon N_2 reduction to NH_3 , rather than cheap and compact hydrogen gas as in industrial ammonia production. But in comparison to the heterogeneous catalyst of the Haber-Bosch process, such soluble model complexes generate intermediates that are much easier to trap and study, which

helps to understand how metals bind the poor ligand dinitrogen and reduce it over intermediates finally to ammonia. Therefore, reproducing the biological transformation of dinitrogen to ammonia that occurs under ambient conditions in nature still challenges chemists. The mimicry of this multi-electron reduction process at milder conditions still proves to be difficult. The Chatt and Schrock cycles have evolved to explain the sequence of reactions involved in biological dinitrogen reduction, but only a low yield catalytic reaction is observed in one of those systems.^[19,23,29–38]

Degree of Activation affected by Binding Mode of the N₂ Molecule

The activation of neutral dinitrogen is furthermore highly affected by the binding mode of the N₂ molecule. Hereby, *side-on* bound dinitrogen is better activated as *end-on* bound N₂ due to the more effective possibilities of π -backbonding into the antibonding π^* states of the ligand thus opening additional pathways for subsequent functionalizing reactions.^[41] A division into weak to highly activated systems is possible regarding the N–N bond lengths and corresponding frequencies of the N–N stretching vibration upon infrared or Raman spectroscopic studies.^[19] The mono-metallic model systems of Chatt and Schrock cycles bind N₂ in general in an *end-on* manner and therefore lead to only weak or moderate activated N₂-intermediates which might be the crucial factor for the missing catalytic reaction. The binding of N₂ in *side-on* manner is usually accessed by homonuclear bi-metallic complexes. Common oxidation states for *side-on* bound N₂ when acting as a ligand are 0, –II or –IV representing non-activated dinitrogen(0), diazenido(–II) or hydrazido(–IV) intermediates. This is not surprising as the dinitrogen ligand is reduced in multiples of two due to the fact that each of the two metal atoms contributes either zero, one or two electrons to the dinitrogen reduction.

Even-Electron Nitrogen-Oxidation States

In general, if N₂ is not or only weakly activated, the observed N–N bond distance of about 1.1 Å is essentially the same as in free dinitrogen (1.097 Å^[42]).^[19,32,43–48] In accordance, the assignment of N₂ as a neutral ligand in such complexes is supported by very high N–N stretching frequencies of around 1900–2200 cm⁻¹ (free N₂: 2331 cm⁻¹^[49]) upon vibrational spectroscopy.^[19,32,45,50,51] For diazenido [N₂]²⁻ ligands, N–N bond lengths are found to be in the range of approximately 1.18–1.28 Å,^[45,52–62] similar to diazene HN=NH, itself exhibiting N–N bond lengths of about 1.21–1.25 Å depending on configuration (*cis*- or *trans*-

isomer).^[4,63] Corresponding stretching frequencies for the N–N double bond in diazenido ligands occur at around 1400–1700 cm⁻¹^[19,45,52–62] as observed for diazene with distinct features ranging from 1150 to 1650 cm⁻¹ based on as-mentioned configuration as well as on infrared- or Raman-active modes.^[63–67] Finally, if dinitrogen is highly activated by a four-electron reduction, [N₂]⁴⁻ ligation results. The hydrazido ligand can be viewed as a N–N single bonded dinitrogen ion with characteristic distances d_{NN} of about 1.38–1.64 Å and N–N stretching frequencies below 1000 cm⁻¹.^[52,68–76] Again these observations are in very good agreement with reported values for the N–N distance and stretching frequencies of protonated hydrazine N₂H₄ ($d_{\text{NN}} = 1.47$ Å, $\tilde{\nu}_{\text{NN}} < 1000$ cm⁻¹).^[77–79]

Odd-Electron Nitrogen-Oxidation States

Odd-electron nitrogen-oxidation states intermediate to those of 0, –II and –IV propose radical character and one-electron reduction mechanisms, but have not been observed so far in Chatt or Schrock cycles. However, this potential intermediacy of [N₂]⁻ or [N₂]³⁻ radical anions in metal complexes proved existence only very recently in dinuclear nickel^[45], iron^[18,80,81] and lanthanide^[52,55,82–84] complexes, respectively.^[85,86] Thereby, *end-on* bound [N₂]⁻ entities revealed a shift of the corresponding N–N stretching vibration towards lower energies (1740–1955 cm⁻¹) consistent with slightly enlarged d_{NN} bond lengths (1.13–1.18 Å) approximately in the range of the non-reduced dinitrogen complexes.^[45,80,81] For the *side-on* bound radical anion [N₂]³⁻, N–N bond lengths of about 1.39–1.41 Å and N–N stretching frequencies of again below 1000 cm⁻¹ have been observed similar to hydrazido ligands.^[18,52,55,82–84] To gain final evidence for the presence of both radical anions [N₂]⁻ and [N₂]³⁻, electron spin resonance (ESR) spectroscopy revealed clearly visible signals in accordance with simulated spectra indicative for unpaired electrons and supporting the radical formulation of dinitrogen ligation.^[45,52,55]

Summarizing, a correlation of N–N bond lengths with N–N stretching frequencies in dinitrogen complexes and in the free molecules of dinitrogen, diazene and hydrazine, all of which have been analyzed by high-quality low-temperature crystal structures is shown in Figure 4. Thereby, a non-linear relationship of d_{NN} and $\tilde{\nu}_{\text{NN}}$ is observed according to *Badger's* rule[†], where $d_{\text{NN}} \propto A\tilde{\nu}^{-2/3} + \delta$.^[87–89] For all protonated reference compounds, the depicted data

[†] *Badger's* rule gives a relation between internuclear distances and bond-force constants, which can be related to stretching frequencies of corresponding intramolecular bonds.

points only represent the general region, where the N–N stretching vibrations at a certain bond length occur. In addition, for N_2H_2 , the low-energy vibration at about 1300 cm^{-1} represents infrared-active modes, whereas the vibration at higher energies refers to Raman-active features.

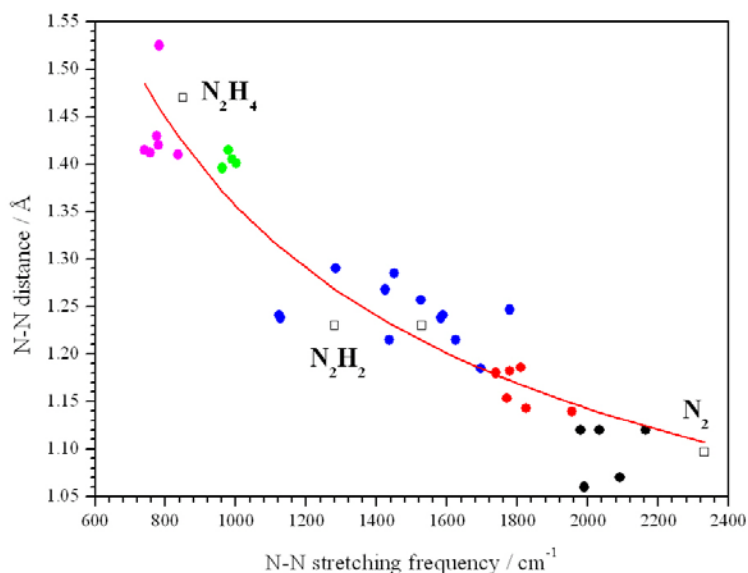


Figure 4. Correlation of N–N bond length with N–N stretching frequencies in dinitrogen complexes. Bond lengths and corresponding stretching frequencies of the dinitrogen ligand can be found in the literature as mentioned in the text. Thereby, the depicted colored circles refer to the N_2 ligand in distinct reduced states according to the following code: $[\text{N}_2]^0$ black, $[\text{N}_2]^-$ red, $[\text{N}_2]^{2-}$ blue, $[\text{N}_2]^{3-}$ green, $[\text{N}_2]^{4-}$ magenta. All points are fitted to *Badger's rule*, where $d_{\text{NN}} \propto A\tilde{\nu}^{-2/3} + \delta$ (red line).^[87–89] Open squares show data for the protonated reference compounds according to the literature.

1.4 NITROGEN FIXATION IN SOLID-STATE CHEMISTRY

Homonuclear Diatomic Carbon Anions

Although homonuclear dinitrogen anions are common intermediates in biological and organo-metallic synthetic chemistry, they have not been observed in solid-state compounds until 2001.^[90–95] This is quite surprising as a variety of ionic solids with homonuclear dianions consisting of the elements to the left and to the right of nitrogen in the periodic table (see Scheme 1) has been fully characterized decades ago.^[4,96–102]

In his review *Binary and ternary carbides of alkali and alkaline earth metals*,^[100] *Ruschewitz* surveys the preparative methods as well as the crystallographic and physical properties (i.e. mainly spectroscopic properties) of many binary and ternary carbides of Group I and II

metals. Thereby, special emphasis is provided for so called acetylenides representing deprotonated acetylene $\text{HC}\equiv\text{CH}$ with a $\text{C}\equiv\text{C}$ triple bond. The corresponding C–C triple bond lengths and C–C stretching frequencies are found to be 1.18–1.29 Å and $\tilde{\nu}_{\text{CC}} = 1800\text{--}2000\text{ cm}^{-1}$, respectively, and are close to the observed values for the gaseous acetylene molecule C_2H_2 ($d_{\text{CC}} = 1.20\text{ Å}$, $\tilde{\nu}_{\text{CC}} = 1974\text{ cm}^{-1}$).^[103,104] Besides these acetylenide anions, *Ruschewitz* additionally summarizes crystallographic, spectroscopic and theoretical evidence for so called methanides or carbides C^{4-} and allylenides with $[\text{C}_3]^{4-}$ anions and touches only slightly the chemistry of further carbon-rich materials such as intercalation compounds, fullerides and partly metallated hydrocarbons. Additional alkali or alkaline earth compounds with homonuclear dicarbon anions of alkali or alkaline earth metals – for example $[\text{C}_2]^{4-}$ or even $[\text{C}_2]^{6-}$ ions formally representing deprotonated ethylene or ethane, respectively – are not known up to date. However, if rare earth halogenides are reacted with graphite, again isolated C^{4-} ions but also C_2 entities are observed. Thereby, the latter ones exhibit C–C distances of about 1.35 or 1.45 Å characteristic for $[\text{C}_2]^{4-}$ or $[\text{C}_2]^{6-}$ anions, respectively.^[105–118]

no. valence electrons	10	11	12	13	14
bonding order (BO)	3	2.5	2	1.5	1
	—	—	—	—	—
	$[\text{C}_2]^{2-}$	$[\text{C}_2]^{3-}$	$[\text{C}_2]^{4-}$	$[\text{C}_2]^{5-}$	$[\text{C}_2]^{6-}$
	acetylenide		ethylenide		ethanide
	N_2	$[\text{N}_2]^-$	$[\text{N}_2]^{2-}$	$[\text{N}_2]^{3-}$	$[\text{N}_2]^{4-}$
	dinitrogen		diazenido diazenide		hydrazido pernitride
		$[\text{O}_2]^+$	O_2	$[\text{O}_2]^-$	$[\text{O}_2]^{2-}$
		dioxygenyl	dioxygen	hyper- superoxide	peroxide

Scheme 1. Hypothetical and experimentally observed homonuclear diatomic molecules and ions of carbon, nitrogen and oxygen. Up to date, there are no commonly accepted chemical names for $[\text{C}_2]^{3-}$, $[\text{C}_2]^{5-}$, $[\text{N}_2]^-$ and $[\text{N}_2]^{3-}$ anions.

Homonuclear Diatomic Oxygen Ions and Molecules

Compared to the homonuclear dicarbon chemistry, an equally rich variability is observed for compounds consisting of homonuclear molecules and ions of oxygen (see Scheme 1). Besides the allotropes O_2 and O_3 , there are peroxides $[\text{O}_2]^{2-}$, hyperoxides $[\text{O}_2]^-$, ozonides $[\text{O}_3]^-$ and

the dioxygenyl cation $[\text{O}_2]^+$.^[4,96–99] With the formal transition by one-electron reduction steps from the dioxygenyl cation to finally peroxide, the distance d_{OO} continuously increases from about 1.12 Å, over approximately 1.21 Å in free gaseous triplet oxygen and 1.28–1.33 Å in the hyperoxide ion to lastly 1.49 Å in $[\text{O}_2]^{2-}$.^[96–99,119–121] In accordance with these crystallographic data, corresponding O–O stretching frequencies decrease starting from roughly 1860 cm^{-1} for the dioxygenyl cation $[\text{O}_2]^+$ to about 740–950 cm^{-1} for peroxide units ($\tilde{\nu}_{\text{OO}}(^3\text{O}_2) \approx 1555 \text{ cm}^{-1}$ and $\tilde{\nu}_{\text{OO}}([\text{O}_2]^-) \approx 1125 \text{ cm}^{-1}$).^[4,122–125]

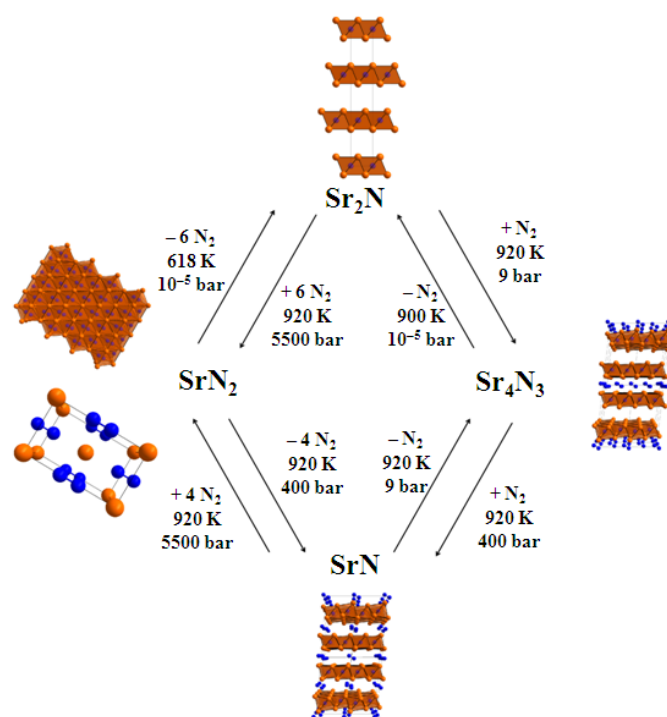
Homonuclear Diatomic Nitrogen Ions and Molecules

In contrast to these manifold representatives of homonuclear di-(an)ions of carbon and oxygen, nitrogen chemistry is considerably less versatile. It is only the nitrogen allotrope N_2 , nitrides N^{3-} and azides $[\text{N}_3]^-$ which have been long known and well characterized, as well as extensively used in industry. Only very recently, they could have been extended by the successful synthesis of the pentazenium cation $[\text{N}_5]^+$.^[126] The existence of potentially reduced dinitrogen molecules in solid-state chemistry proved their existence not before 2001, when *Kniep* et al. succeeded in the synthesis and characterization of the first representatives of inorganic solids containing the homonuclear dinitrogen anion $[\text{N}_2]^{2-}$.^[90–95] Accordingly, representing deprotonated diazene, N_2H_2 with a $\text{N}=\text{N}$ double bond, these anions were named *diazenides* – note that in coordinative chemistry corresponding $[\text{N}_2]^{2-}$ ligands constitute diazenido intermediates (see chapter 1.3). The synthesis of this novel class of materials was carried out using a specially developed autoclave system enabling a controlled temperature and N_2 partial-pressure $p(\text{N}_2)$ adjustment.^[93,127,128]

Initial Synthesis of Diazenides

In more detail, the synthesis of these diazenides is starting from the elements (Sr/Ba were the metals of choice) resulting in subnitride formation at elevated temperatures. In the case of strontium, Sr_2N is formed adopting the layered *anti*- CdCl_2 -type structure.^[90–94,129] Thereby, Sr_2N is built up by alternatingly occupied and vacant layers of $\text{Sr}_{6/3}\text{N}$ octahedra enabling the intercalation of dinitrogen molecules by distinct pressure and temperature conditions (see Scheme 2). In the first step of the initial N_2 redox-intercalation (see equation 1) at $p(\text{N}_2) = 1 \text{ bar}$, $T = 920 \text{ K}$, half of the octahedral voids in every second [001]-orientated layer of Sr_2N are occupied with $[\text{N}_2]^{2-}$ ions, which are formed by a reduction of dinitrogen

molecules. Thereby, the electrons are formally provided by partially oxidizing “Sr^{1.5+}” to common Sr²⁺.[‡] This results in the formation of Sr₄N₃, the first nitride-*diazenide*. Subsequently, increasing $p(\text{N}_2)$ up to about 400 bar at 920 K yields SrN by occupation of all remaining octahedral voids of Sr₄N₃ by diazenide units again formed upon two-electron reduction of the dinitrogen molecule and oxidation of “Sr^{1.5+}” (see equation 2). Finally, all-diazenide containing SrN₂ was obtained by comproportionation of remanent nitride ions and further N₂ molecules at $p(\text{N}_2) = 5.5$ kbar (0.55 GPa) and 920 K. Interestingly, SrN₂ crystallizes isotypically with corresponding alkaline earth acetylenides $M_{\text{AE}}\text{C}_2$, adopting a tetragonally distorted NaCl structure type with the $[\text{C}_2]^{2-}/[\text{N}_2]^{2-}$ units occupying the anion site. Evacuation of the autoclave sample chamber at about 620 K resulted again in the starting compound Sr₂N.



Scheme 2. Schematic representation of N₂ redox-intercalation in Sr₂N host-lattice. The crystal structures of the different strontium-nitrogen (orange-blue) compounds are illustrated next to the respective formulae. Sr₄N₃ and SrN are shown as a 2×2×2 super-cell. The layers of Sr_{6/3}N (nitride) octahedra are represented by orange polyhedra. The intercalated $[\text{N}_2]^{2-}$ ions between these layers are visualized by blue dumbbells. In SrN₂ all octahedral voids of the layers formed by strontium ions are occupied by $[\text{N}_2]^{2-}$ dimers. The crystal structures are depicted in a similar manner for a better understanding of the intercalation processes.

[‡] Note that the formulation of odd oxidation states of “Sr^{1.5+}” are taken from the original work by *Kniep et al.*^[90-94] In chapter 3.2, an alternative scenario of diazenide formation starting from Sr₂N with solely Sr²⁺ ions is presented.



X-ray and neutron diffraction experiments as well as highly precise elemental analysis confirmed the presence of $[\text{N}_2]^{2-}$ ions in all strontium diazenide compounds exhibiting specific N–N distances of about 1.22 Å perfectly matching reported values for diazenido ligands in metal complexes and protonated diazene (see chapter 1.3).^[4,19,45,52–63,90–94] To additionally correlate the obtained N–N distances to $[\text{N}_2]^{2-}$ ions vibrational spectroscopy was targeted. Besides low-energy translational lattice modes ($< 500 \text{ cm}^{-1}$), distinct N–N stretching frequencies at 1380 cm^{-1} (SrN) and 1307 cm^{-1} (SrN₂) were recorded by inelastic neutron scattering spectroscopy (INS) while Raman spectroscopic investigations failed – note that infrared experiments were not attempted.^[91] Interestingly, as-obtained N–N stretching frequencies are in excellent agreement with previously reported values of diazenido ligation and infrared-active modes in N₂H₂ (see chapter 1.3).^[4,19,45,52–62,65–67]

The existence of analogous barium diazenides is reported, but no crystallographic data are provided for the mixed nitride-diazenides Ba₄N₃ and BaN, except for all-diazenide containing BaN₂.^[92,93,95] Accordingly, barium diazenide has been synthesized at 5.6 kbar (0.56 GPa) and 920 K, and shows a close structural relationship to the crystal structure of SrN₂ although the strontium and barium compound do not crystallize isotypically. In BaN₂, the metal ions also form a closed packing, in which the $[\text{N}_2]^{2-}$ ions ($d_{\text{NN}} = 1.22 \text{ Å}$) occupy all octahedral voids, whereby edge and face sharing of octahedral coordination polymers results. However, BaN₂ adopts the ThC₂-type structure with monoclinic symmetry. Besides electronic structure calculations and magnetic susceptibility measurements unraveling metallic behavior of BaN₂,^[95] no vibrational data for the N–N stretching frequency of the $[\text{N}_2]^{2-}$ ion have been reported, but predicted to show up at 1466 cm^{-1} as Raman-active mode.^[130]

Prediction of further Diazenides

Since the successful synthesis of the first representatives of this class of materials in solid-state chemistry in 2001, experimental evidence for further diazenides has not been reported for a decade. Nevertheless, the extraordinary results of 2001 have fueled numerous theoretical

considerations on the prediction of further hitherto unknown diazenides in the following years. Thereby, theory claimed that Li_2N_2 , Na_2N_2 , BeN_2 , MgN_2 , CaN_2 , FeN_2 , ZnN_2 and LaN_2 should be thermodynamically stable at ambient conditions with respect to the elements, but are supposed to form only at high-pressure conditions.^[130–135] Theoretical N–N bond lengths were reported to range from 1.22–1.30 Å in good agreement with experimentally obtained values for diazenide $[\text{N}_2]^{2-}$ ions in Sr_4N_3 , SrN , SrN_2 and BaN_2 .^[90–95] In fact, in 2013 lanthanum diazenide, LaN_2 proved existence by shockwave experiments at peak pressures of 3 GPa starting from $\text{La}(\text{NO}_3)_3$.^[136] Crystallographic analysis resulted in elongated N–N bond lengths of 1.31–1.32 Å consistent with the theoretical N–N distance of 1.30 Å for predicted $\text{La}^{3+}[\text{N}_2]^{2-}\cdot\text{e}^-$ crystallizing in the ThC_2 -type structure.^[130,133,136] Within this context, *Kulkarni et al.* investigated the energy landscapes of $M\text{N}_2$ compounds ($M = \text{Ca}, \text{Sr}, \text{Ba}, \text{La}, \text{Ti}$) at ambient and high-pressure conditions.^[137,138] Besides a variety of hypothetical high-pressure modifications of these compounds, he showed that the dinitrogen anion in TiN_2 -type phases still represents diazenide units $[\text{N}_2]^{2-}$ despite strongly elongated N–N bond lengths of 1.26 up to 1.46 Å according to Bader charge analysis of the metal atom, which for all modifications resulted in Ti^{2+} formulation. However, a potential synthetic route to TiN_2 -type phases was not proposed or reported.

Initial Synthesis of Pernitrides

More recently in 2006/7, related noble metal “nitrides” with an analogous formula type $M_{\text{NM}}\text{N}_2$ ($M_{\text{NM}} = \text{Os}, \text{Ir}, \text{Pd}$ and Pt) have been synthesized in laser-heated diamond-anvil cells (LH-DAC) starting from cryogenically loaded N_2 and the metals themselves at high pressures above 50 GPa and temperatures around 2300 K.^[139–148] The crystallographic characterization of these compounds resulted in N–N distances of about 1.40–1.43 Å which were consistent with theoretical enthalpy-considerations of as-obtained crystal structures. Thereby, N–N bond lengths of around 1.4 Å indicated strongly elongated N_2 dimers compared to the diazenides of 2001. Additional theoretical calculations concerning the valence of expected divalent noble metal ions revealed that $M_{\text{NM}}\text{N}_2$ compounds are constituted of tetravalent noble metals indicating the formulation of $[\text{N}_2]^{4-}$ ions.^[130,133] In accordance with N–N distances of about 1.40–1.43 Å, *in situ* Raman spectroscopy in LH-DACs at various pressures (including zero pressure) as well as phonon calculations resulted in low-energetic N–N stretching frequencies of about 700–1000 cm^{-1} for the dinitrogen anions.^[130,133,139–148] As-mentioned characteristics are in perfect agreement with reported values for hydrazine N_2H_4 and for hydrazido ligands in

corresponding metal complexes.^[52,68–79] Accordingly, as $[\text{N}_2]^{4-}$ is isoelectronic with peroxide $[\text{O}_2]^{2-}$ (see Scheme 1) this class of compounds has been denominated *pernitrides*. Interestingly, all of these pernitrides have been reported experimentally and theoretically as mechanically ultra-hard materials, exceeding the hardness of their constituting noble metals and approaching that of *c*-BN and diamond.^[139–148] The successful synthesis of noble metal pernitrides exhibiting extraordinary materials properties has even expanded the search for further hypothetical nitrogen-rich transition metal “nitrides”. Thereby, $M_{\text{NM}}\text{N}_2$ ($M_{\text{NM}} = \text{W}, \text{Re}, \text{Ru}, \text{Rh}, \text{etc.}$) have been predicted to exist representing *di*-nitrides, but also consisting of pernitrides or even diazenides depending on pressure conditions.^[139,148–164]

Interestingly, already in 2003 *Wehrich* et al. predicted possible $M\text{N}_2$ -type structures of Group IV elements (C, Si and Ge) – indicating anionic $[\text{N}_2]^{4-}$ formulation – but it was not until in 2006/7 that compounds with hypothetical $[\text{N}_2]^{4-}$ ions found significant interest in solid-state but also in materials chemistry.^[165,166] Note that also hypothetical CN_2 is supposed to exhibit ultra-high hardness with a bulk modulus of $B_0 = 405$ GPa exceeding even those of $M_{\text{NM}}\text{N}_2$ pernitrides.^[140,165,166]

Later on, in 2010, finally the first molecular main group metal pernitride with an isolated $[\text{N}_2]^{4-}$ ion coordinated by six gallium atoms was presented by *Uhl* et al.^[167] The crystallographic N–N distance of about 1.55 Å is still in accordance with neutral hydrazine and matches perfectly the wide range of hydrazido ligation of 1.38–1.64 Å.^[52,68–79] In infrared and Raman spectra the N–N stretching vibration of the central hydrazine element was detected at 891 and 892 cm^{-1} , respectively, which is in the range characteristic of hydrazine.^[77–79] Further two years later, in 2012, again *Uhl* et al. succeeded in the synthesis of the first molecular Group III pernitride, namely $[\text{N–N}(\text{Me})]^{3-}$, encapsulated in an aluminum cage constituted of five atoms.^[168] With 1.55 Å, the N–N distance in the latter anion matches the previous bond length in the gallium- N_2 cage compound.

Overview

In summary, the recent success in synthesis of reduced dinitrogen containing solid-state compounds – none the less due to upgraded experimental techniques – has fueled experimental as well as theoretical efforts to characterize novel hitherto unknown diazenides, pernitrides or even – as in bioinorganic and metal-organic chemistry – odd-electron reduced dinitrogen intermediates. A final overview of characteristic N–N bond lengths and stretching

frequency ranges of dinitrogen anions observed in bioinorganic and metal-organic as well as in solid-state chemistry is displayed in Scheme 3.

	$[\text{N}_2]^0$	$[\text{N}_2]^-$	$[\text{N}_2]^{2-}$	$[\text{N}_2]^{3-}$	$[\text{N}_2]^{4-}$
$d_{\text{NN}} / \text{\AA}$	1.06–1.12	1.13–1.18	1.18–1.32 ^a	1.39–1.41	1.40–1.55 ^c 1.38–1.64 ^d
$\tilde{\nu}_{\text{NN}} / \text{cm}^{-1}$	2200–1900	1950–1740	1700–1300	1000–990	890–750 ^c < 1000 ^d
	free N_2 : 1.097 \AA 2331 cm^{-1}		free N_2H_2 : ^b 1.21–1.25 \AA 1150–1650 cm^{-1}		free N_2H_4 : 1.47 \AA < 1000 cm^{-1}

Scheme 3. Overview of characteristic N–N bond lengths and stretching frequencies of dinitrogen ligands/anions observed in (bio-)organo-metallic and solid-state chemistry according to the text. ^aRecent theoretical calculations of TiN_2 -type compounds revealed N–N bond lengths of 1.26 up to even 1.46 \AA for diazenide units. ^bDifferent values for N–N bond lengths and stretching frequencies due to *cis*- and *trans*-configurations as well as due to infrared and Raman active modes. ^{c,d}N–N bond lengths in $[\text{N}_2]^{4-}$ units correspond to solid-state/main group compounds (c) and to bioinorganic/metal-organic ligation (d).

Objective of the Thesis

Except for $M = \text{Sr}, \text{Ba}, \text{La}, \text{Os}, \text{Ir}, \text{Pd}$ and Pt , no other metal diazenides or pernitrides with $M\text{N}_2$ stoichiometry have been synthesized in crystalline form as yet, but have been predicted by a variety of density-functional calculations to form at high-pressure/high-temperature conditions (HP/HT). Although a HP-route using the elements is the correct choice for the synthesis of reported compounds, their realization is hindered due to the employed techniques which are of high-level state-of-the-art and thus not commonly “accessible” – only very specialized equipments were utilized for the synthesis of diazenides and pernitrides so far. An alternative HP-synthesis is only known for BaN_2 starting from ionic barium azide, $\text{Ba}(\text{N}_3)_2$ in a belt apparatus at HP/HT-conditions.^[95] Within this context, *Dronskowski* et al. calculated reaction enthalpies for azide decomposition into diazenides and molecular nitrogen, which resulted in exothermic reactions for the synthesis of strontium and hypothetical calcium diazenides.^[132] For the synthesis of BaN_2 however, the thermal decomposition of $\text{Ba}(\text{N}_3)_2$ is endothermic, which could be and in fact was overcome by HP and HT conditions in the belt apparatus (synthesis temperature: 600 K).^[95,132]

Taking these observations into account, the synthesis of hitherto unknown diazenides using controlled decomposition of highly reactive precursors like the corresponding azides in a multianvil device under HP/HT-conditions represents a promising route. Therefore, the objective of this thesis is the HP/HT-synthesis and structural as well as spectroscopic characterization of novel diazenides by controlled thermal decomposition of ionic Group I

and II azides. The analytical methods used for the identification and characterization combined a manifold of different techniques to properly describe structural and spectroscopic aspects. Structural investigations were mainly based on powder X-ray diffraction (PXRD) while in one case it was supplemented by transmission electron microscopy (TEM). In addition, density-functional theory was also used to verify obtained structural models and spectroscopic aspects. Finally, compared to the classification of valencies in bound N₂ entities in bioinorganic or metal-organic chemistry, their adequate description in solid-state chemistry might be hindered due to, e.g., potential metallicity in such compounds. However, as it is shown in this work, due to complementary use of a variety of different methods including the as-mentioned ones as well as Fourier transform infrared (FTIR), variable temperature solid-state nuclear magnetic (NMR) and electron spin resonance (ESR) spectroscopy the identification of the true oxidation state in [N₂]^{x-} anions remains possible.

Bibliography

- [1] J. R. Jennings, *Catalytic Ammonia Synthesis*, Plenum Press: New York, **1991**.
- [2] W. Laue, M. Thiemann, E. Scheibler, K. W. Wiegand, *Nitrates and Nitrites, Ullmann's Encyclopedia of Industrial Chemistry*, Wiley-VCH: Weinheim, **2000**.
- [3] T. D. Kelly, G. R. Matos, U.S. Geological Survey, *Nitrogen Statistics*, Historical statistics for mineral and material commodities in the United States: U.S. Geological Survey Data Series 140, <http://minerals.usgs.gov/ds/2005/140/>, accessed **24/06/2012**.
- [4] United Nations, Department of Economic and Social Affairs (Population Division), http://esa.un.org/unpd/wpp/unpp/panel_population.htm, selected categories: *Population, World, 1950–2010*, accessed **24/06/2013**.
- [5] A. F. Holleman, E. Wiberg, *Lehrbuch der Anorganischen Chemie*, Vol. 102, de Gruyter: Berlin-New York, **2007**.
- [6] <http://www.basf.com/group/corporate/en/about-basf/history/1902-1924/index>, accessed **24/06/2013**.
- [7] G. Ertl, *Angew. Chem.* **2008**, *120*, 3578; *Angew. Chem., Int. Ed.* **2008**, *47*, 3524.
- [8] International Fertilizer Industry Association, Energy Efficiency and CO₂ Emissions in Ammonia Production, <http://www.fertilizer.org/ifa/HomePage/LIBRARY/Publication->

- database.html/Energy-Efficiency-and-CO2-Emissions-in-Ammonia-Production.html, accessed 24/06/2013.
- [9] F. Tuczek, *Stickstoff-Fixierung bei Raumtemperatur und Normaldruck: Synthetische, spektroskopische und theoretische Untersuchungen*, invited talk at the Ludwig-Maximilians-University: Munich, **2012**.
- [10] H. Schindelin, C. Kisker, J.L. Schlessman, J.B. Howard, D.C. Rees, *Nature* **1997**, 387, 370.
- [11] B.K. Burgess, D.J. Lowe, *Chem. Rev.* **1996**, 96, 2983.
- [12] R.A. Alberty, R.N. Goldberg, *Biochemistry* **1992**, 31, 10610.
- [13] B.K. Burgess, *Chem. Rev.* **1990**, 90, 1377.
- [14] J.S. Kim, D.C. Rees, *Nature* **1992**, 360, 553.
- [15] K.M. Lancaster, M. Roemelt, P. Ettenhuber, Y.L. Hu, M.W. Ribbe, F. Neese, U. Bergmann, S. DeBeer, *Science* **2011**, 334, 974.
- [16] T. Spatzal, M. Aksoyoglu, L.M. Zhang, S.L.A. Andrade, E. Schleicher, S. Weber, D.C. Rees, O. Einsle, *Science* **2011**, 334, 940.
- [17] R.N. F. Thorneley, D.J. Lowe, in: T.G. Spiro, *Molybdenum Enzymes*, Wiley: New York, **1985**.
- [18] B.A. MacKay, M.D. Fryzuk, *Chem. Rev.* **2004**, 104, 385.
- [19] F. Studt, F. Tuczek, *J. Comput. Chem.* **2006**, 27, 1278.
- [20] F. Tuczek, *Adv. Inorg. Chem.* **2004**, 56, 27.
- [21] F. Tuczek, K.H. Horn, N. Lehnert, *Coord. Chem. Rev.* **2003**, 245, 107.
- [22] F. Tuczek, *Electronic Structure Calculations: Dinitrogen Reduction in Nitrogenase and Synthetic Model Systems*, John Wiley & Sons, Ltd, **2009**.
- [23] H. Broda, S. Hinrichsen, F. Tuczek, *Coord. Chem. Rev.* **2013**, 257, 587.
- [24] B.M. Hoffman, D. Lukoyanov, D.R. Dean, L.C. Seefeldt, *Acc. Chem. Res.*, **2013**, 46, 587.

- [25] B.M. Barney, H.I. Lee, P.C. Dos Santos, B.M. Hoffmann, D.R. Dean, L.C. Seefeldt, *Dalton Trans.* **2006**, 2277.
- [26] *RCSB Protein Data Bank*, PDB ID: 1N2C, <http://www.rcsb.org/pdb/explore/explore.do?structureId=1n2c>, accessed 24/06/2013.
- [27] U. Huniar, R. Ahlrichs, D. Coucouvanis, *J. Am. Chem. Soc.* **2004**, *126*, 2588.
- [28] D. Coucouvanis, K.D. Demadis, S.M. Malinak, P.R. Mosier, M.A. Tyson, L.J. Laughlin, *Transition Metal Sulfur Chemistry*, ACS Symp. Ser. 653, ACS: Washington, **1996**.
- [29] C.J. Pickett, *J. Biol. Inorg. Chem.* **1996**, *1*, 601.
- [30] D.V. Yandulov, R.R. Schrock, *Inorg. Chem.* **2005**, *44*, 1103.
- [31] D.V. Yandulov, R.R. Schrock, *Science* **2003**, *301*, 76.
- [32] D.V. Yandulov, R.R. Schrock, A.L. Rheingold, C. Ceccarelli, W.M. Davis, *Inorg. Chem.* **2003**, *42*, 796.
- [33] V. Ritleng, D. V. Yandulov, W. W. Weare, R. R. Schrock, A. S. Hock, W. M. Davis, *J. Am. Chem. Soc.* **2004**, *126*, 6150.
- [34] R. Römer, C. Gradert, A. Bannwarth, G. Peters, C. Näther, F. Tuczek, *Dalton Trans.* **2011**, 3229.
- [35] K. Klatt, G. Stephan, G. Peters, F. Tuczek, *Inorg. Chem.* **2008**, *47*, 6541.
- [36] G. Stephan, G. Peters, N. Lehnert, C. Habeck, C. Näther, F. Tuczek, *Can. J. Chem.* **2005**, *83*, 385.
- [37] G. Stephan, C. Näther, F. Tuczek, *Acta Crystallogr., Sect. E* **2008**, *64*, M629.
- [38] G. Stephan, C. Näther, C. Sivasankara, F. Tuczek, *Inorg. Chim. Acta* **2008**, *361*, 1008.
- [39] A. Dreher, G. Stephan, F. Tuczek, *Adv. Inorg. Chem.* **2009**, *61*, 367.
- [40] G. Stephan, F. Tuczek, in C. Bolm, F.E. Hahn (Eds.), *Activating Unreactive Substrates*, Wiley-VCH: Weinheim, **2009**.
- [41] E.A. MacLachlan, M.D. Fryzuk, *Organometallics* **2006**, *25*, 1530.

- [42] P.G. Wilkinson, N.B. Houk, *J. Chem. Phys.* **1956**, *24*, 528.
- [43] I.E. Buys, L.D. Field, T.W. Hambley, A.E.D. McQueen, *Acta Crystallogr.* **1993**, *C49*, 1056.
- [44] T. Uchida, Y. Uchida, M. Hidai T. Kodama, *Acta Crystallogr.* **1975**, *B31*, 1197.
- [45] S. Pfirrmann, C. Herwig, R. Stößer, B. Ziemer, C. Limberg, *Angew. Chem.* **2009**, *121*, 3407; *Angew. Chem., Int. Ed.* **2009**, *48*, 3357.
- [46] O. Franke, *PhD thesis*, Christian-Albrechts-University: Kiel, **2004**.
- [47] N. Lehnert, F. Tuczek, *Inorg. Chem.* **1999**, *38*, 1671.
- [48] K. Mersmann, K.H. Horn, N. Böres, N. Lehnert, F. Studt, F. Paulat, G. Peters, F. Tuczek, *Inorg. Chem.* **2005**, *44*, 3031.
- [49] F. Rasetti, *Proc. Natl. Acad. Sci. USA* **1929**, *15*, 234.
- [50] O. Franke, B.E. Wiesler, N. Lehnert, F. Tuczek, *Z. Anorg. Allg. Chem.* **2002**, *628*, 2395.
- [51] F. Tuczek, K.H. Horn, N. Lehnert, *Coord. Chem. Rev.* **2003**, *245*, 107.
- [52] W.J. Evans, M. Fang, G. Zucchi, F. Furche, J.W. Ziller, R.M. Hoekstra, J.I. Zink, *J. Am. Chem. Soc.* **2009**, *131*, 11195.
- [53] W.J. Evans, D.S. Lee, D.B. Rego, J.M. Perotti, S.A. Kozimor, E.K. Moore, J.W. Ziller, *J. Am. Chem. Soc.* **2004**, *126*, 14574.
- [54] W.J. Evans, D.L. Lee, C. Lie, J.W. Ziller, *Angew. Chem.* **2004**, *116*, 5633; *Angew. Chem., Int. Ed.* **2004**, *43*, 5517.
- [55] M. Fang, J.E. Bates, S.E. Lorenz, D.S. Lee, D.B. Rego, J.W. Ziller, F. Furche, W.J. Evans, *Inorg. Chem.* **2011**, *50*, 1459.
- [56] W.J. Evans, D.S. Lee, *Can. J. Chem.* **2005**, *83*, 375.
- [57] T. Dubé, M. Ganesan, S. Conoci, S. Gambarotta, G.P.A. Yap, *Organometallics* **2000**, *19*, 3716.

- [58] F. Jaroschik, A. Momin, F. Nief, X.L. Goff, G.B. Deacon, P.C. Junk, *Angew. Chem.* **2009**, *121*, 1137; *Angew. Chem., Int. Ed.* **2009**, *48*, 1117.
- [59] W.J. Evans, N.T. Allen, J.W. Ziller, *J. Am. Chem. Soc.* **2001**, *123*, 7927.
- [60] W.J. Evans, N.T. Allen, J.W. Ziller, *Angew. Chem.* **2002**, *114*, 369; *Angew. Chem., Int. Ed.* **2002**, *41*, 359.
- [61] W.J. Evans, G. Zucchi, J.W. Ziller, *J. Am. Chem. Soc.* **2003**, *125*, 10.
- [62] I. Vidyaratne, J. Scott, S. Gambarotta, P.H.M. Budzelaar, *Inorg. Chem.* **2007**, *46*, 7040.
- [63] N. Wiberg, G. Fischer, H. Bachhuber, *Chem. Ber.* **1974**, *107*, 1456.
- [64] V.E. Bondybey, J.W. Nibler, *J. Chem. Phys.* **1973**, *58*, 2125.
- [65] E.J. Blau, B.F. Hochheimer, *J. Chem. Phys.* **1964**, *41*, 1174.
- [66] K. Rosengren, G.C. Pimentel, *J. Chem. Phys.* **1965**, *43*, 507.
- [67] R. Minkwitz, *Z. Anorg. Allg. Chem.* **1975**, *411*, 1.
- [68] J.A. Pool, E. Lobkovsky, P.J. Chirik, *Nature* **2004**, *427*, 527.
- [69] M. Hirotsu, P.P. Fontaine, P.Y. Zavalij, L.R. Sita, *J. Am. Chem. Soc.* **2007**, *129*, 12690.
- [70] E.A. MacLachlan, F.M. Hess, B.O. Patrick, M.D. Fryzuk, *J. Am. Chem. Soc.* **2007**, *129*, 10895.
- [71] W.H. Bernskoetter, A.V. Olmos, E. Lobkovsky, P.J. Chirik, *Organometallics* **2006**, *25*, 1021.
- [72] T. Dubé, S. Conoci, S. Gambarotta, G.P.A. Yap, G. Vasapollo, *Angew. Chem.* **1999**, *111*, 3890; *Angew. Chem., Int. Ed.* **1999**, *38*, 3657.
- [73] C.D. Bérubé, M. Yazdanbakhsh, S. Gambarotta, G.P.A. Yap, *Organometallics* **2003**, *22*, 3742.
- [74] G. Guillemot, B. Castellano, T. Prangé, E. Solari, C. Floriani, *Inorg. Chem.* **2007**, *46*, 5152.

- [75] J. Jubb, S. Gambarotta, *J. Am. Chem. Soc.* **1994**, *116*, 4477.
- [76] M.D. Fryzuk, J.B. Love, S.J. Rettig, V.G. Young, *Science* **1997**, *275*, 1445.
- [77] N.T. Allen, O. Kennard, D.G. Watson, L. Brammer, A.G. Orpen, R. Taylor, *J. Chem. Soc., Perkin Trans.* **1987**, *2*, S1.
- [78] L.E. Sutton, *Tables of Interatomic Distances and Configuration in Molecules and Ions*, Chemical Society Spec. Publ. 11, Chemical Society: London, **1958**.
- [79] P.A. Giguère, I.D. Liu, *J. Chem. Phys.* **1952**, *20*, 136.
- [80] J.M. Smith, R.J. Lachicotte, K.A. Pittard, T.R. Cundari, G. Lukat-Rodgers, K.R. Rodgers, P.L. Holland, *J. Am. Chem. Soc.* **2001**, *123*, 9222 .
- [81] J.M. Smith, A.R. Sadique, T.R. Cundari, K.R. Rodgers, G. Lukat-Rodgers, R.J. Lachicotte, C.J. Flaschenriem, J. Vela, P.L. Holland, *J. Am. Chem. Soc.* **2006**, *128*, 756.
- [82] M. Fang, D.S. Lee, J.W. Ziller, R.J. Doedens, J.E. Bates, F. Furche, W.J. Evans, *J. Am. Chem. Soc.* **2011**, *133*, 3784.
- [83] J.D. Rinehart, M. Fang, W.J. Evans, J.R. Long, *J. Am. Chem. Soc.* **2011**, *133*, 14236.
- [84] J.D. Rinehart, M. Fang, W.J. Evans, J.R. Long, *Nat. Chem.*, **2011**, *3*, 538.
- [85] P.J. Chirik, *Nat. Chem.* **2009**, *1*, 520.
- [86] W. Kaim, B. Sarkar, *Angew. Chem.* **2009**, *121*, 9573; *Angew. Chem., Int. Ed.* **2009**, *48*, 9409.
- [87] R.M. Badger, *J. Chem. Phys.* **1934**, *2*, 128.
- [88] R.M. Badger, *J. Chem. Phys.* **1935**, *3*, 227.
- [89] P.L. Holland, *Dalton Trans.* **2010**, *39*, 5415.
- [90] G. Auffermann, Y. Prots, R. Kniep, *Angew. Chem.* **2001**, *113*, 565; *Angew. Chem., Int. Ed.* **2001**, *40*, 547.
- [91] G. Auffermann, Y. Prots, R. Kniep, S.F. Parker, S.M. Bennington, *ChemPhysChem* **2002**, *9*, 815.

- [92] G. Auffermann, U. Schmidt, B. Bayer, Y. Prots, R. Kniep, *Anal. Bioanal. Chem.* **2002**, 373, 880.
- [93] G. Auffermann, R. Kniep, W. Bronger, *Z. Anorg. Allg. Chem.* **2006**, 632, 565.
- [94] Y. Prots, G. Auffermann, M. Tovar, R. Kniep, *Angew. Chem.* **2002**, 114, 2392; *Angew. Chem., Int. Ed.* **2002**, 41, 2288.
- [95] G.V. Vajenine, G. Auffermann, Y. Prots, W. Schnelle, R.K. Kremer, A. Simon, R. Kniep, *Inorg. Chem.* **2001**, 40, 4866.
- [96] N.G. Vannerberg, *Prog. Inorg. Chem.* **1962**, 4, 125.
- [97] I.I. Vol'nov, *Peroxides, Superoxides and Ozonides of Alkali and Alkaline Earth Metals*, Vol. II, Plenum Press: New York, **1966**.
- [98] W. Hesse, M. Jansen, W. Schnick, *Prog. Solid State Chem.* **1989**, 19, 47.
- [99] D.H. Lohmann, N. Bartlett, *Proc. Chem. Soc.* **1962**, 115, 5253.
- [100] U. Ruschewitz, *Coord. Chem. Rev.* **2003**, 244, 115.
- [101] U. Ruschewitz, *Z. Anorg. Allg. Chem.* **2006**, 632, 705.
- [102] U. Ruschewitz, M. Kilo, *Nachr. Chem.* **2004**, 52, 260.
- [103] L. Pauling, *The Nature of the Chemical Bond*, 3rd ed., Cornell University Press: Ithaca, **1960**.
- [104] G. Herzberg, *Molecular Spectra and Molecular Structure*, Vol. I: *Spectra of Diatomic Molecules*, Vol. II: *Infrared and Raman Spectra of Polyatomic Molecules*, Van Nostrand Reinhold Co: New York, Toronto, London, Melbourne, **1945**.
- [105] A. Simon, Hj. Mattausch, G.L. Miller, W. Bauhofer, R.K. Kremer, *Handbook on the Physics and Chemistry of Rare Earth*, Elsevier Science Publ.: Amsterdam-London-New York-Tokyo, **1991**.
- [106] D.S. Dudis, J.D. Corbett, *Inorg. Chem.* **1986**, 26, 1933.
- [107] A. Simon, E. Warkentin, R. Masse, *Angew. Chem.* **1981**, 93, 1071; *Angew. Chem., Int. Ed. Engl.* **1981**, 20, 1013.

- [108] S. Uhrlandt, G. Meyer, *Z. Anorg. Allg. Chem.* **1994**, 620, 1872.
- [109] H.M. Artelt, Th. Schleid, G. Meyer, *Z. Anorg. Allg. Chem.* **1992**, 618, 18.
- [110] E. Warkentin, R. Masse, A. Simon, *Z. Anorg. Allg. Chem.* **1982**, 491, 323.
- [111] Hj. Mattausch, E. Warkentin, O. Oeckler, A. Simon, *Z. Anorg. Allg. Chem.* **2000**, 626, 2117.
- [112] U. Schwanitz-Schüller, A. Simon, *Z. Naturforsch.* **1985**, 40b, 710.
- [113] O. Oeckler, Hj. Mattausch, A. Simon, *Z. Kristallogr. Suppl.* **1999**, 16, 2.
- [114] Hj. Mattausch, C. Hoch, A. Simon, *Z. Anorg. Allg. Chem.* **2005**, 631, 1423.
- [115] Hj. Mattausch, C. Hoch, C. Zheng, A. Simon, *Z. Anorg. Allg. Chem.* **2007**, 633, 239.
- [116] Hj. Mattausch, A. Simon, *Z. Kristallogr. NCS* **1995**, 210, 63.
- [117] A. Simon, Y. Yoshiasa, M. Baecker, R.W. Henn, C. Felser, R.K. Kremer, Hj. Mattausch, *Z. Anorg. Allg. Chem.* **1996**, 622, 123.
- [118] Hj. Mattausch, A. Simon, L. Kienle, C. Hoch, C. Zheng, R.K. Kremer, *Z. Anorg. Allg. Chem.* **2006**, 632, 1661.
- [119] S.C. Abrahams, J. Kalnajs, *Acta Crystallogr.* **1995**, 8, 503.
- [120] L. Vaska, *Acc. Chem. Res.* **1976**, 9, 175.
- [121] H. Föppl, *Z. Anorg. Allg. Chem.* **1957**, 291, 12.
- [122] J. Shamir, J. Binenboym, H.H. Claassen, *J. Am. Chem. Soc.* **1968**, 90, 6223.
- [123] H.H. Eysel, S. Thym, *Z. Anorg. Allg. Chem.* **1975**, 411, 97.
- [124] J. Yang, D. Zhai, H.-H. Wang, K.C. Lau, J.A. Schlueter, P. Du, D.J. Myers, Y.-K. Sun, L.A. Curtiss, K. Amine, *Phys. Chem. Chem. Phys.* **2013**, 15, 3764.
- [125] K.C. Lau, L.A. Curtiss, *J. Phys. Chem. C* **2011**, 115, 23625.
- [126] K.O. Christe, W.W. Wilson, J.A. Sheehy, J.A. Boatz, *Angew. Chem.* **2009**, 111, 2112; *Angew. Chem., Int. Ed.* **1999**, 38, 2004.
- [127] W. Bronger, G. Auffermann, *Chem. Mater.* **1998**, 10, 2723.

- [128] W. Bronger, G. Auffermann, *Z. Anorg. Allg. Chem.* **1995**, *621*, 1318.
- [129] N.E. Brese, M. O’Keeffe, *J. Solid State Chem.* **1990**, *87*, 134.
- [130] M. Wessel, R. Dronskowski, *J. Am. Chem. Soc.* **2010**, *132*, 2421.
- [131] X. Zhang, A. Zunger, G. Trimarchi, *J. Chem. Phys.* **2010**, *133*, 194504.
- [132] M. Wessel, R. Dronskowski, *J. Comput. Chem.* **2010**, *31*, 1613.
- [133] M. Wessel, *PhD thesis*, RWTH Aachen University: Aachen, **2010**.
- [134] M. Wessel, R. Dronskowski, *Chem. Eur. J.* **2011**, *17*, 2598.
- [135] S.D. Gupta, S.K. Gupta, P.K. Jha, *Eur. Phys. J. B.* **2013**, *86*, 8.
- [136] O. Tschauner, S.N. Luo, Y.J. Chen, A. McDowell, J. Knoght, S.M. Clark, *High Pressure Res.* **2013**, *33*, 202.
- [137] A. Kulkarni, J.C. Schön, K. Doll, M. Jansen, *Chem. Asian J.* **2013**, *8*, 743.
- [138] A. Kulkarni, *PhD thesis*, University Stuttgart: Stuttgart, **2012**.
- [139] E. Gregoryanz, C. Sanloup, M. Somayazulu, J. Badro, G. Fiquet, H.-K.; Mao, R.J. Hemely, *Nat. Mater.* **2004**, *3*, 294.
- [140] J. von Appen, M.-W. Lumey, R. Dronskowski, *Angew. Chem.* **2006**, *118*, 4472; *Angew. Chem., Int. Ed.* **2006**, *45*, 4365.
- [141] J.C. Crowhurst, A.F. Goncharov, B. Sadigh, C.L. Evans, P.G. Morrall, J.L. Ferreira, A.J. Nelson, *Science* **2006**, *311*, 1275.
- [142] A.F. Young, J.A. Montoya, C. Sanloup, M. Lazzeri, E. Gregoryanz, S. Scandolo, *Phys. Rev. B* **2006**, *73*, 153102.
- [143] J.A. Montoya, A.D. Hernandez, C. Sanloup, E. Gregoryanz, S. Scandolo, *Appl. Phys. Lett.* **2007**, *90*, 011909.
- [144] J.C. Crowhurst, A.F. Goncharov, B. Sadigh, J.M. Zaug, D. Aberg, Y. Meng, V.B. Prakapenka, *J. Mater. Res.* **2008**, *23*, 1.

- [145] Z.W. Chen, X.J. Guo, Z.Y. Liu, M.Z. Ma, Q. Jing, G. Li, X.Y. Zhang, L.X. Li, Q. Wang, Y.J. Tian, R.P. Liu, *Phys. Rev. B* **2007**, 75, 054103.
- [146] R. Yu, Q. Zhan, L.C. De Jonghe, *Angew. Chem.* **2007**, 119, 1154; *Angew. Chem., Int. Ed.* **2007**, 46, 1136.
- [147] W. Chen, J.S. Tse, J.Z. Jiang, *J. Phys.: Condens. Matter* **2010**, 22, 015404.
- [148] A. Salamat, A.L. Hector, P. Kroll, P.F. McMillan, *Coord. Chem. Rev.* **2013**, 257, 2063.
- [149] P. Kroll, T. Schroter, M. Peters, *Angew. Chem.* **2005**, 117, 4321; *Angew. Chem., Int. Ed.* **2005**, 44, 4249.
- [150] H. Wang, Q. Li, Y.E. Li, Y. Xu, T. Cui, A.R. Oganov, Y.M. Ma, *Phys. Rev. B* **2009**, 79, 132109.
- [151] X.F. Li, Z.L. Liu, C.L. Ding, H.Z. Fu, G.F. Ji, *Mater. Chem. Phys.* **2011**, 130, 14.
- [152] L. Song, Y.X. Wang, *Phys. Status Solidi B* **2010**, 247, 54.
- [153] H.A. Wriedt, *Bull. Alloy Phase Diagr.* **1989**, 10, 358.
- [154] S. Wang, X. Yu, Z. Lin, R. Zhang, D. He, J. Qin, J. Zhu, J. Han, L. Wang, H.-k. Mao, J. Zhang, Y. Zhao, *Chem. Mater.* **2012**, 24, 3023.
- [155] Y.L. Li, Z. Zeng, *Solid State Commun.* **2009**, 149, 1591.
- [156] E. Zhao, Z.J. Wu, *Comput. Mater. Sci.* **2008**, 44, 531.
- [157] Y.L. Li, Z. Zeng, *Chem. Phys. Lett.* **2009**, 474, 93.
- [158] X.P. Du, Y.X. Wang, V.C. Lo, *Phys. Lett. A* **2010**, 374, 2569.
- [159] F. Kawamura, H. Yusa, T. Taniguchi, *Appl. Phys. Lett.* **2012**, 100, 251910.
- [160] M.G. Moreno-Armenta, J. Diaz, A. Martinez-Ruiz, G. Soto, *J. Phys. Chem. Solids* **2007**, 68, 1989.
- [161] R. Yu, Q. Zhan, L.C. De Jonghe, *Angew. Chem.* **2007**, 119, 1154; *Angew. Chem., Int. Ed.* **2007**, 46, 1136.

- [162] Y. Wang, T. Yao, J.-L. Yao, J. Zhang, H. Gou, *Phys. Chem. Chem. Phys.* **2013**, *15*, 183.
- [163] W. Chen, J.S. Tse, J.Z. Jiang, *Solid State Commun.* **2010**, *150*, 181.
- [164] E.R. Hernández, E. Canadell, *J. Mater. Chem.* **2008**, *18*, 2090.
- [165] R. Weihrich, S.F. Matar, E. Betranhandy, V. Eyert, *Solid State Sci.* **2003**, *5*, 701.
- [166] R. Weihrich, V. Eyert, S.F. Matar, *Chem. Phys. Lett.* **2003**, *373*, 636.
- [167] W. Uhl, B. Rezaeirad, M. Layh, E. Hagemeyer, E.-U. Würthwein, N. Ghavtadze, I. Kuzu, *Chem. Eur. J.* **2010**, *16*, 12195.
- [168] W. Uhl, A. Hepp, M. Layh, B. Rezaeirad, *Chem. Commun.* **2012**, *48*, 1799.

2. BINARY ALKALINE EARTH DIAZENIDES

Besides the synthesis of SrN_2 and BaN_2 in a specialized autoclave system at high-pressure/high-temperature conditions (HP/HT) starting from the elements, the HP/HT-synthesis of BaN_2 in a belt apparatus by decomposition of $\text{Ba}(\text{N}_3)_2$ has already shown another possibility of accessing (further) diazenide compounds. Therefore, we initially targeted the reproductive HP/HT-synthesis of SrN_2 and BaN_2 by controlled thermal decomposition of corresponding ionic azides in a multianvil device. The successful synthesis of both diazenides encouraged further investigation of the thermal stability of the lighter group II homologue azides under HP/HT-conditions.

2.1. SYNTHESIS OF ALKALINE EARTH DIAZENIDES $M_{\text{AE}}\text{N}_2$ ($M_{\text{AE}} = \text{Ca}, \text{Sr}, \text{Ba}$) BY CONTROLLED THERMAL DECOMPOSITION OF AZIDES UNDER HIGH PRESSURE

Sebastian B. Schneider, Rainer Frankovsky and Wolfgang Schnick

published in *Inorg. Chem.* **2012**, *51*, 2366

DOI: 10.1021/ic2023677

Copyright © 2012, American Chemical Society

<http://pubs.acs.org/doi/full/10.1021/ic2023677>

ABSTRACT

The alkaline earth diazenides $M_{\text{AE}}\text{N}_2$ with $M_{\text{AE}} = \text{Ca}, \text{Sr}$ and Ba were synthesized by a novel synthetic approach, namely a controlled decomposition of the corresponding azides in a multianvil press at high-pressure/high-temperature conditions. The crystal structure of hitherto unknown calcium diazenide (space group $I4/mmm$ (no. 139), $a = 3.5747(6)$, $c = 5.9844(9)$ Å, $Z = 2$, $wR_p = 0.078$) was solved and refined on the basis of powder X-ray diffraction data as well as that of SrN_2 and BaN_2 . Accordingly, CaN_2 is isotypic with SrN_2 (space group $I4/mmm$ (no. 139), $a = 3.8054(2)$, $c = 6.8961(4)$ Å, $Z = 2$, $wR_p = 0.057$) and the corresponding alkaline earth acetylenides ($M_{\text{AE}}\text{C}_2$) crystallizing in a tetragonally distorted NaCl structure type. In accordance with literature data, BaN_2 adopts a more distorted structure in space group $C2/c$ (no. 15) with $a = 7.1608(4)$, $b = 4.3776(3)$, $c = 7.2188(4)$ Å, $\beta = 104.9679(33)^\circ$, $Z = 4$ and $wR_p = 0.049$. The N–N bond lengths of 1.202(4) Å in CaN_2 (SrN_2 1.239(4) Å, BaN_2 1.23(2) Å) correspond well with a double-bonded dinitrogen unit confirming a diazenide ion $[\text{N}_2]^{2-}$. Temperature-dependent *in situ* powder X-ray diffractometry of the three alkaline earth diazenides resulted in formation of the corresponding subnitrides $M_{\text{AE}}\text{N}$ ($M_{\text{AE}} = \text{Ca}, \text{Sr}, \text{Ba}$) at higher temperatures. FTIR spectroscopy revealed a band at about 1380 cm^{-1} assigned to the N–N stretching vibration of the diazenide unit. Electronic structure calculations support the metallic character of alkaline earth diazenides.

2.1.1 INTRODUCTION

Synthesis and characterization of novel binary metal nitrides had a significant impact on solid-state and materials chemistry due to a multitude of applications for such compounds.^[1–9] In 2001, the first members of the novel class of nitrogen-rich alkaline earth compounds $M_{\text{AE}}\text{N}_2$ have been discovered and structurally characterized by *Kniep* et al. revealing dinitrogen anions $[\text{N}_2]^{2-}$ with N=N double bonds. The latter anions represent deprotonated diazene N_2H_2 units and therefore have been named diazenides. In the past SrN_2 and BaN_2 have been synthesized from the corresponding metals at 893 K under nitrogen pressure (0.55–0.56 GPa) in a specialized autoclave system.^[10–14] Recently, related noble metal nitrides with analogous formula type $M_{\text{NM}}\text{N}_2$ ($M_{\text{NM}} = \text{Os, Ir, Pd and Pt}$) have been synthesized in laser-heated diamond-anvil cells in combination with cryogenically loaded nitrogen at high pressure of 50 GPa and temperatures around 2200 K.^[15–23] According to structural and electronic considerations, these noble metal compounds are assumed to contain fourfold negatively charged nitrogen-dimers having the composition $M^{4+}[\text{N}_2]^{4-}$.^[15–24] Unlike the alkaline earth diazenides, the latter anions (bond length about 1.41 Å)^[15–24] are derived from diazane, N_2H_4 , containing N–N single bonds and are isosteric with peroxide $[\text{O}_2]^{2-}$. Accordingly, these compounds $M^{4+}[\text{N}_2]^{4-}$ have been classified as pernitrides^[15–24] and their remarkable properties (e.g. superconductivity, photoluminescence, magnetism and low compressibility comparable to that of *c*-BN)^[15–24] merit the investigation of the crystalline structure, stability, elasticity and electronic structures of the diazenides. However, except for $M = \text{Sr, Ba, Os, Ir, Pd and Pt}$, no other metal diazenides or pernitrides of formula type $M\text{N}_2$ have been synthesized in crystalline form as yet, but have been predicted by density-functional calculations to form under HP/HT-conditions.^[24–29]

In order to extend the class of nitrogen rich metal diazenides or pernitrides, we have targeted new synthetic approaches for these compounds and we were successful using controlled decomposition of highly reactive precursors like the corresponding azides. In this contribution, we present our novel synthesis route for the alkaline earth diazenides SrN_2 and BaN_2 . In addition, we report on the synthesis, structural, spectroscopic and electronic characterization of the novel alkaline earth diazenide CaN_2 and compare its structure to the predicted model.^[26,29]

2.1.2 EXPERIMENTAL SECTION

Synthesis of NH_4N_3

Phase-pure NH_4N_3 is obtained by the metathesis reaction of NH_4NO_3 (3.99 g, 50 mmol, Sigma-Aldrich, 99.0 %) and NaN_3 (3.25 g, 50 mmol, Acros Organics, Geel, Belgium, 99 %) in a silica tube at elevated temperatures. By heating from room temperature to 473 K within 0.5 h, annealing for 12 h and cooling down again to room temperature within 6 h,^[30] NH_4N_3 is precipitated at the cold end of the silica tube separated from NaNO_3 , which crystallizes at the hot end during the reaction.

Synthesis of $\text{Ca}(\text{N}_3)_2$

Aqueous solutions of calcium azide are obtained from the reaction of $\text{Ca}(\text{OH})_2$ with excess of NH_4N_3 (1:4) according to the procedure reported in the literature.^[31] First $\text{Ca}(\text{OH})_2$ (1.5 g, 20.1 mmol, Sigma-Aldrich, 99.995 %) is dissolved in 200 ml of water. Then an excess of NH_4N_3 (4.8 g, 80.5 mmol) is added generating aqueous $\text{Ca}(\text{N}_3)_2$, NH_3 and H_2O . Ammonia is boiled off and calcium azide is precipitated by evaporating the water. The obtained calcium azide is dried over CaCl_2 (Sigma-Aldrich, 99.99 %) using a vacuum desiccator.

Synthesis of $\text{Sr}(\text{N}_3)_2$ and $\text{Ba}(\text{N}_3)_2$

Strontium and barium azide were obtained by the reaction of the corresponding hydroxide (Sigma-Aldrich, 99.995 %) with an aqueous solution of HN_3 , as reported in the literature.^[32,33] The extremely dangerous HN_3 is distilled from NaN_3 (Acros Organics, Geel, Belgium, 99 %) and H_2SO_4 . The solid azides are dried over P_4O_{10} using a vacuum desiccator. A general procedure for the synthesis of the azides of the heavier alkaline earth metals is described in the literature.^[31] **Caution!** Due to the very low thermal and mechanical shock resistance of HN_3 , hydrazoic acid should always be handled with maximum caution. Therefore, whenever working with HN_3 , efficient protective clothing such as face protections, a leather coat and steel reinforced gloves must be worn.

Synthesis of $M_{\text{AE}}\text{N}_2$ ($M_{\text{AE}} = \text{Ca}, \text{Sr}, \text{Ba}$)

The three alkaline earth diazenides were synthesized under high-pressure/high-temperature conditions in a modified Walker-type module in combination with a 1000 t press

(Voggenreiter, Mainleus, Germany). As pressure medium, precastable MgO-octahedra (Cermaic Substrates & Components, Isle of Wight, U.K.) with edge lengths of 14 or 18 mm (14/8 or 18/11 assembly) were employed. Eight tungsten carbide cubes (Hawedia, Marklkofen, Germany) with truncation edge lengths of 8 or 11 mm compressed the octahedra. The three alkaline earth azides were carefully ground, filled into a cylindrical boron nitride crucible (Henze BNP GmbH, Kempten, Germany) and sealed with a fitting boron nitride plate. Details of the setup are described in the literature.^[34–38]

CaN₂ (SrN₂, BaN₂) was synthesized in a 14/8 (18/11, 18/11) assembly which was compressed up to 12 (9, 3) GPa at room temperature within 325 (214, 68) min, then heated up to 1073 (823, 723) K in 300 (30, 30) min, Kept at this temperature for 20 (15, 15) min and cooled down to room temperature in 15 (10, 10) min. Subsequently, the pressure was released over a period of 958 (623, 183) min. The recovered MgO-octahedron was broken apart in a glovebox and the sample carefully isolated from the surrounding boron nitride crucible. A black metallic powder of alkaline earth diazenides is obtained, extremely sensitive to moisture.

Powder X-Ray Diffraction (PXRD), Structure Solution and Rietveld Refinement

The crystal structures of the three alkaline earth diazenides were analyzed on the basis of powder X-ray diffraction data. The powder diffraction patterns were recorded with a STOE Stadi P powder diffractometer (STOE, Darmstadt, Germany) in Debye-Scherrer geometry using Ge(111) monochromated Mo and Cu $K_{\alpha 1}$ radiation (0.7093 Å and 1.54056 Å). For the alkaline earth diazenides of strontium and barium the resulting powder X-ray diffraction patterns fit perfectly the ones reported in the literature.^[10–14] In the case of the novel diazenide of calcium, the indexing resulted unambiguously in a tetragonal unit-cell with $a = 3.57$ and $c = 5.98$ Å. A Rietveld refinement (Figure 1) was performed with the TOPAS package^[39] using the structure of SrN₂ as starting model. The reflection profiles were determined using the fundamental parameter approach^[40] by convolution of appropriate source emission profiles with axial instrument contributions and crystalline microstructure effects. Preferred orientation of the crystallites was described with a spherical harmonics of 5th order. The relevant crystallographic data for the three alkaline earth diazenides and further details of the data collection are summarized in Tables 1 and 2. Further information of the crystal structures may be obtained from the Fachinformationszentrum Karlsruhe, 76344 Eggenstein-Leopoldshafen, Germany (fax: (49) 7247–808–666; e-mail: crysdata@fiz-karlsruhe.de) on

quoting the depository numbers CSD-423721 (CaN_2), CSD-423722 (SrN_2) and CSD-423723 (BaN_2).

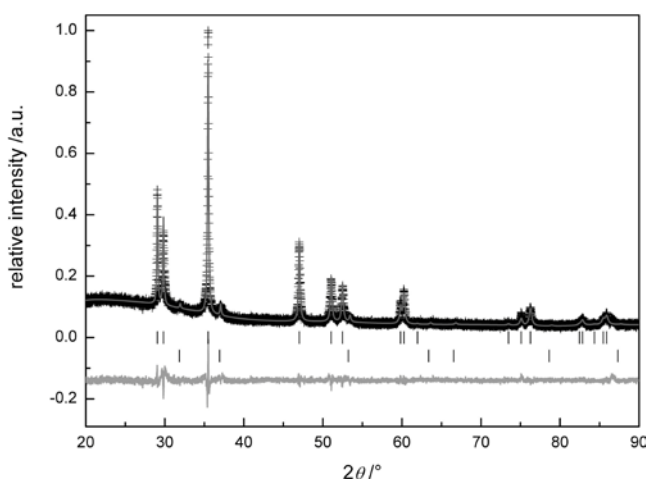


Figure 1. Observed (crosses) and calculated (gray line) powder diffraction pattern as well as difference profile of the Rietveld refinement of CaN_2 ; peak positions of CaN_2 (first row) and of CaO (second row; side phase) are marked by vertical lines.

Temperature-Dependent in situ X-Ray Diffractometry

In situ X-ray powder diffraction data were collected with a STOE Stadi P powder diffractometer ($\text{Mo } K_{\alpha 1}$ radiation (0.7093 \AA)) equipped with a computer controlled STOE resistance graphite furnace. Enclosed in a silica glass capillary under argon, the samples were heated from room temperature to 1173 K at a rate of 5 K/min in steps of 298 K. At each heating step (after holding the temperature for 1 min), a diffraction pattern was recorded with an IP-PSD in the range of $2^\circ \leq 2\theta \leq 80^\circ$.

Infrared Spectroscopy

Fourier transform infrared (FTIR) measurements were carried out on a Bruker IFS 66v/S spectrometer. Spectra of the samples were recorded in an evacuated cell at ambient conditions between 400 and 4000 cm^{-1} after diluting the samples in KBr pellets (2 mg sample, 300 mg KBr, pressed with 10 KN).

Calculation of the Electronic Structure

The LMTO method in its scalar relativistic version (TB-LMTO-ASA program)^[41] was used to perform the calculation of the band structure, electronic density of states (DOS) and crystal

orbital Hamiltonian population (COHP) of CaN_2 and SrN_2 .^[42] Detailed descriptions of the method are given elsewhere.^[43,44] The k point set was extended to a $24 \times 24 \times 24$ array to properly describe the metallic compounds. The basis sets consisted of Ca: $4s/\{4p\}/3d$, Sr: $5s/\{5p\}/4d/\{4f\}$ and N: $2s/2p/\{3d\}$ where orbitals given in parenthesis were downfolded.^[45] The elec-tronic structure calculations converged when the change of the total energy was smaller/equal to 10^{-5} Ry. The COHP method was used for bond analysis. COHP gives the energy contributions of all elec-tronic states for a selected bond. The values are negative for bonding and positive for antibonding interactions. With respect to the COHP diagrams, we plot -COHP(E) to obtain positive values for bonding states. The structural parameters were taken from the Rietveld refinements. The orbital character of the bands was analyzed using the so-called fat-band plots. Magnetic susceptibility measurements and electro-nic structure calculations for BaN_2 already revealed that the compound exhibits Pauli paramagnetism and should be metallic, despite the paramagnetic triplet state of the diazenide ion.^[11] Therefore, a test spin-polarized calculation with nonzero magnetic moments artificially placed on the nitrogen atoms of CaN_2 and SrN_2 was

Table 1. Synthesis Conditions and Crystallographic Data for CaN_2 , SrN_2 and BaN_2 .

	CaN_2	SrN_2	BaN_2
synthesis conditions multianvil assembly	12 GPa @ 1073 K	9 GPa @ 823 K	3 GPa @ 723 K
fw /g·mol ⁻¹	68.0914	115.6334	165.3534
space group	<i>I4/mmm</i> (no. 139)	<i>I4/mmm</i> (no. 139)	<i>C2/c</i> (no. 15)
cell parameters /Å, °	<i>a</i> = 3.5747(6) <i>c</i> = 5.9844(9)	<i>a</i> = 3.8054(2) <i>c</i> = 6.2961(4)	<i>a</i> = 7.1608(4) <i>b</i> = 4.3776(3) <i>c</i> = 7.2188(4) β = 104.9679(33)
<i>V</i> /Å ³	76.47(3)	91.17(1)	218.61(2)
<i>Z</i> /cell	2	2	4
ρ_{calc} /g·cm ⁻³	2.9572(10)	4.212(1)	5.0237(5)
μ_{calc} /mm ⁻¹	30.622(11)	37.068(1)	17.73(2)
<i>d</i> _{NN} /Å	1.202(4)	1.239(4)	1.23(2)
	Data Collection		
type of diffractometer geometry		STOE Stadi P Debye-Scherrer	
radiation, monochromator	Cu <i>K</i> _{α1} , ($\lambda = 1.54056 \text{ \AA}$), Ge(111)	Mo <i>K</i> _{α1} , ($\lambda = 0.7093 \text{ \AA}$), Ge(111)	
<i>T</i> /K		298(2)	
detector		linear PSD ($\Delta\theta = 5^\circ$)	
2θ range /°	10–90	5–90	2–80
number of observed reflections	17	19	690
	Structure Analysis and Refinement		
method of refinement		fundamental parameter model TOPAS Academic	
program package			
atomic parameters	3	3	6
background function / parameters	shifted Chebyshev / 9	shifted Chebyshev / 12	shifted Chebyshev / 15
<i>R</i> indices	GoF(χ^2) = 1.200 <i>R</i> _p = 0.062 <i>wR</i> _p = 0.078	GoF(χ^2) = 1.740 <i>R</i> _p = 0.044 <i>wR</i> _p = 0.057	GoF(χ^2) = 1.495 <i>R</i> _p = 0.037 <i>wR</i> _p = 0.049

performed and converged also back to the metallic state.

2.1.3 RESULTS AND DISCUSSION

Crystal Structure Elucidation of CaN₂ and SrN₂

Both alkaline earth diazenides crystallize in the same structure type, which is isotypic with the corresponding alkaline earth acetylenides ($M_{\text{AE}}\text{C}_2$), namely in a tetragonally distorted NaCl-type. Therefore, they can be topologically derived from

Table 2. Refined Atomic Coordinates and Isotropic Displacement Parameters (in 0.01 \AA^2) for CaN₂, SrN₂ and BaN₂.

atoms	Wyckoff	x	y	z	$U_{\text{iso}}^a \cdot 100$
CaN ₂					
Ca1	2a	0	0	0	3.926(96)
N1	4e	0	0	0.3995(5)	6.15(15)
SrN ₂					
Sr1	2a	0	0	0	3.733(57)
N1	4e	0	0	0.4016(4)	2.60(13)
BaN ₂					
Ba1	4e	0	0.2006(2)	¼	1.413(21)
N1	8f	0.3023(18)	0.1547(39)	0.0508(19)	1.99(13)

$$^a U_{\text{iso}} = B_{\text{eq}} / (8 \cdot \pi^2)$$

Sr₂N (*anti*-CdCl₂-type) by occupying all octahedral voids made up by the strontium ions with [N₂]²⁻ units aligned along [001]. Figure 2 represents a top view of the resulting unit-cell of $M_{\text{AE}}\text{N}_2$ ($M_{\text{AE}} = \text{Ca}, \text{Sr}$) in the (101) plane. The alkaline earth ion is coordinated *side-on* by four and *end-on* by two diazenide units (Figure 3), giving a coordination number of $8 + 2 = 10$. The dinitrogen unit occupies the octahedral voids and is coordinated by six M_{AE}^{2+} ions. The occupied octahedrons are connected to each other by shared edges and faces. The experimentally found N–N bond length of SrN₂ synthesized by *Kniep* et al. was 1.224(2) Å.^[10] Here, we find a distance between the nitrogen atoms of 1.202(4) Å in CaN₂ and 1.239(4) Å in SrN₂, which is in good agreement with the former results.

As already mentioned, *Wessel* et al. have predicted the crystal structures of all alkaline earth diazenides theoretically.^[29] For their theoretical investigation, 15 possible structural models with atomic ratio cation to anion of 1:2 were taken into account and thereby the ground-state structures predicted. The calculations confirm that the experimentally found structures for SrN₂ and BaN₂ are minimum energy structures, thus being the thermodynamically most stable structures. For CaN₂ however, the search for a plausible thermodynamic ground-state structure resulted basically in five possible structure types (Table 3) within a tolerance of $\Delta E_{\text{total}} = 1 \text{ kJ/mol}$ relative to ZnCl₂.

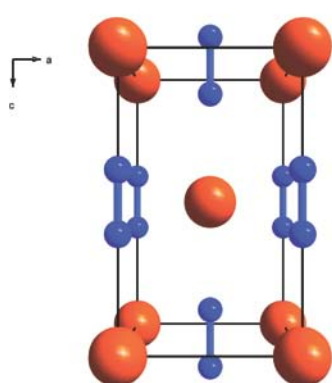


Figure 2. Top view of the unit-cell of CaN_2 and SrN_2 along $[010]$ ($\text{Ca}^{2+}/\text{Sr}^{2+}$ orange, nitrogen blue).

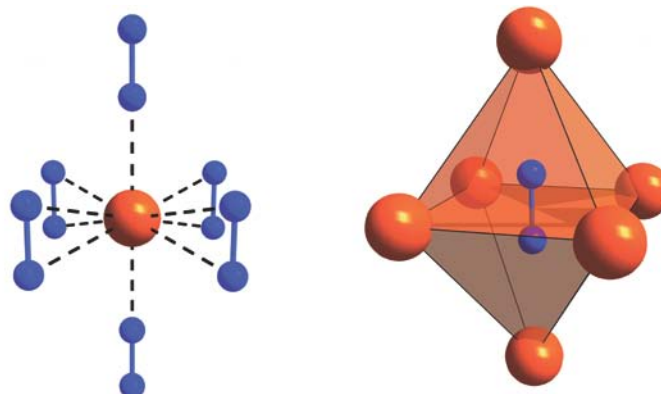


Figure 3. Coordination spheres of $\text{Sr}^{2+}/\text{Ca}^{2+}$ on the left, and of the diazenide on the right ($\text{Ca}^{2+}/\text{Sr}^{2+}$ orange, nitrogen blue).

For the reported ZnCl_2 structure type, the authors additionally analyzed the common crystallographic details (space group, lattice parameters, atomic positions, interatomic N–N distance). In this structural model, the cations are coordinated by four dinitrogen units in an *end-on* and to another two units in a *side-on* mode which results in an effective coordination number of $4 + 4 = 8$. The coordination sphere of the diazenide unit again is octahedral. The resulting N–N distance of 1.255 \AA is in good agreement with the one experimentally found. Synthesized CaN_2 however, is of the $M_{\text{AE}}\text{C}_2$ structure type. Nevertheless, the calculations reveal that the $M_{\text{AE}}\text{C}_2$ structure type is close to the ZnCl_2 type in total energy ($\Delta E_{\text{total}} = 1 \text{ kJ/mol}$).

Crystal Structure Elucidation of BaN_2

BaN_2 shows a close structural relationship to the structure type of SrN_2 and CaN_2 , although the strontium and barium compound do not crystallize isotypically. In BaN_2 , the metal ions also form a closed packing, in which the $[\text{N}_2]^{2-}$ ions occupy all octahedral voids (Figure 4, left). Again, edge and face sharing of octahedra results. However, due to the lower symmetry of BaN_2 compared to CaN_2 and SrN_2 , the octahedral voids are occupied with nitrogen dimers aligned horizontally along the diagonals of the Ba^{2+} octahedra with alternating orientation within each layer. Only along $[100]$, the same orientation of dinitrogen units is found. Therefore, the coordination sphere of Ba^{2+} is quite similar but slightly more distorted (Figure 4, right). Two diazenide units coordinate in an *end-on* and four $[\text{N}_2]^{2-}$ ions in a *side-on* fashion (with two different sets of distances to Ba^{2+}), thus resulting in a coordination number

of $2 + 4 + 4 = 10$. As expected, the experimentally found N–N bond distance of the diazenide ion $1.204(3) \text{ \AA}$ is intermediate between those of a N–N single-bond and triple-bond.

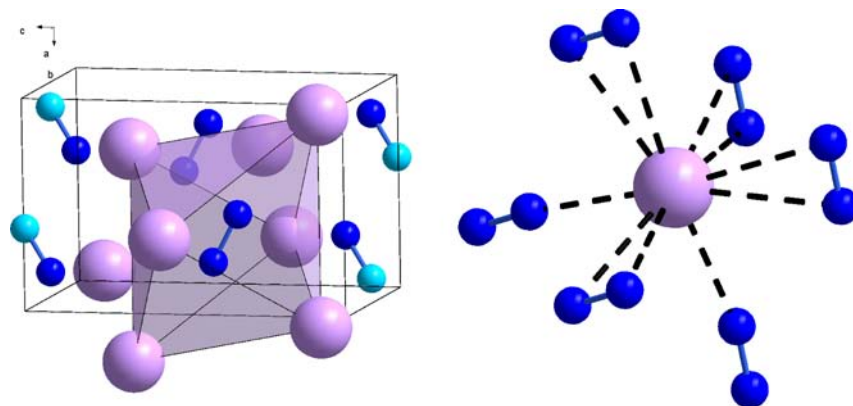


Figure 4. Unit-cell of BaN₂ with coordination of the diazenide unit on the left; Ba²⁺ coordination sphere on the right (Ba²⁺ light purple, nitrogen blue, nitrogen not in unit-cell turquoise).

Vibrational Spectroscopy

For SrN₂ and SrN $\in (\text{Sr}^{2+})_4(\text{N}^{3-})_2([\text{N}_2]^{2-})$, a nitride-diazenide) inelastic neutron scattering (INS) spectroscopy already revealed that an observed feature at 1380 cm^{-1} (SrN) and 1307 cm^{-1} (SrN₂) can be assigned to the N–N stretching vibration of the diazenide ion.^[46] Remaining features at considerable lower wavenumbers ($< 350 \text{ cm}^{-1}$) were assigned to acoustic, optic translational and librational modes of the $[\text{N}_2]^{2-}$ ion.

Concerning a free nitrogen molecule (point symmetry $D_{\infty h}$), the only fundamental vibration (Σ_g) is Raman-active and IR-inactive due to the rule of mutual exclusion.^[47] However, the infrared spectra of $M_{\text{AE}}\text{N}_2$ ($M_{\text{AE}} = \text{Ca}, \text{Sr}, \text{Ba}$), which are shown in Figure 5, exhibit clear features at 1376.9 (CaN₂), 1378.9 (SrN₂) and 1375.9 cm^{-1} (BaN₂), which are assigned to the N–N stretching vibration of the $[\text{N}_2]^{2-}$ ion. Therefore, in comparison to the free dinitrogen molecule with only one Raman-active mode, the corresponding site symmetry of the diazenide ion in the solid has to be reduced to observe IR-active modes. This condition can be verified using the correlation method.^[47] The reduced site symmetry for the dinitrogen unit in CaN₂ and SrN₂ is C_{4v} , resulting in two possible IR-active modes (A_1, E). In BaN₂, there is a $D_{\infty h} \rightarrow C_1$ reduction in symmetry with one IR- and Raman-active vibration (A). Applying the correlation method,^[47] the only IR-active modes for CaN₂ and SrN₂ (factor symmetry D_{4h}) are A_{2u} and E_u , and for BaN₂ (C_{2h}) A_u and B_u . Therefore, in the corresponding crystal, the solely Raman-active mode in the free dinitrogen molecule is split into either one of those IR-active modes for the dinitrogen units, which is clearly observed in the FTIR spectra.

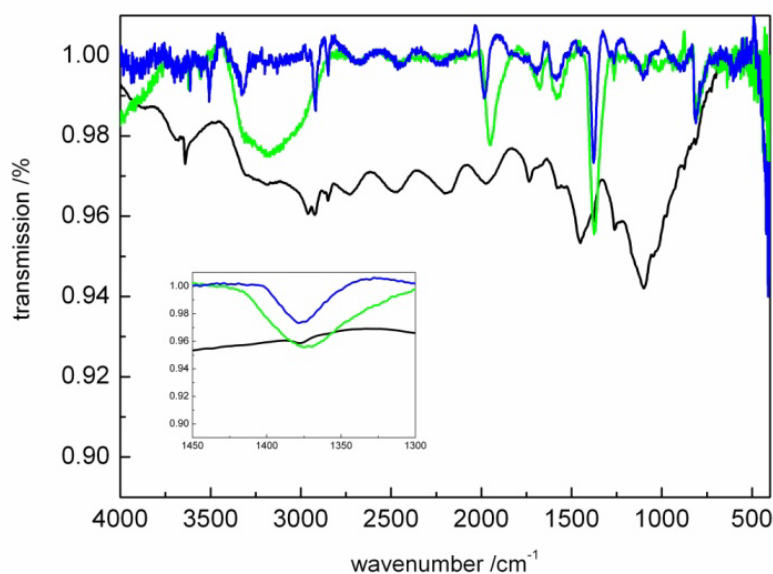


Figure 5. FTIR spectra of CaN_2 (black), SrN_2 (blue) and BaN_2 (green). The region of the $[\text{N}_2]^{2-}$ feature is enlarged (bottom left).

However, there are still a number of unidentified features, which might be caused by additional (translational, acoustic, librational) modes of the diazenide unit due to lattice distortions. On the other hand, due to the extremely high sensitivity to moisture, these compounds tend to hydrolyze very easily. As the KBr-sample pellet is exposed to normal atmosphere upon transfer from the glovebox to the sample chamber of the spectrometer, diverse intermediates could be formed resulting in a variety of possible IR vibrations due to diverse functional groups. Our attempts to record Raman spectra failed. This may be caused by reflection or absorption of the laser by the intensely black alkaline earth diazenides.

Temperature-Dependent in situ X-Ray Diffractometry

The temperature-dependent *in situ* X-ray diffraction patterns for CaN_2 and BaN_2 are depicted in Figure 6. The temperature-dependent powder diffraction patterns of SrN_2 are given in the Supporting Information, Figure S1. It is clearly seen that each alkaline earth diazenide transforms into the subnitride $M_{\text{AE}2}\text{N}$ upon heating. For CaN_2 , the temperature of transformation is about 100 K lower (at approx. 500 K) than for SrN_2 and BaN_2 (both at approx. 600 K). These measurements are in good agreement with the reported value for SrN_2 of 618 K upon heating SrN_2 in vacuum.^[10,14]

It is noteworthy that all three alkaline earth diazenides react analogously forming the respective subnitrides $M_{\text{AE}2}\text{N}$ upon heating. In the case of strontium and barium diazenide this

behavior seems reasonable as the stoichiometric nitrides $M_{\text{AE}3}\text{N}_2$ do not seem to exist.^[48] In contrast, Ca_3N_2 is a stable phase. However it is not formed during thermal decomposition of CaN_2 .

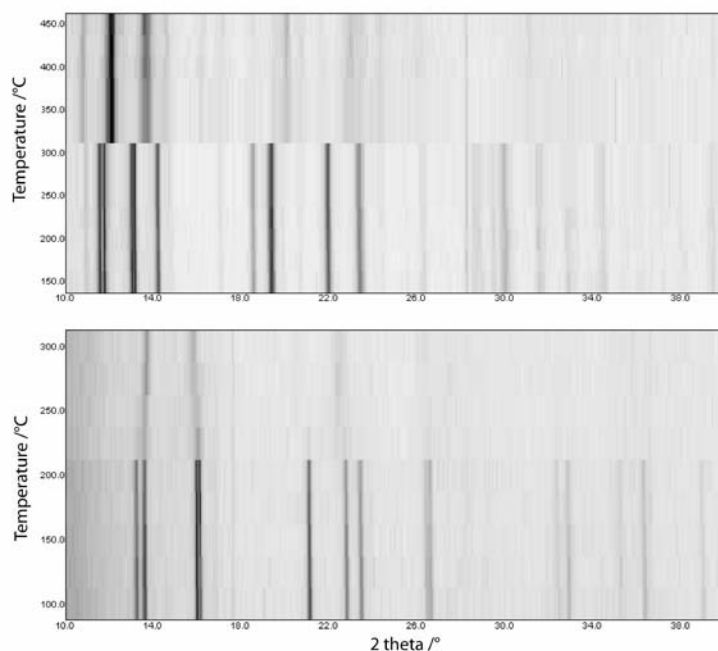


Figure 6. Temperature-dependent *in situ* powder diffraction patterns of CaN_2 (bottom) and BaN_2 (top).

Electronic Structure

To better understand the electronic structure of the alkaline earth diazenides and their bonding situation, first principles calculations on the electronic structure were performed. As the band structure, density of states (DOS) and crystal orbital Hamiltonian population (COHP) of BaN_2 have already been calculated,^[11,24] we here report on the electronic structure of CaN_2 and SrN_2 . In Figure 7 the band structures of both diazenides are depicted. As expected, the electronic structure calculations suggest that the compound should be metallic, which is in good agreement with the observed black metallic color of the samples. In both cases, the main contributions of bands at the Fermi level comes from the $M_{\text{AE}}-d$ (Ca: $3d$, Sr: $4d$) and the N- p ($2p$) states. The contribution of the $M_{\text{AE}}-p$ states (Ca: $4p$, Sr: $5p$) is negligible.

To illustrate the bonding situation, Figure 8 displays a scheme of the molecular-orbital diagram of N_2 and $[\text{N}_2]^{2-}$. Upon forming N_2 by linear combination of the atomic orbitals of elemental nitrogen, the molecular orbitals $1\sigma_g$, $1\sigma_u^*$, $2\sigma_g$, $1\pi_u$, $1\pi_g^*$ and $2\sigma_u^*$ are formed. The bonding orbitals $2\sigma_g$ and $1\pi_u$ are filled up with six electrons resulting in a maximum of bonding multiplicity of three (triple bond). Adding further two electrons into the $1\pi_g^*$

molecular orbital (red vertical lines in Figure 8), results on the one hand in $[\text{N}_2]^{2-}$ and on the other hand in a reduced bonding multiplicity of two which corresponds to the double-bonded nitrogen-dimer. Notice that only 50 % of the antibonding molecular orbital $1\pi_g^*$ are occupied. The $[\text{N}_2]^{2-}$ ion is isosteric to molecular oxygen and $[\text{C}_2]^{4-}$ and therefore should exhibit paramagnetic behavior. However, magnetic susceptibility measurements and electronic structure calculations for BaN_2 revealed that the compound exhibits Pauli paramagnetism and should be metallic, despite the paramagnetic triplet state of the isolated diazenide ion.^[11] Thus, a test spin-polarized calculation with nonzero magnetic moments artificially placed on the nitrogen atoms was conducted for CaN_2 and SrN_2 and converged back to the metallic state. This implies that CaN_2 and SrN_2 should be metallic as well. Further addition of two electrons into the molecular-orbital scheme then results in $[\text{N}_2]^{4-}$ and another reduction in bonding multiplicity by one (single bond).

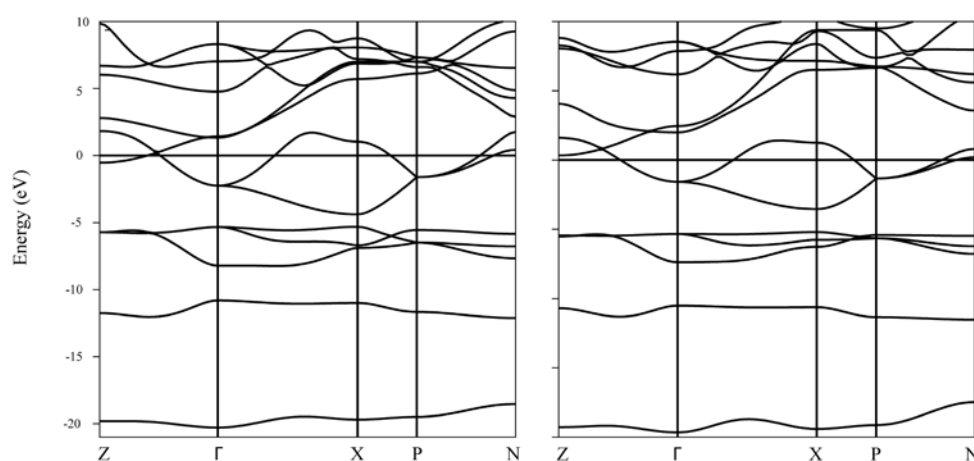


Figure 7. TB-LMTO band structures for CaN_2 (left) and SrN_2 (right).

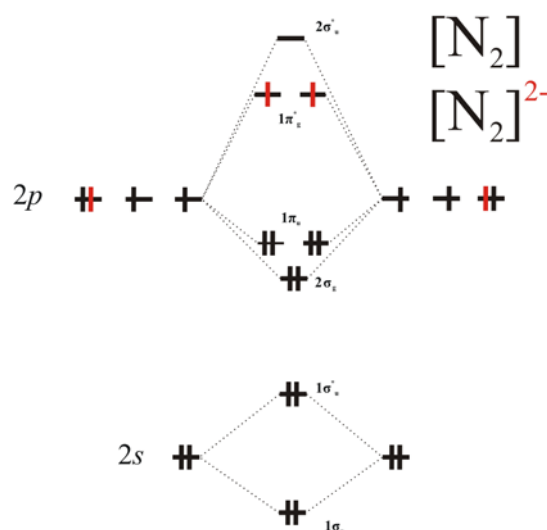


Figure 8. Molecular-orbital scheme of the dinitrogen molecule illustrating the electron filling for N_2 and $[\text{N}_2]^{2-}$.

To elucidate the bonding situation in CaN_2 and SrN_2 , the DOS and COHP ($M_{\text{AE-N}}$ and N-N) were calculated and are depicted in Figure 9 (CaN_2) and Figure S2, Supporting Information (SrN_2). In the COHP plots, the bonding states are given as features to the right, whereas antibonding states show up as features to the left. Since they share the same space groups and crystal structures, the situation for both alkaline earth diazenides is basically the same.

The bonding states at about -20 eV are mainly based on the $1\sigma_s$ orbitals of the dumbbell. At about -12 eV the dinitrogen $1\sigma_u^*$ states can be found mixing with $M_{\text{AE-s}}$, $-p$ and $-d$ states (Ca: $4s$, $4p$, $3d$; Sr: $5s$, $5p$, $4d$). Above that, around -8 to -5 eV the $2\sigma_g$ and the $1\pi_u$ states of the dinitrogen unit show up as bonding states together with an increased contribution of the $M_{\text{AE-d}}$ states and a decreased one of the $M_{\text{AE-p}}$ and $-s$ states. The antibonding bands in the proximity of the Fermi level ranging from -4 to 2 eV are found to be basically built up by the $1\pi_g^*$ states of the dinitrogen unit, which are slightly mixed with the $M_{\text{AE-s}}$ and $-d$ states. These metal-nitrogen interactions are found to be responsible for the significant widths of the corresponding bands in the band structure, and thus probably being also responsible for the metallic character of these compounds. The bands above 2 eV are predominantly formed by $M_{\text{AE-d}}$ states. For the $M_{\text{AE-N}}$ combination (Figure 9, middle; Figure S2, middle), there are basically only bonding states up to E_F . Above the Fermi level (in the region of the unoccupied states), the antibonding $M_{\text{AE-N}}$ interactions are observed. The COHP plots of the N-N combination (Figure 9, right; Figure S2, right) in the range of -4 to 2 eV are clearly dominated by antibonding states where the Fermi level crosses these states at about half of their antibonding character. This perfectly matches with the expected 50 % occupation of the antibonding π -states of the diazenide ion $[\text{N}_2]^{2-}$.

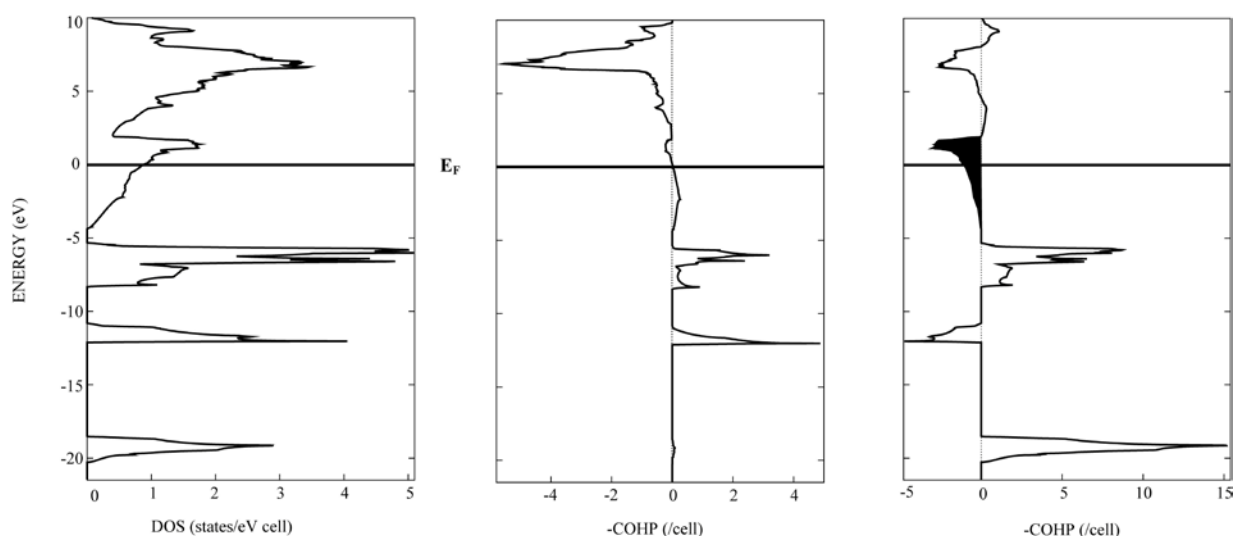


Figure 9. Total DOS (left), COHP analysis of Ca-N (middle) and N-N (right) for CaN_2 .

2.1.4 CONCLUSIONS

By controlled decomposition of the alkaline earth azides of calcium, strontium and barium, the corresponding diazenides $M_{\text{AE}}\text{N}_2$ ($M_{\text{AE}} = \text{Ca, Sr, Ba}$) were synthesized in accord with the pressure-homologue rule (isotypic structures with the heavier homologues can be synthesized by lower pressure; lighter homologues: higher pressure). FTIR spectroscopy of these diazenides resulted in a band at about 1380 cm^{-1} assigned to the N–N stretching vibration of the diazenide ion. Temperature-dependent *in situ* X-ray diffraction revealed that CaN_2 , SrN_2 and BaN_2 transformed into the corresponding subnitrides $M_{\text{AE}2}\text{N}$ at higher temperatures. To better understand the bonding situation in the diazenides, electronic structure calculations were performed for CaN_2 and SrN_2 . As expected, the diazenides show metallic behavior (DOS). In addition, COHP calculations revealed a 50 % occupation of the antibonding π -states of the diazenide ion and therefore support the formulation of a double-bonded, twofold negatively charged $[\text{N}_2]^{2-}$ ion.

2.1.5 BIBLIOGRAPHY

Acknowledgement

We gratefully acknowledge financial support by the Fonds der Chemischen Industrie FCI and the Deutsche Forschungsgemeinschaft DFG (project SCHN377/13-2). The authors thank Prof. Dirk Johrendt for valuable discussion.

References

- [1] G. Matoba, Patent JP-B 50010804, **1975**; G. Matoba, Patent JP-B 50010803, **1975**; H. Kobayashi, Patent JP-A 03006314, **1991**; T. Chokei, Patent JP 55094432, **1980**; H. Willners, Patent SE 115621, **1946**.
- [2] S.H. Jhi, J. Ihm, S.G. Louie, M.L. Cohen, *Nature* **1999**, 399, 132.
- [3] P.F. McMillan, *Nat. Mater* **2002**, 1, 19.
- [4] T. Maruyama, T. Morishita, *Appl. Phys. Lett.* **1996**, 69, 890.
- [5] S. Yamanaka, K. Hotehama, H. Kawaji, *Nature* **1998**, 392, 580.
- [6] A. Zerr, G. Miehe, R. Boehler, *Nat. Mater.* **2003**, 2, 185.

- [7] M. Chhowalla, H.E. Unalan, *Nat. Mater.* **2005**, *4*, 317.
- [8] A. Leineweber, H. Jacobs, S. Hull, *Inorg. Chem.* **2001**, *40*, 5818.
- [9] Z.G. Wu, X.J. Chen, V.V. Struzhkin, R.E. Cohen, *Phys. Rev. B* **2005**, *71*, 214103.
- [10] G. Auffermann, Y. Prots, R. Kniep, *Angew. Chem.* **2001**, *113*, 565; *Angew. Chem., Int. Ed.* **2001**, *40*, 547.
- [11] G.V. Vajenine, G. Auffermann, Y. Prots, W. Schnelle, R.K. Kremer, A. Simon, R. Kniep, *Inorg. Chem.* **2001**, *40*, 4866.
- [12] G. Auffermann, U. Schmidt, B. Bayer, Y. Prots, R. Kniep, *Anal. Bioanal. Chem.* **2002**, *373*, 880.
- [13] G. Auffermann, R. Kniep, W. Bronger, *Z. Anorg. Allg. Chem.* **2006**, *632*, 565.
- [14] Y. Prots, G. Auffermann, M. Tovar, R. Kniep, *Angew. Chem.* **2002**, *114*, 2392; *Angew. Chem., Int. Ed.* **2002**, *41*, 2288.
- [15] E. Gregoryanz, C. Sanloup, M. Somayazulu, J. Badro, G. Fiquet, H.-K. Mao, R.J. Hemely, *Nat. Mater.* **2004**, *3*, 294.
- [16] J. von Appen, M.-W. Lumey, R. Dronskowski, *Angew. Chem.* **2006**, *118*, 4472; *Angew. Chem., Int. Ed.* **2006**, *45*, 4365.
- [17] J.C. Crowhurst, A.F. Goncharov, B. Sadigh, C.L. Evans, P.G. Morrall, J.L. Ferreira, A.J. Nelson, *Science* **2006**, *311*, 1275.
- [18] A.F. Young, J.A. Montoya, C. Sanloup, M. Lazzeri, E. Gregoryanz, S. Scandolo, *Phys. Rev. B* **2006**, *73*, 153102.
- [19] J.A. Montoya, A.D. Hernandez, C. Sanloup, E. Gregoryanz, S. Scandolo, *Appl. Phys. Lett.* **2007**, *90*, 011909.
- [20] J.C. Crowhurst, A.F. Goncharov, B. Sadigh, J.M. Zaug, D. Aberg, Y. Meng, V.B. Prakapenka, *J. Mater. Res.* **2008**, *23*, 1.
- [21] Z.W. Chen, X.J. Guo, Z.Y. Liu, M.Z. Ma, Q. Jing, G. Li, X.Y. Zhang, L.X. Li, Q. Wang, Y.J. Tian, R.P. Liu, *Phys. Rev. B* **2007**, *75*, 054103.

- [22] R. Yu, Q. Zhan, L.C. De Jonghe, *Angew. Chem.* **2007**, *119*, 1154; *Angew. Chem., Int. Ed.* **2007**, *46*, 1136.
- [23] W. Chen, J.S. Tse, J.Z. Jiang, *J. Phys.: Condens. Matter* **2010**, *22*, 015404.
- [24] M. Wessel, R. Dronskowski, *J. Am. Chem. Soc.* **2010**, *132*, 2421.
- [25] M. Wessel, R. Dronskowski, *Chem. Eur. J.* **2011**, *17*, 2598.
- [26] M. Wessel, *PhD thesis*, RWTH Aachen University: Aachen, **2010**.
- [27] X.P. Du, Y.X. Wang, V.C. Lo, *Physics Letters A* **2010**, *374*, 2569.
- [28] H. Wang, Q. Li, Y. Li, Y. Xu, T. Cui, A.R. Oganov, Y. Mal, *Phys. Rev. B* **2009**, *79*, 132109.
- [29] M. Wessel, R. Dronskowski, *J. Comput. Chem.* **2010**, *31*, 1613.
- [30] W.J. Frierson, *Inorg. Synth.* 1946, *8*, 136.
- [31] H.D. Fair, R.F. Walker, *Energetic Materials Vol. 1: Physics and Chemistry of the Inorganic Azides*; Plenum Press: New York **1977**.
- [32] P. Ehrlich, H.J. Seifert, G. Brauer, *Handbuch der Präparativen Anorganischen Chemie Vol. 2*; Ferdinand Enke Verlag: Stuttgart, **1978**.
- [33] P. Remy-Gennete, *Ann. Chim.* **1933**, *19*, 289.
- [34] D. Walker, M.A. Carpenter, C.M. Hitch, *Am. Mineral.* **1990**, *75*, 1020.
- [35] D. Walker, *Am. Mineral.* **1991**, *76*, 1092.
- [36] H. Huppertz, *Z. Kristallogr.* **2004**, *219*, 330.
- [37] D.C. Rubie, *Phase Transitions* **1999**, *68*, 431.
- [38] N. Kawai, S. Endo, *Rev. Sci. Instrum.* **1970**, *8*, 1178.
- [39] A.A. Coelho, *TOPAS-Academic Version 4.1*; Coelho Software: Brisbane, **2007**.
- [40] J. Bergmann, R. Kleeberg, A. Haase, B. Breidenstein, *Mater. Sci. Forum* **2000**, *303*, 347.

- [41] O.K. Andersen, O. Jepsen, *Tight-Binding LMTO Vers. 4.7*, Max-Planck-Institut für Festkörperforschung: Stuttgart, **1994**.
- [42] R. Dronskowski, P. Blöchl, *J. Phys. Chem.* **1993**, *97*, 8617.
- [43] O. Jepsen, M. Snob, O.K. Andersen, *Linearized Band Structure Methods and its Applications*, Springer Lecture Notes, Springer-Verlag: Berlin, **1987**.
- [44] H.L. Skriver, *The LMTO Method*, Springer-Verlag: Berlin, **1984**.
- [45] W.R.L. Lambrecht, O.K. Andersen, *Phys. Rev. B* **1986**, *34*, 2439.
- [46] G. Auffermann, Y. Prots, R. Kniep, S.F. Parker, S.M. Bennington, *ChemPhysChem* **2002**, *9*, 815.
- [47] J. Weidlein, U. Müller, K. Dehnicke, *Schwingungsspektroskopie—Eine Einführung*; Georg Thieme Verlag Stuttgart: New York, **1982**.
- [48] S.R. Römer, T. Dörfler, P. Kroll, W. Schnick, *Phys. Status Solidi B* **2009**, *246*, 1604.

2.2 FURTHER ALKALINE EARTH DIAZENIDES

As the HP/HT-synthesis of alkaline earth diazenides $M_{\text{AE}}\text{N}_2$ ($M_{\text{AE}} = \text{Ca–Ba}$) by a controlled thermal decomposition of the corresponding ionic azides has proven to be successful, it was also targeted to synthesize the lighter homologue MgN_2 . Due to the toxicity of beryllium compounds, the synthesis of BeN_2 was not intended. Taking theoretical calculations into account, the synthesis of MgN_2 (in all hypothetical ground-state structures) is exothermic with respect to the elements and thus should be accessible in synthetic chemistry.^[1] According to our HP/HT-route, binary $\text{Mg}(\text{N}_3)_2$ is required. However, despite numerous efforts binary $\text{Mg}(\text{N}_3)_2$ could not have been synthesized up to date owing to the high acidity of Mg^{2+} ions which tend to form adducts with solvents like ethers or amines as observed upon recent synthesis in liquid ammonia.^[2–6] To avoid any oxygen-content of potential precursors for the HP/HT-synthesis of MgN_2 , we targeted the synthesis of amine-containing precursors in liquid ammonia according to the literature, namely $\text{Mg}(\text{NH}_3)_2(\text{N}_3)_2$ and ammonia reduced $\text{Mg}(\text{N}_3)_{2-x}\text{NH}_3$ ($x \sim 0.7$), the latter one referred to *arMg*(NH_3)₂(N_3)₂.^[5,6]

2.2.1 EXPERIMENTAL SECTION

*Synthesis of $\text{Mg}(\text{NH}_3)_2(\text{N}_3)_2$ and *arMg*(NH_3)₂(N_3)₂*

Diammin magnesium diazide $\text{Mg}(\text{NH}_3)_2(\text{N}_3)_2$ was synthesized from Mg_3N_2 (70.8 mg, 0.70 mmol) and NH_4N_3 (252.8 mg, 4.21 mmol) in 100 ml liquid ammonia at 223 K. Magnesium nitride was previously synthesized from the elements,^[7] whereas NH_4N_3 is synthesized by metathesis reaction of NH_4NO_3 and NaN_3 according to the literature.^[3] After stirring the suspension for 3 days, the finally transparent solution was evaporated and a colorless, moderate crystalline $\text{Mg}(\text{NH}_3)_2(\text{N}_3)_2$ is obtained, which was subsequently analyzed by powder X-ray diffraction and infrared spectroscopy (see Figure 1). For the synthesis of amorphous *arMg*(NH_3)₂(N_3)₂, previously synthesized $\text{Mg}(\text{NH}_3)_2(\text{N}_3)_2$ (100 mg) is further evaporated at 453 K to a minimum pressure of $2 \cdot 10^{-6}$ mbar. Thereby, starting evacuation temperature is set to 363 K and slowly increased over a period of one week that pressure does not exceed $6 \cdot 10^{-6}$ mbar. Once the minimum pressure of $2 \cdot 10^{-6}$ mbar is reached, no additional release of NH_3 is observed and amorphous *arMg*(NH_3)₂(N_3)₂ obtained. *arMg*(NH_3)₂(N_3)₂ is analyzed by means of infrared spectroscopy exhibiting clearly reduced $\delta_{\text{as}}(\text{NHN})$ - and $\delta_{\text{s}}(\text{NHN})$ -features at 1610 and 1190 cm^{-1} , respectively (see Figure 1).

Caution! $\text{Mg}(\text{NH}_3)_2(\text{N}_3)_2$ and $ar\text{Mg}(\text{NH}_3)_2(\text{N}_3)_2$ powders can detonate above 453 K!

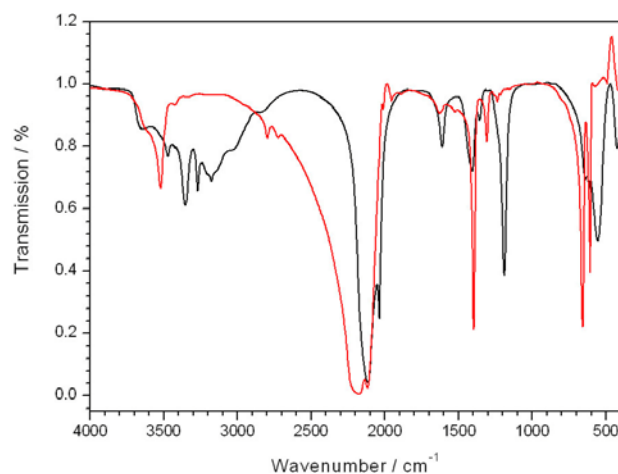


Figure 1. Infrared spectra of $\text{Mg}(\text{NH}_3)_2(\text{N}_3)_2$ (black) and $ar\text{Mg}(\text{NH}_3)_2(\text{N}_3)_2$ (red). Thereby, $ar\text{Mg}(\text{NH}_3)_2(\text{N}_3)_2$ exhibits clearly reduced $\delta_{as}(\text{NHN})$ - and $\delta_s(\text{NHN})$ -features at 1610 and 1190 cm^{-1} compared to $\text{Mg}(\text{NH}_3)_2(\text{N}_3)_2$ indicative for the loss of ammonia. The features at about 2000 and 3500 cm^{-1} are attributed to the stretching vibrations of the azide units in accordance with the literature.^[5,6]

High-Pressure/high-temperature Experiments

For the HP/HT-treatment of as-obtained magnesium azides a modified Walker-type module in combination with a 1000 t press (Voggenreiter, Mainleus, Germany) was used. As pressure medium, precastable MgO-octahedra (Cermaic Substrates & Components, Isle of Wight, U.K.) with edge lengths of 10, 14, 18 or 25 mm (10/5, 14/8, 18/11 or 25/17 assembly) were employed depending on the maximum synthesis pressure. Eight tungsten carbide cubes (Hawedia, Marklkofen, Germany) with truncation edge lengths of 5, 8, 11 or 17 mm compressed the octahedra. The magnesium azides were carefully ground, filled into a cylindrical boron nitride crucible (Henze BNP GmbH, Kempten, Germany) and sealed with a fitting boron nitride plate. A detailed description of the setup can be found in the literature.^[8-12] Compressing and decompression rates were set according to the synthesis pressure. The recovered MgO-octahedra were broken apart in a glovebox (Unilab, MBraun, Garching; $\text{O}_2 < 1 \text{ ppm}$, $\text{H}_2\text{O} < 1 \text{ ppm}$) and the samples carefully isolated from the surrounding boron nitride crucible. All products were analyzed by means of powder X-ray diffraction.

2.2.2 RESULTS, DISCUSSION AND CONCLUSION

In a total number of 33 attempts under various HP/HT-conditions (see Figure 2), no formation of MgN_2 was observed, but of Mg_3N_2 .^[13] This is probably due to the presence of residual

ammonia in both precursors, which upon HT-conditions is released and acts as strong reducing agent for the azide ions to produce nitride N^{3-} ions impeding the stabilization of the intermediate oxidation state of $-I$ in diazenide $[\text{N}_2]^{2-}$ ions. It has to be noted that once ammonia has reduced azides to nitrides, itself is oxidized to nitrogen and hydrogen gas, whereby the latter acts again as strong reducing agent.

Taking these observations into account, novel diazenides by the HP/HT-route are so far only accessible if the corresponding precursors constitute binary, phase-pure azides.

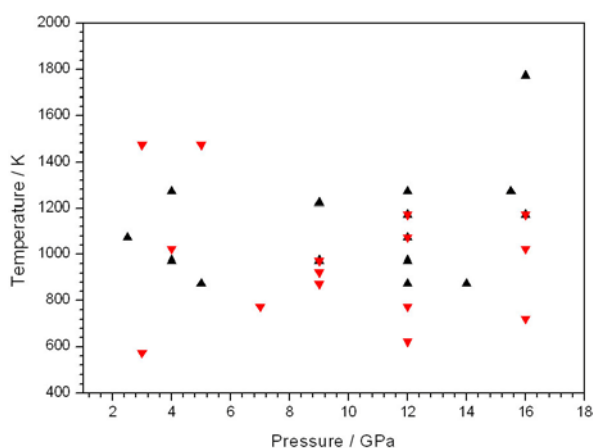


Figure 2. HP/HT-conditions for the synthesis of MgN_2 starting from $\text{Mg}(\text{NH}_3)_2(\text{N}_3)_2$ (black) or $\text{arMg}(\text{NH}_3)_2(\text{N}_3)_2$ (red). In a total number of 33 experiments, no diazenide containing compound was observed. Some experiments have been conducted twice at the same temperature and pressure, but with different heating, holding and cooling rates. A detailed description of the HT/HP-experiments can be found in chapter 2.1.

2.2.3 BIBLIOGRAPHY

- [1] M. Wessel, R. Dronskowski, *J. Comput. Chem.* **2010**, *31*, 1613.
- [2] H.D. Fair, R.F. Walker, *Energetic Materials Vol. 1: Physics and Chemistry of the Inorganic Azides*; Plenum Press: New York **1977**.
- [3] W.J. Frierson, *Inorg. Synth.* **1946**, *8*, 136.
- [4] L.M. Dennis, C.H. Benedict, A.C. Gill, *J. Am. Chem. Soc.* **1898**, *20*, 225.
- [5] F.W. Karau, W. Schnick, *Z. Anorg. Allg. Chem.* **2006**, *632*, 49.
- [6] F. W. Karau, *PhD thesis*; Ludwig-Maximilian-University: Munich, **2007**.
- [7] H. Jacobs, R. Juza, *Z. Anorg. Allg. Chem.* **1969**, *370*, 254.
- [8] D. Walker, M.A. Carpenter, C.M. Hitch, *Am. Mineral.* **1990**, *75*, 1020.
- [9] D. Walker, *Am. Mineral.* **1991**, *76*, 1092.

- [10] H. Huppertz, *Z. Kristallogr.* **2004**, 219, 330.
- [11] D. C. Rubie, *Phase Transitions* **1999**, 68, 431.
- [12] N. Kawai, S. Endo, *Rev. Sci. Instrum.* **1970**, 8, 1178.
- [13] T. Holzmann, *Research internship*; Ludwig-Maximilian-University: Munich, **2011**.

3. BINARY ALKALI DIAZENIDES

As the synthesis of novel alkaline earth diazenides by controlled thermal decomposition of the corresponding ionic azides in a multianvil device under HP/HT-conditions turned out to be the method of choice, it was decided to investigate the thermal decomposition of alkali azides at extreme conditions. Despite the fact that initial attempts in the synthesis of the heavier alkali diazenides with $M = \text{Na} - \text{Cs}$ were truly disappointing, the HP/HT-synthesis of the first alkali diazenide of the lightest alkali metal, namely Li_2N_2 , was even more pleasant but surprising at the same time as described in the following chapter.

3.1. HIGH-PRESSURE SYNTHESIS AND CHARACTERIZATION OF THE ALKALI DIAZENIDE Li_2N_2

Sebastian B. Schneider, Rainer Frankovsky and Wolfgang Schnick

published in *Angew. Chem.* **2012**, *124*, 1909

Angew. Chem., Int. Ed. **2012**, *51*, 1873

DOI: 10.1002/ange.201108252 and 10.1002/anie.201108252

Copyright © 2012, WILEY-VCH Verlag GmbH & Co. KGaA, Weinheim

<http://onlinelibrary.wiley.com/doi/10.1002/ange.201108252/abstract>

<http://onlinelibrary.wiley.com/doi/10.1002/anie.201108252/abstract>

ABSTRACT

Überraschung beim Diazenid: Beim ersten bekannten Alkalimetalldiazenid, Li_2N_2 , wurde ein für Verbindungen der Zusammensetzung A_2B_2 neuartiger Strukturtyp gefunden. Spektroskopische Untersuchungen zeigen bei 1328 cm^{-1} eine signifikante Schwingung, die der Diazenideinheit zugeordnet wird. Die Berechnung der elektronischen Struktur unterstreicht den metallischen Charakter und bestätigt die Besetzung der antibindenden π -Zustände in $[\text{N}_2]^{2-}$ zu 50 %.

Diazenide surprise: Synthesis of the first alkali diazenide, namely Li_2N_2 is presented. Lithium diazenide adopts an unprecedented structure type for compounds with A_2B_2 composition. Spectroscopic analysis shows a significant feature at 1326.8 cm^{-1} which is assigned to the stretching vibration of the $[\text{N}_2]^{2-}$ ion. In addition, electronic structure calculations underline the metallic character and confirm the 50 % occupation of the antibonding π -states in $[\text{N}_2]^{2-}$.

3.1.1 INTRODUCTION WITH RESULTS AND DISCUSSION

In comparison with the versatile chemistry of oxides and their extraordinary impact on mineralogy, materials science, and fundamental research, the chemistry of nitrides appears less varied and their syntheses are usually more elaborate. This observation may be a direct consequence of the high partial pressure of oxygen and the omnipresence of water on our planet. Furthermore, most solid oxides are more stable than nitrides, because chemical bonds to nitrogen are typically weaker than bonds to oxygen^[1-3] And additionally, the electron affinity of nitrogen is significantly lower than that of oxygen, rendering N^{3-} much more endothermic than O^{2-} ; both anions require stabilization by counterions in the solid state.^[2] Accordingly, a broad systematic investigation of nitrides had not been pursued before the last decades.^[4-7]

A similar trend is observed in the variability of homonuclear molecules and ions of oxygen and nitrogen. Besides the allotropes O_2 and O_3 , there are peroxides $[\text{O}_2]^{2-}$, hyperoxides $[\text{O}_2]^-$, ozonides $[\text{O}_3]^-$, and the dioxygenyl cation $[\text{O}_2]^+$.^[2,8-11] In contrast, only the nitrogen allotrope N_2 , nitrides N^{3-} , and azides $[\text{N}_3]^-$ have been long known.^[12] It was not until 2001 that *Kniep* et al. proved the existence of the homonuclear dinitrogen anion $[\text{N}_2]^{2-}$, which is a deprotonated diazene N_2H_2 with a $\text{N}=\text{N}$ bond.^[13-17] These anions were accordingly named diazenides. Unexpectedly, no other binary diazenides except SrN_2 and BaN_2 have been synthesized thus far. Lately, however, the existence of the paramagnetic dinitrogen anions $[\text{N}_2]^-$ and $[\text{N}_2]^{3-}$, as well as compounds containing the pernitride ion $[\text{N}_2]^{4-}$, have been reported.^[18-36]

We have been able to extend the range of diazenide composition through a novel synthetic approach employing controlled thermal decomposition of ionic azides in a multianvil device under high-pressure/high-temperature (HP/HT) conditions.^[37] We thereby obtained calcium diazenide CaN_2 , which is isotypic with SrN_2 and alkaline earth acetylenides crystallizing in a tetragonally distorted NaCl-type structure. To further extend the compositional range of simple metal diazenides, we turned to the investigation of the thermal decomposition of alkali azides under extreme conditions. With respect to the observation that peroxides $M_2\text{O}_2$ and hyperoxides MO_2 are more stable with the heavier alkali metals ($M = \text{K}, \text{Rb}, \text{and Cs}$),^[8-10] we initially targeted synthesis of diazenides in combination with these elements. Surprisingly, we were ultimately successful with the synthesis of a diazenide of the lightest alkali metal, Li_2N_2 .

Lithium diazenide was obtained under HP/HT-conditions (9 GPa, 750 K) in a Walker-type multianvil assembly by decomposition of LiN_3 . It is a black powder with a metallic luster and is extremely sensitive to hydrolysis.

The crystal structure of Li_2N_2 (Table 1) was determined on the basis of powder X-ray diffraction data (Figure 1).^[38]

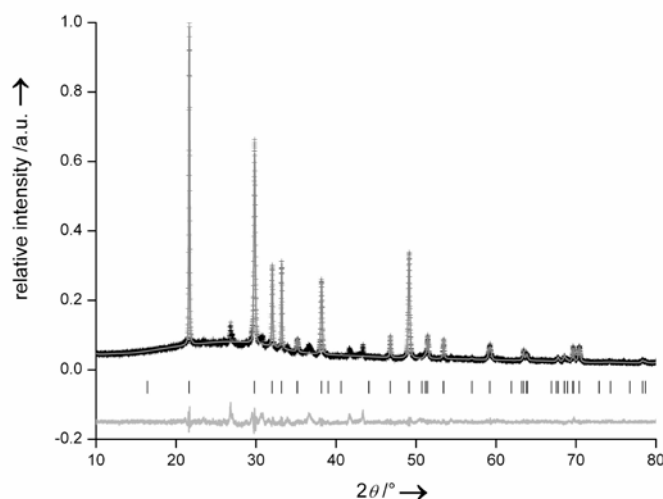


Figure 1. Observed (crosses) and calculated (gray line) powder diffraction pattern ($\text{Cu } K_{\alpha 1}$ radiation (1.54056 Å)) as well as difference profile of the Rietveld refinement of Li_2N_2 ; peak positions are marked by vertical lines.^[39]

Extraction of the peak positions, pattern indexing, structure solution, Fourier calculations, and Rietveld refinements were carried out with the TOPAS software package.^[40] The reflections of the powder pattern were indexed in the orthorhombic crystal system and the space group $Immm$ was derived.

Li_2N_2 , the first alkali metal diazenide, represents an

Table 1. Refined Atomic Coordinates and Isotropic Displacement Factors in 0.01 \AA^2 of Li_2N_2 .^a

Atoms	(Wyckoff)	x	y	z	U_{iso}^b
Li1	2a	0	0	0	0.047(13)
Li2	2c	½	½	0	0.057(14)
Li3	4i	½	½	0.2510(6)	0.022(11)
N1	8l	½	0.1466(5)	0.62321(19)	0.0079(15)

^aspace group $Immm$ (no. 71), $a = 3.1181(4)$, $b = 4.4372(4)$, $c = 10.7912(16)$ Å, $Z = 4$; ^b $U_{iso} = B_{eq}/(8 \cdot \pi^2)$.

unprecedented structure type. The diazenide units are oriented along [010] (Figure 2) and have a bond length $d_{\text{NN}} = 1.301(3)$ Å, which is between a single- and triple-bonded dinitrogen unit. In contrast to diazene itself and the alkaline earth diazenides CaN_2 , SrN_2 , and BaN_2 , which have N–N distances in the range of 1.20–1.24 Å,^[13–17,20,37] the observed bond length in

Li_2N_2 is slightly longer. This might be a direct consequence of the metallic character of this compound, as is also predicted for LaN_2 and FeN_2 .^[33,34]

The $[\text{N}_2]^{2-}$ ions are coordinated in a rhombic prism made up of eight Li atoms. Furthermore, each Li site is coordinated by the diazenide units in a different way: Li1 is coordinated in a square planar shape by four *end-on* diazenide units. Li2 is coordinated by four $[\text{N}_2]^{2-}$ ions in a *side-on* manner, resulting in an eightfold coordination, while Li3 is coordinated by two *side-on* and two *end-on* diazenides, resulting in a coordination number of six. The overall Li–Li and Li–N distances match with reported values.^[41,42] According to *Shannon*^[43], to compare the obtained Li–N distances with the sum of the ionic radii, the radius of the diazenide ion has to be evaluated first, as the ionic radii of Li^+ depends on its coordination. Starting from the structural data of the alkaline earth diazenides CaN_2 , SrN_2 , and BaN_2 ^[37] we estimated the average radius of one nitrogen atom in the diazenide ion to be 1.27 Å. Based on this empirical value, the Li–N distances obtained correspond well with the sum of the ionic radii: $r(\text{Li}^+_{\text{CN}(4)})=0.59$, $r(\text{Li}^+_{\text{CN}(6)})=0.76$, and $r(\text{Li}^+_{\text{CN}(8)})=0.92$ Å.

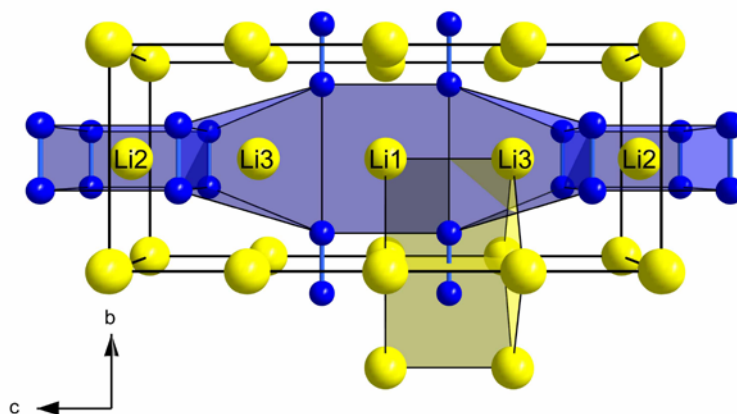


Figure 2. Unit cell of Li_2N_2 , view along $[100]$. Polyhedra around Li atoms marked in blue, around diazenide unit marked in yellow; Li yellow, nitrogen blue.

Recently, *Zhang et al.* attempted to predict the ground-state structure of Li_2N_2 , but the reported data do not match with our experimental results.^[44]

Infrared spectroscopy revealed a significant feature at 1326.8 cm^{-1} , which was assigned to the N–N stretching vibration of the diazenide ion, in accordance with previous vibrational spectroscopic measurements on CaN_2 , SrN (a nitride-diazenide), SrN_2 , and BaN_2 .^[37,45]

To better understand the electronic character of Li_2N_2 and its bonding situation, first-principles calculations on the electronic structure were performed using the LMTO

method.^[46] As expected, the electronic band structure calculations suggest that the compound is metallic, which is in good agreement with the black color of the sample. The crystal orbital Hamilton population (COHP) plot of the N–N combination clearly shows the expected situation for the $[\text{N}_2]^{2-}$ ion: it is not surprising that, on the one hand, the states near the Fermi level are antibonding and that, on the other hand, the Fermi level crosses these states at about half of their antibonding character. These observations match well with the 50 % occupation of the antibonding π states in the isolated diazenide ion.

In summary, the structural, spectroscopic, and electronic characterization of Li_2N_2 confirm it to be the first alkali diazenide and show that it crystallizes in an unprecedented structure type. Furthermore, the experimental approach that is used to generate this class of diazenides is very promising for the synthesis of even more binary compounds in the alkali–nitrogen system.

3.1.2 BIBLIOGRAPHY

Acknowledgements

We thank Thomas Miller (temperature-dependent *in situ* powder diffractometry) and Franziska Hummel (low-temperature powder diffractometry). The authors gratefully acknowledge financial support from the Fonds der Chemischen Industrie (FCI) and the Deutsche Forschungsgemeinschaft (DFG), project SCHN 377/13-2.

References

- [1] W. Schnick, *Angew. Chem.* **1993**, *105*, 846; *Angew. Chem., Int. Ed. Engl.* **1993**, *32*, 806.
- [2] A.F. Holleman, E. Wiberg, *Lehrbuch der Anorganischen Chemie*, Vol. 102, de Gruyter: Berlin-New York, **2007**.
- [3] G.H. Aylward, T.J. Findlay, *Datensammlung Chemie*, Verlag Chemie, Weinheim: **1975**.
- [4] R. Niewa, F.J. DiSalvo, *Chem. Mater.* **1998**, *10*, 2733.
- [5] D.H. Gregory, *J. Chem. Soc. Dalton Trans.* **1999**, 259.

- [6] D.H. Gregory, *Coord. Chem. Rev.* 2001, **215**, 301.
- [7] M. Zeuner, S. Pagano, W. Schnick, *Angew. Chem.* **2011**, *123*, 7898; *Angew. Chem., Int. Ed.* **2011**, *50*, 7754.
- [8] N.G. Vannerberg, *Prog. Inorg. Chem.* **1962**, *4*, 125.
- [9] I.I. Vol'nov, *Peroxides, Superoxides and Ozonides of Alkali and Alkaline Earth Metals*, Vol. II, Plenum Press: New York, **1966**.
- [10] W. Hesse, M. Jansen, W. Schnick, *Prog. Solid State Chem.* **1989**, *19*, 47.
- [11] D.H. Lohmann, N. Bartlett, *Proc. Chem. Soc.* **1962**, *115*, 5253.
- [12] Recently, the pentazenium cation $[N_5]^+$ has been characterized in detail, see: K.O. Christe, W.W. Wilson, J.A. Sheehy, J.A. Boatz, *Angew. Chem.* **2009**, *111*, 2112; *Angew. Chem., Int. Ed.* **1999**, *38*, 2004.
- [13] G. Auffermann, Y. Prots, R. Kniep, *Angew. Chem.* **2001**, *113*, 565; *Angew. Chem., Int. Ed.* **2001**, *40*, 547.
- [14] G.V. Vajenine, G. Auffermann, Y. Prots, W. Schnelle, R.K. Kremer, A. Simon, R. Kniep, *Inorg. Chem.* **2001**, *40*, 4866.
- [15] G. Auffermann, U. Schmidt, B. Bayer, Y. Prots, R. Kniep, *Anal. Bioanal. Chem.* **2002**, *373*, 880.
- [16] G. Auffermann, R. Kniep, W. Bronger, *Z. Anorg. Allg. Chem.* **2006**, *632*, 565.
- [17] Y. Prots, G. Auffermann, M. Tovar, R. Kniep, *Angew. Chem.* **2002**, *114*, 2392; *Angew. Chem., Int. Ed.* **2002**, *41*, 2288.
- [18] S. Pfirrmann, C. Herwig, R. Stößer, B. Ziemer, C. Limberg, *Angew. Chem.* **2009**, *121*, 3407; *Angew. Chem., Int. Ed.* **2009**, *48*, 3357.
- [19] P.J. Chirik, *Nat. Chem.* **2009**, *1*, 520.
- [20] W.J. Evans, M. Fang, G. Zucchi, F. Furche, J.W. Ziller, R.M. Hoekstra, J.I. Zink, *J. Am. Chem. Soc.* **2009**, *131*, 11195.
- [21] W. Kaim, B. Sarkar, *Angew. Chem.* **2009**, *121*, 9573; *Angew. Chem., Int. Ed.* **2009**, *48*, 9409.

- [22] W. Uhl, B. Rezaeirad, M. Layh, E. Hagemeyer, E.-U. Würthwein, N. Ghavtadze, I. Kuzu, *Chem. Eur. J.* **2010**, *16*, 12195.
- [23] J.D. Rinehart, M. Fang, W.J. Evans, J.R. Long, *Nat. Chem.*, **2011**, *3*, 538.
- [24] E. Gregoryanz, C. Sanloup, M. Somayazulu, J. Badro, G. Fiquet, H.-K.; Mao, R.J. Hemely, *Nat. Mater.* **2004**, *3*, 294.
- [25] J. von Appen, M.-W. Lumey, R. Dronskowski, *Angew. Chem.* **2006**, *118*, 4472; *Angew. Chem., Int. Ed.* **2006**, *45*, 4365.
- [26] J.C. Crowhurst, A.F. Goncharov, B. Sadigh, C.L. Evans, P.G. Morrall, J.L. Ferreira, A.J. Nelson, *Science* **2006**, *311*, 1275.
- [27] A.F. Young, J.A. Montoya, C. Sanloup, M. Lazzeri, E. Gregoryanz, S. Scandolo, *Phys. Rev. B* **2006**, *73*, 153102.
- [28] J.A. Montoya, A.D. Hernandez, C. Sanloup, E. Gregoryanz, S. Scandolo, *Appl. Phys. Lett.* **2007**, *90*, 011909.
- [29] J.C. Crowhurst, A.F. Goncharov, B. Sadigh, J.M. Zaug, D. Aberg, Y. Meng, V.B. Prakapenka, *J. Mater. Res.* **2008**, *23*, 1.
- [30] Z.W. Chen, X.J. Guo, Z.Y. Liu, M.Z. Ma, Q. Jing, G. Li, X.Y. Zhang, L.X. Li, Q. Wang, Y.J. Tian, R.P. Liu, *Phys. Rev. B* **2007**, *75*, 054103.
- [31] R. Yu, Q. Zhan, L.C. De Jonghe, *Angew. Chem.* **2007**, *119*, 1154; *Angew. Chem., Int. Ed.* **2007**, *46*, 1136.
- [32] W. Chen, J.S. Tse, J.Z. Jiang, *J. Phys.: Condens. Matter* **2010**, *22*, 015404.
- [33] M. Wessel, R. Dronskowski, *J. Am. Chem. Soc.* **2010**, *132*, 2421.
- [34] M. Wessel, R. Dronskowski, *Chem. Eur. J.* **2011**, *17*, 2598.
- [35] M. Wessel, R. Dronskowski, *J. Comput. Chem.* **2010**, *31*, 1613.
- [36] M. Wessel, *PhD thesis*, RWTH Aachen University: Aachen, **2010**.
- [37] S.B. Schneider, R. Frankovsky, W. Schnick, *Inorg. Chem.* **2012**, *51*, 2366.

- [38] Further information of the crystal structure may be obtained from the Fachinformationszentrum Karlsruhe, 76344 Eggenstein-Leopoldshafen, Germany (fax: (49) 7247-808-666; e-mail: crysdata@fiz-karlsruhe.de) on quoting the depository number CSD-423831.
- [39] Non-indexed reflections do definitively not belong to Li_2N_2 , which is confirmed by a slight variation of synthesis conditions (only a few K and about 0.5 GPa) and by temperature-dependent *in situ* X-ray diffractometry (see Supporting Information).
- [40] A.A. Coelho, *TOPAS-Academic* Version 4.1; Coelho Software: Brisbane, **2007**.
- [41] O. Reckeweg, A. Simon, *Z. Naturforsch.* **2003**, *85b*, 1097.
- [42] a) E. Zintl, G.Z. Brauer, *Elektrochem.* **1935**, *41*, 102; b) A. Rabenau, H. Schultz, *J. Less-Common Met.* **1976**, *50*, 155; c) N.E. Brese, M. O'Keeffe, *Structural Bonding*, Vol. 79, Springer Verlag: Berlin-Heidelberg, **1992**.
- [43] R.D. Shannon, *Acta Crystallogr., Sect. A* **1976**, *32*, 751.
- [44] X. Zhang, A. Zunger, G. Trimarchi, *J. Chem. Phys.* **2010**, *133*, 194504.
- [45] G. Auffermann, Y. Prots, R. Kniep, S.F. Parker, S.M. Bennington, *ChemPhysChem* **2002**, *9*, 815.
- [46] K.O. Andersen, O. Jespen, Tight-Binding LMTO Version 4.7, Max-Planck-Institut für Festkörperforschung: Stuttgart, **1994**.

3.2 FURTHER ALKALI DIAZENIDES

In contrast to the elaborated alkali-oxygen chemistry, where homonuclear anions like peroxides M_2O_2 and hyperoxides MO_2 are more stable with the heavier alkali metals ($M = K, Rb,$ and Cs),^[1-3] the existence of corresponding homologue alkali compounds with homonuclear dinitrogen anions still lacks evidence. With Li_2N_2 , the first representative of related peroxide composition with $[N_2]^{2-}$ ions was obtained by thermal decomposition of LiN_3 under extreme conditions. To extend the compositional range of M_2N_2 ($M = Na-Cs$) diazenides, we also targeted the investigation of thermal behavior of the heavier alkali azides under extreme conditions.

3.2.1 EXPERIMENTAL SECTION

Synthesis of Alkali Azides MN_3 ($M = Na-Cs$)

Besides sodium azide, which was purchased commercially from Acros Organics (Geel, Belgium, 99 %), the heavier homologue alkali azides have been synthesized according to the literature.^[4-7] Potassium, rubidium and cesium azides are obtained by the reaction of the corresponding hydroxides (Sigma-Aldrich, 99.995 %) with an aqueous solution of HN_3 . The extremely dangerous HN_3 is distilled from NaN_3 and H_2SO_4 . The solid azides are dried over P_4O_{10} using a vacuum desiccator. A general procedure for the synthesis of the azides of the heavier alkaline earth metals is described in the literature.^[4,5] As-obtained azides can be handled without special precautions.

Caution! Due to the very low thermal and mechanical shock resistance of HN_3 , hydrazoic acid should always be handled with maximum caution. Therefore, whenever working with HN_3 , efficient protective clothing such as face protections, a leather coat and steel reinforced gloves must be worn.

Ex situ High-pressure Investigations

According to the synthesis of Li_2N_2 , the thermal behavior of the heavier alkali azides has also been investigated under HP/HT-conditions. For the HP/HT-treatment of as-obtained azides a modified Walker-type module in combination with a 1000 t press (Voggenreiter, Mainleus, Germany) was used. As pressure medium, precastable MgO-octahedra (Ceramic Substrates &

Components, Isle of Wight, U.K.) with edge lengths of 10, 14, 18 or 25 mm (10/5, 14/8, 18/11 or 25/17 assembly) were employed depending on the maximum synthesis pressure. Eight tungsten carbide cubes (Hawedia, Marklkofen, Germany) with truncation edge lengths of 5, 8, 11 or 17 mm compressed the octahedra. The alkali azides were carefully ground, filled into a cylindrical boron nitride crucible (Henze BNP GmbH, Kempten, Germany) and sealed with a fitting boron nitride plate. A detailed description of the setup can be found in the literature.^[8–12] Compressing and decompression rates were set according to the synthesis pressure. The recovered MgO-octahedra were broken apart in a glovebox (Unilab, MBraun, Garching; O₂ < 1 ppm, H₂O < 1 ppm) and the samples carefully isolated from the surrounding boron nitride crucible.

In situ High-Pressure Investigations

In addition, the thermal behavior of MN_3 azides ($M = \text{Na}$ and K) under extreme conditions was also investigated *in situ* at the *Hamburger Synchrotronstrahlungslabor (HASYLAB, Beamline F2.1* operated by the Geoforschungszentrum (GFZ) Potsdam until 2012). Energy-dispersive diffraction patterns were recorded using white X-rays from the storage-ring DORIS III. The pressure was measured by using the high-pressure equation of state for admixed NaCl by *Decker*.^[13] The beamline was equipped with a Ge solid-state detector, situated at the press frame and tracking the adjustment of the whole apparatus in relation to the X-ray beam. The multianvil apparatus is equipped with six tungsten carbide anvils, which are driven by a 2.5 kN uniaxial hydraulic ram. The top and bottom anvil are driven directly, the lateral anvils by two load frames and four reaction bolsters. The maximum pressure for the 8 mm cube setup is approximately 9 GPa with temperatures up to 1900 K, which are produced by an internal graphite heater. The high-pressure cell consists of a cube made of boron epoxy resin. The gaskets between the anvils are formed from the boron epoxy cube material during the runs. The boron nitride high-pressure cell itself is filled with the ground alkali azides, the graphite heater, the pressure standard (NaCl) and the thermocouple, which is insulated by boron nitride. All sample preparation was done in a glovebox (Unilab, MBraun, Garching; O₂ < 1 ppm, H₂O < 1 ppm). Rings made from heated pyrophyllite provide electrical insulation and act as a quasi-hydrostatic pressure transmitting medium. Copper rings contact the heater at the top and bottom anvils.

3.2.2 RESULTS, DISCUSSION AND CONCLUSION

Surprisingly, independently of the synthesis conditions as well as of the investigated alkali azides, the products of each *ex situ* HP/HT-experiment (see Figure 1) showed typical properties of elemental alkali metals, namely metallic brilliance and ductility, indicating a decomposition of the heavier alkali azides into the elements in contrast to the synthesis of Li_2N_2 .

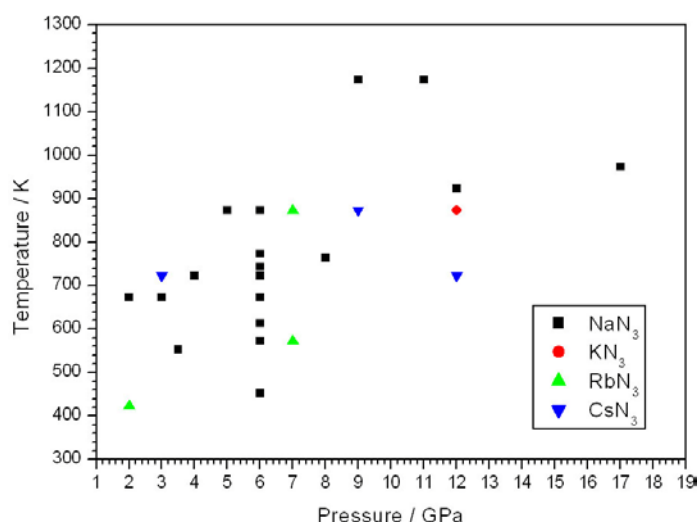


Figure 1. Conditions of the HP/HT-experiments with sodium (black), potassium (red), rubidium (green) and cesium (blue) azide. In a total number of 27 experiments, no diazenide was formed, but always the corresponding elemental alkali metal indicating the decomposition of the azides into the elements. Some experiments have been conducted twice at the same temperature and pressure, but with different heating, holding and cooling rates.

The *in situ* experiments are in accordance with previous *ex situ* results, as the investigated alkali azides do not transform into another product but the alkali metal itself upon HP/HT-treatment (see Figure 2), which indicates again a decomposition of the alkali azide into the elements.

In the case of NaN_3 a pressure-induced phase-transition from rhombohedral $\beta\text{-NaN}_3$ ($R\bar{3}m$, no. 166) to monoclinic $\alpha\text{-NaN}_3$ ($C2/m$, no. 12) is observed at pressures < 1 GPa in good agreement with the literature (data not shown).^[14] Once the assembly-dependent final pressure of e.g. 3.5 GPa (see Figure 2, red squares) is reached, the temperature is slowly raised. Up to 523 K, the reflection profile of $\alpha\text{-NaN}_3$ is still observed. At 523 K $\alpha\text{-NaN}_3$ rapidly transforms into body-centered metallic sodium, which after a further increase in temperature melts at about 823 K in agreement with literature data.^[15,16] An *in situ* investigation of NaN_3 at

4.9 GPa shows the same features as the experiment at 3.5 GPa. For KN_3 no pressure-induced phase-transition is observed up to a maximum investigated pressure of 3.9 GPa.^[17] Like NaN_3 , potassium azide first decomposes to elemental potassium which finally melts upon increasing temperature. Corresponding melting points of potassium are also in good agreement with the literature.^[18]

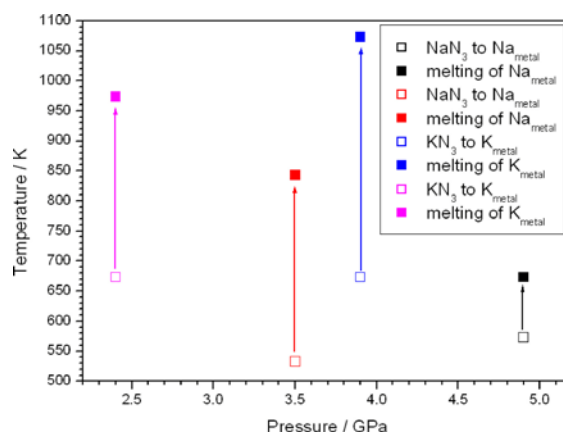
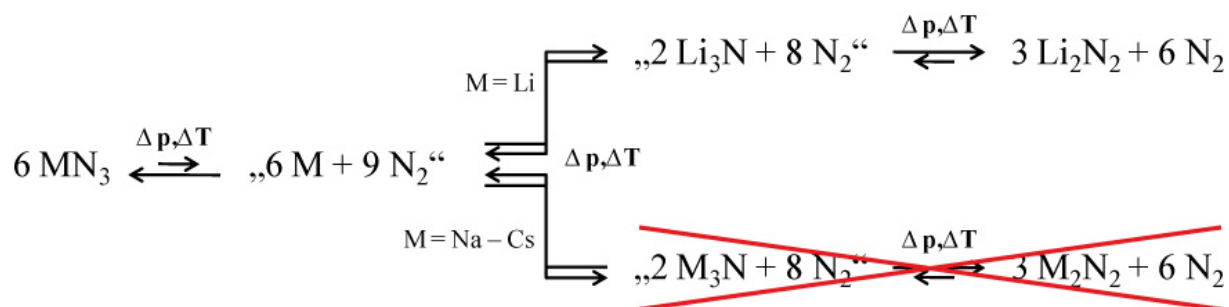


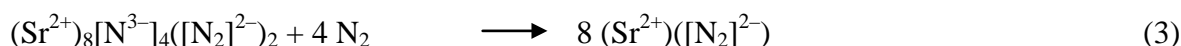
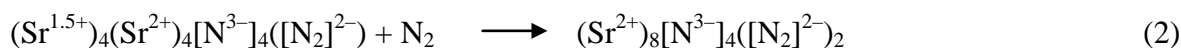
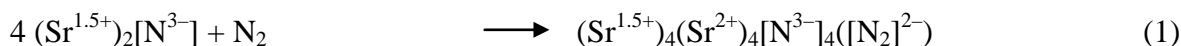
Figure 2. Conditions of the *in situ* HP/HT-experiments with sodium (black, red) and potassium (blue, magenta) azide. Hollow squares represent the onset of azide-metal transition. A further rise in temperature (arrow) finally results in a total melting (squares) of the assembly.

Summarizing, the (di-)nitrogen-chemistry of the heavier alkali metals does not follow the trend as observed in oxygen-rich alkali compounds, namely in the formation of representatives with homonuclear anions of M_2X_2 or MX_2 stoichiometry ($M = \text{alkali}$, $X = \text{O, N}$). Corresponding azides rather decompose into the elements upon temperature increase at a given pressure. So far, Li_2N_2 represents the only known alkali diazenide accessible by thermal decomposition of the ionic azide under extreme conditions. A reason for this observation might be the following, however rather hypothetical scenario (see Scheme 1). Upon the synthesis of Li_2N_2 , once LiN_3 decomposes into the elements (as observed for NaN_3 and KN_3), lithium and molecular nitrogen can rearrange to form thermodynamically stable Li_3N as it is commonly observed for the elements at high temperatures.^[19] According to *LeChatelier's* principle, the chemical equilibrium further shifts to the side with less gaseous components at high-pressure conditions, which then is the comproportionation of nitride ions and dinitrogen molecules to diazenide entities formally represented by the reaction of intermediate Li_3N to Li_2N_2 . Note that this comproportioning has already been proposed by *Kniep* et al. (see equations 1–3) for the final step upon initial synthesis of SrN_2 (see also scheme 2 in chapter 1.4).^[20–24] However, *Kniep's* redox-intercalation process of molecular N_2 into various

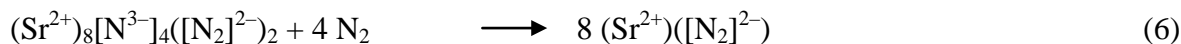
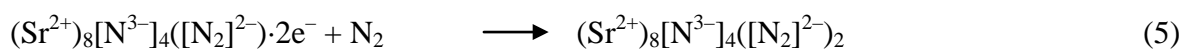
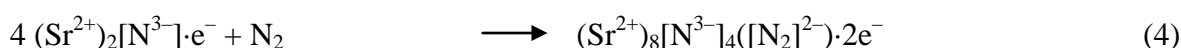
host lattices remains questionable as uncommon oxidation states of strontium differing from +II are involved.



Scheme 1. Hypothetical intermediates upon thermal decomposition of alkali azides. Due to the minor gaseous contributions at the right side of the chemical equilibrium, the synthesis of the product Li_2N_2 is favoured upon HP/HT-treatment of LiN_3 . In contrast, the formation of a diazenide of the heavier alkalis is not observed at all.



On the other hand, if strontium exhibits the common oxidation state +II for all intermediate reactions, the corresponding equations 4–6 for the formation of Sr_4N_3 , SrN and SrN_2 starting again from Sr_2N could be formulated as follows:



Thereby, N_2 molecules ions are reduced to $[\text{N}_2]^{2-}$ entities, whereby the electrons are most probably provided by $\text{Sr}_2\text{N} \cdot e^-$ itself. Nevertheless, in both scenarios the last step of SrN_2 formation involves comproportioning of remanent nitride ions in $\text{Sr}_8\text{N}_4(\text{N}_2)_2$ and dinitrogen molecules to yield solely $[\text{N}_2]^{2-}$ containing compounds.

Coming back to the question of missing representatives of the heavier alkali diazenides, lattice energies of M_3N nitrides ($M = \text{Li}, \text{Na}, \text{K}$) have to be taken into account. Thereby, the lattice energy of Li_3N mounts to about 6330 kJ/mol, and shows an enormously decreased

value for Na_3N and K_3N , which is only of 5250 and 4200 kJ/mol, respectively.^[25] This clearly indicates the difficulty in nitride formation of the heavier alkali homologues – note that the synthesis of Na_3N or K_3N starting from the elements is only observed for extraordinary extreme conditions with specialized equipments.^[26,27] In addition, the existence of Cs_3N and Rb_3N still leaks evidence. In accord with Scheme 1, the *in situ* investigations for NaN_3 and KN_3 did not show any nitride formation upon HP/HT-treatment, thus possibly impeding a further reaction to potential diazenides by comproportionation reactions. However it has to be stated that the true behavior of LiN_3 under HP/HT-conditions is yet not known, as LiN_3 was not investigated by *in situ* experiments. Thus, the postulated nitride formation remains hypothetical. Electrostatic conditions might also play the crucial role upon diazenide formation, which are so far completely unidentified. Moreover, it has to be stated that the necessity of nitride formation is also not proven.

In addition, transferring the as-postulated reaction scheme to the successful HP/HT-synthesis of alkaline earth diazenides $M_{\text{AE}}\text{N}_2$ ($M_{\text{AE}} = \text{Ca}, \text{Sr}$ and Ba) starting again from the corresponding azides, it further remains questionable. Up to date there are no *in situ* investigations of the thermal behavior of alkaline earth azides upon HP/HT-conditions. Thus their decomposition into the elements and the recombination into nitrides still leaks evidence, especially as strontium and barium nitrides, Sr_3N_2 and Ba_3N_2 , are not unambiguously known to exist so far. In fact, the synthesis of $M_{\text{AE}}\text{N}_2$ starting from the corresponding azides also has to be investigated *in situ* to prove the postulated reaction mechanism as nitride-diazenides synthesized by *Kniep* et al. can constitute possible intermediates.^[20–24,28] If decomposition into the elements and formation of nitrides do not constitute any intermediate steps, another mechanism for diazenide formation has to be formulated possibly involving the direct recombination of azide ions themselves into dinitrogen molecules and $[\text{N}_2]^{2-}$ entities.

3.2.3 BIBLIOGRAPHY

- [1] N.G. Vannerberg, *Prog. Inorg. Chem.* **1962**, 4, 125.
- [2] I.I. Vol'nov, *Peroxides, Superoxides and Ozonides of Alkali and Alkaline Earth Metals*, Vol. II, Plenum Press: New York, **1966**.
- [3] W. Hesse, M. Jansen, W. Schnick, *Prog. Solid State Chem.* **1989**, 19, 47.
- [4] H.D. Fair, R.F. Walker, *Energetic Materials Vol. 1: Physics and Chemistry of the Inorganic Azides*; Plenum Press: New York **1977**.

- [5] P. Ehrlich, H.J. Seifert, G. Brauer, *Handbuch der Präparativen Anorganischen Chemie Vol. 2*; Ferdinand Enke Verlag: Stuttgart, **1978**.
- [6] P. Remy-Gennete, *Ann. Chim.* **1933**, *19*, 289.
- [7] P. Gray, T.C. Waddington, *Proc. R. Soc. London, Ser. A.* **1956**, *235*, 106.
- [8] D. Walker, M.A. Carpenter, C.M. Hitch, *Am. Mineral.* **1990**, *75*, 1020.
- [9] D. Walker, *Am. Mineral.* **1991**, *76*, 1092.
- [10] H. Huppertz, *Z. Kristallogr.* **2004**, *219*, 330.
- [11] D.C. Rubie, *Phase Transitions* **1999**, *68*, 431.
- [12] N. Kawai, S. Endo, *Rev. Sci. Instrum.* **1970**, *8*, 1178.
- [13] D.L. Decker, *J. Appl. Phys.* **1971**, *42*, 3239.
- [14] M.I. Eremets, M.Yu. Popov, I.A. Trojan, V.N. Denisov, R. Böehler, R.J. Hemley, *J. Chem. Phys.* **2004**, *120*, 10618.
- [15] C.-S. Zha, R. Boehler, *Phys. Rev. B* **1985**, *31*, 3199.
- [16] E. Gregoryanz, O. Degtyareva, M. Somayazulu, R.J. Hemley, H. Mao, *Phys. Rev. Lett.* **2005**, *94*, 185502.
- [17] C. Ji, F. Zhang, D. Hou, H. Zhu, J. Wua, M.-C. Chyu, V.I. Levitas, Y. Maa, *J. Phys. Chem. Sol.* **2011**, *72*, 736.
- [18] O. Narygina, E.E. McBride, G.W. Stinton, M.I. McMahon, *Phys. Rev. B*, **2011**, *84*, 054111.
- [19] A. Rabenau, *Solid State Ion.* **1982**, *6*, 277.
- [20] G. Auffermann, Y. Prots, R. Kniep, *Angew. Chem.* **2001**, *113*, 565; *Angew. Chem., Int. Ed.* **2001**, *40*, 547.
- [21] G. Auffermann, Y. Prots, R. Kniep, S.F. Parker, S.M. Bennington, *ChemPhysChem* **2002**, *9*, 815.

- [22] G. Auffermann, U. Schmidt, B. Bayer, Y. Prots, R. Kniep, *Anal. Bioanal. Chem.* **2002**, 373, 880.
- [23] G. Auffermann, R. Kniep, W. Bronger, *Z. Anorg. Allg. Chem.* **2006**, 632, 565.
- [24] Y. Prots, G. Auffermann, M. Tovar, R. Kniep, *Angew. Chem.* **2002**, 114, 2392; *Angew. Chem., Int. Ed.* **2002**, 41, 2288.
- [25] a) R.D. Shannon, *Acta Crystallogr., Sect. A* **1976**, 32, 751; b) R. Hübenthal, Vers. 4 ed.; Universität Gießen: **1993**; c) R. Hoppe, *Angew. Chem.* **1966**, 78, 52; *Angew. Chem., Int. Ed. Engl.* **1966**, 5, 95; d) R. Hoppe, *Angew. Chem.* **1970**, 82, 7; *Angew. Chem., Int. Ed. Engl.* **1970**, 9, 25.
- [26] D. Fischer, M. Jansen, *Angew. Chem.* **2002**, 114, 1831; *Angew. Chem., Int. Ed.* **2002**, 41, 1755.
- [27] D. Fischer, Z. Cancarevic, J.C. Schön, M. Jansen, *Z. Anorg. Allg. Chem.* **2004**, 630, 156.
- [28] G.V. Vajenine, G. Auffermann, Y. Prots, W. Schnelle, R.K. Kremer, A. Simon, R. Kniep, *Inorg. Chem.* **2001**, 40, 4866.

4. MATERIALS PROPERTIES OF BINARY DIAZENIDES

In the following chapters, as-synthesized binary diazenides are investigated regarding their materials properties, such as electronic, ionic and pressure-dependent mechano-physical characteristics. Whether the alkaline earth diazenides $M_{\text{AE}}\text{N}_2$ ($M_{\text{AE}} = \text{Ca}, \text{Sr}, \text{Ba}$) and Li_2N_2 despite their rather ionic characteristics show true metallic behavior in accordance with density functional considerations or insulating and therefore ionic properties, can be found out in the first chapter. Again, it is the alkali diazenide Li_2N_2 that proves another exciting characteristic.

4.1. ELECTRONIC AND IONIC CONDUCTIVITY IN ALKALINE EARTH DIAZENIDES $M_{AE}N_2$ ($M_{AE} = CA, SR, BA$) AND IN Li_2N_2

Sebastian B. Schneider, Martin Mangstl, Gina M. Friederichs, Rainer Frankovsky, Jörn Schmedt auf der Günne and Wolfgang Schnick

published in Chem. Mater. **2013**, 25, 4149

DOI: 10.1021/cm4011629

Copyright © 2013, American Chemical Society

<http://pubs.acs.org/doi/abs/10.1021/cm4011629>

ABSTRACT

Electrical conductivity measurements of alkaline earth diazenides SrN_2 and BaN_2 revealed temperature-dependent metal-like behavior. As CaN_2 is isotypic with SrN_2 its electronic properties are supposed to show similar characteristics. For the alkali diazenide Li_2N_2 , the corresponding measurement shows not only the typical characteristics of metallic materials but also an unexpected rise in electrical conductivity above 250 K, which is consistent with an ionic contribution. This interpretation is further corroborated by static 6Li and 7Li nuclear magnetic resonance measurements (NMR) of the spin-lattice relaxation time (T_1) over an extended temperature range from 50 to 425 K. We observe a constant Heitler-Teller product (T_1T) as expected for metals at low temperatures and a maximum in the temperature-dependent relaxation rates, which reflects the suggested ionic conductivity. A topological structural analysis indicates possible 3D ion migration pathways between two of the three crystallographic independent Li positions. A crude estimate of temperature-dependent self-diffusion coefficients $D(T)$ of the lithium motion classifies Li_2N_2 as a mixed electronic/ionic conductor.

4.1.1 INTRODUCTION

Due to numerous applications of binary metal-nitrogen compounds, their synthesis and characterization had and still has a remarkable impact on solid-state and materials chemistry.^[1-9] Besides the long known nitrides and azides with N^{3-} and $[\text{N}_3]^-$ anions, respectively, a third class of nitrogen based anions proved their existence only very recently, the latter consisting of homonuclear dinitrogen units, namely $[\text{N}_2]^{x-}$ ($x = 1-4$).¹⁰⁻³³ Besides the paramagnetic dinitrogen anions $[\text{N}_2]^-$ and $[\text{N}_2]^{3-}$, which so far have only been observed in molecular complexes,^[10-16] it was $[\text{N}_2]^{2-}$ and $[\text{N}_2]^{4-}$ ions that could have been synthesized in solid-state compounds.^[17-33] The 14 electron ion $[\text{N}_2]^{4-}$ is isosteric with peroxide $[\text{O}_2]^{2-}$ and thus was named pernitride,^[24-33] whereas $[\text{N}_2]^{2-}$, representing a deprotonated diazene N_2H_2 with a $\text{N}=\text{N}$ double bond has been denominated diazenide.^[17-23]

The first binary representatives containing $[\text{N}_2]^{2-}$ anions were SrN_2 and BaN_2 , which have been synthesized under nitrogen pressure in a specialized autoclave system.^[17-21] In order to further extend this class of metal diazenides, we recently have targeted new synthetic approaches and were successful employing controlled thermal decomposition of ionic azides in a multianvil device under high-pressure/high-temperature (HP/HT) conditions.^[22,23] Besides the two known diazenides, we obtained and characterized novel CaN_2 and the first alkali diazenide, namely Li_2N_2 .^[22,23]

With a high difference in electronegativity between cations and anions, these diazenide compounds suggest rather ionic behavior, although having a black metallic luster. In addition, corresponding theoretical calculations on their electronic structure revealed that these compounds should exhibit metallic characteristics.^[18,22,23,34] This is somehow surprising as simple compounds containing corresponding homonuclear anions made up of elements on either side of the element nitrogen in the PSE, namely acetylenide $[\text{C}_2]^{2-}$ or peroxide compounds clearly show ionic and thus insulating or at least semiconductive behavior.^[35-37] In addition, stretching vibrations of the double-bonded dinitrogen anions were observed in FTIR measurements of the mentioned diazenides as distinct features at about $1325\text{--}1375\text{ cm}^{-1}$ (see Figure S1 in the Supporting Information, SI).^[22,23] In fact, applying the correlation method^[38] for allowed vibrations of the diazenide ions in the corresponding crystal structures, we were successful by predicting infrared-active modes for all of these diazenides.^[22,23] This observation rather contradicts metal-like behavior as for metallic compounds infrared-active features at such high energies usually do not occur. Additional theoretical considerations on

the existence of hitherto unknown diazenide compounds revealed that FeN_2 , ZnN_2 and LaN_2 should be thermodynamically stable at ambient conditions and exhibit again metallicity.^[33,39,40] However, the true character of an either metallic or ionic formulation of diazenides based on experimental data still lacks evidence.

In the case of Li_2N_2 potential lithium ionic conduction is however thought to interfere with assumed metallic, electronic conductivity. As the interest in and demand for Li^+ ion conductors still increase due to their industrial applications such as solid-state batteries,^[41–43] it is important to fully characterize Li_2N_2 . In order to investigate a potential ionic conduction lithium nuclear magnetic resonance (NMR) is a suitable tool.^[44–46] As it already has been shown for Li_3N and various Li^+ containing compounds,^[47–53] it is possible to estimate activation energies E_A and diffusion coefficients $D(T)$ for the lithium migration from temperature-dependent ^6Li and ^7Li spin-lattice relaxation (SLR) experiments.

In the present work we report on an experimental study of unsettled metal-like behavior in diazenide compounds. Conductivity measurements between 3.5 and 300 K are presented and measured specific conductivities are classified and discussed with respect to those of metals, semiconductors and insulators. Ionic and electronic contributions to the electrical conductivity in Li_2N_2 were further investigated from temperature-dependent ^6Li and ^7Li NMR. The results obtained with different experimental techniques combined with a topological analysis of lithium migration pathways allow us to estimate a activation energy E_A , the dimensionality and temperature-dependent self-diffusion coefficients $D(T)$ of the lithium motion.

4.1.2 EXPERIMENTAL SECTION

Synthesis of Azides

Nondoped LiN_3 was obtained by precipitation from its aqueous solution (Sigma-Aldrich, 20 wt% solution in water) by evaporation in vacuum, whereas $^6\text{LiN}_3$ was precipitated in diethylether by addition of excess NaN_3 (Acros Organics, 99 %) to a suspension of $^6\text{LiCl}$ (Sigma-Aldrich, 95 atom% ^6Li , 99 %) in absolute ethanol as described in the literature.^[54–56] Strontium and barium azide are obtained by the reaction of the corresponding hydroxides (Sigma-Aldrich, 99.995 %) with an aqueous solution of HN_3 , as reported in the literature.^[54,55] The extremely dangerous HN_3 is distilled from NaN_3 (Acros Organics, Geel, Belgium, 99 %) and H_2SO_4 . The solid azides are dried over P_4O_{10} using a vacuum desiccator (24 h). A general

procedure for the synthesis of the azides of the heavier alkaline earth metals is described in the literature.^[56]

Caution! Due to the very low thermal and mechanical shock resistance of HN_3 , only very small quantities should be used. Therefore, whenever working with HN_3 , efficient protective clothing such as face protection, a leather coat and steel reinforced gloves must be worn.

Synthesis of Diazenides

${}^6\text{Li}_2\text{N}_2$, nondoped Li_2N_2 , SrN_2 and BaN_2 were synthesized at distinct HP/HT-conditions in a modified Walker-type module in combination with a 1000 t press (both devices from the company Voggenreiter, Mainleus, Germany) according to literature.^[22,23] The as-obtained azide was carefully ground, filled into a cylindrical copper (Li_2N_2) or boron nitride ($M_{\text{AE}}\text{N}_2$) crucible (Henze BNP GmbH, Kempten, Germany) and sealed with a fitting boron nitride plate. As pressure medium, precastable MgO-octahedra (Ceramic Substrates & Components, Isle of Wight, U.K.) with edge lengths of 18 mm (18/11 assembly) were applied. Eight tungsten carbide cubes (Hawedia, Marklkofen, Germany) with truncation edge lengths of 11 mm compressed the octahedra. Details of the setup can be found in the literature.^[57-61] Li_2N_2 (SrN_2 , BaN_2) was synthesized in a 18/11 (18/11, 18/11) assembly which was compressed up to 9 (9, 3) GPa at room temperature within 217 (214, 68) min, then heated up to 750 (850, 750) K in 10 (30, 30) min, kept at this temperature for 50 (15, 15) min and cooled to room temperature in 10 (10, 10) min. Subsequently, pressure was released over a period of 633 (623, 183) min. The recovered MgO-octahedron was broken apart under inert conditions in a glovebox (Unilab, MBraun, Garching; $\text{O}_2 < 1$ ppm, $\text{H}_2\text{O} < 1$ ppm) and the sample was carefully isolated from the surrounding boron nitride crucible. A black metallic powder of the corresponding diazenide is obtained, extremely sensitive to moisture. Each diazenide was analyzed by means of powder X-ray diffraction patterns which were recorded with a STOE Stadi P powder diffractometer (STOE, Germany) in Debye-Scherrer geometry using Ge(111) monochromated Mo and Cu $K_{\alpha 1}$ radiation, respectively (0.7093 Å and 1.54056 Å).

Li_2N_2 crystallizes in space group *Immm* (no. 71) with $a = 3.1181(4)$, $b = 4.4372(4)$, $c = 10.7912(16)$ Å, $V = 149.31(3)$ Å³ and $Z = 4$; Li1 in (2*a*), Li2 in (2*c*), Li3 in (4*i*) with $z = 0.2510(6)$ and N1 in (8*l*) with $y = 0.1466(5)$ and $z = 0.62321(19)$.^[22] SrN_2 crystallizes in a tetragonally distorted NaCl-type structure in space group *I4/mmm* (no. 139) with

$a = 3.8054(2)$, $c = 6.8961(4)$ Å, $V = 91.17(1)$ Å³ and $Z = 2$; Sr1 in (2a) and N1 in (4e) with $z = 0.4016(4)$.²³ The crystal structure of BaN₂ is of monoclinic symmetry ($C2/c$ no. 15) with $a = 7.1608(4)$, $b = 4.3776(3)$, $c = 7.2188(4)$ Å, $\beta = 104.9679(33)^\circ$, $V = 218.61(2)$ Å³ and $Z = 4$; Ba1 in (4e) with $y = 0.2006(2)$ and N1 in (8f) with $x = 0.3023(18)$, $y = 0.1547(39)$ and $z = 0.0508(19)$.^[23] The crystallographic data of the corresponding diazenides are taken from literature.^[22,23]

Conductivity Measurements

For the measurements of SrN₂ and BaN₂, two reaction batches of each diazenide were combined, whereas for the measurement of Li₂N₂ an overall of eight batches had to be merged due to the small sample amount obtained upon synthesis. In addition, each product of a HP/HT-synthesis was analyzed separately by means of powder X-ray diffraction to rely on a successful synthesis of the corresponding diazenide.

The electrical measurements were performed with a self-built susceptometer consisting of a Janis shi-950 two-stage closed-cycle Cryostate with ⁴He exchange gas (Janis Research Company, Wilmington, U.S.A.) and a dual-channel temperature controller (model 332 by LakeShore, Westerville, U.S.A.). A Keithley Source-Meter 2400 (Cleveland, U.S.A.) was available as current source, which was used to create square waves with amplitudes of 2 μA to 5 mA and frequencies of either 2 or 0.4 Hz (1 or 5 PLC, respectively). The differential voltage drop between signal-high and signal-low was recorded with a Keithley 2182 Nano-Voltmeter and used to calculate the sample resistance in one direction according to Ohm's law and the specific resistance according to the Van-der-Pauw approximation.^[62]

For the measurements cold pressed (10 kN) pellets of nonsintered diazenides (diameter: 4.0 mm, thickness: 0.5–0.9 mm) were produced. Applying the four-probe method, the pellet was contacted with four equidistant probes using silver conducting paint. As the diazenides were extremely sensitive to moisture, all preparations had to be done under inert atmosphere in a glovebox. A current of 0.15–0.3·10⁻³ A was applied and the potential difference was measured as a function of the temperature upon cooling and heating (300 to 3.5 K) yielding the specific conductivity. No superconductivity was observed.

⁶Li and ⁷Li solid-State Nuclear Magnetic Resonance

The static ⁷Li and ⁶Li NMR spectra were recorded with a Bruker Avance III NMR spectrometer at a frequency of 194.37 and 73.60 MHz, respectively which corresponds to an external magnetic field of 11.7 T. For temperature-dependent measurements, the spectrometer was equipped with different commercial static variable-temperature probes. For temperatures above approximately 160 K a double-resonance SOL5 probe from Bruker Biospin was used, for temperatures below 160 K a probe from the same company was used which consists of a He continuous flow cryostat (model STVP-XG, Janis Research Company, Wilmington, MA, U.S.A.) and a single channel probe with two CERNOX temperature sensors and self-made coils. The sample was inserted into the coils made of manganin wire for the low-temperature ⁷Li experiments and silver plated copper wire in case of the ⁶Li experiments. The sample was sealed in an airtight glass tube under vacuum. T_1 spin-relaxation times were measured with a saturation recovery experiment. The one-dimensional ⁷Li static NMR spectra were acquired with a $\pi/2$ pulse length of 1.5 μ s and a recycle delay minimum three times bigger than T_1 . The solid-echo ⁶Li static NMR spectra were acquired with a $\pi/2$ pulse length of 1.31 μ s and a recycle delay minimum three times bigger than T_1 .^[63]

4.1.3 RESULTS AND DISCUSSION

Conductivity Measurements

For metals, resistance is temperature-dependent and supposed to decrease with decreasing temperature. The resistance of a semiconductor decreases with increasing temperature and shows an abrupt decay, once the electrons can be excited from the valence band into the conductive band. Insulators only become conductive at very high temperatures and show exceptional high specific resistances at ambient temperature. Taking these classifications into account and comparing them to the observed conductivity curve of the diazenides, the ambiguity whether there is metallicity in diazenides or not can now be referenced.

Figure 1, parts a, b and c show the specific resistance curves for SrN₂, BaN₂ and Li₂N₂, respectively, obtained upon cooling the prefabricated pellets. Figure 1d depicts the pellet of black colored Li₂N₂ mounted onto the sample holder for conductivity measurements.

SrN_2 and BaN_2 show a decrease of specific resistance with decreasing temperature, typical for metals. However, it has to be stated that the pellets have not been sintered before the measurements but were only cold pressed to avoid any oxidation of these highly moisture-sensitive compounds.^[64]

For Li_2N_2 , the specific resistance increases up to a maximum temperature of about 250 K and finally decreases with a further decrease of temperature as expected for metals. Thus, true metal-like behavior is only observed at temperatures below 250 K. The change in conductivity from 250 K to higher temperatures needs a different explanation, for example Li^+ ion conductivity, thermal activation across a band gap (intrinsic doping), or a phase transition (1st or 2nd order). However, the latter explanation of unexpected resistivity in Li_2N_2 can be excluded as previous temperature-dependent *in situ* powder X-ray diffraction already revealed no phase transition below ambient conditions.^[22] Interestingly, it is only the Li^+ ion containing diazenide showing such a distinct feature in its specific resistance.

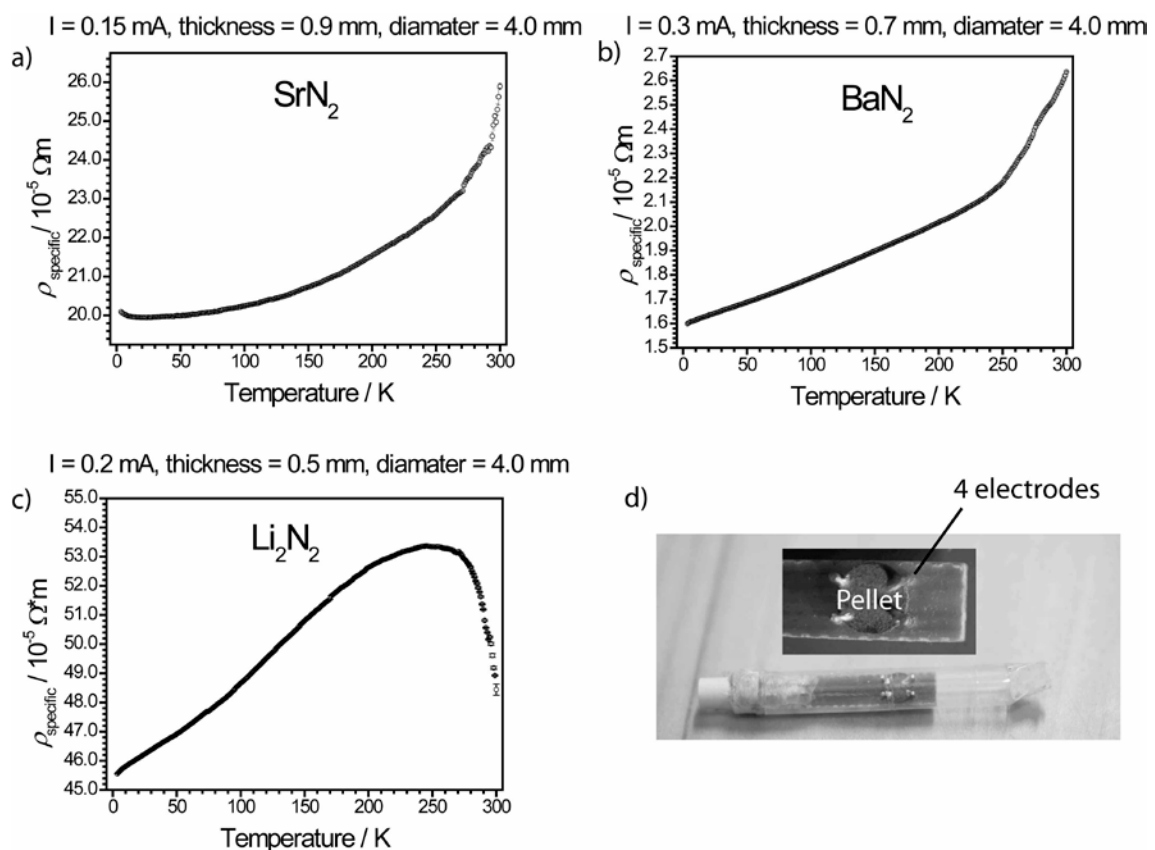


Figure 1. Specific resistance for SrN_2 (a), BaN_2 (b), and Li_2N_2 (c) with temperature; experimental setup for the measurements illustrating the pellet placed between four electrodes (d).

Table 1 lists the obtained resistivity values for SrN_2 , BaN_2 and some selected elements^[65,66] at ambient temperature (300 K) and for Li_2N_2 at 250 K.

Obviously, the specific values of the diazenides are intermediate to those of pure metals and semiconductors. However, as the pellets have not been sintered for the measurements, they definitively do contain a large number of grain boundaries inhibiting perfect conductivity properties. In addition, the products upon HP/HT-synthesis still show oxide impurities in case of the alkaline earth diazenides and an unknown minor side phase with Li_2N_2 .^[22,23] Taking all these facts into account, the true values of resistivity are thought to match better with pure metals. Thus, it is the curve progression indicating true metal-like behavior for all diazenides.

Table 1. Specific Resistance of Diazenides (SrN_2 and BaN_2 at Ambient Temperature; Li_2N_2 at 250 K) and Selected Elements^[65,66] As Well As Their Corresponding Color and Resulting Electronic Behavior.

Compd.	$\rho_{\text{specific}} [\Omega\text{m}]$	color	characteristics
Li_2N_2	$5.33 \cdot 10^{-4}$	black	this work
SrN_2	$2.32 \cdot 10^{-4}$	black-bronze	this work
BaN_2	$0.23 \cdot 10^{-4}$	black-bronze	this work
$\text{Fe}^{[65]}$	$1.0 \cdot 10^{-7}$	gray-metallic	metallic
$\text{Pb}^{[65]}$	$2.2 \cdot 10^{-7}$	gray-metallic	metallic
$\text{Mn}^{[66]}$	$1.43 \cdot 10^{-6}$	steelwhite-metallic	metallic
amorphous carbon ^[66]	$\sim 6 \cdot 10^{-5}$	black	semiconductive
$\text{Te}^{[66]}$	$\sim 3 \cdot 10^{-3}$	silverwhite-metallic	semiconductive
diamond ^[65]	$> 0.1 \cdot 10^9$	transparent	insulating

temperature regime which, consistently with the macroscopic electrical conductivity measurements, gives evidence of the metallic character of Li_2N_2 . Then we will discuss the observed anomaly at increased temperatures reaching up to the decomposition point at about 385 K (depending on synthesis conditions).^[67]

Metals at low temperatures have a characteristic relaxation behavior due to the unpaired electrons close to the Fermi level which leads to a constant Heitler-Teller product $T_1 T$.^[68–70]

⁶Li and ⁷Li solid-State Nuclear Magnetic Resonance

In order to investigate the hypothesis of a beginning Li^+ ion conduction at elevated temperatures being responsible for the unexpected change in resistivity with temperature, variable temperature measurements of the spin-lattice relaxation (SLR) times (T_1) of ^6Li and ^7Li nuclei were performed from 170 to 390 K and from 50 to 425 K, respectively. In the following, we will first discuss the low-

Often this is accompanied by a drastic change of the chemical shift. The difference in chemical shift to diamagnetic materials is termed Knight shift K and often specified in % because of its enormous size in some cases. In case of metallic Li the Knight shift K is small and only of the order of 400 ppm. Even with modern quantum chemical methods it is difficult to predict the Knight shift. Korringa^[69,71] derived a formula that relates the Knight shift K to the Heitler-Teller product T_1T (see equation 1) given the conduction electrons form a free electron gas, where γ_e and γ_n refer to the electron and nuclear gyromagnetic ratios, respectively.

$$T_1T = \frac{h}{8\pi^2 k_B K^2} \frac{\gamma_e^2}{\gamma_n^2} \quad (1)$$

In the case of Li_2N_2 , we obtained temperature SLR time constants both for ^6Li and for ^7Li (^7Li , Figure 2; ^6Li , Figure S2). As expected, we observe constant Heitler-Teller products T_1T in the low-temperature region. The Korringa formula (see equation 1) predicts a quotient of the Heitler-Teller products

$$\frac{T_1T(^7\text{Li})}{T_1T(^6\text{Li})} = \left(\frac{\gamma(^6\text{Li})}{\gamma(^7\text{Li})} \right)^2 \approx 0.14 \quad (2)$$

which is within the range of the experimental value of 0.12 (see Supporting Information, SI).

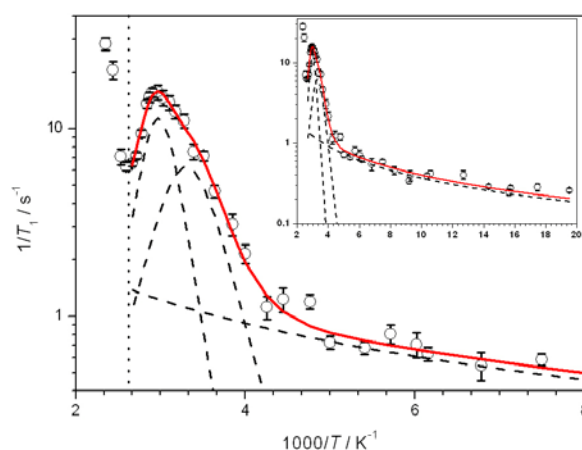


Figure 2. Experimental inverse-temperature dependence of the ^7Li (circles) NMR SLR rates on a logarithmic scale. The fit (solid line) to the experimental data is given by the extended BPP relation (see equation 4). The dashed curves below refer to three different relaxation processes (individual terms in equation 4). The inset shows an overview over the complete data set including the low-temperature region. Decomposition of Li_2N_2 is observed at about $1000/T = 2.6 \text{ K}^{-1}$ (385 K) marked by a dotted line, in good agreement with previous temperature-dependent *in situ* X-ray diffraction analysis.^[22]

Because of the documented deviations^[71] between observed and calculated Knight shift K we consider it to be a fitting parameter which here amounts to 80 ppm. We conclude that the ${}^6\text{Li}$ and ${}^7\text{Li}$ SLR NMR data in the low-temperature regime are consistent with the macroscopic metallic properties of Li_2N_2 .

In the temperature-dependent T_1 relaxation rate diagram (see Figure 2), we observe a flat low-temperature regime in agreement with metallic relaxation; then, we pass through a maximum at about 300 K which is followed by another rise caused by the decomposition of Li_2N_2 to $\alpha\text{-Li}_3\text{N}$. The decomposition product $\alpha\text{-Li}_3\text{N}$ was confirmed by powder X-ray diffraction after the NMR experiments, in line with previous observations.^[22]

We interpret the maximum at 300 K as a consequence of Li ion conduction because other explanations such as decomposition to other products because of humidity or temperature can be ruled out on the basis of IR spectroscopy and XRD diffractometry, which show no evidence of decomposition of Li_2N_2 .

In the following, we analyze the presented relaxation rates for activation energies and jump rates. In good approximation, the relaxation rates $1/T_1$ for ${}^{6,7}\text{Li}$ of different relaxation mechanisms add up to the observable relaxation rate $1/T_1$:

$$\frac{1}{T_1} = \frac{1}{T_1^{\text{quadrupolar}}} + \frac{1}{T_1^{\text{dipolar}}} + \frac{1}{T_1^{\text{paramagnetic}}} + \dots \quad (3)$$

The most important mechanisms, which are commonly considered for ${}^{6,7}\text{Li}$ NMR of dielectric materials, are relaxation by dipolar, quadrupolar, and paramagnetic mechanisms. The temperature dependence of the first two terms can be estimated from a theory suggested by Bloembergen, Purcell, and Pound (BPP theory).^[72] In the low temperature regime, we already realized that an extra term will be necessary, which takes into account the relaxation caused by the random field caused by the conduction electrons. This extra term can be derived from equation 1. For least-squares fitting we neglected the paramagnetic term, we used the following equation which describes quadrupolar/dipolar relaxation through two different terms^[73] and added a last term for relaxation through the conduction electrons

$$\frac{1}{T_1} = C_1 \left(\frac{\tau_{c1}}{1+\omega_0^2\tau_{c1}^2} + \frac{4\tau_{c1}}{1+4\omega_0^2\tau_{c1}^2} \right) + C_2 \left(\frac{\tau_{c2}}{1+\omega_0^2\tau_{c2}^2} + \frac{4\tau_{c2}}{1+4\omega_0^2\tau_{c2}^2} \right) + \left(\frac{8\pi^2 T k_B K^2 \gamma_n^2}{h \gamma_e^2} \right) \quad (4)$$

where τ_{c1} and τ_{c2} are the correlation times of two motional processes, which can be justified for example by motional heterogeneity.^[73] We achieve good agreement (see Figure 2) with the experimental data by assuming that these processes are thermally activated and follow an Arrhenius law $\tau_c = \tau_0 \exp(E_A/k_B T)$. Clearly this is a crude approximation neglecting for example the existence of different crystallographic orbits for Li in the crystal structure of Li_2N_2 , biexponential longitudinal relaxation, relaxational anisotropy, correlated motion, different relaxation rates in the satellite and central transitions.

From least-squares fitting of the ^7Li NMR SLR experiments, we obtain two different activation energies of 0.57 and 0.34 eV (Table 2), which could reflect the mentioned motional heterogeneity of the Li atoms migrating through the complex structure of Li_2N_2 . We note that such a two-component fit yields rather uncommon values τ_0 . For comparison, a single component fit yields an activation energy E_A of 0.36 eV, a τ_0 of $1.3 \cdot 10^{-15}$ s, and a C of

Table 2. Resulting Refined Parameters of the Analysis of ^7Li SLR Rates According to Equation 4.

parameter	i = 1	i = 2
$E_{A,i} / \text{eV}$	0.57	0.34
C_i / s^{-2}	$9.8 \cdot 10^9$	$5.4 \cdot 10^9$
$\tau_{0,i} / \text{s}$	$2.0 \cdot 10^{-18}$	$9.9 \cdot 10^{-16}$

$13.5 \cdot 10^9 \text{ s}^{-2}$. A corresponding analysis of SLR rates of ^6Li NMR measurements (see SI Figure S2) is hampered by the poor signal-to-noise ratio, due to the small amount of available material, despite isotopic labeling and a handmade sample-container-adapted coil. However we

can use the obtained ^6Li SLR data set to check whether relaxation is dominated by a quadrupolar or dipolar mechanism. The isotope-dependent factor in the prefactor C in equation 4 is proportional to $[I(I + 1)] \gamma^4$ and $Q^2 \left[\frac{2I+3}{I^2(2I-1)} \right]$ for a homonuclear dipolar or quadrupolar mechanism,^[74–76] respectively, where I refers to the spin-quantum number, Q to the quadrupolar moment and γ to the gyromagnetic ratio, as tabulated by IUPAC.^[77] For a dipolar relaxation mechanism neglecting isotope effects the prefactor ratio becomes

$$\frac{C(^6\text{Li})}{C(^7\text{Li})} \approx 0.011 \quad (5)$$

and for quadrupolar relaxation

$$\frac{C(^6\text{Li})}{C(^7\text{Li})} \approx 0.0015 \quad (6)$$

Thus the SLR of ${}^6\text{Li}$ can be predicted on the basis of the ${}^7\text{Li}$ least-squares fitting results for the two limiting cases. The resulting comparison with the experimental ${}^6\text{Li}$ SLR data (see Supporting Information Figure S3) indicates that the dominating mechanism is dipolar in nature.

Dimensionality of the Motional Process

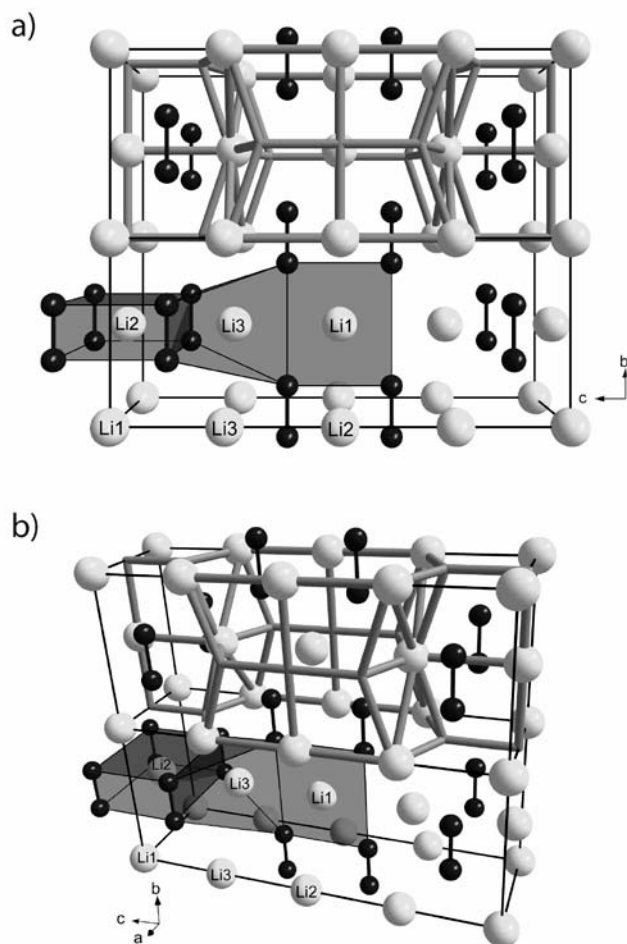


Figure 3. [010]-doubled crystal structure of Li_2N_2 (Li white, N black) illustrating the calculated possible Li^+ ion pathways (thick dark gray) according to the voids in the structure obtained by topological analysis. Polyhedra (gray) around Li sites illustrate the coordination spheres of the Li^+ ions. Cell edges of the unit-cells are marked by black lines.

Efficient macroscopic Li ion conduction requires three-dimensional (3D) motion of the ions which is further supported by topological analysis of possible lithium migration pathways inside the Li_2N_2 structure, as implemented in the software package TOPOS.^[78–81] Lithium ions are assumed to be able to jump between different sites if open channels between two sites exist. Formally, a channel is considered accessible for lithium motion if the sum of radii of a lithium ion and a framework atom does not exceed the channel radius more than by 10–15%.^[81] The TOPOS software allows to calculate channels and voids with the help of Voronoi-Dirichlet polyhedra. On the basis of such an analysis of the Li_2N_2 crystal structure (see Figure 3) it is clear that migration pathways in all three dimensions exist.

Interestingly, only two of the three crystallographic independent Li sites (Li2 and Li3) contribute to possible pathways, whereas Li1 is not free to leave its position (see Figure 3) and thus does not contribute to charge transport. This is due to the fact, that the Li1–N distance of 2.055(1) Å is the shortest of all Li–N distances (2.055–2.180(1) Å), whereby Li1 seems to be trapped at its crystallographic

site by $[\text{N}_2]^{2-}$ ions.^[22] Due to the limited resolution power of the static ^7Li NMR experiments, however, only a single, averaged activation energy can be resolved.

Temperature-Dependent Self-Diffusion Coefficients

In case of an material with a single Li site only the inverse correlation time τ_c^{-1} corresponds to the Li^+ jump rate, which allows for an estimate of the self-diffusion coefficient $D(T)$ of the Li ions according to the Einstein–Smoluchowski relation:^[82,83]

$$D(T) = \frac{l^2}{2d\tau_c} \quad (7)$$

We use this equation to obtain a crude estimate for the self-diffusion of lithium diazenide. To this end we assume an average jump length l for the lithium ions between Li sites exists, which contribute to ionic conduction (see SI Figure S4). In addition, each Li^+ jump is assumed to have the same activation energy, which is actually supposed to vary concerning the topostructural analysis. With $l = 2.25(1) \text{ \AA}$ and three-dimensional lithium migration ($d = 3$), the calculated self-diffusion coefficients for lithium motion according to the single fit of SLR rates are of the order of 10^{-14} to $10^{-12} \text{ m}^2/\text{s}$ within the corresponding Li^+ ion conductive temperature range. As-obtained self-diffusion coefficients are approximately within the range of typical cathode and electrolyte materials for Li-ion batteries ($\text{LiCoO}_2 \sim 10^{-16} \text{ m}^2/\text{s}$, $\text{LiBF}_4 \sim 10^{-13} \text{ m}^2/\text{s}$, $(\text{Li}_2\text{S})_7(\text{P}_2\text{S}_5)_3 \sim 10^{-12} \text{ m}^2/\text{s}$).^[84–86]

4.1.4 CONCLUSION

With our experimental study of the unsettled electronic behavior of diazenide compounds, we have shown that alkaline earth diazenides are of true metallic nature. For Li_2N_2 the electrical conductivity, unusually, has both electronic and ionic contributions, especially in the high temperature regime. Our investigations concerning lithium ionic conductivity in Li_2N_2 reveal that lithium diazenide is a potential 3D ionic conductor with high Li self-diffusion coefficients. Analysis of spin-lattice relaxation data from ^6Li and ^7Li NMR experiments is consistent with contributions from different relaxational mechanisms, namely an electronic contribution describable with the Korringa equation and an ionic contribution of dipolar origin.

4.1.5 BIBLIOGRAPHY

Acknowledgment

The authors would like to thank Prof. Dirk Johrendt (LMU Munich) for providing the equipment for the conductivity measurements, as well as Dr. Thomas Bräuniger and Christian Minke for technical support with the NMR spectrometer (both LMU Munich). The authors also gratefully acknowledge financial support from the Fonds der Chemischen Industrie (FCI) and the Deutsche Forschungsgemeinschaft (DFG), project SCHN 377/13-2.

References

- [1] G. Matoba, Patent No. JP-B 50010804, **1975**; G. Matoba, Patent No. JP-B 50010803, **1975**; H. Kobayashi, Patent No. JP-A 03006314, **1991**; T. Chokey, Patent No. JP 55094432, **1980**; H. Willners, Patent No. SE 115621, **1946**.
- [2] S.H. Jhi, J. Ihm, S.G. Louie, M.L. Cohen, *Nature* **1999**, 399, 132.
- [3] P.F. McMillan, *Nat. Mater.* **2002**, 1, 19.
- [4] T. Maruyama, T. Morishita, *Appl. Phys. Lett.* **1996**, 69, 890.
- [5] S. Yamanaka, K. Hotehama, H. Kawaji, *Nature* **1998**, 392, 580.
- [6] A. Zerr, G. Miehe, R. Böhler, *Nat. Mater.* **2003**, 2, 185.
- [7] M. Chhowalla, H.E. Unalan, *Nat. Mater.* **2005**, 4, 317.
- [8] A. Leineweber, H. Jacobs, S. Hull, *Inorg. Chem.* **2001**, 40, 5818.
- [9] Z.G. Wu, X.J. Chen, V.V. Struzhkin, R.E. Cohen, *Phys. Rev. B* **2005**, 71, 214103.
- [10] S. Pfirrmann, C. Herwig, R. Stößer, B. Ziemer, C. Limberg, *Angew. Chem.* **2009**, 121, 3407; *Angew. Chem., Int. Ed.* **2009**, 48, 3357.
- [11] P.J. Chirik, *Nat. Chem.* **2009**, 1, 520.
- [12] W.J. Evans, M. Fang, G. Zucchi, F. Furche, J.W. Ziller, R.M. Hoekstra, J.I. Zink, *J. Am. Chem. Soc.* **2009**, 131, 11195.

- [13] W. Kaim, B. Sarkar, *Angew. Chem.* **2009**, *121*, 9573; *Angew. Chem., Int. Ed.* **2009**, *48*, 9409.
- [14] W. Uhl, B. Rezaeirad, M. Layh, E. Hagemeyer, E.-U. Würthwein, N. Ghavtadze, I. Kuzu, *Chem. Eur. J.* **2010**, *16*, 12195.
- [15] J.D. Rinehart, M. Fang, W.J. Evans, J.R. Long, *Nat. Chem.* **2011**, *3*, 538.
- [16] J.H. Farnaby, M. Fang, J.W. Ziller, W.J. Evans, *Inorg. Chem.* **2012**, *51*, 11168.
- [17] G. Auffermann, Y. Prots, R. Kniep, *Angew. Chem.* **2001**, *113*, 565; *Angew. Chem., Int. Ed.* **2001**, *40*, 547.
- [18] G.V. Vajenine, G. Auffermann, Y. Prots, W. Schnelle, R.K. Kremer, A. Simon, R. Kniep, *Inorg. Chem.* **2001**, *40*, 4866.
- [19] G. Auffermann, U. Schmidt, B. Bayer, Y. Prots, R. Kniep, *Anal. Bioanal. Chem.* **2002**, *373*, 880.
- [20] G. Auffermann, R. Kniep, W. Bronger, *Z. Anorg. Allg. Chem.* **2006**, *632*, 565.
- [21] Y. Prots, G. Auffermann, M. Tovar, R. Kniep, *Angew. Chem.* **2002**, *114*, 2392; *Angew. Chem, Int. Ed.* **2002**, *41*, 2288.
- [22] S.B. Schneider, R. Frankovsky, W. Schnick, *Angew. Chem.* **2012**, *124*, 1909; *Angew. Chem., Int. Ed.* **2012**, *51*, 1873.
- [23] S.B. Schneider, R. Frankovsky, W. Schnick, *Inorg. Chem.* **2012**, *51*, 2366.
- [24] E. Gregoryanz, C. Sanloup, M. Somayazulu, J. Badro, G. Fiquet, H.-K. Mao, R.J. Hemely, *Nat. Mater.* **2004**, *3*, 294.
- [25] J. von Appen, M.-W. Lumey, R. Dronskowski, *Angew. Chem.* **2006**, *118*, 4472; *Angew. Chem., Int. Ed.* **2006**, *45*, 4365.
- [26] J.C. Crowhurst, A.F. Goncharov, B. Sadigh, C.L. Evans, P.G. Morrall, J.L. Ferreira, A.J. Nelson, *Science* **2006**, *311*, 1275.
- [27] A.F. Young, J.A. Montoya, C. Sanloup, M. Lazzeri, E. Gregoryanz, S. Scandolo, *Phys. Rev. B* **2006**, *73*, 153102.

- [28] J.A. Montoya, A.D. Hernandez, C. Sanloup, E. Gregoryanz, S. Scandolo, *Appl. Phys. Lett.* **2007**, *90*, 011909.
- [29] J.C. Crowhurst, A.F. Goncharov, B. Sadigh, J.M. Zaug, D. Aberg, Y. Meng, V.B. Prakapenka, *J. Mater. Res.* **2008**, *23*, 1.
- [30] Z.W. Chen, X.J. Guo, Z.Y. Liu, M.Z. Ma, Q. Jing, G. Li, X.Y. Zhang, L.X. Li, Q. Wang, Y.J. Tian, R.P. Liu, *Phys. Rev. B* **2007**, *75*, 054103.
- [31] R. Yu, Q. Zhan, L.C. De Jonghe, *Angew. Chem.* **2007**, *119*, 1154; *Angew. Chem., Int. Ed.* **2007**, *46*, 1136.
- [32] W. Chen, J.S. Tse, J.Z. Jiang, *J. Phys.: Condens. Matter.* **2010**, *22*, 015404.
- [33] M. Wessel, R. Dronskowski, *J. Am. Chem. Soc.* **2010**, *132*, 2421
- [34] M. Wessel, R. Dronskowski, *J. Comput. Chem.* **2010**, *31*, 1613.
- [35] U. Ruschewitz, *Coord. Chem. Rev.* **2003**, *244*, 115.
- [36] W. Kockelmann, U. Ruschewitz, *Angew. Chem.* **1999**, *111*, 3697; *Angew. Chem., Int. Ed.* **1999**, *38*, 3492.
- [37] S. Hemmersbach, B. Zibrowius, W. Kockelmann, U. Ruschewitz, *Chem. Eur. J.* **2001**, *7*, 1952.
- [38] J. Weidlein, U. Müller, K. Dehnicke, *Schwingungsspektroskopie—Eine Einführung*; Georg Thieme Verlag: Stuttgart, NY, **1982**.
- [39] M. Wessel, R. Dronskowski, *Chem. Eur. J.* **2011**, *17*, 2598.
- [40] M. Wessel, *PhD thesis*, RWTH Aachen University: Aachen, **2010**.
- [41] P. Knauth, *Solid State Ionics* **2009**, *180*, 911.
- [42] M. Park, X. Zhang, M. Chung, G.B. Less, A.M. Sastry, *J. Power Sources* **2010**, *195*, 7904.
- [43] Oudenhoven, J. F. M.; Baggetto, L.; Notten, P. H. L. *Adv. Energy Mater.* **2011**, *1*, 10.
- [44] P. Heitjans, S. Indris, *J. Phys.: Condens. Matter* **2003**, *15*, R1257.

- [45] C.P. Grey, N. Dupré, *Chem. Rev.* **2004**, *104*, 4493.
- [46] R. Böhmer, K.R. Jeffrey, M. Vogel, *Prog. Nucl. Magn. Reson. Spectrosc.* **2007**, *50*, 87.
- [47] B.A. Boukamp, R.A. Huggins, *Phys. Lett.* **1976**, *58A*, 231.
- [48] U. von Alpen, A. Rabenau, G.H. Talat, *Appl. Phys. Lett.* **1977**, *30*, 621.
- [49] Z. Wang, M. Gobet, V. Sarou-Kanian, D. Massiot, C. Bessada, M. Deschamps, *Phys. Chem. Chem. Phys.* **2012**, *14*, 13535.
- [50] M. Mali, J. Roos, M. Sonderegger, D. Brinkmann, P. Heitjans, *J. Phys. F: Met. Phys.* **1988**, *18*, 403.
- [51] A. Kuhn, S. Narayanan, L. Spencer, G. Goward, V. Thangadurai, M. Wilkening, *Phys. Rev. B* **2011**, *83*, 094302.
- [52] A. Kuhn, P. Sreeraj, R. Pöttgen, H.-D. Wiemhöfer, M. Wilkening, P. Heitjans, *J. Am. Chem. Soc.* **2011**, *133*, 11018.
- [53] B. Koch, M. Vogel, *Solid State Nucl. Magn. Reson.* **2008**, *34*, 37.
- [54] P. Ehrlich, H.-J. Seifert, G. Brauer, *Handbuch der Präparativen Anorganischen Chemie Vol. 2*; Ferdinand Enke Verlag: Stuttgart, **1978**.
- [55] P. Remy-Gennete, *Ann. Chim.* **1933**, *19*, 289.
- [56] H.D. Fair, R.F. Walker, *Energetic Materials Vol. 1: Physics and Chemistry of the Inorganic Azides*, Plenum Press: New York, **1977**.
- [57] D. Walker, M.A. Carpenter, C.M. Hitch, *Am. Mineral.* **1990**, *75*, 1020.
- [58] D. Walker, *Am. Mineral.* **1991**, *76*, 1092.
- [59] H. Huppertz, *Z. Kristallogr.* **2004**, *219*, 330.
- [60] D.C. Rubie, *Phase Transitions* **1999**, *68*, 431.
- [61] N. Kawai, S. Endo, *Rev. Sci. Instrum.* **1970**, *8*, 1178.
- [62] L.J. van-der-Pauw, *Philips Research Reports* **1958**, *13*, 1.

- [63] J.G. Powles, H. Strange, *Proc. Phys. Soc* **1963**, 6, 82.
- [64] The actual measurements have been performed with nonsintered pellets due to the observation that upon sintering using different conditions (temperatures, crucibles, atmospheres) always the beginning of hydrolysis of the pellets (white surrounding) was detected. Thus, the white hydroxide layer inhibits the contact of the inner-sphere diazenide to the electrodes making conductivity measurements impossible.
- [65] R.C. Weast, *Handbook of Chemistry and Physics*; CRC Press: Cleveland, OH, **1975**.
- [66] G.W.C. Kaye, T.H. Laby, *Tables of Physical and Chemical Constants*, 15th ed.; Longman: London, **1993**.
- [67] Upon variable temperature NMR measurements, the decomposition temperature of ${}^7\text{Li}_2\text{N}_2$ is found to be approximately 385 K due to a further sharp increase in inverse T_1 data. However, a corresponding NMR analysis of ${}^6\text{Li}_2\text{N}_2$ yields a decomposition temperature about 40 K lower. On the one hand, the divergence in decomposition temperature is referred to the limited data quality of ${}^6\text{Li}$ measurements, hindering a proper identification of the phase transition from Li_2N_2 to Li_3N . On the other hand, the synthesis of ${}^6\text{Li}_2\text{N}_2$ includes many more steps as compared to ${}^7\text{Li}_2\text{N}_2$ synthesis, whereby the final product ${}^6\text{Li}_2\text{N}_2$ might be afflicted with more side phases possibly changing the true decomposition temperature of ${}^6\text{Li}_2\text{N}_2$.
- [68] J.J. van der Klink, H.B. Brom, *Prog. Nucl. Magn. Reson. Spectrosc.* **2000**, 36, 89.
- [69] J. Korryng, *Physica*, **1950**, 16, 601.
- [70] Y.S. Avadhut, J. Weber, E. Hammarberg, C. Feldmann, J. Schmedt auf der Gönne, *Phys. Chem. Chem. Phys.* **2012**, 14, 11610.
- [71] C.P. Slichter, *Principles of Magnetic Resonance*; Springer-Verlag: Berlin, **1992**.
- [72] N. Bloembergen, E.M. Purcell, R.V. Pound, *Phys. Rev.* **1948**, 73, 679.
- [73] K. Arbi, M.A. París, J. Sanz *Dalton Trans.* **2011**, 40, 10195.
- [74] I. Solomon, *Phys. Rev.* **1955**, 99, 559.
- [75] C. León, M.L. Lucìa, J. Santamarià, M.A. París, J. Sanz, A. Várez, *Phys. Rev. B* **1996**, 54, 184.

- [76] J.L. Sudmeier, S.E. Anderson, J.S. Frye, *Concepts Magn. Reson.* **1990**, 2, 197.
- [77] R.K. Harris, E.D. Becker, S.M. Cabral de Menezes, R. Goodfellow, P. Granger, *Solid State Nucl. Mag.* **2002**, 22, 458.
- [78] V.A. Blatov, *IUCr Comp. Comm. Newsletter* **2006**, 7, 4.
- [79] V.A. Blatov, *Acta Crystallogr., Sect. A* **2000**, 56, 178.
- [80] V.A. Blatov, A.P. Shevchenko, V.N. Serezhkin, *J. Appl. Crystallogr.* **1999**, 32, 377.
- [81] V.A. Blatov, G.D. Ilyushin, O.A. Blatova, N.A. Anurova, A.K. Ivanov-Schits, L.N. Dem'yanets, *Acta Crystallogr., Sect. B* **2006**, B62, 1010.
- [82] A. Einstein, *Ann. Phys.* **1905**, 17, 549.
- [83] M. von Smoluchowski, *Ann. Phys.* **1906**, 21, 756.
- [84] Y.I. Jang, B.J. Neudecker, N.J. Dudney, *Electrochem. Solid-State Lett.* **2001**, 4, A74.
- [85] T.-Y. Wu, L. Hao, C.-W. Kuo, Y.-C. Lin, S.-G. Su, P.-L. Kuo, I.-W. Sun, *Int. J. Electrochem. Sci.* **2012**, 7, 2047.
- [86] K. Hayamizu, Y. Aihara, *Solid State Ionics* **2013**, 238, 7.

4.2 HIGH-PRESSURE BEHAVIOR OF BINARY DIAZENIDES

The effect of pressure on the structural and mechano-physical properties of binary diazenides has been examined *in situ* at the *European Synchrotron Radiation Facility (ESRF, Grenoble, France)* in diamond-anvil cells at room temperature. The results of these investigations are presented in the following chapter.

4.2.1 INTRODUCTION

The most common homonuclear diatomic anion with carbon is the acetylenide $[C_2]^{2-}$ with a $C\equiv C$ triple bond representing deprotonated acetylene C_2H_2 . The first synthesis of the most prominent member of this class of materials, namely CaC_2 ($I4/mmm$, no. 139), goes back to the year 1890.^[1] In the first structural investigation a body centered tetragonal unit-cell was found,^[2] which was confirmed later on by neutron powder and X-ray single crystal diffraction experiments, thereby referred to as CaC_2 -I structure-type.^[3,4] Although the main structural aspects of binary to even quaternary acetylenides have been long established, their crystal structures have been characterized in more detail only a few years ago.^[5-7] Thus, structural transformations in alkali and alkaline earth acetylenides were studied as a function of temperature and revealed the stability ranges of an enormous diversity of further low- and high-temperature phases with $M_{A,2}C_2$ and $M_{AE}C_2$ stoichiometry ($M_{A/AE}$ = alkali or alkaline earth metals).

While temperature-dependent structural phase-transitions have been observed for several binary acetylenides,^[5-7] the effect of pressure on the crystal structures with homonuclear dimeric anions has not been investigated thoroughly despite a few experimental exceptions. Thereby, it has only been shown for LaC_2 ,^[8] UC_2 ,^[9] CaC_2 ,^[10] BaC_2 ^[11] and Li_2C_2 ^[10] that at high-pressure conditions the structural variability of homonuclear dimeric compounds is even enlarged. Note that except for Li_2C_2 ($Immm$, no. 71, Rb_2O_2 -type), as-investigated acetylenides crystallize in the CaC_2 -I-type structure at ambient conditions. Upon *in situ* high-pressure studies, acetylenides transform into well established crystal structures, which have already been observed in temperature-dependent investigations,^[5-8] but also yet unidentified and unprecedented crystal structures are observed upon HP-investigations.^[9-11]

Recently, also the structural and vibrational behavior of barium peroxide, BaO_2 at high pressures has been reported, which crystallizes at ambient conditions also in the CaC_2 -I-type structure.^[12] These experiments represent the first HP-investigations of compounds with homonuclear dimeric oxygen anions, namely $[\text{O}_2]^{2-}$ ions. Again, the crystal chemistry of structures with homonuclear dianions could be enriched by these findings.

Interestingly, at very high pressures of 20–30 GPa, yet unidentified high-pressure phases might even constitute polymeric anionic structural motifs such as graphitic layers or sulfidic chains of homonuclear atoms as considered for CaC_2 , BaC_2 , Li_2C_2 and BaO_2 .^[10–13]

In addition, besides the identification and structural characterization of novel high-pressure phases, mechano-physical properties such as the bulk modulus of investigated ambient and high-pressure phases could be obtained supporting a further insight into the crystal chemistry of homonuclear dimeric anions.^[8–12]

As no *in situ* high-pressure experiments for alkaline earth diazenides $M_{\text{AE}}\text{N}_2$ ($M_{\text{AE}} = \text{Ca–Ba}$) and Li_2N_2 have been conducted up to date, and as corresponding investigations for acetylenides and peroxides already revealed interesting observations, we targeted the structural and mechano-physical characterization of $[\text{N}_2]^{2-}$ ion containing compounds at *in situ* high-pressure conditions for the first time at the *European Synchrotron Radiation Facility* (*ESRF*, Grenoble, France). The results of as-obtained data are presented in the following chapters.

4.2.2 EXPERIMENTAL SECTION

In situ High-Pressure X-Ray Powder Diffraction

In situ powder X-ray diffraction experiments at high pressure for CaN_2 , SrN_2 and Li_2N_2 were carried out on beamline ID27 at the *ESRF*.^[14] Membrane driven diamond-anvil cells equipped with 150- (CaN_2) and 250- μm (SrN_2 and Li_2N_2) culet diamonds and rhenium gaskets were used with an automated pressure drive.^[15] The gaskets were pre-indented to 40 μm and 70- (CaN_2) and 120- μm holes (SrN_2 and Li_2N_2) working as a sample chamber were drilled into the gasket using a Nd:YAG laser. Helium (gas loading) served as the pressure transmitting medium (PTM) for the investigations of CaN_2 and SrN_2 , whereas no PTM at all was used for Li_2N_2 . The pre-synthesized samples^[16,17] were loaded onto a bedding of three ruby spheres. As the diazenides are extremely sensitive to moisture, the entire loading procedure had to be

performed in an argon filled glovebox (Unilab, MBraun, Garching; $O_2 < 1$ ppm, $H_2O < 1$ ppm). The pressure was determined by the ruby fluorescence scale according to the calibration (Ne) described by *Mao et al.*^[18] For the high-pressure experiment monochromatic radiation with a wavelength of $\lambda = 0.3738 \text{ \AA}$ ($E = 55.04 \text{ keV}$) was selected. The beam was focused on a $3 \times 3 \mu\text{m}^2$ area and diffraction images were collected at pressures ranging from about 0.2 to 50 GPa. The pressure at each diffraction image was measured before and after the data collection and averaged to its final value. Diffracted intensities were recorded with a MAR165 CCD detector. Exposure time was typically 10 to 60 seconds, depending on saturation of the detector. To average on texture and strain effects for selected images, the cell was oscillated in general by $\pm 5^\circ$ relative to the beam. A precise calibration of the detector parameters was performed with LaB_6 powder as reference material. The diffraction images were processed and integrated using the program Fit2D.^[19] Individual single diffraction spots from the diamond-anvils were masked manually and excluded from integration. All attempts to record the high-pressure behavior of BaN_2 failed as it hydrolyzed immediately once it touched the diamond-anvils.

Rietveld refinement for investigated diazenides was performed with the TOPAS package.^[20] The crystallographic data at ambient conditions^[16,17] were taken as starting values for stepwise Rietveld refinement up to higher pressures. The reflection profiles were determined using the fundamental parameters approach^[21] by convolution of appropriate source emission profiles with axial instrument contributions and crystalline microstructure effects. Preferred orientation of the crystallites was described with a spherical harmonics function of 8th order. For each investigated diazenides at least one structural phase-transition at high-pressure conditions was observed. However, due to an extreme peak broadening observed for all diazenides at high pressures an unambiguous indexing of as-obtained diffraction patterns was not possible. Thus, structure solutions did not yield a satisfactory model for the high-pressure phases.

Equation of state

The isothermal bulk modulus B_0 and its pressure derivative B' for CaN_2 , SrN_2 and Li_2N_2 were obtained from fits of a second- and third-order Birch–Murnaghan (BM) equation of state (EoS)^[22,23] to the p – V data at 298 K:

$$p = 3B_0f(1 + 2f)^{\frac{5}{2}}[1 + \frac{3}{2}(B' - 4)f] \quad (1)$$

$$\text{where } f = \frac{\left(\frac{V}{V_0}\right)^{-\frac{2}{3}} - 1}{2} \quad (2)$$

represents the Eulerian strain, where V_0 is the volume at zero pressure, so

$$p = \frac{3}{2} B_0 \left[\left(\frac{V}{V_0}\right)^{-\frac{7}{3}} - \left(\frac{V}{V_0}\right)^{-\frac{5}{3}} \right] \left[1 - \frac{3}{4} (4 - B') \left[\left(\frac{V}{V_0}\right)^{-\frac{2}{3}} - 1 \right] \right] \quad (3)$$

For B' fixed to 4, the second-order BM-EoS is obtained. To check the quality of the EoS fit, the BM-EoS was also expressed in terms of the Eulerian strain f and the normalized pressure F :

$$F = \frac{p}{3f(1+2f)^{\frac{5}{2}}} \quad (4)$$

The compression data are therefore additionally presented in a $F(f)$ -plot,^[24] where the intercept with the F -axis yields B_0 , whereas the slope is $3 \times B_0(B' - 4)/2$ and thus provides B' :

$$F = B_0 + \frac{[3B_0(B' - 4)f]}{2} \quad (5)$$

The $F(f)$ form of representation of the p - V data is very sensitive to scattering of data and to experimental uncertainties as the bulk modulus and its first pressure derivative are obtained by a linear fit.^[23] All expressions of B_0 and B' , the second- and third-order BM-EoS fits and the $F(f)$ -plot calculations were done using the software Origin.^[25] For all calculations the error in pressure was set to 0.5 GPa.

4.2.3 RESULTS AND DISCUSSION

High-Pressure Behavior of CaN₂ and SrN₂

In general, both CaN₂ and SrN₂ transform into yet unknown high-pressure polymorphs (see Figures 1 and 2, respectively). For CaN₂, the phase transition starts at 14.7 GPa and is completed at about 17 GPa as the intensity of reflections of ambient CaN₂ continuously diminishes and additional reflections appear (see Figure 1a and 1b as well as Table 1). The high-pressure polymorph of CaN₂ remains stable up to the maximum applied pressure of

41.8 GPa. Diffraction patterns upon further decompression to 15.2 GPa still indicate the presence of the high-pressure phase.

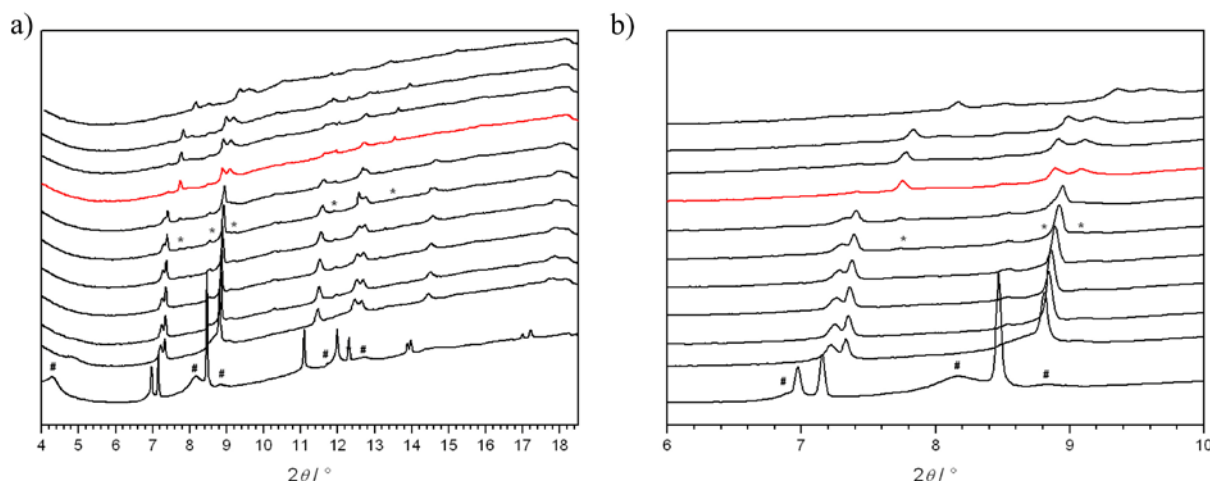


Figure 1. Diffraction patterns at various pressures illustrating the phase transition from ambient CaN_2 to a yet unknown high-pressure polymorph starting at 14.7 GPa (asterisks) and completed at 17.1 GPa (red). The pressure increases from 0.4 GPa (bottom) to an applied maximum of 41.8 GPa (top). Rhombs indicate the reflection profile of Ca(OH)_2 which originates from the hydrolysis of CaN_2 . To better illustrate the phase transition, the corresponding diffraction patterns in a) are depicted in b) from only 6 to 10° 2θ .

Ambient SrN_2 starts to transform into a high-pressure polymorph at 25.2 GPa as additional reflections emerge, which continuously gain intensity while the reflections of ambient SrN_2 disappear upon further pressure increase (see Figure 2a and 2b as well as Table 1). The pressure-induced phase transition is completed at approximately 32 GPa and no further transformation is observed up to the maximum applied pressure of 53.4 GPa. Upon decompression to 6.4 GPa, ambient SrN_2 could be recovered, indicating a reversible high-pressure phase transition. For both experiments, a further decompression to ambient conditions was not possible due to a mechanic defect of the diamond-anvil cell.

Interestingly, if diffraction profiles of both high-pressure phases are compared to each other, yet unidentified crystal structures of both polymorphs might be isotypic with each other (see Figure 3) due to a similar reflection profile. On the one hand, this is not surprising as both diazenides crystallize at ambient conditions in the same crystal structure which is of CaC_2 -I-type and therefore might behave similar upon extreme conditions. On the other hand, as recent *in situ* high-pressure investigations of CaC_2 -I-type structures with $[\text{C}_2]^{2-}$ and $[\text{O}_2]^{2-}$ ions already revealed, a variety of complex, unprecedented and different crystal structures were obtained.^[8–13] However, due to the low intense and extremely broad reflections of both

high-pressure polymorphs, especially those of HP-CaN₂, the identification of their crystal structures remains an open question (see next section).

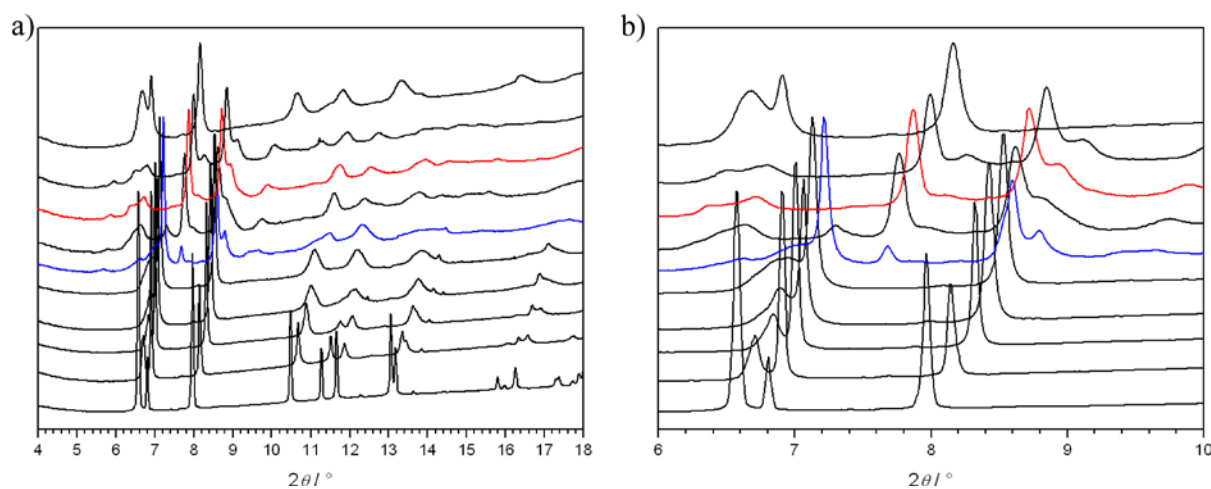


Figure 2. Diffraction patterns at various pressures illustrating the phase transition from ambient SrN₂ to a yet unknown high-pressure polymorph starting at 25.2 GPa (blue) and completed at 31.8 GPa (red). The pressure increases from 0.4 GPa (bottom) to an applied maximum of 53.4 GPa (top). To better illustrate the phase transition, the corresponding diffraction patterns in a) are depicted in b) from only 6 to 10° 2 θ .

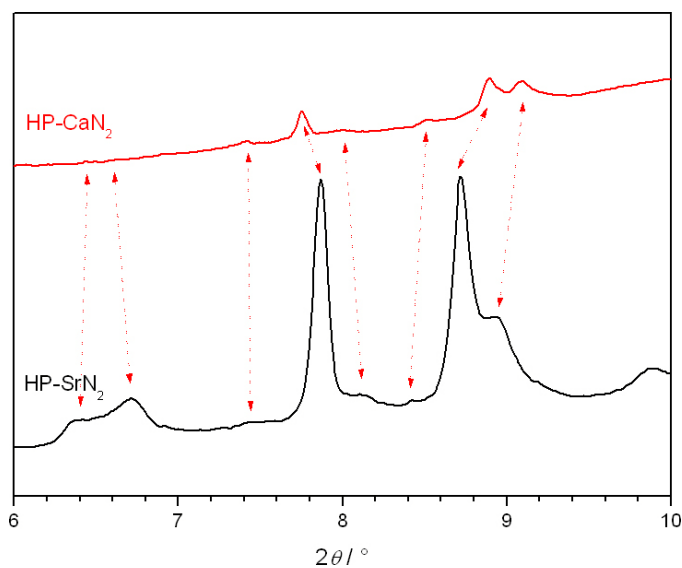


Figure 3. Diffraction patterns of HP-CaN₂ at 17.1 GPa (red) and of HP-SrN₂ at 40.2 GPa (black). With respect to the shift in 2 θ and the low intensity of reflections of the diffraction pattern of HP-CaN₂, both high-pressure phases might be isotypic with each other as they show the same basic reflection profiles.

High-Pressure Behavior of Li₂N₂

Li₂N₂ transforms into two yet unknown high-pressure polymorphs, thereby referred to as β - and γ -Li₂N₂ (see Figure 4). Ambient Li₂N₂ starts to transform into β -Li₂N₂ at 6.8 GPa as additional reflections emerge, which continuously gain intensity while the reflections of

ambient Li_2N_2 disappear upon further pressure increase (see Figure 4a and Table 1). The completion pressure of the pressure-induced phase transition is found to be 13.2 GPa as the reflection profile contains no more reflections of ambient Li_2N_2 . Upon further pressure increase, a second phase

Table 1. Starting and Final Pressure of the Phase Transition Observed for CaN_2 , SrN_2 and Li_2N_2 .

Phase transition	$p(\text{start})$ / GPa	$p(\text{final})$ / GPa
ambient $\text{CaN}_2 \rightarrow \text{HP-CaN}_2$	14.7	~17
ambient $\text{SrN}_2 \rightarrow \text{HP-SrN}_2$	25.2	~32
ambient $\text{Li}_2\text{N}_2 \rightarrow \beta\text{-Li}_2\text{N}_2$	6.8	13.2
$\beta\text{-Li}_2\text{N}_2 \rightarrow \gamma\text{-Li}_2\text{N}_2$	19.3	~30

transition from $\beta\text{-Li}_2\text{N}_2$ into $\gamma\text{-Li}_2\text{N}_2$ is observed (see Figure 4b and Table 1). The transformation starts at 19.3 GPa and is completed at pressures around 30 GPa. However, the true identification of the completion pressure is hindered due to the fact that the first visible reflection of $\beta\text{-Li}_2\text{N}_2$ at about $6^\circ 2\theta$ still is part of the reflection profile of $\gamma\text{-Li}_2\text{N}_2$. Thus it is the especially the reflection profile of $\beta\text{-Li}_2\text{N}_2$ at about $8\text{--}9^\circ 2\theta$, which continuously changes at up to around 30 GPa, that enables a rough determination of the final transformation pressure. Up to the maximum applied pressure of 45.4 GPa no further pressure-induced phase transition is observed. Decompression data show that all phase transitions are reversible. Thereby, the $\gamma\text{-}\beta$ re-transformation is complemented at 11.4 GPa. The final diffraction pattern upon decompression obtained for the lowest accessible pressure at 9.4 GPa shows the presence of $\beta\text{-Li}_2\text{N}_2$ and the ambient pressure phase. Decompression to ambient conditions was not possible due to a mechanic defect of the diamond-anvil cell.

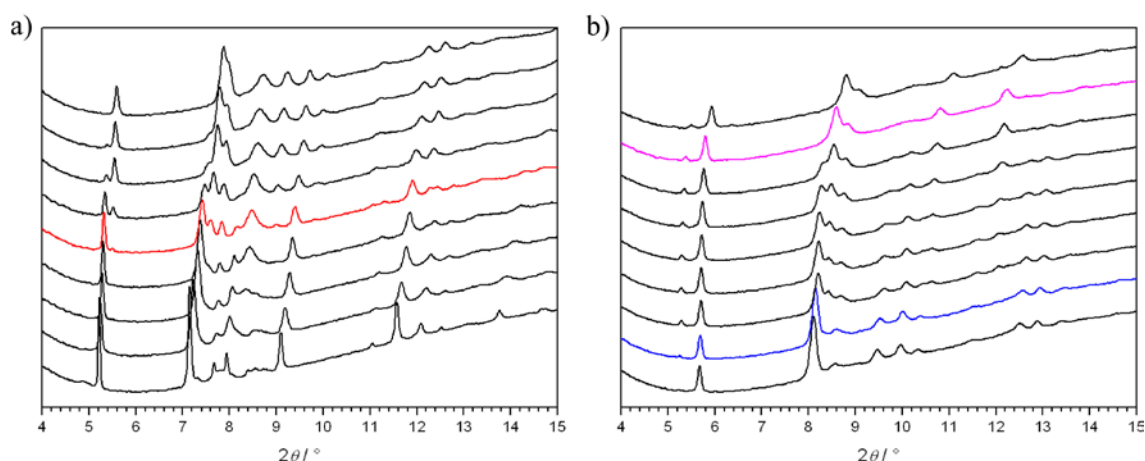


Figure 4. a) Diffraction patterns at various pressures illustrating the phase transition from ambient Li_2N_2 (bottom, 0.2 GPa) to a yet unknown high-pressure polymorph, referred to as $\beta\text{-Li}_2\text{N}_2$ starting at 6.8 GPa (red) and completed at 13.2 GPa (top). b) Diffraction patterns at various pressures illustrating the phase transition from $\beta\text{-Li}_2\text{N}_2$ (bottom, 17.9 GPa) to a second high-pressure polymorph, named $\gamma\text{-Li}_2\text{N}_2$ starting at 19.3 GPa (blue) and completed at 30.4 GPa (magenta).

Attempts of Crystal Structure Solutions

An unambiguous identification of the crystal structures of HP-CaN₂, HP-SrN₂ as well as of β - and γ -Li₂N₂ was extremely impeded as indexing and subsequent structure solutions always resulted in a complex variety of different hypothetical models, which could not be fitted to experimental data. This was due to the very broad and low intense reflection profiles of diffraction patterns of as-obtained high-pressure polymorphs inhibiting the true identification of reflection singlets or multiplets. As no distinct structural models could be obtained, the question arises whether the change in the diffraction patterns is due to pressure-induced phase transitions or due to decomposition of ambient diazenides. However, as no decomposition products (elements, nitrides, subnitrides) could be identified upon high-pressure conditions and due to the reversibility of the phase transitions, the presence of high-pressure polymorphs of CaN₂, SrN₂ and Li₂N₂ seems probable.

In addition, for the high-pressure polymorphs of $M_{\text{AE}}\text{N}_2$ diazenides the corresponding diffraction profiles were compared to those of well characterized crystal structures with homonuclear dianions^[5-7,26-30] but were not consistent or at least similar with those. Recent *in situ* investigations of the high-pressure behavior of as-mentioned CaC₂-I-type structures^[9-12] did also not result in structural hints for the crystal structure solution of HP-CaN₂ and HP-SrN₂. Finally, experimental diffraction profiles of the high-pressure polymorphs were compared to recently predicted promising structural candidates,^[31] but again no analogy was observed.

For the high-pressure polymorphs of Li₂N₂, a systematic search of matching diffraction profiles of well characterized A_2B_2 ($A = \text{alkali metal}, B = \text{C, O}$) structure types^[5,26-30] as well as of predicted Na_{*n*}N₂ ($n = 2, 6$) diazenides^[32] did also not succeed in the crystal structure determination of β - and γ -Li₂N₂.

Furthermore, the diffraction patterns of HP-CaN₂, HP-SrN₂ as well as of β - and γ -Li₂N₂ do not agree with corresponding patterns of recently considered and predicted polymeric crystal structures in lithium and calcium acetylenides observed upon high-pressure conditions.^[10-13]

EoS Analysis and Structural Aspects of Ambient CaN₂ and SrN₂

To obtain appropriate lattice parameters and unit-cell volumes of the ambient pressure phases at high-pressure conditions, only those diffraction patterns were taken into account, in which

no high-pressure polymorph was observed. Thereby, the maximum pressure for the bulk moduli calculations was found to be 13.4 GPa for CaN_2 and 23.1 GPa for SrN_2 . Fits of a second- and third-order Birch-Murnaghan equation of state to the experimental p - V data are presented in the Supporting Information in Figure S1a and S1c (CaN_2) as well as in S1b and S1d (SrN_2) in the Supporting Information (see chapter 8.1.4). The corresponding linear fits of the $F(f)$ -plots are illustrated in Figure S1e (CaN_2) and S1f (SrN_2). The results of all fits are summarized in Table 2. For CaN_2 , the experimentally obtained bulk moduli for all fits range in between 89–115 GPa. However, the strong scattering and huge error bars of the data in the $F(f)$ plots and the deviation of the value of the first pressure derivative B' from 4 after fitting a BM-EoS of third-order to the experimental p - V data, might be a direct consequence of non-hydrostatic conditions and demand theoretical confirmation of the calculated bulk moduli. Within this context, *Kulkarni et al.* recently predicted the bulk modulus of ambient CaC_2 -I-type CaN_2 , which is roughly in the same range as experimental values and gives a bulk modulus of 81–82 GPa (PBE and GGA calculations, respectively).^[31] Therefore, the experimental bulk modulus can be considered as appropriate.

Since the differences in B_0 and B' for SrN_2 obtained from EoS analysis and the linear fit of the $F(f)$ -plot have the

Table 2. Bulk Moduli B_0 and First Pressure Derivatives B' of CaN_2 and SrN_2 Obtained from Second- and Third-Order Birch-Murnaghan EoS and Normalized Strain Fits to Experimental p - V data.

	BM 2 nd	BM 3 rd	Natural Strain 3 rd
CaN_2			
B_0 (GPa)	89(1)	106(2)	115(3)
B'	4 (fixed)	3(1)	2.7(4)
SrN_2			
B_0 (GPa)	78(2)	74(8)	81(1)
B'	4 (fixed)	4(1)	1.8(5)

same order of magnitude and range between 74 and 81 GPa, the EoS fit of SrN_2 can be considered of good quality, especially as the experimental values are in good agreement with predicted ones (64 and 65 GPa).^[31,33] Interestingly, predicted bulk moduli for experimentally synthesized (Ca–Ba) and theoretical predicted (Be, Mg) alkaline earth diazenides follow a distinct trend, which is a steadily reduction of bulk moduli from the lighter to the heavier homologues.^[31,33] In our study, we obtained the first experimental data for bulk moduli of alkaline earth diazenides, which show the same trend as already theoretically observed, although representing in general higher values for bulk moduli.

As-obtained values are in the same range as observed for other binary compounds with homonuclear dianions crystallizing in the CaC_2 -I-type structure at ambient conditions (LaC_2 : 76 GPa^[8], BaO_2 : 105 GPa^[12]). Compared to noble metal pernitrides $M_{\text{NM}}\text{N}_2$ ($M_{\text{NM}} = \text{Os, Ir,}$

Pd, Pt) with $[\text{N}_2]^{4-}$ anions, which have bulk moduli of $B_0 > 250$ GPa, alkaline earth diazenides lack mechanical hardness.^[34–43] The higher hardness of the pernitrides is thereby attributed to the stiffer $[\text{N}_2]^{4-}$ anions consisting of completely filled π^* antibonding orbitals impeding a massive contraction of the N–N bonds.

Lattice parameters and unit-cell volumes of ambient CaN_2 and SrN_2 decrease with increasing pressure (see Figure S2 in the Supporting Information). Thereby, the unit-cell volumes shrink by about 12 (CaN_2) and 19 % (SrN_2) compared to the initial unit-cell volumes at zero pressure. Interestingly, also the N–N distances in both diazenides decrease continuously. For CaN_2 , up to the investigated pressure of 13.4 GPa, the d_{NN} decreases from 1.206(13) to 1.099(13) Å, which is about 9 % compared to the initial bond length. The interatomic distance in the diazenide units in SrN_2 shrinks for about 8 % from 1.231(19) to 1.141(23) Å up to 23.1 GPa. These observations are in good agreement with the predicted low stiffness of the $[\text{N}_2]^{2-}$ ions^[33] compared to the extremely inflexible pernitride anions. Hereby, the N–N distance of the latter ions is reported to change only within about 3 % up to 18 GPa compared to its initial distance at ambient pressure.^[42]

EoS Analysis of and Structural Aspects of Ambient Li_2N_2

To obtain correct lattice parameters and unit-cell volumes of the ambient Li_2N_2 at high-pressure conditions, only those diffraction patterns were taken into account, in which no high-pressure polymorph was detected. Thereby, the maximum pressure for the bulk modulus calculations was found to be 5.5 GPa. As the investigated maximum pressure is only at the lower border of true high-pressure conditions (below 10 GPa), we restricted to a second-order equation of state analysis. Fits of a second-order Birch-Murnaghan equation of state to the experimental p – V data are presented in Figure S3a. The corresponding linear fit of the $F(f)$ -plot is illustrated in Figure S3b. As-obtained bulk moduli of ambient Li_2N_2 are found to be 92(1) GPa with $B' = 4$ (fixed) using the second-order BM-EoS and 94(2) GPa with $B' = 3(2)$ if the $F(f)$ -plot is considered. Since the differences in B_0 and B' for Li_2N_2 obtained from EoS analysis and the linear fit of the $F(f)$ -plots are in the same range, the EoS fit of Li_2N_2 can be considered of high quality. The calculated bulk moduli of Li_2N_2 are in good agreement with the corresponding values of CaN_2 and SrN_2 , again revealing the low hardness of diazenides. In addition, both the rapidly decreasing unit-cell volume of about 5 % up to only 5.5 GPa compared to the unit-cell volume at zero pressure (see Figure 3c) as well as the shrinking N–N

distances of the diazenide units (1.3089(49) Å at ambient conditions; 1.193(70) Å at 5.5 GPa) further support this observation.

4.2.4 CONCLUSION

By *in situ* high-pressure experiments on $M_{\text{AE}}\text{N}_2$ ($M_{\text{AE}} = \text{Ca}$ and Sr) and Li_2N_2 in diamond-anvil cells, we were able to identify reversible, pressure-induced phase transitions from the ambient diazenide phases to overall four high-pressure polymorphs. However, due to stressed reflection profiles including very broad and low intense reflections, the identification of the crystal structures of these high-pressure polymorphs was hindered. Additionally, we were able to determine the bulk moduli and first pressure derivatives of the ambient pressure phases by fitting a second- and third-order BM-EoS to the experimental p - V data. These data were compared to the values obtained from an Eulerian strain versus normalized stress plot resulting in overall bulk moduli of 80–100 GPa for investigated diazenides. As-obtained values are in good agreement with previously reported bulk moduli of binary acetylenides or peroxides also crystallizing in the CaC_2 -I-type structure at ambient conditions. For CaN_2 and SrN_2 as-obtained bulk moduli perfectly match the predicted trend in alkaline earth diazenides. In addition, analyses of the behavior of N–N bond lengths of investigated diazenides at high-pressure conditions renders them far more compressible than pernitrides $[\text{N}_2]^{4-}$, in which the higher electron count is responsible for their extremely high hardness.

4.2.5 BIBLIOGRAPHY

- [1] C. Winkler, *Ber. Dtsch. Chem. Ges.* **1890**, 23, 2642.
- [2] a) M. v. Stackelberg, *Naturwissenschaften* **1930**, 18, 305; b) M. v. Stackelberg, *Z. Phys. Chem. Abt. B* **1930**, 9, 437.
- [3] M. Atoji, R. C. Medrud, *J. Chem. Phys.* **1959**, 31, 332.
- [4] O. Reckeweg, A. Baumann, H.A. Mayer, J. Glaser, H.-J. Meyer, *Z. Anorg. Allg. Chem.* **1999**, 625, 1686.
- [5] U. Ruschewitz, *Coord. Chem. Rev.* **2003**, 244, 115.

- [6] M. Knapp, U. Ruschwitz, *Chem. Eur. J.* **2001**, *7*, 874.
- [7] V. Vohn, W. Kockelmann, U. Ruschwitz, *J. Alloys Compd.* **1999**, *284*, 132.
- [8] X.Wang, I. Loa, K. Syassen, R.K. Kremer, A. Simon, M. Hanfland, K. Ahn, *Phys. Rev. B* **2005**, *72*, 064520.
- [9] J.-P. Dancausse, S. Heathman, U. Benedict, L. Gerward, J.S. Olsen, F. Hulliger, *J. Alloys Compd.* **1993**, *191*, 309.
- [10] J. Nylém, S. Konar, P. Lazor, D. Benson, U. Häussermann, *J. Chem. Phys.* **2012**, *137*, 224507.
- [11] I. Efthimiopoulos, K. Kunc, G.V. Vazhenin, E. Stavrou, K. Syassen, M. Hanfland, St. Liebig, U. Ruschwitz, *Phys. Rev. B.* **2012**, *85*, 054105.
- [12] I. Efthimiopoulos, K. Kunc, S. Karmakar, K. Syassen, M. Hanfland, G. Vajenine, *Phys. Rev. B* **2012**, *82*, 134125.
- [13] D. Benson, Y. Li, W. Luo, R. Ahuja, G. Svensson, U. Häussermann, *Inorg. Chem.* **2013**, *52*, 6402.
- [14] M. Mezouar, *J. Synchrotron Radiat.* **2005**, *12*, 659.
- [15] R. Letoullec, J.P. Pinceaux, P. Loubeyre, *High Pressure Res.* **1988**, *1*, 77.
- [16] S.B. Schneider, R. Frankovsky, W. Schnick, *Inorg. Chem.* **2012**, *51*, 2366.
- [17] S.B. Schneider, R. Frankovsky, W. Schnick *Angew. Chem.* **2012**, *124*, 1909; *Angew. Chem., Int. Ed.* **2012**, *51*, 1873
- [18] H.-K. Mao, J. Xu, M.J. Bell, *Geophys. Res.* **1986**, *91*, 4673.
- [19] A.P. Hammersley, S.O. Svensson, M. Hanfland, A.N. Fitch, D. Hausermann, *High Pressure Res.* **1996**, *14*, 235.
- [20] A.A. Coelho, *TOPAS-Academic*, Version 4.1, Coelho Software, Brisbane, **2007**.
- [21] J. Bergmann, R. Kleberg, A. Haase, B. Breidenstein, *Mater. Sci. Forum* **2000**, *303*, 347.
- [22] F. Birch, *Phys. Rev.* **1947**, *71*, 809.

- [23] F. Murnaghan, *Proc. Natl. Acad. Sci. USA* **1944**, 30, 244.
- [24] D.L. Heinz, R. Jeanloz, *J. Appl. Phys.* **1984**, 55, 885.
- [25] Origin 6.1, v6.1052 (B232), OriginLab Corporation, **2000**.
- [26] A.F. Holleman, E. Wiberg, *Lehrbuch der Anorganischen Chemie*, Vol. 102, de Gruyter: Berlin-New York, **2007**.
- [27] N.G. Vannerberg, *Prog. Inorg. Chem.* **1962**, 4, 125.
- [28] I.I. Vol'nov, *Peroxides, Superoxides and Ozonides of Alkali and Alkaline Earth Metals*, Vol. II, Plenum Press: New York, **1966**.
- [29] W. Hesse, M. Jansen, W. Schnick, *Prog. Solid State Chem.* **1989**, 19, 47.
- [30] D.H. Lohmann, N. Bartlett, *Proc. Chem. Soc.* **1962**, 115, 5253.
- [31] A. Kulkarni, J.C. Schön, K. Doll, M. Jansen, *Chem. Asian J.* **2013**, 8, 743.
- [32] X. Zhang, A. Zunger, G. Trimarchi, *J. Chem. Phys.* **2010**, 133, 194504.
- [33] M. Wessel, R. Dronskowski, *J. Comput. Chem.* **2010**, 31, 1613.
- [34] E. Gregoryanz, C. Sanloup, M. Somayazulu, J. Badro, G. Fiquet, H.-K.; Mao, R.J. Hemely, *Nat. Mater.* **2004**, 3, 294.
- [35] J. von Appen, M.-W. Lumey, R. Dronskowski, *Angew. Chem.* **2006**, 118, 4472; *Angew. Chem., Int. Ed.* **2006**, 45, 4365.
- [36] J.C. Crowhurst, A.F. Goncharov, B. Sadigh, C.L. Evans, P.G. Morrall, J.L. Ferreira, A.J. Nelson, *Science* **2006**, 311, 1275.
- [37] A.F. Young, J.A. Montoya, C. Sanloup, M. Lazzeri, E. Gregoryanz, S. Scandolo, *Phys. Rev. B* **2006**, 73, 153102.
- [38] J.A. Montoya, A.D. Hernandez, C. Sanloup, E. Gregoryanz, S. Scandolo, *Appl. Phys. Lett.* **2007**, 90, 011909.
- [39] J.C. Crowhurst, A.F. Goncharov, B. Sadigh, J.M. Zaug, D. Aberg, Y. Meng, V.B. Prakapenka, *J. Mater. Res.* **2008**, 23, 1.

- [40] Z.W. Chen, X.J. Guo, Z.Y. Liu, M.Z. Ma, Q. Jing, G. Li, X.Y. Zhang, L.X. Li, Q. Wang, Y.J. Tian, R.P. Liu, *Phys. Rev. B* **2007**, 75, 054103.
- [41] R. Yu, Q. Zhan, L.C. De Jonghe, *Angew. Chem.* **2007**, 119, 1154; *Angew. Chem., Int. Ed.* **2007**, 46, 1136.
- [42] W. Chen, J.S. Tse, J.Z. Jiang, *J. Phys.: Condens. Matter* **2010**, 22, 015404.
- [43] M. Wessel, R. Dronskowski, *J. Am. Chem. Soc.* **2010**, 132, 2421.

5. TERNARY DIAZENIDES

The controlled thermal decomposition of solely alkali *or* alkaline earth azides in a multianvil device under HP/HT-conditions has proven to be an excellent strategy in the synthesis of hitherto unknown binary diazenides with intriguing properties. The synthesis of even ternary diazenides has not yet been attempted, and thus was part within this thesis. If the combination of alkali *and* alkaline earth azides for the HP/HT-synthesis of even ternary diazenides was equally successful as for their famous binary representatives can be read in the following two chapters.

5.1. HIGH-PRESSURE SYNTHESIS AND CHARACTERIZATION OF $\text{Li}_2\text{Ca}_3[\text{N}_2]_3$ – AN UNCOMMON METALLIC DIAZENIDE WITH $[\text{N}_2]^{2-}$ IONS

Sebastian B. Schneider, Markus Seibald, Volker L. Deringer, Ralf P. Stoffel, Rainer Frankovsky, Gina M. Friederichs, Henryk Laqua, Viola Duppel, Gunnar Jeschke, Richard Dronskowski and Wolfgang Schnick

published in *J. Am. Chem. Soc.* **2013**, *135*, 16668

DOI: 10.1021/ja408816t

Copyright © 2013, American Chemical Society

<http://pubs.acs.org/doi/abs/10.1021/ja408816t>

ABSTRACT

Dinitrogen (N_2) ligation is a common and well-characterized structural motif in bioinorganic synthesis. In solid-state chemistry, on the other hand, homonuclear dinitrogen entities as structural building units proved existence only very recently. High-pressure/high-temperature (HP/HT) syntheses have afforded a number of binary diazenides and pernitrides with $[\text{N}_2]^{2-}$ and $[\text{N}_2]^{4-}$ ions, respectively. Here, we report on the HP/HT-synthesis of the first ternary diazenide. $\text{Li}_2\text{Ca}_3[\text{N}_2]_3$ (space group *Pmma*, no. 51, $a = 4.7747(1)$, $b = 13.9792(4)$, $c = 8.0718(4)$ Å, $Z = 4$, $wR_p = 0.08109$) was synthesized by controlled thermal decomposition of a stoichiometric mixture of lithium azide and calcium azide in a multianvil device under a pressure of 9 GPa at 1023 K. Powder X-ray diffraction analysis reveals strongly elongated N–N bond lengths of $d_{\text{NN}} = 1.34(2)–1.35(3)$ Å exceeding those of previously known, binary diazenides. In fact, the refined N–N distances in $\text{Li}_2\text{Ca}_3[\text{N}_2]_3$ would rather suggest the presence of $[\text{N}_2]^{3-}$ radical ions. Also, characteristic features of the N–N stretching vibration occur at lower wavenumbers ($1260–1020\text{ cm}^{-1}$) than in the binary phases, and these assignments are supported by first-principles phonon calculations. Ultimately, the true character of the N_2 entity in $\text{Li}_2\text{Ca}_3[\text{N}_2]_3$ is probed by a variety of complementary techniques, including electron diffraction, electron spin resonance spectroscopy (ESR), magnetic and electric conductivity measurements, as well as density-functional theory calculations (DFT). Unequivocally, the title compound is shown to be metallic containing diazenide $[\text{N}_2]^{2-}$ units according to the formula $(\text{Li}^+)_2(\text{Ca}^{2+})_3([\text{N}_2]^{2-})_3 \cdot (\text{e}^-)_2$.

5.1.1 INTRODUCTION

Among the most important processes in modern chemistry is the conversion of dinitrogen molecules (N_2) into environmentally sustainable intermediates or products. This process is referred to as “nitrogen fixation”. In industry, this process is named after its inventors *Fritz Haber* and *Carl Bosch*, the Haber–Bosch cycle,^[1] which offers rapid access to synthetic fertilizers and has become essential for the nutrition of a large amount of the world population. In nature, this enormously expensive and complex industrial process is replaced by the enzyme nitrogenase, whose crystal structure has been determined only recently.^[2] Nitrogenases can cleave the $N\equiv N$ triple bond already at ambient conditions and transform it into ammonia, which however consumes huge amounts of energy (adenosine triphosphate, ATP).^[3,4] Nitrogenase fixes atmospheric dinitrogen through an inimitable class of various metal clusters.^[2,5–9] However, despite detailed knowledge of these structural motifs, a basic mechanism for the biological process still lacks evidence. Hence, the activation and conversion of free N_2 to ammonia including the characterization of a diversity of intermediates with bound dinitrogen is one of the major challenges in bioinorganic and organo-metallic chemistry, to finally unravel nature’s mystery.^[10]

Synthetic nitrogen fixation focuses on the binding, activation, and reduction of N_2 on mono-, di-, and polynuclear transition metal centers coordinated by capacious steric ligands. Mono- and dinuclear transition metal complexes have long been known to activate dinitrogen in various ways: they enable protonation, reduction, functionalization, and even N–N bond cleavage steps. Besides a handful of examples of transition metal complexes with trapped and activated N_2 , up to date only two distinct classes of molybdenum- or tungsten- based model systems have emerged, involving a full set of well-defined intermediates, such as diazenido, hydrazido, nitrido, imido, amido, or amine intermediates, on the way from N_2 to NH_3 . These systems form the basis of the Chatt and the Schrock cycles.^[11,12]

However, true mimicry of the multielectron reduction process still proves difficult because both cycles explain the sequence of reactions involved in biological dinitrogen reduction, on the one hand, but only a low yield catalytic reaction is observed in one of those systems, on the other hand.^[11–23] The monometallic model systems of Chatt and Schrock cycles bind N_2 in an *end-on* manner and therefore lead to only weakly or moderately activated N_2 -intermediates, which might be the crucial factor for the absence of a catalytic reaction. The binding of N_2 in a *side-on* manner is usually accessed by homonuclear bimetallic complexes.

Common oxidation states for *side-on* bound N_2 when acting as a ligand are 0, $-II$ or $-IV$ representing non-activated dinitrogen(0), diazenido $[N_2]^{2-}$, or hydrazido $[N_2]^{4-}$ intermediates. This is not surprising as the dinitrogen ligand is reduced in multiples of two electrons, because each of the two metal atoms contributes either zero, one, or two electrons to nitrogen reduction. Odd-electron nitrogen oxidation states, instead, propose radical character and one-electron reduction mechanisms, but have not been observed in Chatt or Schrock cycles so far. However, this potential intermediacy of $[N_2]^{-}$ or $[N_2]^{3-}$ radical ions in metal complexes proved existence only very recently in dinuclear nickel, iron, and lanthanide complexes, respectively.^[10,24–33] Thereby, $[N_2]^{-}$ were found to exhibit N–N bond lengths of about 1.13–1.18 Å and N–N stretching frequencies of 1740–1950 cm^{-1} ,^[10,24–26,32,33] whereas the d_{NN} in $[N_2]^{3-}$ ions was found to be at 1.39–1.41 Å with shifted N–N stretching energies of below 1000 cm^{-1} .^[27–33] To gain final evidence for the presence of such radical anions $[N_2]^{-}$ or $[N_2]^{3-}$, electron spin resonance spectroscopy (ESR) revealed clearly visible signals in accordance with simulated spectra indicative of unpaired electrons and supporting the radical formulation of dinitrogen ligation.^[24,27,28]

Gauging “weakly” to “highly” activated systems is possible at the hand of N–N bond lengths and corresponding N–N stretching frequencies in spectroscopic studies of bound dinitrogen molecules or ions. For such purpose, reliable crystallographic and spectroscopic data for protonated reference compounds, such as diazene $HN=NH$ and hydrazine N_2H_4 , are required to facilitate the classification of even- and odd-electron nitrogen-oxidation states.

Surprisingly, given the importance of homonuclear dinitrogen anions in biological and organo-metallic chemistry, it was not before 2001 that such ions have been observed in solid-state chemistry for the first time.^[34–39] Pioneering works by *Kniep* et al. introduced the hitherto unknown compounds Sr_4N_3 ($\equiv Sr_8N_4[N_2] \cdot (e^-)_2$), SrN ($\equiv Sr_8N_4[N_2]_2$), SrN_2 , and BaN_2 , which are the first so-called diazenides with ionic $[N_2]^{2-}$ units. The latter show characteristic N–N bond lengths (1.22 Å) and stretching frequencies (1307 cm^{-1} in SrN_2 and 1380 cm^{-1} in SrN), which may be compared to protonated diazene N_2H_2 (1.21–1.25 Å, 1400–1700 cm^{-1}).^[34–45] Only 5 years later, high-pressure/high-temperature (HP/HT) experiments revealed the existence of noble metal compounds with MN_2 stoichiometry ($M = Os, Ir, Pd, \text{ and } Pt$) exhibiting ultrahigh hardness and bulk moduli of about 250–350 GPa.^[46–53] Theoretical investigations finally concluded the presence of tetravalent metals and $[N_2]^{4-}$ anions, with N–N bond lengths (about 1.40 Å) and stretching frequencies (700–1000 cm^{-1}) similar to those of hydrazine N_2H_4 ($d_{NN} = 1.47$ Å, $\tilde{\nu}_{NN} < 1000$ cm^{-1}).^[46–57]

The latter anions are isoelectronic with peroxides $[\text{O}_2]^{2-}$, and so they were dubbed “pernitrides”. In 2012, we were able to extend the compositional range of binary diazenides by subjecting ionic azides to HP/HT-conditions in a multianvil device.^[58,59] We succeeded in synthesizing SrN_2 and BaN_2 , as well as the unprecedented (but theoretically predicted) CaN_2 and also Li_2N_2 , the latter one representing the first alkali diazenide.^[58–61] Crystallographic, spectroscopic, and theoretical investigations confirmed the presence of $[\text{N}_2]^{2-}$ anions in these crystal structures.^[58,59] Only very recently, LaN_2 ($\equiv \text{La}^{3+}[\text{N}_2]^{2-}\cdot\text{e}^-$) proved existence in shockwave experiments in accord with theoretical predictions^[54,62] Again, crystallographic studies showed the presence of diazenide anions with slightly elongated N–N bonds (1.30–1.32 Å), possibly due to the metallic character of the crystalline host.

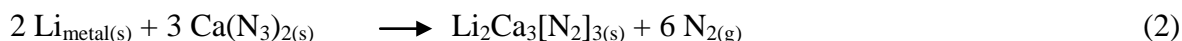
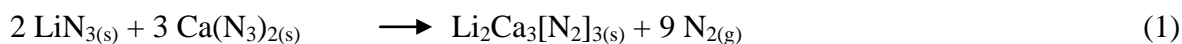
In summary, the recent success in identifying diazenides and pernitrides in solid-state chemistry has fueled various theoretical and synthetic efforts to predict and characterize further compounds containing dinitrogen anions. However, despite the as-mentioned examples, no further representatives of diazenides, pernitrides or even intermediate dinitrogen ions are known to date in ionic solids.

In this contribution, we present the successful synthesis and structural elucidation of $\text{Li}_2\text{Ca}_3[\text{N}_2]_3$, the first ternary compound with dinitrogen anions. Detailed crystallographic, spectroscopic, and theoretical studies at the respective state-of-the-art support the presence of solely $[\text{N}_2]^{2-}$ anions in the crystal structure. As we demonstrate, the title compound may be seen as the first ternary sub-diazenide with $(\text{Li}^+)_2(\text{Ca}^{2+})_3([\text{N}_2]^{2-})_3\cdot(\text{e}^-)_2$ formulation.

5.1.2 EXPERIMENTAL SECTION

Synthesis of $\text{Li}_2\text{Ca}_3[\text{N}_2]_3$

$\text{Li}_2\text{Ca}_3[\text{N}_2]_3$ was prepared under HP/HT-conditions in a modified Walker-type module in combination with a 1000 t press (Voggenreiter, Mainleus, Germany). As pressure medium, Cr_2O_3 doped (5 %) MgO-octahedra (Ceramic Substrates & Components, Isle of Wight, U.K.) with edge lengths of 18 mm (18/11 assembly) were employed. Eight tungsten carbide cubes (Hawedia, Marklkofen, Germany) with truncation edge lengths of 11 mm compressed the octahedron. $\text{Li}_2\text{Ca}_3[\text{N}_2]_3$ can be synthesized from two different stoichiometric mixtures of lithium and calcium azides according to equations 1 and 2. For a detailed description of the synthesis of both azides, see the Supporting Information.



The corresponding mixtures were carefully ground, filled into a cylindrical boron nitride crucible (Henze BNP GmbH, Kempten, Germany), and sealed with a fitting boron nitride plate. Details of the setup are described in the literature.^[63–67] The assembly was compressed to 9 GPa at room temperature within 213 min, then heated up to 1023 K in 10 min, kept at this temperature for 20 min and cooled to room temperature in 10 min again. Subsequently, the pressure was released over a period of 620 min. The recovered MgO-octahedron was broken apart in a glovebox (Unilab, MBraun, Garching; O₂ < 1 ppm, H₂O < 1 ppm), and the sample was carefully isolated from the surrounding boron nitride crucible. Besides a golden metallic powder of the title compound (see Figure S1 in the Supporting Information), which is very sensitive to moisture, small amounts of a red, but yet not identified side-phase were obtained.

Powder X-Ray Diffraction (PXRD)

For powder X-ray diffraction experiments, ground Li₂Ca₃[N₂]₃ was loaded into tube capillaries (Hilgenberg, Malsfeld, Germany) with diameters of 0.2–0.3 mm in a glovebox. Data were recorded with a STOE Stadi P powder diffractometer (STOE, Darmstadt, Germany) in Debye–Scherrer geometry using Ge(111) monochromated Cu and Mo K_{α1} radiation (1.54056 and 0.7093 Å) with a step size of 0.01°. Data acquisition was done using the STOE software (WinXPOW). The indexing, integration, and extraction of the intensities as well as the structure solution and Rietveld refinement were performed with the TOPAS package (see Figure 1).^[68]

The reflection profiles were determined using the fundamental parameter approach^[69] by convolution of appropriate source emission profiles with axial instrument contributions and crystalline microstructure effects. Preferred orientation of the crystallites was described with a spherical harmonic of fourth order. A search for potential higher symmetry obtained after structure solutions and Rietveld refinements was carried out using the program PLATON.^[70] The relevant crystallographic data for the title compound as well as further details of the data collection are summarized in Tables 1 and S1 in the Supporting Information. Further information of the crystal structure may be obtained from the Fachinformationszentrum

Karlsruhe, 76344 Eggenstein-Leopoldshafen, Germany (fax, (49) 7247-808-666; e-mail, crysdata@fiz-karlsruhe.de) on quoting the depository number CSD-426449.

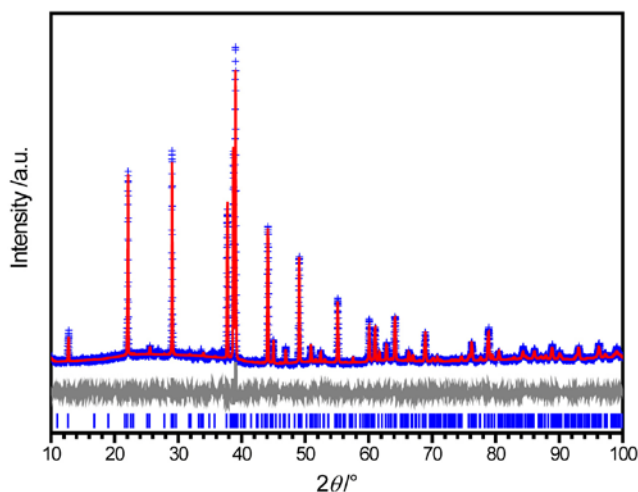


Figure 1. Observed (blue) and calculated (red) powder diffraction pattern (Cu $K_{\alpha 1}$ radiation, 1.54056 Å) and difference profile (gray) of the Rietveld refinement of $\text{Li}_2\text{Ca}_3[\text{N}_2]_3$. Peak positions are marked by vertical blue lines (bottom).

High-temperature *in situ* X-ray powder diffraction data were collected with a STOE Stadi P powder diffractometer (Mo $K_{\alpha 1}$ radiation (0.7093 Å)) equipped with a computer-controlled STOE resistance graphite furnace. Enclosed in a silica glass capillary under argon, the samples were heated from room temperature to 700 K at a rate of 5 K/min in steps of 25 K (see Figure S2 in the Supporting Information). At each heating step (after holding the temperature for 1 min), a diffraction pattern was recorded with an IP-PSD in the range of $2^\circ \leq 2\theta \leq 80^\circ$. At about 610 K, the sample decomposed spontaneously.

Low-temperature *in situ* X-ray powder diffraction data were collected in intervals of 5 K using a Huber G670 Guinier imaging plate diffractometer (Co $K_{\alpha 1}$ radiation (1.7890 Å)) equipped with a closed cycle He-cryostat. The samples were cooled down from room temperature to 10 K in 5 K/min. At each cooling step (after holding the temperature for 1 min), a diffraction pattern was recorded in the range of $10^\circ \leq 2\theta \leq 80^\circ$. No phase transition was observed.

Transmission Electron Microscopy (TEM)

All manipulations for the preparation and transfer of the sample were carried out under argon atmosphere. Data were recorded with a Philips CM30/ST (LaB₆ cathode) at 300 kV. Selected

area electron diffraction (SAED) as well as precession electron diffraction patterns (PED) were collected with a GATAN slow-scan CCD camera. Simulations of diffraction patterns were calculated with the EMS program package.^[71] Elemental analysis by EDX was performed with a Si/Li detector (Thermo Fischer, NSS). Tilt series of diffraction patterns were obtained using a double tilt sample holder with a maximum tilt angle of $\pm 25^\circ$.

Computational Details

Periodic density-functional theory (DFT) computations in the generalized gradient approximation of Perdew, Burke, and Ernzerhof (PBE)^[72] were done using the projector augmented-wave (PAW)^[73] method as implemented in the Vienna *ab initio* Simulation Package (VASP).^[74] The cutoff energy for the plane-wave expansion was set to 500 eV,

and the Brillouin zone was sampled on a dense Monkhorst–Pack mesh of reciprocal-space points.^[75] Electronic wave functions (crystal structures) were optimized until the energy difference between two iterative steps fell below 10^{-8} eV/cell (10^{-6} eV/cell), respectively.

Chemical-bonding analyses were performed by computing the crystal orbital Hamilton population (COHP),^[76] which allows one to identify bonding and antibonding contributions to the electronic band structure by weighting the off-site projected DOS with the corresponding Hamiltonian matrix elements (hence, negative COHP values denote stabilizing interactions). These computations were done for the previously optimized structures using the TB-LMTO-ASA program,^[77] version 4.7, as in our previous studies of diazenides.^[54,58–60] In this case, the local von Barth–Hedin exchange–correlation functional^[78] had to be employed to ensure

Table 1. Refined Atomic Coordinates and Isotropic Displacement Factors of $\text{Li}_2\text{Ca}_3[\text{N}_2]_3$.^a

atom (Wyckoff)	x	y	z	U_{iso} (0.01 Å ²) ^b
Li1 (4g)	0	0.346(2)	0	0.033(9)
Li2 (4h)	0	0.847(3)	½	0.02(1)
Ca1 (2e)	¼	0	0.697(1)	0.039(3)
Ca2 (2f)	¼	½	0.195(2)	0.042(4)
Ca3 (4k)	¼	0.1446(5)	0.164(1)	0.055(3)
Ca4 (4k)	¼	0.6435(5)	0.651(1)	0.057(3)
N1 (4k)	¼	0.177(1)	0.7043(9)	0.027(6)
N2 (4k)	¼	0.6656(8)	0.2002(9)	0.048(9)
N3 (4k)	¼	0.048(2)	0.410(4)	0.06(1)
N4 (4k)	¼	0.548(1)	0.91(3)	0.027(7)
N5 (4k)	¼	0.2860(8)	0.343(2)	0.026(5)
N6 (4k)	¼	0.803(1)	0.867(1)	0.04(1)

^aSpace group *Pmma* (no. 51), $a = 4.7747(1)$, $b = 13.9792(4)$, $c = 8.0718(4)$ Å, $Z = 4$.^b $U_{iso} = B_{eq}/(8 \cdot \pi^2)$.

convergence. Vibrational properties such as phonon densities of states were calculated by the *ab initio* force-constant method^[79] as implemented in the FROPHO code^[80] based on forces obtained from VASP.

Electron Spin Resonance Spectroscopy (ESR)

ESR measurements were carried out on powdered samples covering a temperature range of 10–525 K. For that, the sample was filled into a quartz Mark tube capillary (diameter 0.3 mm) and sealed under inert conditions. Low-temperature (ambient temperature to 10 K) continuous-wave (CW) ESR measurements at X-band frequencies were performed on three spectrometers: (a) on a Bruker Elexsys 500 CW ESR spectrometer equipped with a Bruker ER 4122 SHQ resonator with or without an Oxford Helium flow cryostat, (b) on a Bruker Elexsys 580 X-band CW/pulse ESR spectrometer equipped with a Bruker dielectric ENDOR resonator and an Oxford Helium flow cryostat, and (c) on a Magnetech MS 400 miniscope spectrometer equipped with a nitrogen flow cryostat. High-temperature (ambient temperature to 525 K) measurements were carried out on spectrometer (a). All measurements were properly calibrated and referenced to standards as detailed in the Supporting Information.

Fourier Transform Infrared Spectroscopy (FTIR)

Fourier transform infrared spectroscopy measurements were carried out on a Bruker FTIR-IS66 V-S spectrometer. Spectra of the samples were recorded at ambient conditions between 400 and 4000 cm^{-1} after the samples were diluted in dried KBr pellets under inert conditions.

Magnetic and Electric Conductivity Measurements

The magnetic measurements were performed on a Quantum Design MPMS XL5 SQUID magnetometer. Electric resistivity (and conductivity) were determined from a cold pressed (10 kN) pellet of nonsintered $\text{Li}_2\text{Ca}_3[\text{N}_2]_3$ (diameter 4.0 mm, thickness 1.28 mm) using the four-probe method. For the measurement, three batches of previously synthesized $\text{Li}_2\text{Ca}_3[\text{N}_2]_3$ had to be combined due to the small sample amount obtained upon one HP/HT-experiment. In addition, each product of synthesis was analyzed separately by means of powder X-ray diffraction to rely on a successful synthesis. The pellet was contacted with four equidistant probes using silver conducting paint. As the compound is very sensitive to moisture, all preparations had to be done in a glovebox. A current of 5.0 mA was applied and the potential

difference was measured as a function of temperature (3.5–300 K) yielding the resistivity. No superconductivity was observed.

5.1.3 RESULTS AND DISCUSSION

Unit-Cell Metrics

The unit-cell metrics was analyzed on the basis of powder X-ray diffraction (PXRD) and transmission electron microscopy (TEM) data. The indexing of PXRD patterns suggested a unit-cell with hexagonal metrics ($a = 8.06$, $c = 4.76$ Å). From systematic absences, as well as from the integration and extraction of the intensities, a first structural model in space group $P6_3/mcm$ (no. 193) was derived (see Figures S4–S6 in the Supporting Information). However, SAEDs with the hexagonal $[001]_{\text{hex}}$ zone axis of all investigated crystallites significantly differed from simulated ones (see Figure 2). Hereby, the experimental diffraction patterns of $[001]_{\text{hex}}$ zone axes contain additional reflections that suggest a doubling of the unit-cell axes a and b . Although simulated diffraction patterns of $[001]_{\text{hex}}$ zone axes of an isomorphic subgroup with $a' = 2a$ and $b' = 2b$ ($P6_3/mcm$, no. 193) would result in the experimentally observed diffraction profile, the simple doubling of the lattice parameters does *not* fit other zone axes due to a simulated, doubled spot density that is absent in the experimental diffraction patterns. Therefore, a simple doubling of the lattice parameters does not suffice to reconcile experimental and simulated diffraction patterns.

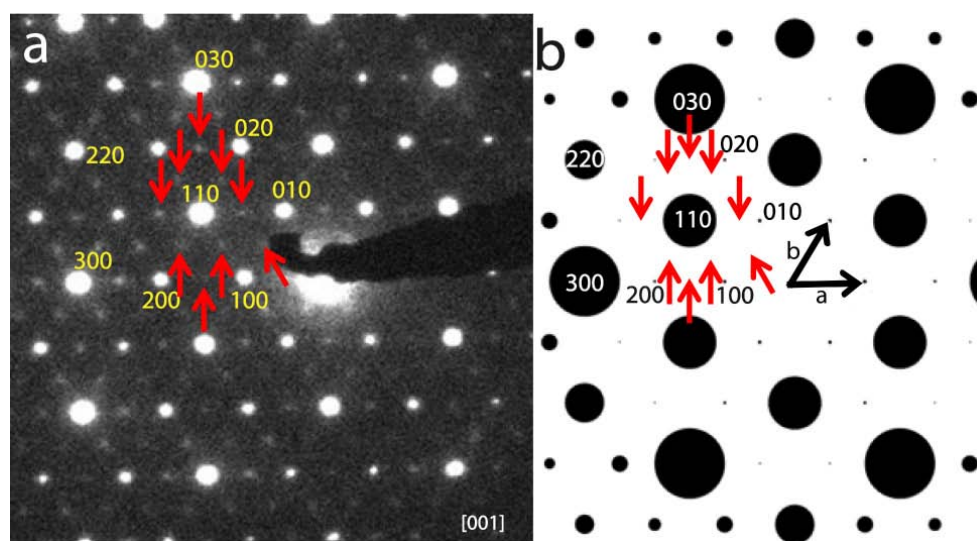


Figure 2. Experimental (a) and simulated (b, hexagonal model with $a = 8.06$, $c = 4.76$ Å) SAED pattern of $[001]_{\text{hex}}$ zone axis of hexagonal “LiCaN₂”. In the experimental SAED pattern, between each indexed spot, there are further residual spots (red arrows). According to the simulated SAED pattern, these additional reflections suggest a doubling of the unit-cell according to $a' = 2a$ and $b' = 2b$.

As it was not possible to describe all diffraction patterns with the obtained hexagonal model, reduction of symmetry was done referring to group–subgroup relations. A first *translationsgleich* reduction in symmetry of index 3 (structure model in hexagonal space group $P6_3/mcm$, no. 193) results in the orthorhombic space group $Cmcm$ (no. 63) with $a = 13.96$, $b = 8.06$, and $c = 4.76$ Å. The C -centering, however, still results in an extinction of reflections with $h+k = 2n+1$, and hence the simulated diffraction pattern of the $[001]$ zone axis in $Cmcm$ is similar to the one of the hexagonal model. Thus, the C -centering has to be omitted and the symmetry further reduced in a second step. This *klassengleich* symmetry reduction of index 2 into space group $Pmma$ (no. 51) finally results in an adequate model. The simulated diffraction pattern of the resulting $[100]_{\text{orth}}$ zone axis (former $[001]$ zone axes in $P6_3/mcm$ and $Cmcm$) matches the experimental reflection profile for the latter model by additional stepwise tilting by 120° around the origin of $[100]_{\text{orth}}$ zone axes quite well (see Figure 3) and indicates a $[100]_{\text{orth}}$ ($= [001]_{\text{hex}}$) stacked 3-fold twin.

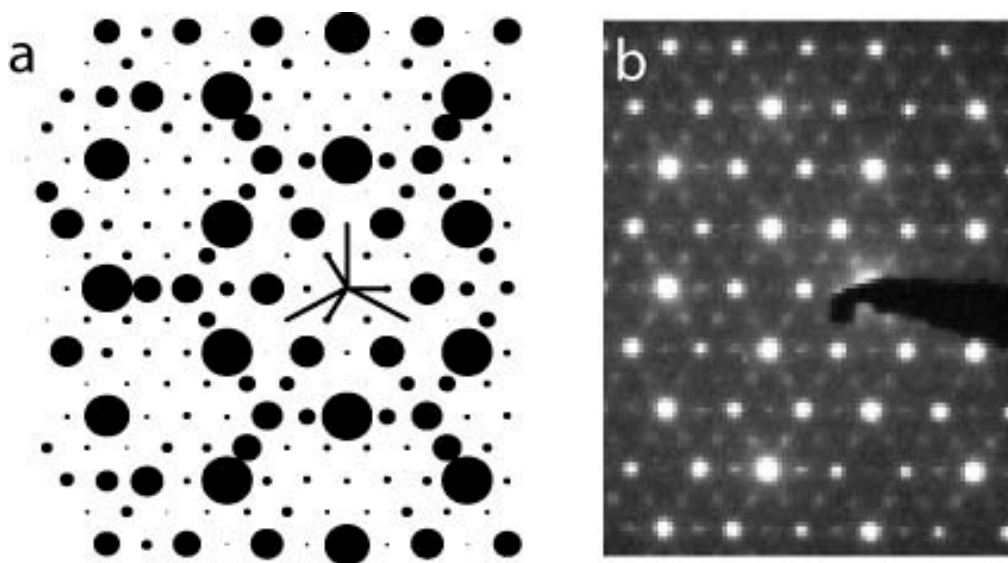


Figure 3. (a) Simulated SAED pattern of 3-fold twin by rotation in orthorhombic space group $Pmma$ (no. 51) obtained after stepwise tilting the simulated $[100]_{\text{orth}}$ pattern by 120° around the origin. (b) Experimental SAED pattern of former hexagonal $[001]_{\text{hex}}$ zone axis matching the diffraction profile of the 3-fold twin.

The latter, orthorhombic unit-cell metrics is supported by comparison of experimental SAED patterns to simulated ones; zone axes and lattice parameters have been obtained by transformations of the former hexagonal model (see the Supporting Information).

In addition, the theoretical positions of reflections of the as-obtained model are consistent with the experimentally observed positions in the corresponding PXRD patterns, resulting in

Pawley-fitted parameters of $a = 4.7747(1)$, $b = 13.9792(4)$, and $c = 8.0718(4)$ Å in space group $Pmma$ (no. 51). Note that as-investigated hexagonal and orthorhombic models mentioned in this section exhibit stoichiometric compositions of “LiCaN₂” diverging from elemental analysis which suggested lithium-deficiency (see the following sections).

Theoretical Considerations on the Hexagonal Model

The complex nature of the problem at hand called for a complementary quantum-theoretical analysis in search of the structure, and the first computations were performed for the initially assigned, hexagonal model with “LiCaN₂” composition ($P6_3/mcm$, see Supporting Information Figure S4). Surprisingly, at first sight, this structure showed pronounced instability during relaxation: the Hellmann–Feynman forces computed at temperature zero were enough to totally destroy the Li–Ca coordination environment. Moreover, phonon computations characterize this structure as dynamically unstable, proven by the presence of several imaginary eigenmodes (see Figure 4a). To improve this structural model, we applied a multistep procedure that has been described in more detail recently.^[81] First, we applied eigenvectors of the imaginary modes at the Γ point followed by structural optimization, for which the $E(V)$ plot is shown in Figure 4b. This process, labeled (1) in Figure 4b for two distinct eigenmodes, leads to the new $E(V)$ curves shown in green and light blue, respectively. This structural change is accompanied by an energy gain of over 30 kJ/mol, quite impressively. For both of these structures, subsequent energy–volume scans were performed (labeled (2)). Upon compressing the simulated cells, both still showed an inherent instability upon decreasing the unit-cell volume below ~ 28 cm³/mol (green dots) or ~ 25 cm³/mol, respectively. The most favorable structure, finally, was obtained upon relaxation (labeled (3); dark blue line in Figure 4b) and led to an energy gain of ~ 55 kJ/mol as compared to the initial $P6_3/mcm$ guess.

The new theoretical structure with “LiCaN₂” composition was found in space group $Pmma$ (no. 51). It must be noted, however, that the resulting space group equals that of the TEM model (see previous section) *only by coincidence*, and the reason is as follows. Despite the large energetic stabilization of ~ 55 kJ/mol gained during the optimization procedure that started from the initial model ($P6_3/mcm$, Figure 4b), a simulated diffraction pattern for the optimized “LiCaN₂” model could not be reconciled with the experimental diffractogram. In particular, the computational result so far did not correspond to the revised unit-cell metrics but to those of the initial model, which had been falsified in the sequel. Consequently, what

was initially believed to be the “correct” answer from theory (Figure 4b, dark blue curve) had to be discarded in the light of experiment.

On the other hand, the revised structural model derived from TEM (sketched in Figure 5, top) again proved unstable during quantum-chemical relaxation. This led us to conclude that the results of the elemental analysis (see the Supporting Information) had to be recalled as the compound obtained from HP/HT-experiments might differ in stoichiometry as compared to the originally proposed sum formula of LiCaN_2 .

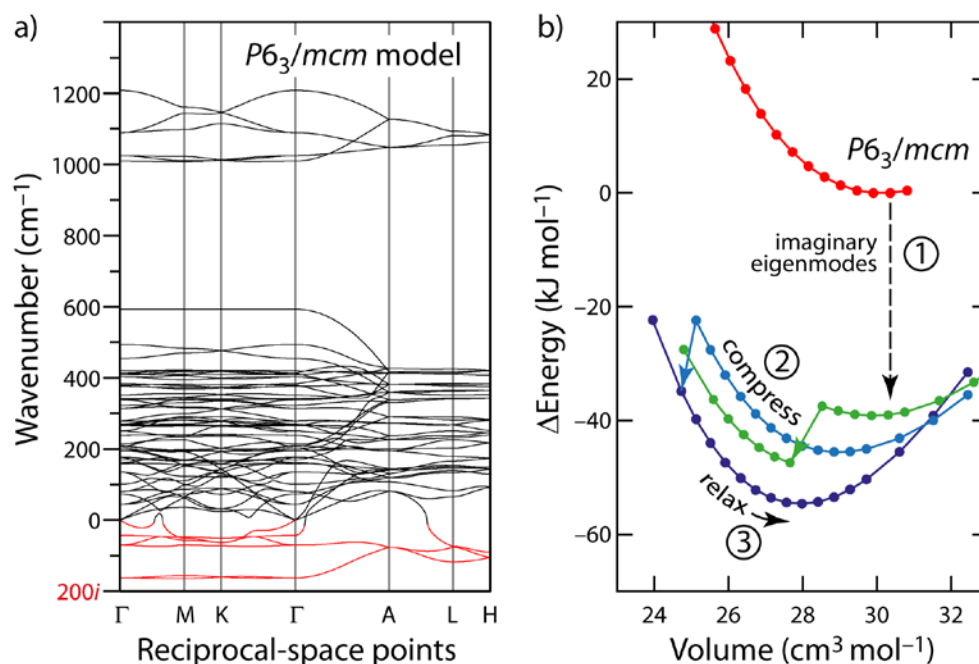


Figure 4. (a) Phonon band structure computed for the hexagonal $P6_3/mcm$ model exhibiting “ LiCaN_2 ” stoichiometry. Several imaginary eigenvalues (highlighted in red), seemingly extending throughout the entire Brillouin zone, are visible. (b) Energy–volume plots for the different structural models of “ LiCaN_2 ”, with arrows describing how one is obtained from the other. Lines connecting data points are only guides to the eye. See text for discussion.

Improving the Structural Model

The elemental analysis, albeit with some uncertainty, suggested a Li deficiency with a atomic ratio $\text{Li:Ca} \sim 0.8:1$ in the title compound, whereas a Ca:N ratio of $\sim 1:2$ had been observed. Also, the exclusively Ca-coordinated Li positions in the $Pmma$ structure model (2a and 2d) were the ones that experienced the most pronounced structural change/instability in the theoretical computations. Hence, it became obvious that the structural model with $\text{Li:Ca} = 1$ did not suffice because it did not lead to an agreement of experiment and theory.

Indeed, upon removing the Li atoms in question, the stoichiometric composition was changed to $\text{Li}_2\text{Ca}_3[\text{N}_2]_3$, and we again carried out structural optimizations (see Tables S3 and S4 in the Supporting Information), starting from the TEM-based experimental, orthorhombic “ LiCaN_2 ” model in space group $Pmma$ (see Figure 5) but with Li deficiency at $2a$ and $2d$ sites.

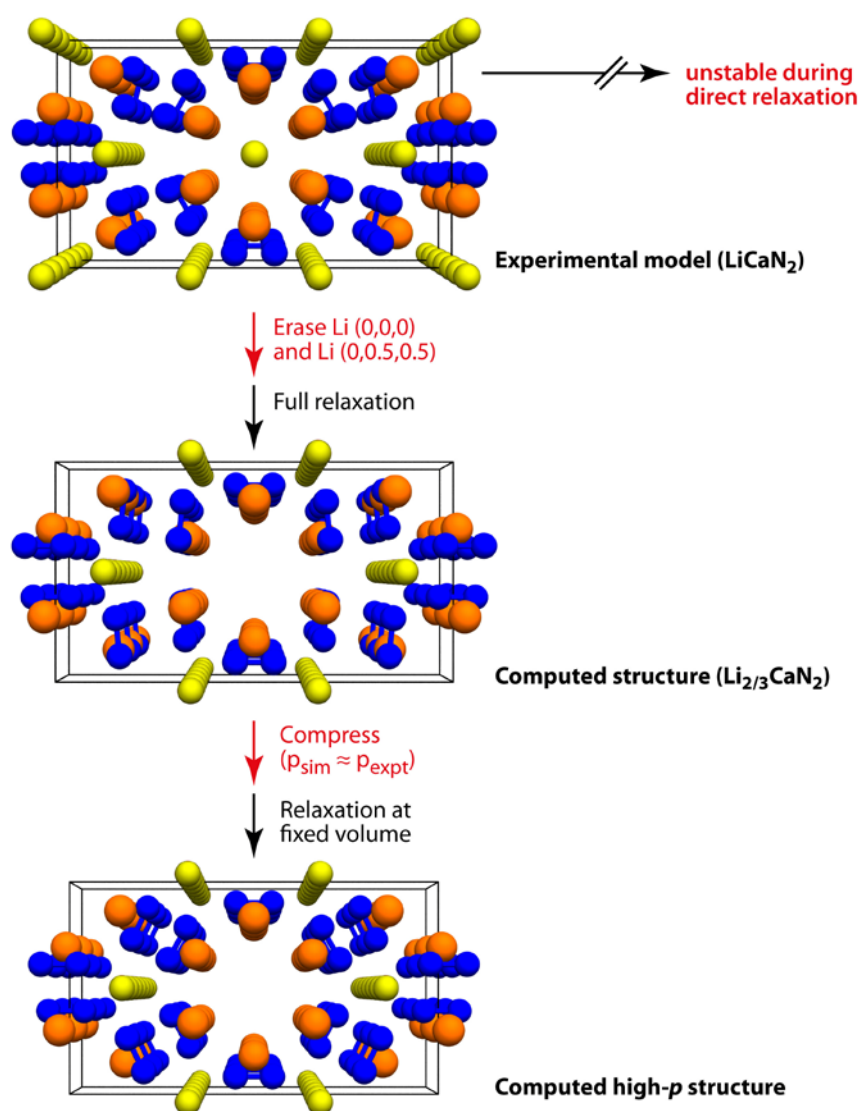


Figure 5. Schematic drawing of the route from the initial experimental, orthorhombic “ LiCaN_2 ” model to the final, Li-deficient model with $\text{Li}_2\text{Ca}_3[\text{N}_2]_3$ stoichiometry, both of which exhibit space group $Pmma$ (no. 51). Cell sizes are not to scale; Li yellow, Ca orange, N blue.

In the absence of external pressure, the structure seemed to be unstable again as indicated by the presence of imaginary phonon modes (albeit less strongly pronounced than in the $P6_3/mcm$ model characterized in Figure 4a). Nonetheless, by decreasing the simulation cell volume, the proposed structure could be stabilized. The imaginary modes disappeared entirely once the simulated pressure increased to ~ 13 GPa and above (see Figure 6), which is close to

synthesis conditions (9 GPa). The imaginary eigenmodes at zero pressure might propose further instability of the crystal structure at ambient conditions; however, a collapse of the crystal structure at these conditions seems to be kinetically hindered as $\text{Li}_2\text{Ca}_3[\text{N}_2]_3$ could be analyzed experimentally even after releasing high pressure.

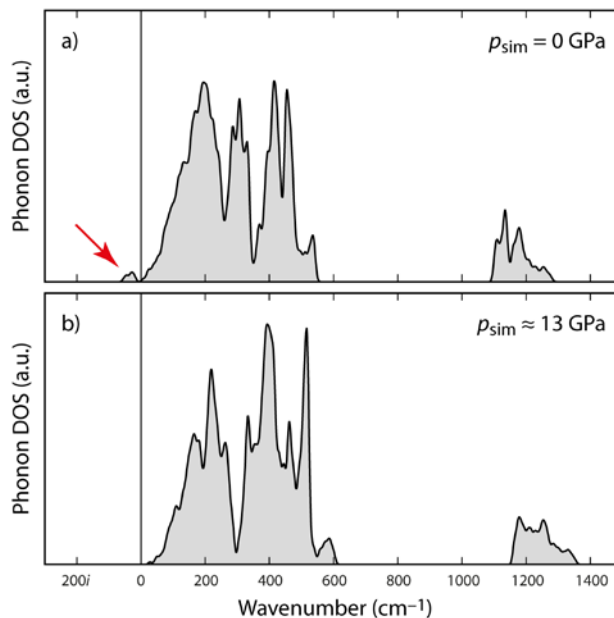


Figure 6. Computed phonon DOS for the final structural model with $\text{Li}_2\text{Ca}_3[\text{N}_2]_3$ stoichiometry without external pressure (a) and at a simulated pressure of approximately 13 GPa (b). In the upper panel, a small number of imaginary eigenmodes are visible as indicated by a red arrow. In the lower panel, these imaginary modes have disappeared and the structural model proves dynamically stable.

Note that the spot density in simulated diffraction patterns of $\text{Li}_2\text{Ca}_3[\text{N}_2]_3$ (data not shown) is equal to orthorhombic “ LiCaN_2 ” in space group $Pmma$ (no. 51, TEM-based model). It is only the intensity of the spots that slightly varies due to the lithium depletion of Wyckoff positions $2a$ and $2d$ in “ LiCaN_2 ” resulting in the composition $\text{Li}_2\text{Ca}_3[\text{N}_2]_3$. Thus, the simulated diffraction patterns are also in good agreement with the final crystal structure.

Description of the Crystal Structure

$\text{Li}_2\text{Ca}_3[\text{N}_2]_3$ shows a close structural relationship to hexagonal Mn_5Si_3 -type structures ($P6_3/mcm$, no. 193), better known as Nowotny phases.^[82–84]

$\text{Li}_2\text{Ca}_3[\text{N}_2]_3$ contains four pairs of crystallographically independent nitrogen dumbbells exhibiting N–N bond lengths of $d_{\text{NN}}=1.337(17)\text{--}1.353(32)$ Å (see Figure 7 and Table 2).

These N–N distances are intermediate to those in experimentally reported diazenides MN_2 ($M = \text{Ca}, \text{Sr}, \text{Ba}$), Li_2N_2 and LaN_2 having distances of about 1.20–1.32 Å,^[58,59,62] and to pernitride $[\text{N}_2]^{4-}$ ions with N–N bond lengths of about 1.40 Å.^[46–54] For $\text{Li}_2\text{Ca}_3[\text{N}_2]_3$, this suggests a $[\text{N}_2]^{3-}$ formulation, which would correspond to a radical character of the dinitrogen anion. In more detail, as-obtained N–N distances are in good agreement with corresponding characteristics of $[\text{N}_2]^{3-}$ ligation observed in already mentioned bimetallic lanthanide complexes ($d_{\text{NN}} = 1.39\text{--}1.41$ Å).^[10,27–31] However, recent theoretical calculations considering hypothetical TiN_2 also support diazenide $[\text{N}_2]^{2-}$ units with N–N bond lengths up to even 1.46 Å.^[85]

To elucidate the electronic character of the dinitrogen anion, we targeted chemical bonding analysis by means of the crystal orbital Hamiltonian population (COHP) method, as done previously for different diazenide/pernitride compounds.^[54,58–60]

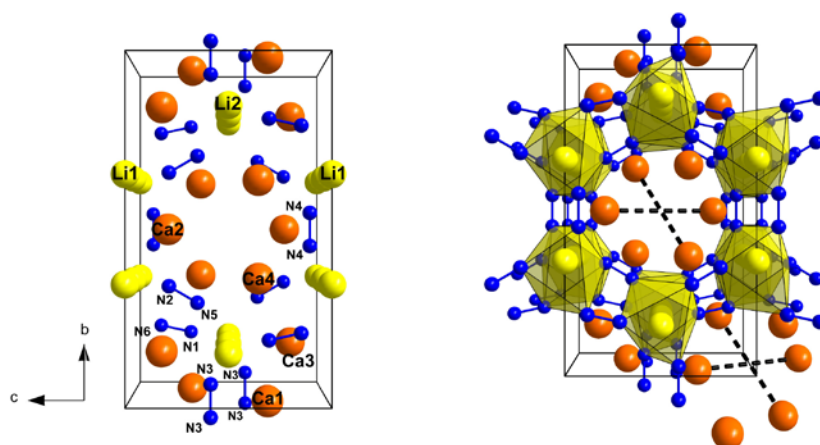


Figure 7. Unit-cell of $\text{Li}_2\text{Ca}_3[\text{N}_2]_3$ viewed along $[100]$ as resulting from the final refinement. Polyhedra around Li atoms are marked in yellow; Li yellow, Ca orange, N blue. Dashed lines in the right figure represent Ca–Ca distances in the center of the unit-cell with $d_{\text{Ca1-Ca1}} = 5.45(1)$, $d_{\text{Ca2-Ca2}} = 5.47(2)$, $d_{\text{Ca3-Ca3}} = 5.39(1)$ and $d_{\text{Ca4-Ca4}} = 5.267(9)$ Å, respectively. For further information see Table S6 in the Supporting Information.

Figure 8 shows the well-known electronic „fingerprint” of the dinitrogen entity in the region close to the Fermi level ε_{F} .^[54] In agreement with Scheme 1, a set of π bonding and π^* antibonding bands may be discerned. The four dinitrogen dumbbells, despite overall similarities, have a unique bonding fingerprint each (shown in different colors), which is in accord with the experimental observation of several N–N stretching modes in the vibrational spectrum. For a more quantitative analysis, we calculate the “filling” of the π^* orbitals as reflected in the integrated COHPs. (We are aware of difficulties in integrating over an unoccupied area of the band structure; relative comparison is however well permitted) We derive the filling as

$$\left(\int_{\varepsilon_-}^{\varepsilon_F} \text{COHP}(E) dE \right) / \left(\int_{\varepsilon_-}^{\varepsilon_+} \text{COHP}(E) dE \right)$$

where ε_- denotes a suitably chosen lower energy limit (in Figure 8, 4 eV below the Fermi level) and ε_+ is the upper one (2 eV above ε_F). The resulting values of the π^* filling up to the Fermi level are given in Table 2. Note that these values have also been averaged over the four bonds present in equal amounts.

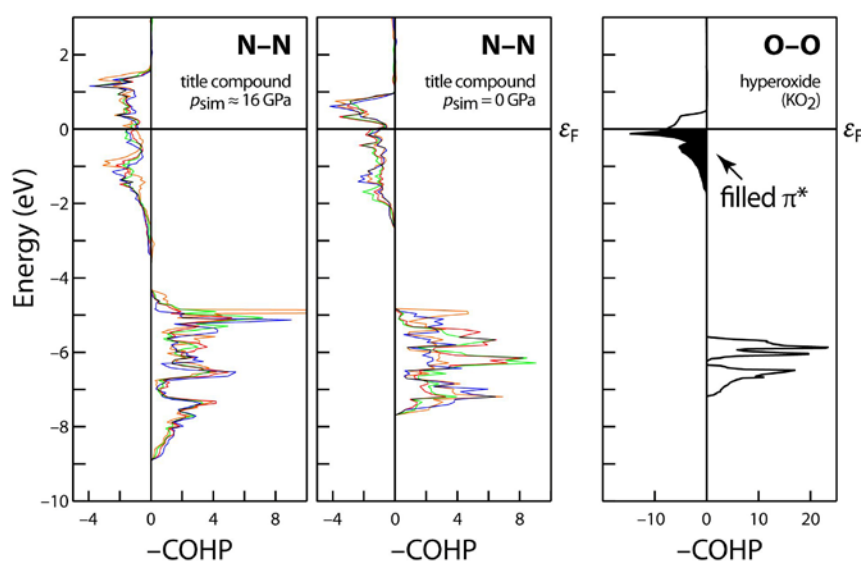
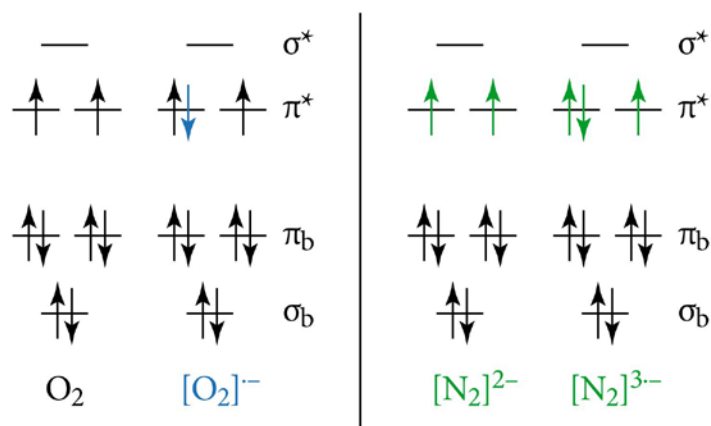


Figure 8. Left and middle: COHP analysis for the 4 $[\text{N}_2]$ entities in $\text{Li}_2\text{Ca}_3[\text{N}_2]_3$ depicted in different arbitrarily chosen colors, computed under a pressure of 16 GPa (left) and for the fully relaxed structure at zero pressure (middle), respectively. For the definition of π^* filling, see the text. Right: Same but for the $[\text{O}_2]$ entity in potassium hyperoxide KO_2 .



Scheme 1. Schematic molecular-orbital diagrams (not drawn to scale) for the species discussed. Electrons in excess of the neutral diatomic ground-state are indicated in color.

For comparison, an O–O COHP curve has been computed for potassium hyperoxide as a well-characterized representative compound with an anion isoelectronic to $[\text{N}_2]^{3-}$.^[86] Thereby, the calculated filling is 73 %, well matching the ideally expected percentage of 75 % according to Scheme 1. The individual and averaged electronic character of the four N_2 entities in $\text{Li}_2\text{Ca}_3[\text{N}_2]_3$ are listed in Table 2. Accordingly, with an averaged π^* filling of 57 % at zero pressure (53 % at 16 GPa) resembling an expected value of 50 % for diazenides, the N_2 units in $\text{Li}_2\text{Ca}_3[\text{N}_2]_3$ clearly exhibit different electronic behavior as compared to hypothetical $[\text{N}_2]^{3-}$ radical anions.

Taking these theoretical considerations into account, $\text{Li}_2\text{Ca}_3[\text{N}_2]_3$ is conjectured to consist of diazenide $[\text{N}_2]^{2-}$ ions rather than $[\text{N}_2]^{3-}$ radical anions. This assignment is probed by

Table 2. Experimental and Computationally Optimized N–N Bond Lengths in angstroms of Nitrogen Dumbbells in $\text{Li}_2\text{Ca}_3[\text{N}_2]_3$, Together with π^* Orbital Fillings (See Text).

$\text{N}_x\text{--N}_y^a$	1–6	2–5	3–3	4–4	Average
exp.	1.342(14)	1.337(17)	1.353(32)	1.348(26)	
calc at 0 GPa	1.308	1.308	1.313	1.313	
π^* filling	55%	59%	59%	56%	57%
calc at 16 GPa	1.293	1.293	1.291	1.289	
π^* filling	55%	51%	59%	46%	53%

^aThe pairing of six crystallographically independent nitrogen sites (all Wyckoff site 4k), thereby referring to Table 1, results in four crystallographically independent N_2 entities.

such compounds, suboxides or subnitrides come to mind.^[87–97] Interestingly, each nitrogen atom of the diazenide entities is octahedrally coordinated by four calcium and two lithium cations. Both octahedra share one common face which is similar to the Rb_9O_2 -type cluster observed in the rubidium suboxides Rb_9O_2 and Rb_6O (see Figure 9).^[87–90]

These compounds represent oxygen-deficient (or, again, electron-rich) structures. Formally, Rb_9O_2 and Rb_6O can also be written as $(\text{Rb}^+)_9(\text{O}^{2-})_2 \cdot (\text{e}^-)_5$ or $(\text{Rb}^+)_6(\text{O}^{2-}) \cdot (\text{e}^-)_4$, respectively. As the $[\text{N}_2]^{2-}$ coordination spheres resemble those of the oxygen ions in suboxides and due to potential formulation of $\text{Li}_2\text{Ca}_3[\text{N}_2]_3$ as $(\text{Li}^+)_2(\text{Ca}^{2+})_3([\text{N}_2]^{2-})_3 \cdot (\text{e}^-)_2$, the title compound might also constitute the first representative of hitherto unknown ternary sub-diazenides. However, as compared to the Rb_9O_2 structure (see Figure 9b), with isolated Rb_9O_2 units in the rubidium-

experiment in the next sections.

The presence of only diazenide ions in $\text{Li}_2\text{Ca}_3[\text{N}_2]_3$ and the reasonable requirement of singly (doubly) positively charged Li (Ca) ions, respectively, results in a more precise formulation as in $(\text{Li}^+)_2(\text{Ca}^{2+})_3([\text{N}_2]^{2-})_3 \cdot (\text{e}^-)_2$, an anion-deficient or vice-versa electron-rich structure. As prominent representatives of

based lattice, the resulting structural motifs of N₂-coordination in Li₂Ca₃[N₂]₃ are exclusively interconnected again by sharing octahedral faces (see Supporting Information Figure S8).

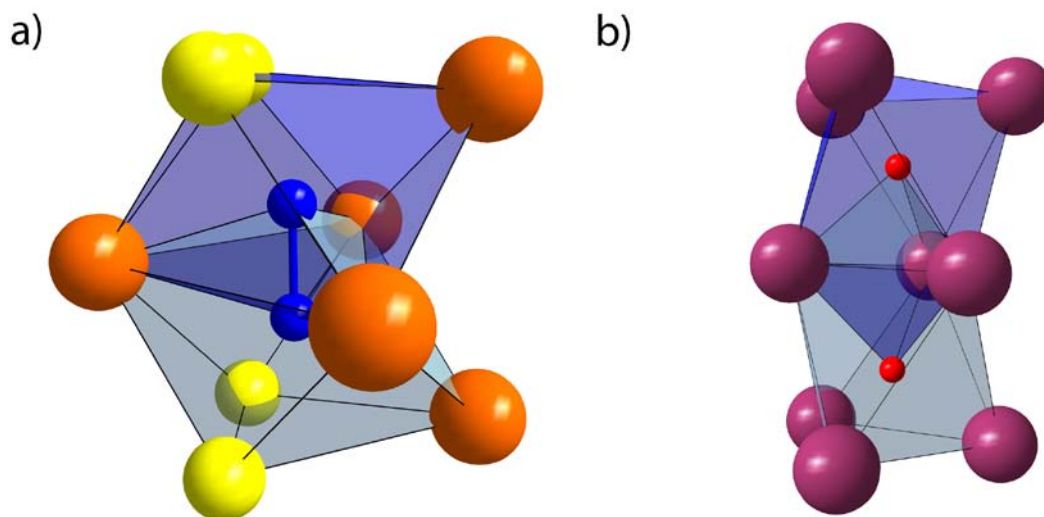


Figure 9. Coordination sphere of diazenide ions in Li₂Ca₃[N₂]₃ (a). Thereby each nitrogen atom is octahedrally coordinated by Li⁺ and Ca²⁺. The resulting octahedra share a common face, representing the basic motif of anion coordination in rubidium suboxides Rb₉O₂ and Rb₆O (b); Li yellow, Rb violet, Ca orange, N blue, O red.

The two independent lithium sites are coordinated by six [N₂]²⁻ ions in an *end-on* manner, building up a strand of face-sharing octahedra (see Figures 7 and S9 in the Supporting Information). These strands are interconnected to other ²_∞[Li(N₂)_{6/2}]-strands by diazenide units. The refined Li–Li distances (see Table S5 in the Supporting Information) match with reported ones.^[59,98–103] Additionally, we compared the obtained Li–N distances with the sum of the ionic radii. Preliminary investigations already resulted in an average radius of one nitrogen atom in a diazenide ion to be 1.27 Å.⁶⁰ According to Shannon,^[104] the ionic radius of 6-fold coordinated Li⁺ is 0.76 Å. On the basis of on this empirical values, the refined Li–N distances correspond well with the sum of the ionic radii.

Like hexagonal Mn₅Si₃, Li₂Ca₃[N₂]₃ contains structural voids, which due to the orthorhombic metric are located at (0,0,0) and (0,½,½). Many A₅B₃-type compounds were observed to incorporate nonmetal atoms like B, C, N, O, or even metals into these cavities to result in A₅B₃Z-type compounds.^[82] However, a clear tendency for occupying the voids is very hard to predict. Moreover, nonstoichiometric intercalation of Z elements into the cavities is supposed to stabilize A₅B₃-type structures.^[82] In Li₂Ca₃[N₂]₃, the average void diameter is found to be 3.15 Å (see Supporting Information Table S6), which is within the range of those in the

aforementioned A_5B_3 compounds and thus formally enables incorporation of further elements into these voids. However, elemental analysis (see the Supporting Information) resulted in no significant stoichiometric atom content other than Li, Ca, and N. In addition, due to electrostatic reasons, the incorporation of cations/metals is supposed to be rather energetically unstable as shown by theoretical consideration finally resulting in $Li_2Ca_3[N_2]_3$ after removing Li atoms of Wyckoff positions $2a$ and $2d$.

Infrared Spectroscopy

In bioinorganic chemistry, the valency of dinitrogen anions is routinely assigned according to the N–N bond lengths and their corresponding N–N stretching vibrations upon infrared or Raman spectroscopy. Recently, it has been shown experimentally that the infrared spectra of the diazenides MN_2 ($M=Ca, Sr, Ba$), as well as of Li_2N_2 , exhibit clear features in the range of $1380\text{--}1330\text{ cm}^{-1}$, which had been assigned to the N–N stretching vibration of the diazenide units.^[58,59] Pernitride units as observed in noble metal $M_{NM}N_2$ compounds ($M_{NM} = Os, Ir, Pd$ and Pt) also exhibit distinct features around 800 cm^{-1} , attributed to the stretching of $[N_2]^{4-}$ units.^[46–54] In addition, radical dinitrogen ions $[N_2]^{3\cdot-}$ have recently been observed, and they show characteristic N–N vibrations at wavenumbers shortly below 1000 cm^{-1} .^[27–31]

For $Li_2Ca_3[N_2]_3$, infrared spectroscopy revealed significant features at $1260, 1100, 1020$ and 802 cm^{-1} besides overtones at about 3000 cm^{-1} (see Figure 10). The nitrogen dumbbells in $Li_2Ca_3[N_2]_3$ exhibit bond lengths of $d_{NN} = 1.34(2)\text{--}1.35(3)\text{ \AA}$, which are intermediate to previous reports for $[N_2]^{2-}$ and $[N_2]^{3\cdot-}$ ions. In accord with this observation, the wavenumbers of the observed features in the infrared spectrum of $Li_2Ca_3[N_2]_3$ are also intermediate to those of the latter two anions. Thus, the theoretical COHP analysis of the N–N bonding in the title compound (suggesting diazenide $[N_2]^{2-}$ ions, rather than radicals) despite elongated N–N bond lengths is in good agreement with the vibrational measurements.

Seeking again a corroboration of experimental findings, we also performed pressure-dependent phonon calculations to assign the vibrational modes from first principles, and also to look at the high-pressure trend in vibrational properties that is much more difficult to determine experimentally.

For the fully optimized (pressure-free) structural model, as well as with simulated pressures of a few GPa applied, the phonon calculations give imaginary vibrational modes (see Figure 11), which indicates dynamical instability already seen in Figure 6a (red arrow). With increasing

(simulated) pressure, the imaginary modes disappear, which points toward the structure being stable under pressure.

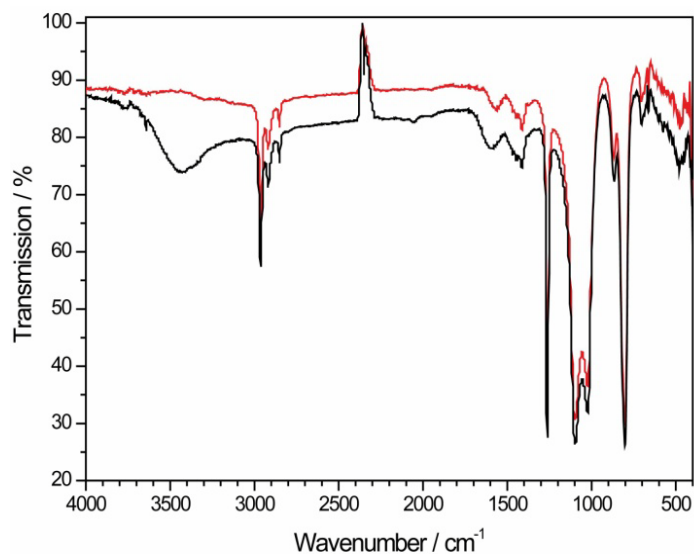


Figure 10. FTIR spectra of $\text{Li}_2\text{Ca}_3[\text{N}_2]_3$ (black) and after exposure to moisture for 5 min (red). The absorption features at about 2250 cm^{-1} are artifacts of the spectrometer.

As can further be seen in Figure 11, the theoretical phonon DOS shows a broad signal in the range from 1100 to 1300 cm^{-1} without external pressure applied, which is shifted to higher wavenumbers with increasing pressure due to shorter atomic distances. This part of the spectrum is related to the N–N stretching vibrations of the diazenide ions, and the signals are broadened because of their interaction. The experimentally obtained features at 1260 , 1100 , and 1020 cm^{-1} can be confirmed by the theoretical calculations, albeit caution must be taken because not all lattice modes are infrared active, and hence the IR spectrum and the computed PDOS may not be compared to each other without care.

As our calculations reveal, the feature at 800 cm^{-1} cannot be assigned to the N–N stretching vibrations of one of the diazenide units. However, the product of the high-pressure synthesis is always affected with an unknown impurity (see the Experimental Section), which might constitute an oxo- or nitridoborate originating from the BN crucible used. Such compounds exhibit distinct features at wavenumbers $< 1000\text{ cm}^{-1}$ assigned to lattice vibrations of the oxo- or nitridoborate units,^[105–109] and thus might account for the unexplained signal in the IR spectrum of the title compound. A more detailed assignment of observed features in the experimental and theoretical vibrational spectrum to N–N bond lengths can be found in the Supporting Information.

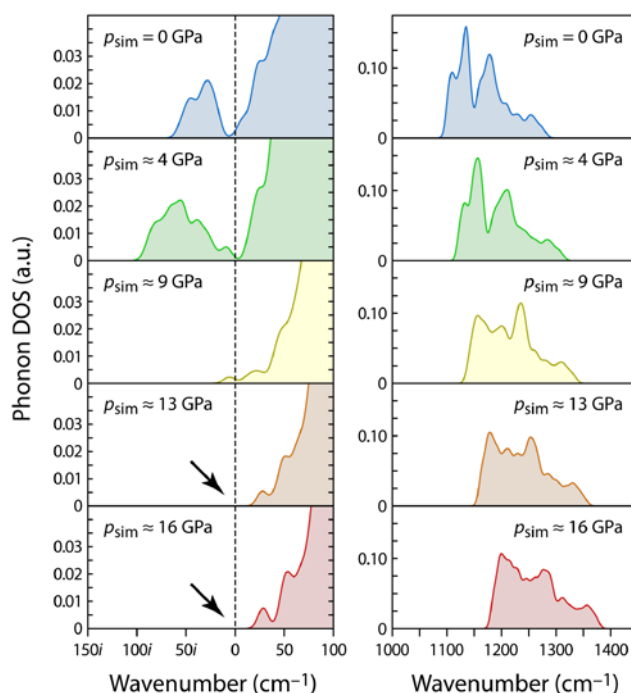


Figure 11. Excerpts from phonon densities of states computed at different simulated pressures, evolving from pressure-free structures (top) to 16 GPa. Note the absence of dynamic instabilities (that would be indicated by complex-valued vibrational modes), which sets in at increased pressure (arrows).

Electron Spin Resonance (ESR) Spectroscopy

To settle the character of the nitrogen dumbbells experimentally, we next employed electron spin resonance spectroscopy, which is routinely used for the detection and further analysis of unpaired electrons. As the $[\text{N}_2]^{2-}$ ion is isoelectronic to molecular oxygen O_2 , it should exhibit paramagnetic behavior (see Scheme 1). However, despite the paramagnetic character, the detection of an ESR-signal for molecular oxygen is hindered due to the enormous zero field splitting of the triplet state, which in general leads to a broadening and therefore makes detection of an ESR signal impossible. On the contrary, $[\text{N}_2]^{3-}$ radical anions are shown to give a very sharp signal as they are isoelectronic to hyperoxides $[\text{O}_2]^-$ (see Scheme 1).^[27,28] Indeed, ESR measurements of alkali and alkaline earth hyperoxides resulted in distinct signals at a g -factor ranging from 2.001 to 2.004, close to the g -factor of free electrons (2.0023).^[110,111]

Figure 12a displays the ESR spectrum of $\text{Li}_2\text{Ca}_3[\text{N}_2]_3$, whereas in Figure 12b that of BaN_2 is depicted, the latter serving as diazenide reference. The spectrum of $\text{Li}_2\text{Ca}_3[\text{N}_2]_3$ contains a narrow-line and a broad-line signal at $g_{\text{narrow}}=2.0052(1)$ and $g_{\text{broad}}=2.0052(10)$, which would, in principle, be consistent with the presence of free electrons and support a potential $[\text{N}_2]^{3-}$

formulation. However, the ESR spectrum of BaN_2 also consists of a signal at about the g -factor of free electrons contradicting the unambiguous correlation of the signals in the spectrum of $\text{Li}_2\text{Ca}_3[\text{N}_2]_3$ to $[\text{N}_2]^{3-}$ radical anions.

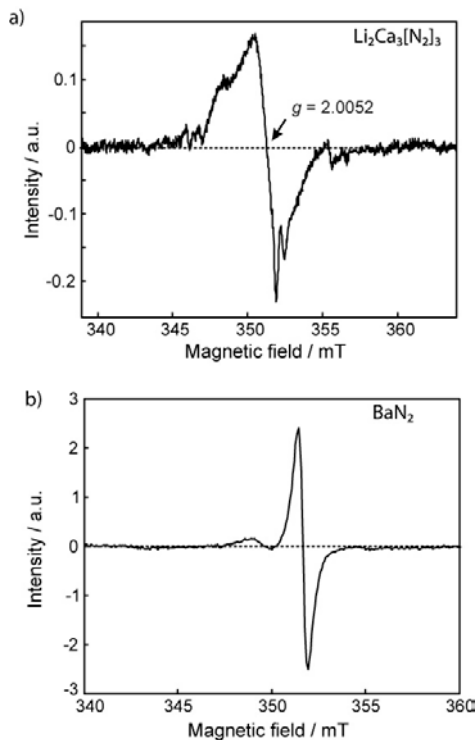


Figure 12. (a) Detail ESR spectrum at ambient temperature after background correction (black). In addition to the narrow-line signal shown here in detail, an overview spectrum (see Supporting Information Figure S3) reveals the presence of a broad-line signal. The g values for the narrow-line and the broad-line signal are 2.0052(1) and 2.0052(10), respectively. The dotted line only serves as a guide to the eyes for the zero crossing of the spectrum. (b) ESR spectrum of BaN_2 after background correction recorded at ambient temperature.

Additionally, we analyzed the spin concentration of the obtained signals in $\text{Li}_2\text{Ca}_3[\text{N}_2]_3$ and BaN_2 and referenced them to common ESR standards. For BaN_2 , the obtained spin concentration of 16.6 mM is far below the expected value of 60.8 M for the biradical $[\text{N}_2]^{2-}$. These data are in good agreement with as-mentioned difficulties in signal detection due to triplet state splitting of paramagnetic diazenide ions. Thus, the visible signal of the HP/HT-product is attributed either to impurities in the mmol range or surface defects in BaN_2 evolving unpaired electrons, which then can be detected.

The ratio of double integrals of the broad-line signal of $\text{Li}_2\text{Ca}_3[\text{N}_2]_3$ to the one of the utilized one-electron references is 1:373, suggesting an effective spin concentration in $\text{Li}_2\text{Ca}_3[\text{N}_2]_3$ of 373(60) mM. The spin concentration of the narrow-line signal is only in the 10^{-3} mM range. In any case, a rough estimate indicates that the number of spins is too low for a compound

with all or at least one nitrogen dumbbell in a $[\text{N}_2]^{3-}$ radical anion state. Therefore, even considering a 20 % uncertainty in determining spin concentration, the observed concentration is much too low for assigning an electronic structure with $[\text{N}_2]^{3-}$ radical anions. Again, the presence of the signals is presumably due to surface defects or impurities in the sample. Taking all of these facts into account, $\text{Li}_2\text{Ca}_3[\text{N}_2]_3$ rather consists of $[\text{N}_2]^{2-}$ ions than $[\text{N}_2]^{3-}$ radical anions, which is in sound agreement with electronic-structure theory (see Figure 8).

Magnetic and Electric Conductivity Measurements

Magnetic measurements are supposed to ultimately end speculations on the potential presence of $[\text{N}_2]^{3-}$ radical anions in $\text{Li}_2\text{Ca}_3[\text{N}_2]_3$. If $\text{Li}_2\text{Ca}_3[\text{N}_2]_3$ contained $[\text{N}_2]^{3-}$ radical anions, magnetic characteristics like antiferro- or ferromagnetism would be expected as observed for the isoelectronic hyperoxides.^[112] However, susceptibility measurements of $\text{Li}_2\text{Ca}_3[\text{N}_2]_3$ at 1 and 0.01 T show nearly temperature-independent (Pauli-paramagnetic) behavior down to low temperatures (see Figure 13a).

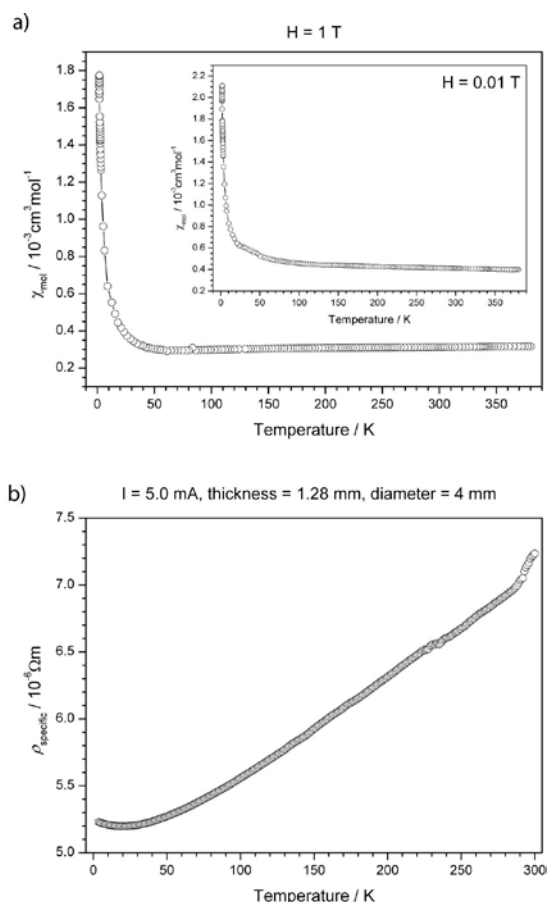


Figure 13. Course of the molar susceptibility of $\text{Li}_2\text{Ca}_3[\text{N}_2]_3$ with temperature (a) at an applied external field of 1 and 0.01 T (inset); specific resistance with temperature upon cooling (b). Error bars are not shown. The lines only serve as a guide to the eyes.

To rely on this observation especially in the low-temperature region where the susceptibility slightly increases again (see Figure 13a), we also plotted the product of $\chi_{\text{mol}}T$ versus T (see Figure S11 in the Supporting Information), which resulted in a continuous increase of $\chi_{\text{mol}}T$ with increasing temperature indicative for true temperature-independent behavior of the susceptibility. This observation is in good agreement with previous magnetic measurements of again BaN_2 revealing that the dominant magnetic behavior in BaN_2 is also Pauli-paramagnetism.^[39]

As shown in Figure 13b, the resistivity of $\text{Li}_2\text{Ca}_3[\text{N}_2]_3$ decreases with decreasing temperature, as is typical for metals. The resistivity at ambient temperature is found to be $7.23 \cdot 10^{-6} \Omega\text{m}$ which is in the range of good metallic conduction and qualitatively in accord with electronic-structure computations that predict a finite density of electronic states at the Fermi level (see Figure 8). Again, as-obtained results are in very good agreement with the presence of solely $[\text{N}_2]^{2-}$ ions in $\text{Li}_2\text{Ca}_3[\text{N}_2]_3$.

5.1.4 CONCLUSION

We were able to synthesize the first ternary compound with homonuclear dinitrogen entities by thermal decomposition of stoichiometric mixtures of ionic lithium and calcium azides under HP/HT-conditions. In contrast to binary diazenides such as Li_2N_2 , $M\text{N}_2$ ($M = \text{Ca}, \text{Sr}$ and Ba) and LaN_2 , the ternary title compound $\text{Li}_2\text{Ca}_3[\text{N}_2]_3$ exhibits pronounced elongation of the N–N bond lengths which would intuitively contradict the presence of $[\text{N}_2]^{2-}$ ions. In fact, these N–N distances would be better described by $[\text{N}_2]^{3-}$ units, as has been previously observed in metal-organic reference compounds.

Much to the contrary, the true character of the N_2 entity was finally elucidated by complementary use of various analytical methods. Experimental and theoretical studies excluded the presence of $[\text{N}_2]^{3-}$ radical anions, but instead supported the presence of only $[\text{N}_2]^{2-}$ ions in the crystal structure. Therefore, the ionic formulation of $\text{Li}_2\text{Ca}_3[\text{N}_2]_3$ is better described as $(\text{Li}^+)_2(\text{Ca}^{2+})_3([\text{N}_2]^{2-})_3 \cdot (\text{e}^-)_2$.

Interestingly, $\text{Li}_2\text{Ca}_3[\text{N}_2]_3$ exhibits distinct structural motifs with regard to anion coordination that have been observed in Rb_9O_2^- and Rb_6O -type suboxides, which represent anion-deficient (or, depending on perspective, electron-rich) structures. Within this context, the title compound might also be interpreted as the second representative of “sub-diazenides”.

Finally, as compared to the classification of valencies in bound N₂ entities observed in bioinorganic or metal-organic chemistry, their adequate description in solid-state chemistry is hindered due to, for example, potential metallicity in such compounds. However, by the use of a variety of complementary methods as presented, the identification of the true oxidation state in [N₂]^{x-} anions remains possible.

5.1.5 BIBLIOGRAPHY

Acknowledgment

We would like to thank Prof. Dirk Johrendt (LMU Munich) for providing the equipment for the electric conductivity and SQUID measurements, Prof. Bettina Lotsch for providing the TEM (MPI Stuttgart), Franziska Hummel and Thomas Miller (both LMU Munich) for the low- and high-temperature powder X-ray diffraction measurements, Dr. Constantin Hoch (LMU Munich) for helpful discussions concerning the structural analysis, Nicole Dannenbauer (JMU Würzburg) for the FTIR measurements, Andreas Groß and Dr. Malte Drescher (both University Konstanz) for preliminary ESR experiments, as well as Christian Minke (LMU Munich) for solid-state MAS-NMR measurements.

References

- [1] J.R. Jennings, *Catalytic Ammonia Synthesis*, Plenum Press: New York, **1991**.
- [2] F.A. Tezcan, S.L. A. Andrade, B. Schmid, M. Yoshida, J.B. Howard, D.C. Rees, O. Einsle, *Science* **2002**, 297, 1696.
- [3] B.K. Burgess, D.J. Lowe, *Chem. Rev.* **1996**, 96, 2983.
- [4] R.A. Alberty, R.N. Goldberg, *Biochemistry* **1992**, 31, 10610.
- [5] B.K. Burgess, *Chem. Rev.* **1990**, 90, 1377.
- [6] J.S. Kim, D.C. Rees, *Nature* **1992**, 360, 553.
- [7] K.M. Lancaster, M. Roemelt, P. Ettenhuber, Y.L. Hu, M.W. Ribbe, F. Neese, U. Bergmann, S. DeBeer, *Science* **2011**, 334, 974.
- [8] T. Spatzal, M. Aksoyoglu, L. M. Zhang, S.L.A. Andrade, E. Schleicher, S. Weber, D.C. Rees, O. Einsle, *Science* **2011**, 334, 940.

- [9] R.N.F. Thorneley, D. J. Lowe, *Molybdenum Enzymes*; Wiley:New York, **1985**.
- [10] B.A. MacKay, M.D. Fryzuk, *Chem. Rev.* **2004**, *104*, 385.
- [11] C.J. Pickett, *J. Biol. Inorg. Chem.* **1996**, *1*, 601.
- [12] D.V. Yandulov, R.R. Schrock, *Inorg. Chem.* **2005**, *44*, 1103.
- [13] F. Studt, F. Tuczek, *J. Comput. Chem.* **2006**, *27*, 1278.
- [14] H. Broda, S. Hinrichsen, F. Tuczek, *Coord. Chem. Rev.* **2013**, *257*, 587.
- [15] D.V. Yandulov, R.R. Schrock, *Science* **2003**, *301*, 76.
- [16] D.V. Yandulov, R.R. Schrock, A.L. Rheingold, C. Ceccarelli, W.M. Davis, *Inorg. Chem.* **2003**, *42*, 796.
- [17] V. Ritleng, D.V. Yandulov, W.W. Weare, R.R. Schrock, A.S. Hock, W.M. Davis, *J. Am. Chem. Soc.* **2004**, *126*, 6150.
- [18] R. Römer, C. Gradert, A. Bannwarth, G. Peters, C. Näther, F. Tuczek, *Dalton Trans.* **2011**, 3229.
- [19] K. Klatt, G. Stephan, G. Peters, F. Tuczek, *Inorg. Chem.* **2008**, *47*, 6541.
- [20] G. Stephan, G. Peters, N. Lehnert, C. Habeck, C. Näther, F. Tuczek, *Can. J. Chem.* **2005**, *83*, 385.
- [21] G. Stephan, C. Näther, F. Tuczek, *Acta Crystallogr., Sect. E* **2008**, *64*, M629.
- [22] G. Stephan, C. Näther, C. Sivasankara, F. Tuczek, *Inorg. Chim. Acta* **2008**, *361*, 1008.
- [23] A. Dreher, G. Stephan, F. Tuczek, *Advances in Inorganic Chemistry. Metal Ion Controlled Reactivity*; Elsevier:Amsterdam, 2009.
- [24] S. Pfirrmann, C. Herwig, R. Stößer, B. Ziemer, C. Limberg, *Angew. Chem.* **2009**, *121*, 3407; *Angew. Chem., Int. Ed.* **2009**, *48*, 3357.
- [25] J.M. Smith, R. J. Lachicotte, K.A. Pittard, T.R. Cundari, G. Lukat-Rodgers, K.R. Rodgers, P.L. Holland, *J. Am. Chem. Soc.* **2001**, *123*, 9222.

- [26] J.M. Smith, A.R. Sadique, T.R. Cundari, K.R. Rodgers, G. Lukat-Rodgers, R.J. Lachicotte, C.J. Flaschenriem, J. Vela, P.L. Holland, *J. Am. Chem. Soc.* **2006**, *128*, 756.
- [27] W.J. Evans, M. Fang, G. Zucchi, F. Furche, J.W. Ziller, R.M. Hoekstra, J.I. Zink, *J. Am. Chem. Soc.* **2009**, *131*, 11195.
- [28] M. Fang, J.E. Bates, S.E. Lorenz, D.S. Lee, D.B. Rego, J.W. Ziller, F. Furche, W.J. Evans, *Inorg. Chem.* **2011**, *50*, 1459.
- [29] M. Fang, D.S. Lee, J.W. Ziller, R.J. Doedens, J.E. Bates, F. Furche, W.J. Evans, *J. Am. Chem. Soc.* **2011**, *133*, 3784.
- [30] J.D. Rinehart, M. Fang, W.J. Evans, J.R. Long, *J. Am. Chem. Soc.* **2011**, *133*, 14236.
- [31] J.D. Rinehart, M. Fang, W.J. Evans, J.R. Long, *Nat. Chem.* **2011**, *3*, 538.
- [32] P.J. Chirik, *Nat. Chem.* **2009**, *1*, 520.
- [33] W. Kaim, B. Sarkar, *Angew. Chem.* **2009**, *121*, 9573; *Angew. Chem., Int. Ed.* **2009**, *48*, 9409.
- [34] G. Auffermann, Y. Prots, R. Kniep, *Angew. Chem.* **2001**, *113*, 565; *Angew. Chem., Int. Ed.* **2001**, *40*, 547.
- [35] G. Auffermann, Y. Prots, R. Kniep, S. F. Parker, S. M. Bennington, *ChemPhysChem* **2002**, *9*, 815.
- [36] G. Auffermann, U. Schmidt, B. Bayer, Y. Prots, R. Kniep, *Anal. Bioanal. Chem.* **2002**, *373*, 880.
- [37] G. Auffermann, R. Kniep, W. Bronger, *Z. Anorg. Allg. Chem.* **2006**, *632*, 565.
- [38] Y. Prots, G. Auffermann, M. Tovar, R. Kniep, *Angew. Chem.* **2002**, *114*, 2392; *Angew. Chem., Int. Ed.* **2002**, *41*, 2288.
- [39] G.V. Vajenine, G. Auffermann, Y. Prots, W. Schnelle, R. K. Kremer, A. Simon, R. Kniep, *Inorg. Chem.* **2001**, *40*, 4866.
- [40] A.F. Holleman, E. Wiberg, *Lehrbuch der Anorganischen Chemie*, de Gruyter: Berlin-New York, **2007**.

- [41] N. Wiberg, G. Fischer, H. Bachhuber, *Chem. Ber.* **1974**, *107*, 1456.
- [42] V.E. Bondybey, J.W. Nibler, *J. Chem. Phys.* **1973**, *58*, 2125.
- [43] E.J. Blau, B.F. Hochheimer, *J. Chem. Phys.* **1964**, *41*, 1174.
- [44] K. Rosengren, G.C. Pimentel, *J. Chem. Phys.* **1965**, *43*, 507.
- [45] R. Minkwitz, *Z. Anorg. Allg. Chem.* **1975**, *411*, 1.
- [46] E. Gregoryanz, C. Sanloup, M. Somayazulu, J. Badro, G. Fiquet, H.-K. Mao, R.J. Hemely, *Nat. Mater.* **2004**, *3*, 294.
- [47] J. von Appen, M.-W. Lumey, R. Dronskowski, *Angew. Chem.* **2006**, *118*, 4472; *Angew. Chem., Int. Ed.* **2006**, *45*, 4365.
- [48] J.C. Crowhurst, A.F. Goncharov, B. Sadigh, C.L. Evans, P.G. Morrall, J.L. Ferreira, A.J. Nelson, *Science* **2006**, *311*, 1275.
- [49] A.F. Young, J.A. Montoya, C. Sanloup, M. Lazzeri, E. Gregoryanz, S. Scandolo, *Phys. Rev. B* **2006**, *73*, 153102.
- [50] J.A. Montoya, A.D. Hernandez, C. Sanloup, E. Gregoryanz, S. Scandolo, *Appl. Phys. Lett.* **2007**, *90*, 011909.
- [51] J.C. Crowhurst, A.F. Goncharov, B. Sadigh, J.M. Zaug, D. Aberg, Y. Meng, V.B. Prakapenka, *J. Mater. Res.* **2008**, *23*, 1.
- [52] Z.W. Chen, X.J. Guo, Z.Y. Liu, M.Z. Ma, Q. Jing, G. Li, X.Y. Zhang, L.X. Li, Q. Wang, Y.J. Tian, R.P. Liu, *Phys. Rev. B* **2007**, *75*, 054103.
- [53] R. Yu, Q. Zhan, L.C. De Jonghe, *Angew. Chem.* **2007**, *119*, 1154; *Angew. Chem., Int. Ed.* **2007**, *46*, 1136.
- [54] M. Wessel, R. Dronskowski, *J. Am. Chem. Soc.* **2010**, *132*, 2421.
- [55] N.T. Allen, O. Kennard, D.G. Watson, L. Brammer, A.G. Orpen, R. Taylor, *J. Chem. Soc., Perkin Trans.* **1987**, *2*, S1.
- [56] L.E. Sutton, *Tables of Interatomic Distances and Configuration in Molecules and Ions*, Chemical Society Spec. Publ. 11, Chemical Society: London, **1958**.

- [57] P.A. Giguère, I.D. Liu, *J. Chem. Phys.* **1952**, *20*, 136.
- [58] S.B. Schneider, R. Frankovsky, W. Schnick, *Inorg. Chem.* **2012**, *51*, 2366.
- [59] S.B. Schneider, R. Frankovsky, W. Schnick, *Angew. Chem.* **2012**, *124*, 1909; *Angew. Chem., Int. Ed.* **2012**, *51*, 1873.
- [60] M. Wessel, R. Dronskowski, *J. Comput. Chem.* **2010**, *31*, 1613.
- [61] X. Zhang, A. Zunger, G. Trimarchi, *J. Chem. Phys.* **2010**, *133*, 194504.
- [62] O. Tschauer, S.N. Luo, Y.J. Chen, A. McDowell, J. Knight, S.M. Clark, *High Pressure Res.* **2013**, *33*, 202.
- [63] D. Walker, M.A. Carpenter, C.M. Hitch, *Am. Mineral.* **1990**, *75*, 1020.
- [64] D. Walker, *Am. Mineral.* **1991**, *76*, 1092.
- [65] H. Huppertz, *Z. Kristallogr.* **2004**, *219*, 330.
- [66] D.C. Rubie, *Phase Transitions* **1999**, *68*, 431.
- [67] N. Kawai, S. Endo, *Rev. Sci. Instrum.* **1970**, *8*, 1178.
- [68] A.A. Coelho, *TOPAS-Academic*, Version 4.1; Coelho Software: Brisbane, **2007**.
- [69] J. Bergmann, R. Kleeberg, A. Haase, B. Breidenstein, *Mater. Sci. Forum* **2000**, *303*, 347.
- [70] A.L. Spek, *PLATON, A Multipurpose Crystallographic Tool*, v1.07, Utrecht University, Netherlands, **2003**.
- [71] P.A. Stadelmann, *Ultramicroscopy* **1987**, *21*, 131
- [72] J.P. Perdew, K. Burke, M. Ernzerhof, *Phys. Rev. Lett.* **1996**, *77*, 3865–3868.
- [73] P.E. Blöchl, *Phys. Rev. B* **1994**, *50*, 17953.
- [74] (a) G. Kresse, J. Hafner, *Phys. Rev. B* **1993**, *47*, 558. (b) G. Kresse, J. Furthmüller, *Comput. Mater. Sci.* **1996**, *6*, 15. (c) G. Kresse, J. Furthmüller, *Phys. Rev. B* **1996**, *54*, 11169. (d) G. Kresse, D. Joubert, *Phys. Rev. B* **1999**, *59*, 1758.
- [75] H.J. Monkhorst, J.D. Pack, *Phys. Rev. B* **1976**, *13*, 5188.

- [76] R. Dronskowski, P.E. Blöchl, *J. Phys. Chem.* **1993**, *97*, 8617.
- [77] (a) O.K. Andersen, *Phys. Rev. B* **1975**, *12*, 3060. (b) O.K. Andersen, O. Jepsen, *Phys. Rev. Lett.* **1984**, *83*, 2571.
- [78] U. von Barth, L. Hedin, *J. Phys. C: Solid State Phys.* **1972**, *5*, 1629.
- [79] K. Parlinski, Z.Q. Li, Y. Kawazoe, *Phys. Rev. Lett.* **1997**, *78*, 4063.
- [80] A. Togo, F. Oba, I. Tanaka, *Phys. Rev. B* **2008**, *78*, 134106.
- [81] R.P. Stoffel, R. Dronskowski, *Z. Anorg. Allg. Chem.* **2013**, *639*, 1227.
- [82] J.D. Corbett, E. Carcia, A.M. Guloy, W.-M. Hurng, Y.-U. Kwon, E.A. Leon-Escamilla, *Chem. Mater.* **1998**, *10*, 2824.
- [83] B. Aronsson, *Acta Chem. Scand.* **1960**, *14*, 1414.
- [84] H. Schachner, E. Cerwenka, H. Nowotny, *Monatsh. Chem.* **1954**, *85*, 241.
- [85] A. Kulkarni, J.C. Schön, K. Doll, M. Jansen, *Chem. Asian J.* **2013**, *8*, 743.
- [86] The structure was taken from an earlier experimental report in: H.G. Smith, R.M. Nicklow, L.J. Raubenheimer, M.K. Wilkinson, *J. Appl. Phys.* **1966**, *37*, 1047, with $d(\text{O}-\text{O}) = 1.25 \text{ \AA}$. Test computations including full relaxation at the GGA level were also performed, giving a quite different $d(\text{O}-\text{O}) = 1.34 \text{ \AA}$. Nonetheless, COHPs computed for the analogous optimized structure lead to a π^* occupation of 74 %, which is within 1 % of that given in Figure 8 (right) for the experimental structure. We conclude that the relative filling of the π^* orbital does not seem strongly affected by the structural optimization.
- [87] A. Simon, *Z. Anorg. Allg. Chem.* **1977**, *431*, 5.
- [88] A. Simon, H.J. Deiseroth, *Rev. Chim. Miner.* **1976**, *13*, 98.
- [89] A. Simon, *Molecular Clusters of the Main Group Elements*; Wiley-VCH: Weinheim, **2004**.
- [90] A. Simon, *Crystal Structure and Chemical Bonding in Inorganic Chemistry*; North-Holland Publ. Comb.: Amsterdam, **1975**.

- [91] A. Simon, *Z. Anorg. Allg. Chem.* **1973**, 395, 301.
- [92] A. Simon, *Z. Anorg. Allg. Chem.* **1977**, 428, 187.
- [93] K.-R. Tsai, P. Harris, E. Lassette, *J. Phys. Chem.* **1956**, 60, 338.
- [94] A. Simon, *Struct. Bonding (Berlin)* **1979**, 36, 81.
- [95] P. Rauch, A. Simon, *Angew. Chem.* **1992**, 104, 1505; *Angew. Chem., Int. Ed. Engl.* **1992**, 31, 1519.
- [96] G. Snyder, A. Simon, *J. Am. Chem. Soc.* **1995**, 117, 1996.
- [97] G. Snyder, A. Simon, *Angew. Chem.* **1994**, 106, 713; *Angew. Chem., Int. Ed. Engl.* **1994**, 33, 689.
- [98] A. Rabenau, H. Schulz, *J. Less-Common Met.* **1976**, 50, 155.
- [99] L.G. Cota, P. De La Mora, *Acta Crystallogr., Sect. B* **2005**, 61, 133.
- [100] D. Fischer, M. Jansen, *Z. Anorg. Chem.* **2003**, 629, 1934.
- [101] E. Hellner, F. Laves, *Z. Kristallogr.* **1943**, 105, 134.
- [102] O. Reckeweg, A. Simon, *Z. Naturforsch. B* **2003**, 85, 1097.
- [103] (a) E. Zintl, G.Z. Brauer, *Elektrochemistry* **1935**, 41, 102; (b) A. Rabenau, H. Schultz, *J. Less-Common Met.* **1976**, 50, 155; (c) N. E. Brese, M. O' Keeffe, *Structural Bonding*, Springer: Berlin, **1992**.
- [104] R.D. Shannon, *Acta Crystallogr., Sect. A* **1976**, 32, 751.
- [105] M. Ren, J.H. Lin, Y. Dong, L.Q. Yang, M.Z. Su, L.P. You, *Chem. Mater.* **1999**, 11, 1576.
- [106] J.P. Laperches, P. Tarte, *Spectrochim. Acta* **1966**, 22, 1201.
- [107] G. Blasse, G.P.M. van den Heuvel, *Phys. Status Solidi* **1973**, 19, 111.
- [108] M. Somer, *Z. Naturforsch.* **1991**, 46b, 1664.
- [109] R. Kaindl, G. Sohr, H. Huppertz, *Spectrochim. Acta, Part A* **2013**, 116, 408.
- [110] A.U. Khan, S.D. Mahanti, *J. Chem. Phys.* **1975**, 63, 2271.

[111] V.N. Belevskii, I. I. Vol'nov, S. A. Tokareva, *Bull. Acad. Sci. USSR* **1972**, 21, 1366.

[112] A. Zumsteg, M. Ziegler, W. Känzig, M. Bösch, *Phys. Condens. Matter* **1974**, 17, 267.

5.2 FURTHER TERNARY DIAZENIDES

With the successful synthesis of $\text{Li}_2\text{Ca}_3[\text{N}_2]_3$ the first representative of a ternary diazenide by thermal decomposition of stoichiometric mixtures of LiN_3 and $\text{Ca}(\text{N}_3)_2$ under extreme conditions was presented. As SrN_2 and BaN_2 could also have been synthesized by the high-pressure route, the combination of LiN_3 and $\text{Sr}(\text{N}_3)_2$ or $\text{Ba}(\text{N}_3)_2$ seems to be very promising for the synthesis of further ternary diazenides in the corresponding Li-Sr-N₂ or Li-Ba-N₂ systems. To additionally extend the compositional range of ternary $M^{\text{I}}M^{\text{II}}_y$ -diazenides (M^{III} = alkali or alkaline earth metal), we also targeted the investigation of the thermal behavior under extreme conditions of various stoichiometric combinations of alkali (Na–Cs) and alkaline earth (Ca–Ba) azides despite the previously reported observation that $M\text{N}_3$ ($M = \text{Na–Cs}$) azides decompose into the elements at high-pressure and high-temperature conditions.

5.2.1 EXPERIMENTAL SECTION

Alkali and alkaline earth azides were prepared as described in the chapters 3 and 4. For the synthesis of hypothetical ternary $M^{\text{I}}M^{\text{II}}_y$ -diazenides (M^{III} = alkali or alkaline earth metal), alkali and alkaline earth azides have been initially mixed with each other in a glovebox (Unilab, MBraun, Garching; $\text{O}_2 < 1$ ppm, $\text{H}_2\text{O} < 1$ ppm) with a molar ratio of 1 to gain a first insight in the miscibility of cations in the corresponding systems. For lithium containing compounds, additional mixtures with molar ratios of $\text{LiN}_3:M^{\text{II}}(\text{N}_3)_2$ of 2:1 and 4:1 have been prepared, which were supposed to yield $\text{Li}_2M^{\text{II}}[\text{N}_2]_2$ and $\text{Li}_4M^{\text{II}}[\text{N}_2]_3$ diazenides, respectively. For the HP/HT-treatment of as-obtained mixtures a modified Walker-type module in combination with a 1000 t press (Voggenreiter, Mainleus, Germany) was used. As pressure medium, precastable MgO-octahedra (Cermaic Substrates & Components, Isle of Wight, U.K.) with edge lengths of 14, 18 or 25 mm (14/8, 18/11 or 25/17 assembly) were employed depending on the maximum synthesis pressure. Eight tungsten carbide cubes (Hawedia, Marklkofen, Germany) with truncation edge lengths of 8, 11 or 17 mm compressed the octahedra. The azide mixtures were carefully ground, filled into a cylindrical boron nitride or in the case of lithium containing mixtures into copper crucibles (Henze BNP GmbH, Kempten, Germany) and sealed with a fitting boron nitride plate. A detailed description of the setup can be found in the literature.^[1–4] Compressing and decompression

rates were set according to the synthesis pressure. The recovered MgO-octahedra were broken apart in a glovebox and the samples carefully isolated from the surrounding boron nitride crucible. Whenever possible, HP/HT-products were analyzed by means of powder X-ray diffraction.

5.2.2 RESULTS, DISCUSSION AND CONCLUSION

Unfortunately, in a total number of 57 attempts (26 in the Li-Sr/Ba-N₂ system) under various HP/HT-conditions (see Figure 1), the synthesis of a further ternary diazenide was not successful. Though the combination of LiN₃ with alkaline earth azides resulted in crystalline HP/HT-products, they turned out to be mainly composed of the corresponding binary diazenides SrN₂ or BaN₂ with only minor and depending on conditions varying side-phases, which could not be identified. The HP/HT-treatment of combinations of MN₃ ($M = \text{Na–Cs}$) and $M_{\text{AE}}(\text{N}_3)_2$ ($M_{\text{AE}} = \text{Ca–Ba}$) azides (see Figure 1b) yielded always the corresponding elemental alkali metal with dispersed black inclusions of $M_{\text{AE}}\text{N}_2$ diazenides.

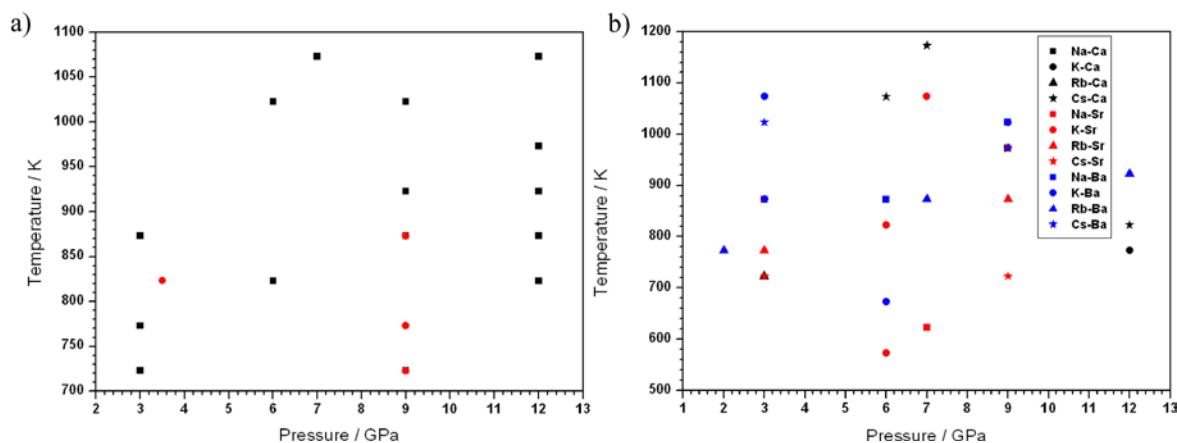


Figure 1. HP/HT-conditions for the synthesis of ternary diazenides starting from stoichiometric mixtures of alkali and alkaline earth azides. In a total number of 57 experiments, no ternary diazenide could be identified. Some experiments have been conducted twice at the same temperature and pressure, but with different heating, holding and cooling rates. a) Investigations in the systems Li-Sr-N₂ (black) and Li-Ba-N₂ (red); b) Corresponding investigated systems are explained by the input legend.

Summarizing, the synthesis of further ternary diazenides by the high-pressure/high-temperature route was not yet possible. Attempting the synthesis of lithium containing ternary diazenides, only minor unidentified side-phases besides the corresponding alkaline earth diazenides representing the main phases have been observed. Whenever the heavier alkali azides have been tried in combination with $M_{\text{AE}}(\text{N}_3)_2$ ($M_{\text{AE}} = \text{Ca–Ba}$), a decomposition into

the elemental alkali metal has been observed with enclosed alkaline earth diazenides. This observation matches the reported behavior of alkali azides upon HP/HT-conditions (see chapter 3).

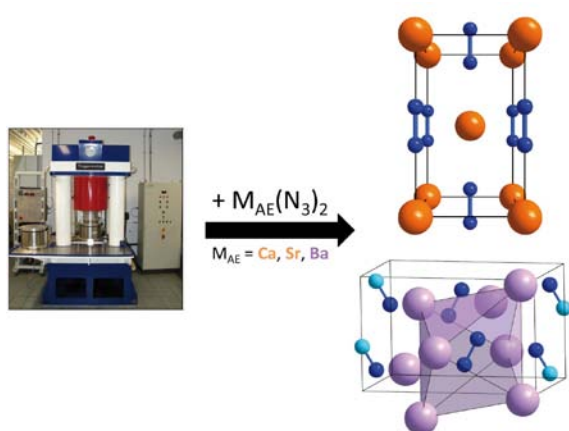
5.2.3 BIBLIOGRAPHY

- [1] D. Walker, M.A. Carpenter, C.M. Hitch, *Am. Mineral.* **1990**, 75, 1020.
- [2] D. Walker, *Am. Mineral.* **1991**, 76, 1092.
- [3] H. Huppertz, *Z. Kristallogr.* **2004**, 219, 330.
- [4] D.C. Rubie, *Phase Transitions* **1999**, 68, 431.
- [5] N. Kawai, S. Endo, *Rev. Sci. Instrum.* **1970**, 8, 1178.

6. SUMMARY

1. Synthesis of Alkaline Earth Diazenides $M_{\text{AE}}\text{N}_2$ ($M_{\text{AE}} = \text{Ca, Sr, Ba}$) by Controlled Thermal Decomposition of Azides under High Pressure

The alkaline earth diazenides $M_{\text{AE}}\text{N}_2$ ($M_{\text{AE}} = \text{Ca, Sr and Ba}$) are synthesized by a controlled decomposition of the corresponding ionic azides in a Walker-type multianvil device at high-pressure/high-temperature conditions of 3–12 GPa at 723–1023 K. The structural model of hitherto unknown calcium diazenide ($I4/mmm$ (no. 139), $a = 3.5747(6)$, $c = 5.9844(9)$ Å,



$Z = 2$, $wR_p = 0.078$) is derived and refined on the basis of powder X-ray diffraction data. The crystal structures of all alkaline earth diazenides are elucidated and compared to well characterized models with homonuclear dianions. Refined N–N bond lengths, FTIR spectroscopy revealing distinct features at about

1375 cm^{-1} attributed to the N–N stretching vibration of the diazenide units, and electronic structure calculations underline the formulation of a double-bonded, twofold negatively charged $[\text{N}_2]^{2-}$ entity.

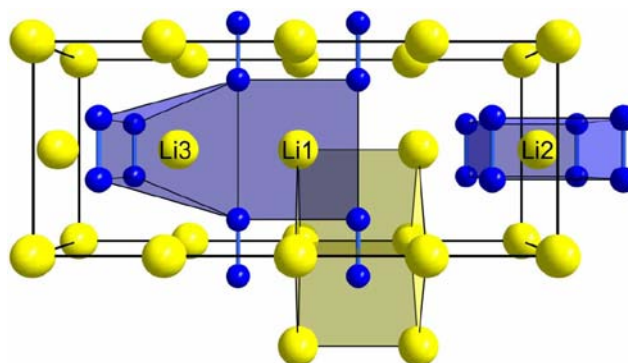
2. Further Alkaline Earth Diazenides

According to the literature, theoretically predicted formation enthalpies for $M_{\text{AE}}\text{N}_2$ compounds ($M_{\text{AE}} = \text{Be–Ba}$) were found to be exothermic with respect to the elements. As the HP/HT-synthesis of alkaline earth diazenides $M_{\text{AE}}\text{N}_2$ ($M_{\text{AE}} = \text{Ca–Ba}$) by controlled thermal

decomposition of the corresponding ionic azides has proven to be successful, the synthesis of hitherto unknown MgN_2 is targeted – due to the toxicity of beryllium compounds, the synthesis BeN_2 is not intended. As ideally binary $\text{Mg}(\text{N}_3)_2$ is required but not known, two oxygen-deficient precursors, namely $\text{Mg}(\text{NH}_3)_2(\text{N}_3)_2$ and $\text{Mg}(\text{N}_3)_{2 \cdot x} \text{NH}_3$ ($x < 1$), have been synthesized and subjected to various HP/HT-conditions. Unfortunately the formation of MgN_2 could not be observed and reasons are presented. Concluding, novel diazenides by the high-pressure/high-temperature route are so far only accessible if the corresponding precursors constitute binary, phase-pure azides.

3. High-Pressure Synthesis and Characterization of the Alkali Diazenide Li_2N_2

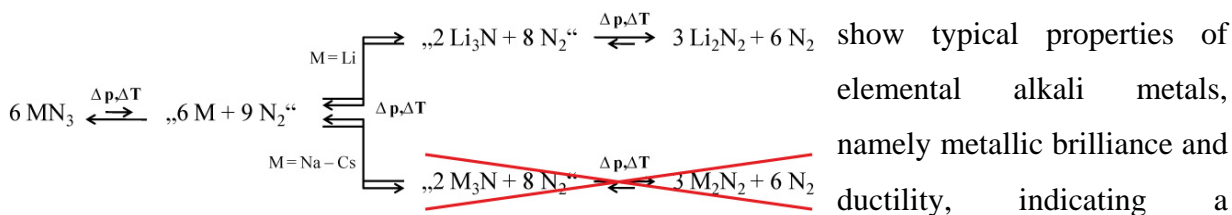
In order to further extend the compositional range of simple metal diazenides, the thermal decomposition of alkali azides, namely Li_2N_2 , under extreme conditions is investigated. Lithium diazenide Li_2N_2 (*Immm* (no. 71), $a = 3.1181(4)$, $b = 4.4372(4)$, $c = 10.7912(16)$ Å, $Z = 4$, $wR_p = 0.0498$) is obtained under HP/HT-conditions of 9 GPa and 750 K in a Walker-type multianvil assembly. The crystal structure of Li_2N_2 is solved and refined on the basis of powder X-ray diffraction data. Li_2N_2 , the first alkali diazenide, represents an unprecedented structure type for A_2B_2 compounds. In contrast to the alkaline earth diazenides CaN_2 , SrN_2 and BaN_2 or even diazene N_2H_2 itself, exhibiting N–N distances in the range of 1.20–1.24 Å, the N–N bond length in Li_2N_2 of 1.301(3) Å is slightly elongated and reasons are presented. The formulation of a $[\text{N}_2]^{2-}$ entity is further supported by FTIR spectroscopy and first principles calculations with the LMTO method.



4. Further Alkali Diazenides

The successful synthesis of Li_2N_2 encouraged the investigation of the thermal decomposition behavior of the heavier alkali azides $M\text{N}_3$ ($M = \text{Na}–\text{Cs}$) under extreme conditions. Thereby, *ex situ* HP/HT-experiments are conducted in a multianvil device at various conditions ranging from 2–18 GPa at temperatures of 423–1173 K. Independently of the synthesis conditions as

well as of the investigated alkali azides, the recovered products of each HP/HT-experiment

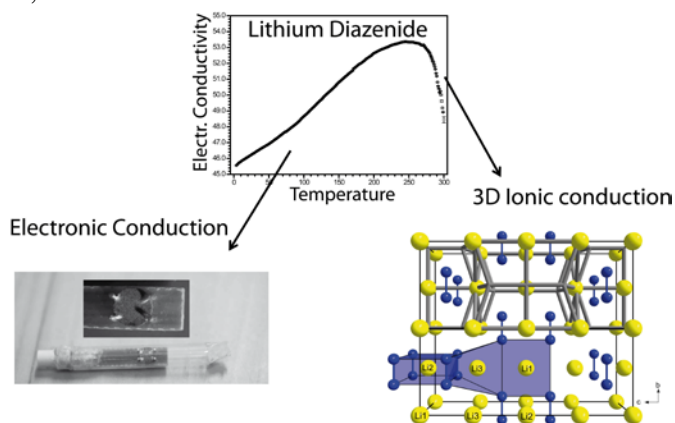


show typical properties of elemental alkali metals, namely metallic brilliance and ductility, indicating a decomposition of the heavier alkali azides into the elements. These findings are supported by *in situ* investigations of pressure-dependent thermal behavior of NaN_3 and KN_3 at the *Hamburger Synchrotronstrahlungslabor* (HASYLAB, Beamline F2.1 operated by the Geoforschungs-zentrum (GFZ) Potsdam until 2012). Both azides also decompose into the elements at increasing temperatures under high pressure conditions. A mechanistic scenario for the differences in reaction behavior of alkali azides (Li vs. Na–Cs) under extreme conditions is presented, however remains only hypothetically.

5. Electronic and Ionic Conductivity in Alkaline Earth Diazenides $M_{\text{AE}}\text{N}_2$ ($M_{\text{AE}} = \text{Ca}, \text{Sr}, \text{Ba}$) and in Li_2N_2

Electrical conductivity measurements of alkaline earth diazenides SrN_2 and BaN_2 reveal temperature-dependent true metal-like behavior. As CaN_2 is isotopic with SrN_2 its electronic properties are supposed to show similar characteristics. For Li_2N_2 , the corresponding measurement also shows typical characteristics of metallic materials, but also an unexpected rise in electrical conductivity above 250 K, which is consistent with the onset of an ionic contribution. This interpretation is further corroborated by static ^6Li and ^7Li nuclear magnetic resonance measurements (NMR) of the spin-lattice relaxation time T_1 over an extended temperature range from 50–425 K. We observe a constant Heitler-Teller product

$T_1 T$ as expected for metals at low temperatures and a maximum in the temperature-dependent relaxation rates, which reflects the suggested ionic conductivity. A topological structural analysis indicates possible 3D ion migration pathways between two of the three crystallographic independent Li positions. A crude estimate of temperature-dependent self-



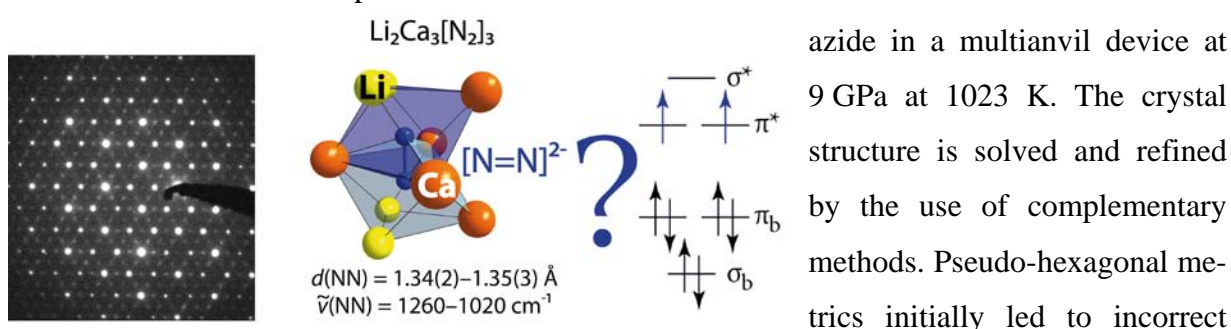
diffusion coefficients $D(T)$ of the lithium motion classifies Li_2N_2 as a mixed electronic/ionic conductor.

6. High-Pressure Behavior of Binary Diazenides

The effect of pressure on the structural and mechano-physical properties of binary diazenides of calcium, strontium and lithium is examined *in situ* at the *European Synchrotron Radiation Facility* (ESRF, Grenoble, France) in diamond-anvil cells at room temperature up to maximum pressures of about 50 GPa. All diazenides show reversible, pressure-induced phase transitions from the ambient structure phases into overall four high-pressure polymorphs (HP- CaN_2 , HP- SrN_2 , β - and γ - Li_2N_2). A comparison of diffraction data of HP- CaN_2 and HP- SrN_2 might indicate possible isotypic high-pressure polymorphs. Decompression data show that all phase transitions are reversible. The bulk moduli B_0 of the ambient pressure phases were determined by fitting a second- and third-order BM-EoS to the experimental p - V data. These data are compared to the values obtained from an Eulerian strain versus normalized stress plot resulting in overall bulk moduli of 80–100 GPa for investigated diazenides. These values are compared to previously reported bulk moduli of binary compounds with homonuclear dianions. Analyses of the behavior of N–N bond lengths of investigated diazenides at high-pressure conditions renders them far more compressible than pernitrides $[\text{N}_2]^{4-}$, in which the higher electron count is responsible for their extremely high incompressibility.

7. High-Pressure Synthesis and Characterization of $\text{Li}_2\text{Ca}_3[\text{N}_2]_3$ – An Uncommon Metallic Diazenide with $[\text{N}_2]^{2-}$ Ions

$\text{Li}_2\text{Ca}_3[\text{N}_2]_3$ (*Pmma* (no. 51), $a = 4.7747(1)$, $b = 13.9792(4)$, $c = 8.0718(4)$ Å, $Z = 4$, $wR_p = 0.08109$) is the first representative of a ternary diazenide. It has been synthesized by a controlled thermal decomposition of a stoichiometric mixture of lithium azide and calcium



structural models supported by theoretical calculations (DFT). Detailed crystallographic analyses including PXRD investigations, SAED simulations and comparison to experimental TEM diffraction patterns finally result in a reliable structural model, which is further corroborated and underlined by quantum-theoretical considerations. Refined N–N bond lengths in the correct space group show strongly elongated values of 1.34(2)–1.35(3) Å exceeding those of previously known, binary diazenides. In fact, observed N–N distances rather suggest the presence of $[\text{N}_2]^{3-}$ radical ions. Characteristic features of the N–N stretching vibration occur at lower wavenumbers than in the binary phases, and these assignments are again supported by first-principles phonon calculations. Detailed electron diffraction, electron spin resonance (ESR) spectroscopy, magnetic and electric conductivity measurements as well as density-functional theory calculations (DFT) finally and unequivocally show that the title compound solely consists of diazenide $[\text{N}_2]^{2-}$ units according to the formula $(\text{Li}^+)_2(\text{Ca}^{2+})_3([\text{N}_2]^{2-})_3 \cdot (\text{e}^-)_2$ presenting the first representative of ternary sub-diazenides.

8. Further Ternary Diazenides

To extend the compositional range of ternary $M^I_x M^{II}_y$ -diazenides (M^{II} = alkali or alkaline earth metal), the thermal behavior of various stoichiometric mixtures of alkali (Na–Cs) and alkaline earth (Ca–Ba) azides under extreme conditions is investigated. Unfortunately, the synthesis of further ternary diazenides under various HP/HT-conditions was not successful. Though the combination of LiN_3 with alkaline earth azides results in crystalline reaction products, they turn out to be mainly composed of the corresponding binary alkaline earth diazenides with only minor, but unidentified and depending on conditions varying side-phases. The HP/HT-treatment of combinations of $M\text{N}_3$ ($M = \text{Na–Cs}$) and $M_{\text{AE}}(\text{N}_3)_2$ ($M_{\text{AE}} = \text{Ca–Ba}$) azides yields always the corresponding elemental alkali metal with dispersed black inclusions of most probably $M_{\text{AE}}\text{N}_2$ diazenides. This observation matches the reported behavior of alkali azides upon HP/HT-conditions that is decomposition into the elements.

7. CONCLUSION AND OUTLOOK

In solid-state chemistry, the existence of homonuclear diatomic nitrogen anions has proven existence only very recently,^[1-19] although the latter represent a common and well-characterized structural motif in biological and synthetic chemistry. Thereby, high-pressure/high-temperature (HP/HT) syntheses starting from the elements and using specialized equipments have introduced binary *diazenides* ($M = \text{Sr, Ba, La}$)^[1-7] and *pernitrides* ($M = \text{Os, Ir, Pd, Pt}$)^[8-19] with $M\text{N}_2$ stoichiometry consisting of $[\text{N}_2]^{2-}$ and $[\text{N}_2]^{4-}$ ions, respectively. Nevertheless, synthesis and characterization of only a handful of examples of both materials classes since their identification in 2001 is quite surprising. Within this context, it is likewise remarkable that solids with isoelectronic, homonuclear diatomic ions consisting of elements to the left (carbon) and to the right (oxygen) of nitrogen in the periodic table have already been synthesized and characterized decades ago.

Introducing the approach of controlled thermal decomposition of ionic azides of Group I and II metals in a multianvil device at extreme conditions resulted in a renaissance of homonuclear diatomic nitrogen chemistry.^[20-23] This high-pressure route proved as excellent tool for the synthesis of hitherto unknown binary and even ternary materials with homonuclear diatomic nitrogen anions. However, compared to the classification of valencies in bound N_2 entities observed in bioinorganic or metal-organic chemistry, their adequate description in solid-state chemistry is hindered due to, for example potential metallicity in such compounds. Nevertheless, by the use of a variety of complementary experimental and theoretical methods, the identification of the true oxidation state in $[\text{N}_2]^{x-}$ ($x = 1-4$) anions is possible.

Moreover, a chemist's aim should not only be to *synthesize* novel materials with extraordinary properties, but also to *transfer* the knowledge of characterized properties to possible applications or if hindered to *establish* synthesis conditions or materials classes to basics in

fundamental research. Within this context both, diazenides and pernitrides are very promising candidates although they are very sensitive to moisture unfortunately hindering industrial applications. PERNITRIDES, for example have been reported as mechanically ultra-hard materials even approaching the hardness of *c*-BN or diamond.^[8–19] An observation, which is attributed to the high electron-count in stiff $[\text{N}_2]^{4-}$ ions, which consist of completely filled π^* antibonding orbitals and therefore impede a massive contraction of the N–N bonds. Furthermore, Li_2N_2 has shown to be a mixed electronic/ionic conductor depending on temperature.^[22] Its self-diffusion coefficients are thereby within the range of typical cathode and electrolyte materials for Li-ion batteries.^[24–26] On the other hand, as homonuclear diatomic nitrogen species have been discovered in solid-state chemistry only very recently, the identification of their crystal structures contributes to a detailed understanding of fundamental research in inorganic chemistry.

By now, only a few members of binary and ternary diazenides and pernitrides are known in solid-state chemistry, all of them having been synthesized under extreme conditions starting from both, either the elements in specialized equipments or ionic azides in a multianvil device.^[1–23] As the HP/HT-route starting from ionic azides has proven to be an excellent method, and has been intensively investigated within this thesis, an adaption for covalent azides, for example of Groups 11 or 12 (AgN_3 or $\text{Zn}(\text{N}_3)_2$, respectively) might result in hitherto unknown diazenides with interesting properties. Thereby, especially the synthesis of ZnN_2 seems to be practicable as thermodynamic investigations showed that it should be stable with respect to dissociation to the elements ($\Delta H_{\text{reaction}} < 0$).^[19] Furthermore, re-visiting the initial synthesis procedures for diazenides and pernitrides, namely the reaction of the elements, still could be a very promising way in chemistry for obtaining nitrogen-rich materials as predicted by a variety of different groups.^[17–19,27–32] Thereby, even industrial synthesis procedures such as hot isostatic pressing (HIP) in nitrogen atmosphere might constitute a promising approach for the synthesis of unprecedented homonuclear diatomic representatives as these devices are able to establish pressures of about 0.3 GPa (3000 bar) in maximum – a pressure which is within the range of initial diazenide synthesis (9–5500 bar).^[1–6,33]

Not only HP/HT-experiments might result in further representatives with homonuclear diatomic nitrogen anions, but also conventional methods in solid-state chemistry, such as metathesis reactions. This unique type of reaction is very efficient because it uses the intrinsic energy of the reaction partners being involved. Desired stoichiometries are achieved by

appropriate starting materials for the reactions controlled through the heating procedure and potentially by using a reactive flux, which lowers the ignition temperature of a reaction mixture and might even promote crystal growth of products. This approach has already shown to be successful for the synthesis of various materials, such as nitridoborates, carbodiimides, tetracyanoborates, tetracyanamidosilicates and carbon-nitrides.^[34] A further big advantage is the reduced temperature upon synthesis due to the as-mentioned intrinsic energy of reaction partners. In the most metathesis reactions chlorides are reacted with lithium compounds bearing the anion of choice to be transferred. The successful synthesis of Li_2N_2 perfectly matches the pre-conditions of potential metathesis reactions and might clear the way for future chemists to exploratively study the existence of novel homonuclear diatomic nitrogen representatives and characterize their properties to expand fundamental research of main group solid-state chemistry.

References

- [1] G. Auffermann, Y. Prots, R. Kniep, *Angew. Chem.* **2001**, *113*, 565; *Angew. Chem., Int. Ed.* **2001**, *40*, 547.
- [2] G. Auffermann, Y. Prots, R. Kniep, S.F. Parker, S. M. Bennington, *ChemPhysChem* **2002**, *9*, 815.
- [3] G. Auffermann, U. Schmidt, B. Bayer, Y. Prots, R. Kniep, *Anal. Bioanal. Chem.* **2002**, *373*, 880.
- [4] G. Auffermann, R. Kniep, W. Bronger, *Z. Anorg. Allg. Chem.* **2006**, *632*, 565.
- [5] Y. Prots, G. Auffermann, M. Tovar, R. Kniep, *Angew. Chem.* **2002**, *114*, 2392; *Angew. Chem., Int. Ed.* **2002**, *41*, 2288.
- [6] G.V. Vajenine, G. Auffermann, Y. Prots, W. Schnelle, R.K. Kremer, A. Simon, R. Kniep, *Inorg. Chem.* **2001**, *40*, 4866.
- [7] O. Tschauer, S.N. Luo, Y.J. Chen, A. McDowell, J. Knoght, S.M. Clark, *High Pressure Res.* **2013**, *33*, 202.
- [8] E. Gregoryanz, C. Sanloup, M. Somayazulu, J. Badro, G. Fiquet, H.-K.; Mao, R.J. Hemely, *Nat. Mater.* **2004**, *3*, 294.

- [9] J. von Appen, M.-W. Lumey, R. Dronskowski, *Angew. Chem.* **2006**, 118, 4472; *Angew. Chem., Int. Ed.* **2006**, 45, 4365.
- [10] J.C. Crowhurst, A.F. Goncharov, B. Sadigh, C.L. Evans, P.G. Morrall, J.L. Ferreira, A.J. Nelson, *Science* **2006**, 311, 1275.
- [11] A.F. Young, J.A. Montoya, C. Sanloup, M. Lazzeri, E. Gregoryanz, S. Scandolo, *Phys. Rev. B* **2006**, 73, 153102.
- [12] J.A. Montoya, A.D. Hernandez, C. Sanloup, E. Gregoryanz, S. Scandolo, *Appl. Phys. Lett.* **2007**, 90, 011909.
- [13] J.C. Crowhurst, A.F. Goncharov, B. Sadigh, J.M. Zaug, D. Aberg, Y. Meng, V.B. Prakapenka, *J. Mater. Res.* **2008**, 23, 1.
- [14] Z.W. Chen, X.J. Guo, Z.Y. Liu, M.Z. Ma, Q. Jing, G. Li, X.Y. Zhang, L.X. Li, Q. Wang, Y.J. Tian, R.P. Liu, *Phys. Rev. B* **2007**, 75, 054103.
- [15] R. Yu, Q. Zhan, L.C. De Jonghe, *Angew. Chem.* **2007**, 119, 1154; *Angew. Chem., Int. Ed.* **2007**, 46, 1136.
- [16] W. Chen, J.S. Tse, J.Z. Jiang, *J. Phys.: Condens. Mater* **2010**, 22, 015404.
- [17] A. Salamat, A. L. Hector, P. Kroll, P.F. McMillan, *Coord. Chem. Rev.* **2013**, 257, 2063.
- [18] M. Wessel, R. Dronskowski, *J. Am. Chem. Soc.* **2010**, 132, 2421.
- [19] M. Wessel, *PhD thesis*, RWTH Aachen University: Aachen, **2010**.
- [20] S.B. Schneider, R. Frankovsky, W. Schnick, *Inorg. Chem.* **2012**, 51, 2366.
- [21] S.B. Schneider, R. Frankovsky, W. Schnick, *Angew. Chem.* **2012**, 124, 1909; *Angew. Chem., Int. Ed.* **2012**, 51, 1873.
- [22] S.B. Schneider, M. Mangstl, G.M. Friederichs, R. Frankovsky, J. Schmedt auf der Günne, W. Schnick, *Chem. Mater.* **2013**, 25, 4149.
- [23] S.B. Schneider, M. Seibald, V.L. Deringer, R.P. Stoffel, R. Frankovsky, G.M. Friederichs, H. Laqua, V. Duppel, G. Jeschke, R. Dronskowski, W. Schnick, *J. Am. Chem. Soc.* **2013**, 135, 16668.

- [24] Y.I. Jang, B.J. Neudecker, N.J. Dudney, *Electrochem. Solid-State Lett.* **2001**, *4*, A74.
- [25] T.-Y. Wu, L. Hao, C.-W. Kuo, Y.-C. Lin, S.-G. Su, P.-L. Kuo, I.-W. Sun, *Int. J. Electrochem. Sci.* **2012**, *7*, 2047.
- [26] K. Hayamizu, Y. Aihara, *Solid State Ionics* **2013**, *238*, 7.
- [27] X. Zhang, A. Zunger, G. Trimarchi, *J. Chem. Phys.* **2010**, *133*, 194504.
- [28] M. Wessel, R. Dronskowski, *J. Comput. Chem.* **2010**, *31*, 1613.
- [29] M. Wessel, R. Dronskowski, *Chem. Eur. J.* **2011**, *17*, 2598.
- [30] S. D. Gupta, S.K. Gupta, P.K. Jha, *Eur. Phys. J. B.* **2013**, *86*, 8.
- [31] A. Kulkarni, J.C. Schön, K. Doll, M. Jansen, *Chem. Asian J.* **2013**, *8*, 743.
- [32] A. Kulkarni, *PhD thesis*, University Stuttgart: Stuttgart, **2012**.
- [34] http://www.alcoa.com/howmet/en/service_category.asp?cat_id=40,
accessed 23/10/2013.
- [34] H.-J. Meyer, *Dalton Trans.* **2010**, *39*, 5973

8. APPENDIX

8.1 SUPPORTING INFORMATION

8.1.1 SUPPORTING INFORMATION FOR CHAPTER 2.1

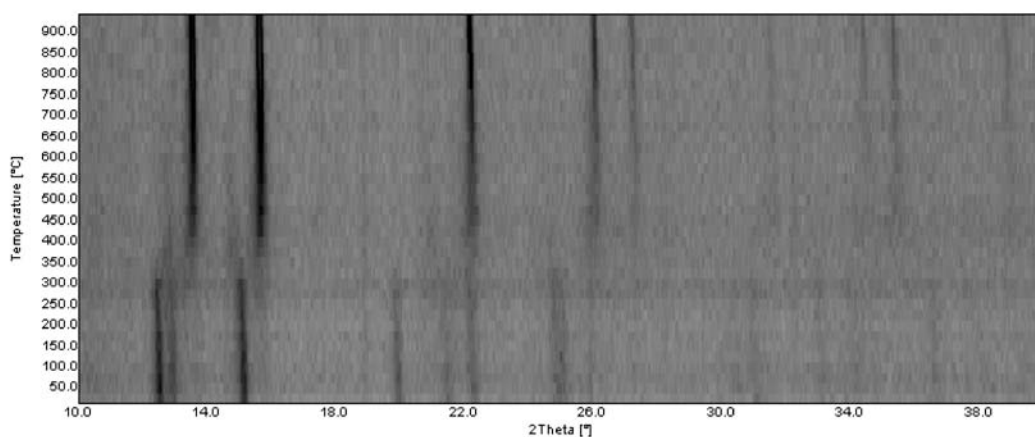


Figure S1. Temperature-dependent *in situ* powder diffraction patterns of SrN₂ (Mo K_{α1} radiation (0.7093 Å)).

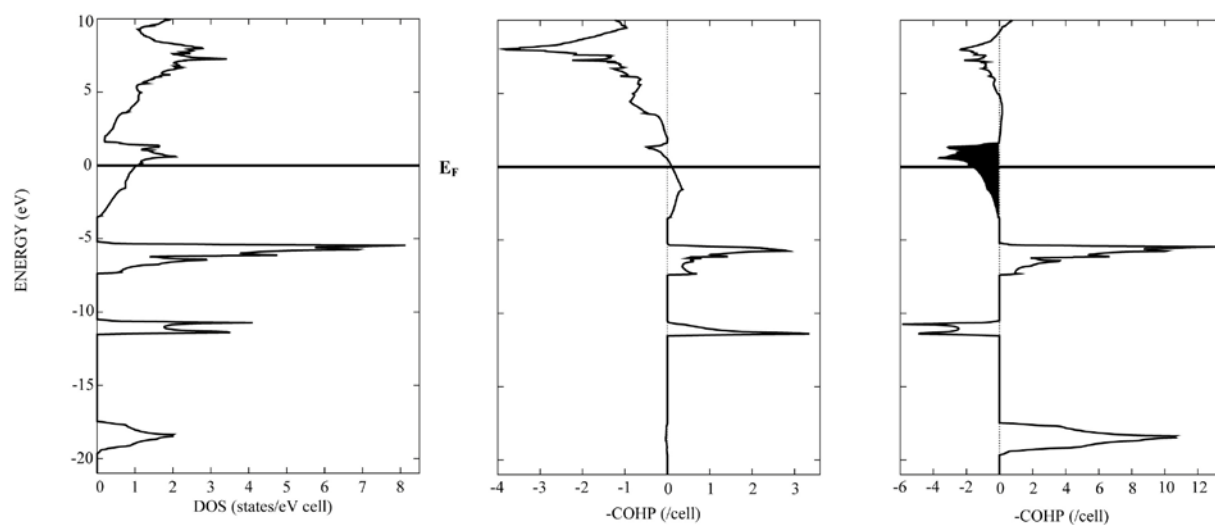


Figure S2. Total DOS (left), COHP analysis of Sr-N (middle) and N-N (right) for SrN₂.

8.1.2 SUPPORTING INFORMATION FOR CHAPTER 3.1

Experimental details of the HP/HT-synthesis

Lithium diazenide was synthesized under HP/HT-conditions in a modified Walker-type module in combination with a 1000 t press (both devices from the company Voggenreiter, Mainleus, Germany). Starting material for the synthesis was crystalline lithium azide, which was precipitated from its aqueous solution (Sigma-Aldrich, 20 wt% solution in water) by evaporation in vacuum. The product was dried over P_4O_{10} using a vacuum desiccator (24h) and analyzed by means of infrared spectroscopy and X-ray diffractometry. Then, LiN_3 was carefully ground, filled into a cylindrical copper crucible, placed into a boron nitride crucible (Henze BNP GmbH, Kempten, Germany) and sealed with a fitting boron nitride plate. As pressure medium, precastable MgO-octahedra (Ceramic Substrates & Components, Isle of Wight, U.K.) with edge lengths of 18 mm (18/11 assembly) were applied. Eight tungsten carbide cubes (Hawedia, Marklkofen, Germany) with truncation edge lengths of 11 mm compressed the octahedra. The details of the setup can be found in literature.^[1-5] The assembly was compressed up to 9 GPa at room temperature within 217 min, then heated up to 750 K in 10 min, kept at this temperature for 50 min and finally cooled down to room temperature in 10 min again. Subsequently, the pressure was released over a period of 633 min. The recovered MgO-octahedron was broken apart in a glovebox and the sample was carefully isolated from the surrounding boron nitride and copper crucibles. A black metallic powder of lithium diazenide is obtained. No chemical analysis was performed due to the fact that there is still an unknown side phase present.^[6]

Information about the data collection and selected crystallographic details of the Rietveld refinement of Li_2N_2

The crystal structure of Li_2N_2 was analyzed on the basis of powder X-ray diffraction data. The powder diffraction patterns were recorded with a STOE Stadi P powder diffractometer (STOE, Darmstadt, Germany) in Debye-Scherrer geometry using Ge(111) monochromated Cu $K_{\alpha 1}$ radiation (1.54056 Å). The indexing resulted unambiguously in an orthorhombic unit-cell with $a = 3.11$, $b = 4.43$ and $c = 10.79$ Å. From systematic absences the space groups $I222$, $I2_12_12_1$, $Imm2$ and $Immm$ were considered. The integration and extraction of the intensities as well as the structure solution was carried out by using the TOPAS package.^[7] The position of all atoms on chemically plausible sites was only possible in space groups $Immm$ and $I222$.

However, a distinct differentiation of the two possible space groups was not possible. Therefore, the space group with the highest symmetry (*Immm*) was chosen for structure refinement. The Rietveld refinement was performed with the TOPAS package using the atomic positions found upon structure solution. The reflection profiles were determined using

Table S1. Information About the Data Collection and Selected Crystallographic Details of the Rietveld Refinement of Li_2N_2 .

<i>Formula</i>	Li_2N_2
Synthesis Conditions	
$d_{\text{NN}}/\text{\AA}$	9 GPa @ 750 K
fw /g·mol ⁻¹	1.301(3)
space group	41.89
cell parameters / \AA	<i>Immm</i> (no. 71)
	$a = 3.1181(4)$
	$b = 4.4372(4)$
	$c = 10.7912(16)$
$V/\text{\AA}^3$	149.31(3)
Z/cell	4
$\rho_{\text{calc}}/\text{g}\cdot\text{cm}^{-3}$	1.8640(4)
$\mu_{\text{calc}}/\text{mm}^{-1}$	1.17
Data Collection	
type of diffractometer	STOE Stadi P
geometry	Debye-Scherrer
radiation, monochromator	Cu- $K_{\alpha 1}$ ($\lambda = 1.54056 \text{\AA}$), Ge(111)
T/K	298(2)
detector	linear PSD ($\Delta 2\theta = 5^\circ$)
2θ range /°	10–80
number of observed reflections	38
Structure Analysis and Refinement	
method of refinement	fundamental parameter approach ^[10]
program package	TOPAS Academic
atomic parameters	7
background function /parameters	shifted Chebyshev /16
R indices	$\text{GoF}(\chi^2) = 1.755$ $R_p = 0.07061$ $wR_p = 0.09488$

the fundamental parameter approach^[8] by convolution of appropriate source emission profiles with axial instrument contributions and crystalline microstructure effects. Preferred orientation of the crystallites was described with a spherical harmonics of 4th order. To prove the novelty of the structure type a precise search within several structural databases was performed, resulting in the Sc_3TMC_4 ($\text{TM} = \text{Fe}, \text{Co}, \text{Ni}, \text{Rh}, \text{Ru}, \text{Os}, \text{Ir}$)^[9] structure type having similar atomic positions and crystallizing in space group *Immm* as well. However, both structural models (Li_2N_2 and Sc_3TMC_4) differ in one of their four atomic positions (Li_2N_2 : 4i, Sc_3TMC_4 : 4j). The differing positions cannot be converted into each other underlining Li_2N_2 being not isotypic with Sc_3TMC_4 and therefore confirming the hitherto unknown structure type. The relevant crystallographic data for lithium

diazene and further details of the data collection are summarized in Table S1.

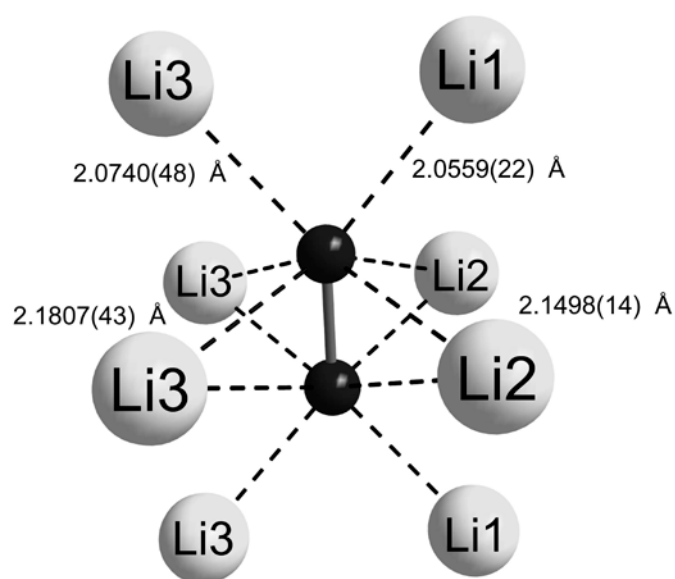
Li-N distances in Li₂N₂

Figure S1. Coordination sphere of diazenide unit with corresponding Li-N distances; Li gray, nitrogen black.

Structural investigation and comparison of the novel structure type to related structural models

Comparing the structural model of Li₂N₂ to reported structures, there are only two models crystallizing in a similar structure. For structures with A₂B₂ composition, it is Li₂C₂ (Figure S2 left, Table S2 top).^[11] However, there is no direct symmetry relation between Li₂N₂ and Li₂C₂

Table S2. Atomic Positions in Li₂C₂ and Sc₃CoC₄.^[9,11]

Atoms (Wyckoff)	x	y	z
Li₂C₂			
Li1(4i)	0	0	0.236
C1(4g)	0	0.3731	0
Sc₃CoC₄			
Co1(2a)	0	0	0
Sc2(2c)	½	½	0
Sc1(4j)	½	0	0.188
C1(8l)	0	0.332	0.124

converting both structures into each other. The anionic lattices are not convertible at all, whereas the cationic lattices derive from the same aristotype, which is the γ -Sn-type (*Cmmm*).^[12] In Li₂C₂ however, the unit-cell is doubled, while in Li₂N₂ it is quadruplicated.

To prove our novel structural model, we even expanded our search for related compounds to ternary and multinary phases. It were the scandium transition metal carbides Sc₃TMC₄ (TM = Fe, Co, Ni, Ru, Rh, Os, Ir) in space group *Immm*^[9] which attracted our interest due to a very similar atomic arrangement (Figure S2 right, Table S2 bottom). Replacing the Sc2 and TM1 site by Li and the carbide dimers by diazenide units, it is only the Sc1 site which makes

a full symmetric conversion of both structures impossible. Therefore, as we can not find any structural model isotopic to our model, Li_2N_2 crystallizes in a novel, unprecedented structure type (resembling that of Sc_3TMC_4).

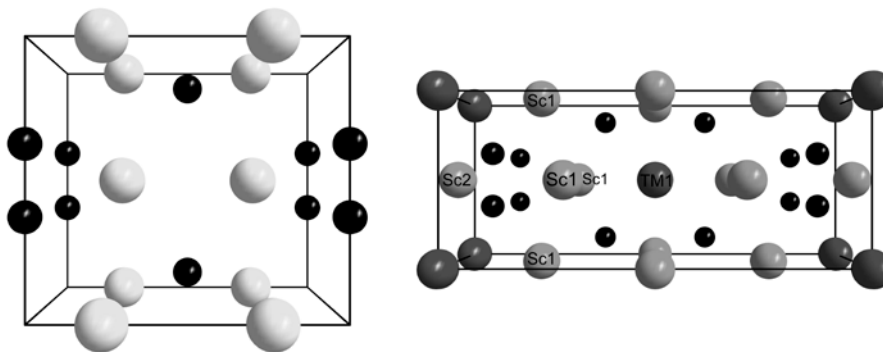


Figure S2. Unit-cell of Li_2C_2 (left) and Sc_3CoC_4 (right) along [100]; lithium white, scandium light gray, cobalt representing transition metals dark gray, carbon black. Structure data taken from the literature.^[9,11]

Temperature-dependent in situ X-Ray diffraction from 8 to 1173 K

A) Experimental details

Low-temperature X-ray diffraction data were collected using a Huber G670 Guinier imaging plate diffractometer (Co $K_{\alpha 1}$ radiation (1.7890 Å)) equipped with a closed cycle He-cryostat. The samples were cooled down from room temperature to 8 K in 5 K/min in steps of 25 K. At each cooling step (after holding the temperature for 1 min) a diffraction pattern was recorded in the range of $0^\circ \leq 2\theta \leq 80^\circ$.

High-temperature *in situ* X-ray powder diffraction data were collected with a STOE Stadi P powder diffractometer (Mo $K_{\alpha 1}$ radiation (0.7093 Å)) equipped with a computer controlled STOE resistance graphite furnace. Enclosed in a silica glass capillary under argon, the samples were heated from room temperature to 1173 K in 5 K/min in steps of 25 K. At each heating step (after holding the temperature for 1 min) a diffraction pattern was recorded with an IP-PSD in the range of $7^\circ \leq 2\theta \leq 80^\circ$.

B) Results

Low-temperature measurements from room temperature down to 8 K resulted in no observable transformation of Li_2N_2 . Figure S3 shows the high-temperature *in situ* X-ray diffraction patterns of Li_2N_2 from room temperature to 1173 K. At 475 K a transformation of Li_2N_2 into $\alpha\text{-Li}_3\text{N}$ occurs. Reaching 800 K, $\alpha\text{-Li}_3\text{N}$ decomposes forming Li_2O , which finally

(950 K) reacts with the quartz capillary to Li_2SiO_3 . Another prove, that the non-indexed lines in the powder diffraction pattern of Li_2N_2 (Figure 1 in publication) do definitely not belong to Li_2N_2 , is the fact, that these lines do not transform into $\alpha\text{-Li}_3\text{N}$ at about 475 K, but only shift to smaller 2θ angles with respect to the higher temperature.

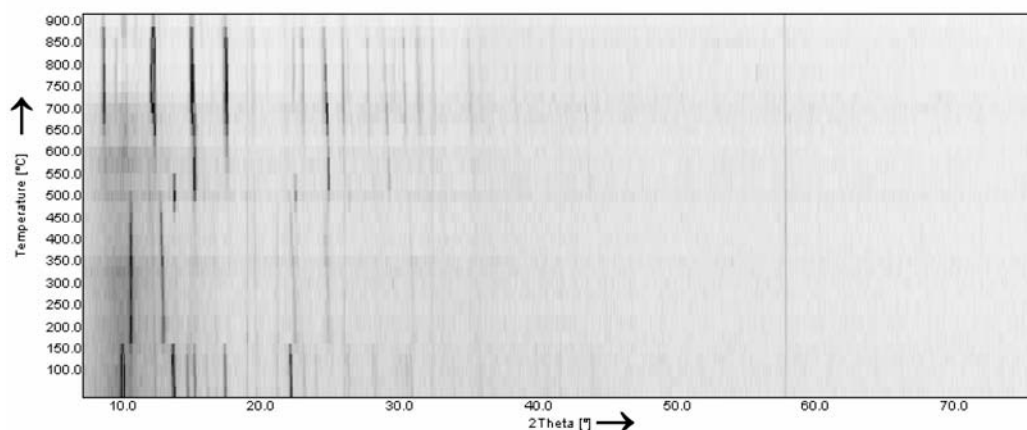


Figure S3. High-temperature *in situ* X-ray diffraction patterns of Li_2N_2 (Mo $K_{\alpha 1}$ radiation (0.7093 Å)).

FTIR spectroscopy of Li_2N_2

A) Experimental details

Fourier transform infrared (FTIR) measurements were carried out on a Bruker IFS 66v/S spectrometer. Spectra of the samples were recorded in an evacuated cell at ambient conditions between 400 and 4000 cm^{-1} after diluting the samples in KBr pellets (2 mg sample, 300 mg KBr, pressed with 10 kN).

B) Results

Concerning a free diazenide ion (point symmetry $D_{\infty h}$), the only basic vibration is Raman-active and IR-inactive due to the rule of mutual exclusion.^[13] Therefore, to observe an IR-active mode of $[\text{N}_2]^{2-}$, its corresponding site symmetry in the solid has to be reduced. This condition is actually fulfilled, as the diazenide ion adopts the reduced site symmetry C_s . Figure S4 illustrates the infrared spectrum of Li_2N_2 . As already mentioned, the significant feature at 1326.8 cm^{-1} is assigned to the N–N stretching vibration of the diazenide ion due to previous vibrational measurements on CaN_2 , SrN , SrN_2 and BaN_2 .^[14,15] Additional features at considerable lower wavenumbers (at about 500 cm^{-1}) are assigned to acoustic, optic translational and librational modes of the $[\text{N}_2]^{2-}$ ion as reported in literature.^[14] The modes at

about 2000 cm^{-1} are so far unexplained. However, as there is still an unknown side phase in the bulk sample present, these features might be assigned to the side phase. In addition, because of the extremely high sensitivity to moisture, the diazenides tend to hydrolyze very easily. As the KBr-sample pellet is exposed to normal atmosphere upon the transfer from the glovebox to the sample chamber of the spectrometer, LiOH is formed definitively. Therefore, the feature at 3675.7 cm^{-1} is assigned to the stretching vibration of the hydroxide ion.

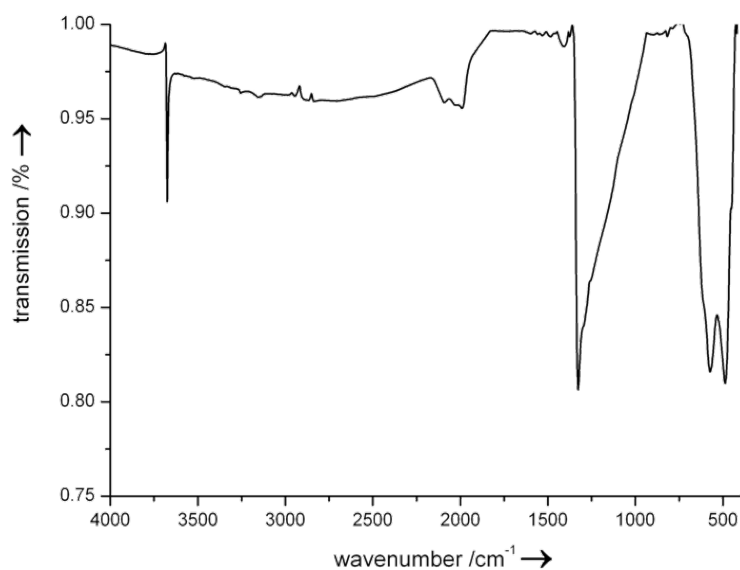


Figure S4. FTIR Spectrum of Li_2N_2 .

First principle calculations on the electronic structure of Li_2N_2

A) Experimental details

The LMTO method in its scalar relativistic version (TB-LMTO-ASA program)^[16] was used to perform the band structure, electronic density of states (DOS) and crystal orbital Hamiltonian population (COHP) calculations.^[17] Detailed descriptions of the method are given elsewhere.^[18,19] The k point set was extended to a $12 \times 24 \times 24$ array to properly describe the metallic compound. The basis set consisted of Li: $2s/\{2p\}/\{3d\}$ and N: $2s/2p/\{3d\}$ where orbitals given in parenthesis were downfolded.^[20] The electronic structure calculations converged when the change of the total energy was smaller/equal to 10^{-5} Ry. The COHP method was used for the bond analysis. COHP gives the energy contributions of all electronic states for a selected bond. The values are negative for bonding and positive for antibonding interactions. With respect to the COHP diagrams, we plot $-\text{COHP}(E)$ to get positive values

for bonding states. The structural parameters were taken from the Rietveld refinement. The orbital character of the bands was analyzed using the so-called fat-band plots.

B) Results

As already mentioned in the publication, the electronic band structure calculations (Figure S5) suggest that the compound is metallic. The main contribution of bands at the Fermi level comes from N-p ($2p$, $1\pi_g^*$) states with only little contribution of the Li states ($2s$, $2p$). To elucidate the bonding situation, the DOS (Figure S6 left) and COHP of the interactions of Li-N (Figure S7) and N-N (Figure S6 right) were calculated as well.

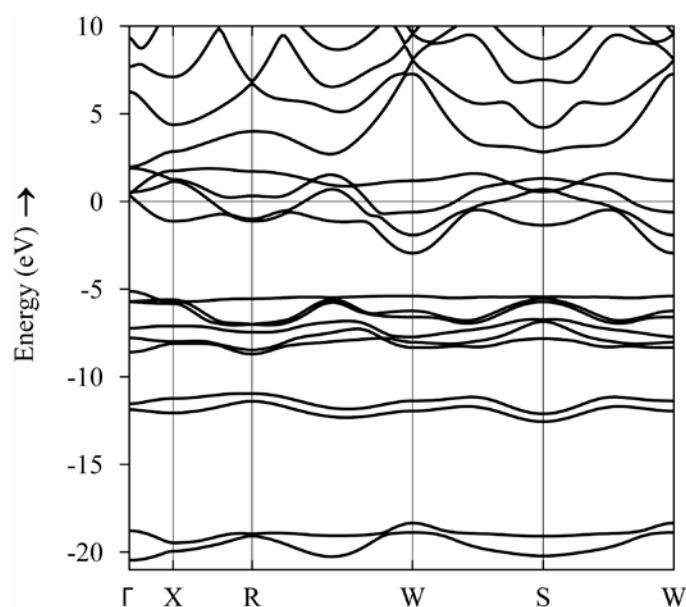


Figure S5. TB-LMTO band structure of Li_2N_2 .

At about -20 eV the states of the $1\sigma_g$ orbitals of the nitrogen dumbbell are located. The nitrogen $1\sigma_u^*$ states can be found at about -12 eV, mixing with Li- s and $-p$ states. Above that, around -8 to -5 eV the $2\sigma_g$ and the $1\pi_u$ bonding states of the diazenide together with an increased contribution of the lithium states can be found. The states in the proximity of the Fermi level ranging from -3 to 3 eV are basically the $1\pi_g^*$ states of the diazenide ion which are only slightly mixed with lithium states. These metal-nitrogen interactions are found to be responsible for the significant widths of the corresponding bands in the band structure, and thus probably being also responsible for the metallic character of these compounds. The states above 3 eV are predominantly formed by Li- s and $-p$ states. The COHP plot of the N-N combination clearly shows the situation as expected for the $[\text{N}_2]^{2-}$ ion: to understand the

bonding situation, the molecular-orbital diagram of N_2 has to be taken into account. Upon forming N_2 by linear combination of the atomic orbitals of elemental nitrogen, the molecular orbitals $1\sigma_g$, $1\sigma_u^*$, $2\sigma_g$, $1\pi_u$, $1\pi_g^*$ and $2\sigma_u^*$ of molecular nitrogen are formed.

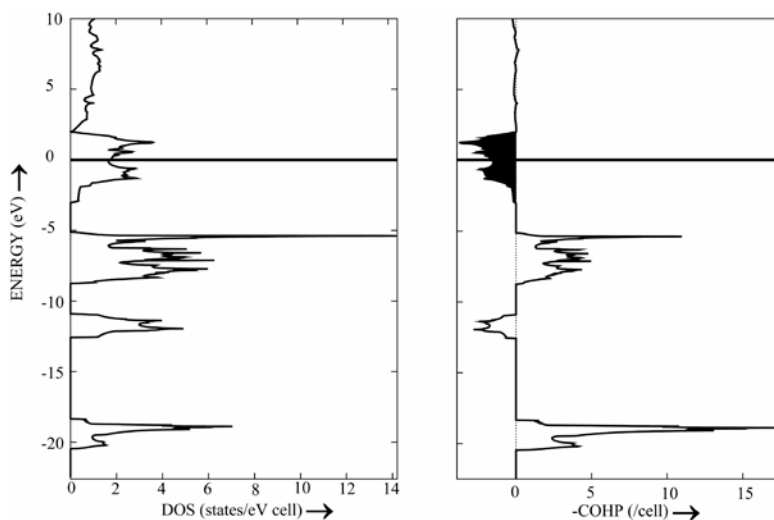


Figure S6. Total DOS (left) and COHP analysis of the N–N bond (right) in states/eV per formula unit of Li_2N_2 . In the COHP plot, the bonding states are given as features to the right, whereas antibonding states show up as features to the left.

The bonding orbitals $2\sigma_g$ and $1\pi_u$ are filled up with six electrons resulting in a maximum of bonding multiplicity of 3 (triple bond, N_2). Adding further 2 electrons into the $1\pi_g^*$ molecular orbital, then results in $[N_2]^{2-}$ and a 50 % occupation of these antibonding $1\pi_g^*$ orbitals. Therefore, the bonding multiplicity is reduced to a value of 2 which corresponds with a double-bonded dinitrogen unit as observed in $[N_2]^{2-}$. This anion is isosteric to molecular oxygen and to $[C_2]^{4-}$. Therefore, it should exhibit paramagnetic behavior. However, magnetic susceptibility measurements and electronic structure calculations for BaN_2 already revealed that the compound exhibits only Pauli paramagnetism and is metallic, despite the paramagnetic triplet state of the isolated diazenide ion.^[21] Thus, a test spin-polarized calculation with nonzero magnetic moments artificially placed on the nitrogen atoms was conducted for Li_2N_2 and converged back to the metallic state. This confirms that Li_2N_2 is metallic as well, which was already assumed for the band structure. Coming back to the COHP of N–N, it is not surprising that on the one hand the states near the Fermi level are antibonding, and that on the other hand the Fermi level crosses these states at about half of their antibonding character. This perfectly matches with the 50 % occupation of the antibonding π -states of the diazenide ion. Concerning the Li–N combinations, there are

basically only bonding states up to E_F . Above the Fermi level (in the region of the unoccupied states), the antibonding Li–N interactions are settled.

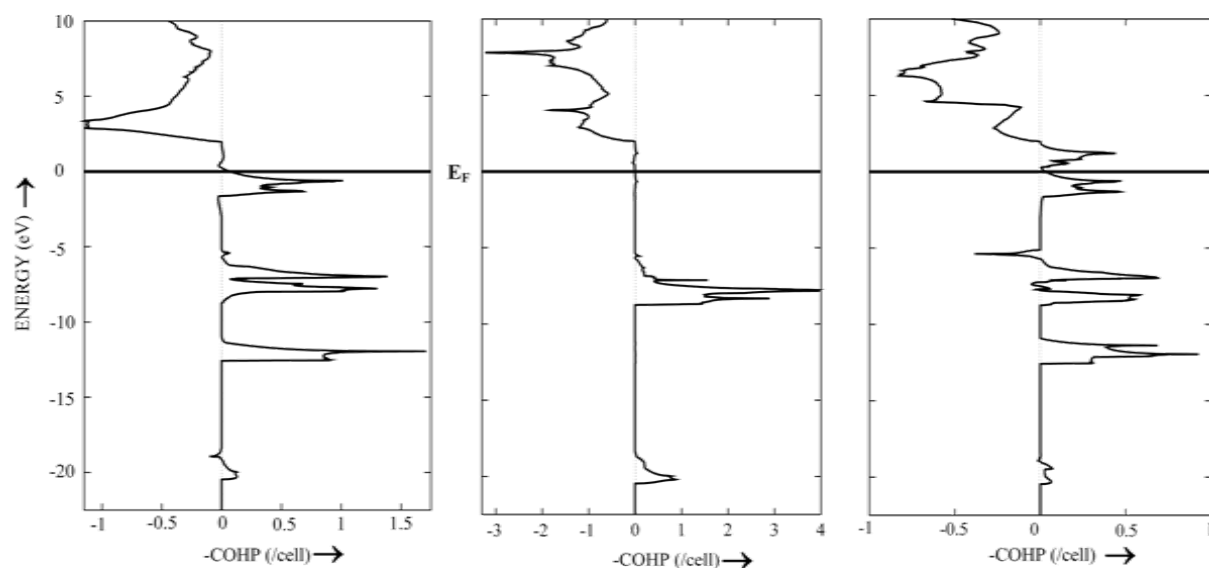


Figure S7. COHP analysis of the Li–N interactions of Li_2N_2 in states/eV per formula unit. In these plots, the bonding states are given as features to the right, whereas antibonding states show up as features to the left. As there are three different Li sites in Li_2N_2 , at least three different Li–N COHP plots result: Li1–N (left), Li2–N (middle) and Li3–N (right). Additionally, only the nearest Li–N interactions are taken into account ($d_{\text{Li1–N}} = 2.0559(22) \text{ \AA}$, $d_{\text{Li2–N}} = 2.1498(14) \text{ \AA}$, $d_{\text{Li3–N}} = 2.0740(48) \text{ \AA}$).

References

- [1] D. Walker, M.A. Carpenter, C. M. Hitch, *Am. Mineral.* **1990**, 75, 1020.
- [2] D. Walker, *Am. Mineral.* **1991**, 76, 1092.
- [3] H. Huppertz, *Z. Kristallogr.* **2004**, 219, 330.
- [4] D.C. Rubie, *Phase Transitions* **1999**, 68, 431.
- [5] N. Kawai, S. Endo, *Rev. Sci. Instrum.* **1970**, 8, 1178.
- [6] Non-indexed reflections do definitively not belong to Li_2N_2 , which is confirmed by a slight variation of synthesis conditions (only a few K and about 0.5 GPa) and by temperature-dependent *in situ* X-ray diffractometry (see supporting information). If the synthesis conditions are slightly varied, the reflection intensities of the side phase vary with respect to the observed lines compared to the optimum conditions. However, the true nature of the side phase is still unknown.

- [7] A.A. Coelho, *TOPAS-Academic* Version 4.1, Coelho Software, Brisbane, **2007**.
- [8] J. Bergmann, R. Kleeberg, A. Haase, B. Breidenstein, *Mater. Sci. Forum* **2000**, 303, 347.
- [9] a) A.O. Tsokol', O.I. Bodak, E.P. Marusin, *Sov. Phys. Crystallogr.* **1986**, 31, 466; b) R.-D. Hoffmann, R. Pöttgen, W. Jeitschko, *J. Solid State Chem.* **1992**, 99, 134.
- [10] J. Bergmann, R. Kleeberg, A. Haase, B. Breidenstein, *Mater. Sci. Forum* **2000**, 303, 347.
- [11] a) R. Juza, V. Wehle, *Naturwissenschaften* **1965**, 52, 537; b) R. Juza, V. Wehle, H.-U. Schuster, *Z. Anorg. Allg. Chem.* **1967**, 352, 252.
- [12] R. Kubiak, *J. Less-Common Met.* **1986**, 116, 307.
- [13] J. Weidlein, U. Müller, K. Dehnicke, *Schwingungsspektroskopie—Eine Einführung*, Georg Thieme Verlag Stuttgart: New York, **1982**.
- [14] G. Auffermann, Y. Prots, R. Kniep, S.F. Parker, S.M. Bennington, *ChemPhysChem* **2002**, 9, 815.
- [15] S.B. Schneider, R. Frankovsky, W. Schnick, *Inorg. Chem.* **2012**, 51, 2366.
- [16] O.K. Andersen, O. Jepsen, *Tight-Binding LMTO*, Version 4.7, Max-Planck-Institut für Festkörperforschung: Stuttgart **1994**.
- [17] R. Dronskowski, P. Blöchl, *J. Phys. Chem.* **1993**, 97, 8617.
- [18] O. Jepsen, M. Snob, O.K. Andersen, *Linearized Band Structure Methods and its Applications*, Springer Lecture Notes, Springer-Verlag: Berlin **1987**.
- [19] H.L. Skriver, *The LMTO Method*, Springer-Verlag: Berlin **1984**.
- [20] W.R.L. Lambrecht, O.K. Andersen, *Phys. Rev. B* **1986**, 34, 2439.
- [21] G.V. Vajenine, G. Auffermann, Y. Prots, W. Schnelle, R.K. Kremer, A. Simon, R. Kniep, *Inorg. Chem.* **2001**, 40, 4866.

8.1.3 SUPPORTING INFORMATION FOR CHAPTER 4.1

Infrared Spectra of $^{6,7}\text{Li}_2\text{N}_2$ and $M_{\text{AE}}\text{N}_2$ ($M_{\text{AE}} = \text{Ca}, \text{Sr}, \text{Ba}$)

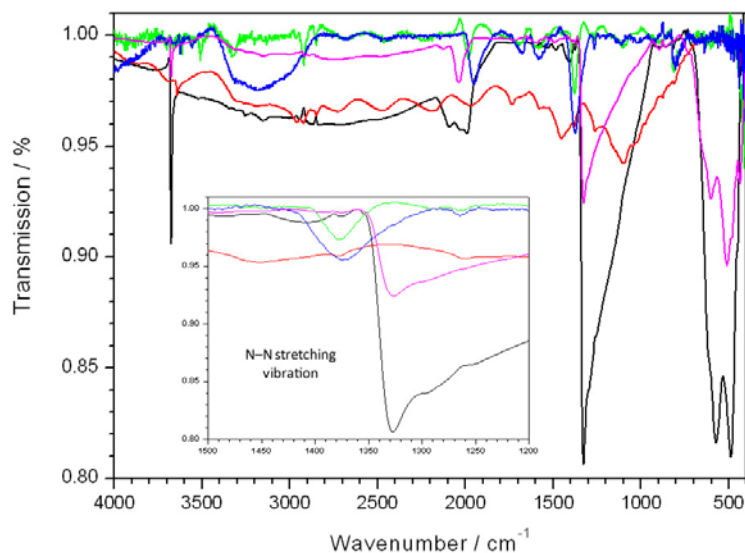


Figure S1. FTIR spectra of $^7\text{Li}_2\text{N}_2$ (black), $^6\text{Li}_2\text{N}_2$ (magenta), CaN_2 (red), SrN_2 (green) and BaN_2 (blue). The region of the $[\text{N}_2]^{2-}$ feature is enlarged. Thereby, vibrational features for $^7\text{Li}_2\text{N}_2$ and $^6\text{Li}_2\text{N}_2$ are located both at 1326.8 cm^{-1} , and for CaN_2 , SrN_2 and BaN_2 at 1376.9 , 1378.9 and 1375.9 cm^{-1} , respectively.^[1,2]

Note that a detailed evaluation of corresponding FTIR spectra has been previously presented in references [1] and [2].

Plot of $1/(T_1T)$ versus Temperature for ^6Li and ^7Li NMR

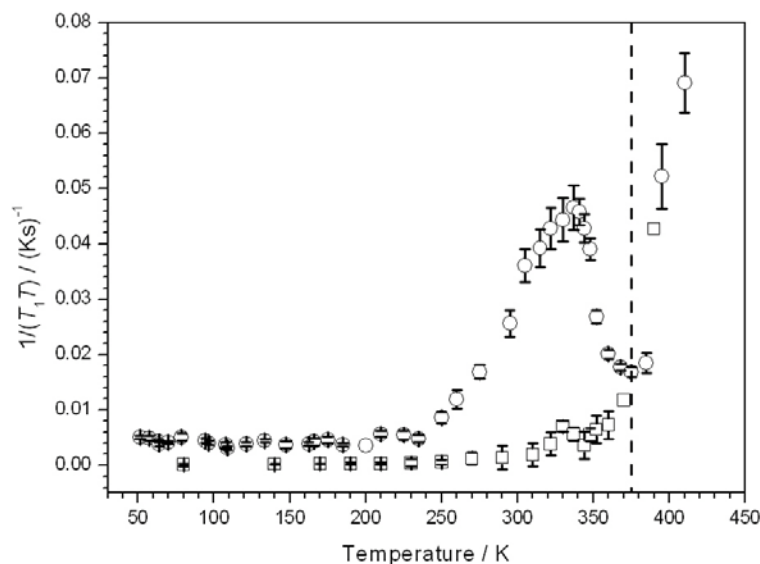


Figure S2. Plot of $1/(T_1T)$ versus T for ^6Li (squares) and ^7Li (circles) NMR SLR rates from $^6\text{Li}_2\text{N}_2$ and undoped Li_2N_2 , respectively. The dashed line indicates the decomposition temperature for undoped Li_2N_2 .

In Figure S2 the temperature dependent spin-lattice relaxation rates for ^7Li and ^6Li are plotted as a function of temperature. Below 250 K, the inverse product of T_1T (Heitler-Teller product) remains approximately constant indicating metallic behavior. Above 250 K, a sharp increase of $1/(T_1T)$ is observed in ^7Li NMR. Decomposition of Li_2N_2 into Li_3N is observed at above

385 K for ^7Li NMR measurements (dashed line) in accordance with previous *in situ* X-ray diffraction measurements.^[1] For the ^6Li doped Li_2N_2 a slightly different decomposition temperature is observed possibly because of the different synthesis route which we had to use because of different starting materials. For ^6Li and ^7Li NMR measurements we obtained a Heitler-Teller product (T_1T) from the low-temperature data of 2226 Ks and 266 Ks, respectively.

NMR SLR Rates versus Temperature

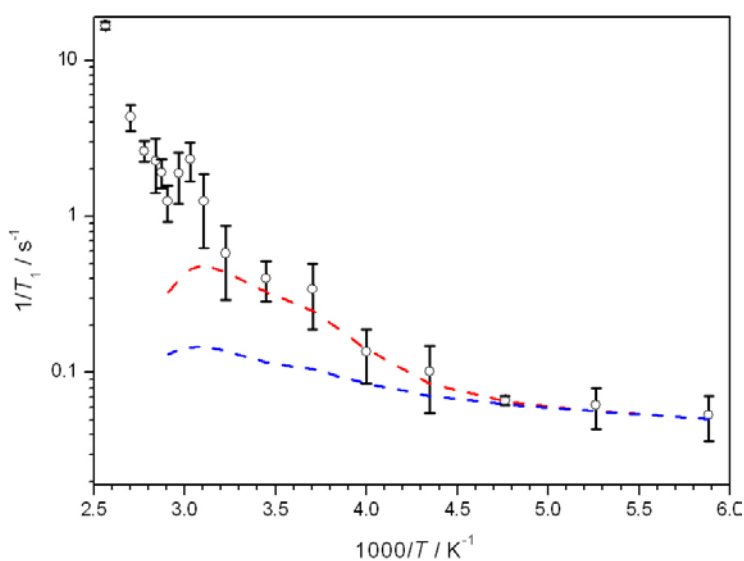


Figure S3. Experimental inverse-temperature dependence of the ^6Li (circles) NMR SLR rates on a logarithmic scale. The dashed curves below refer to a relaxation behavior which was calculated from the fitted ^7Li NMR SLR data (see Figure 2) assuming a pure dipolar (red) and quadrupolar (blue) relaxation mechanism. Isotope effects were neglected and the isotope depending prefactors (spin quantum number, quadrupole moment and gyromagnetic ratio) were taken into account.

Linewidth and Chemical Shift of the ^6Li NMR Signal in $^6\text{Li}_2\text{N}_2$

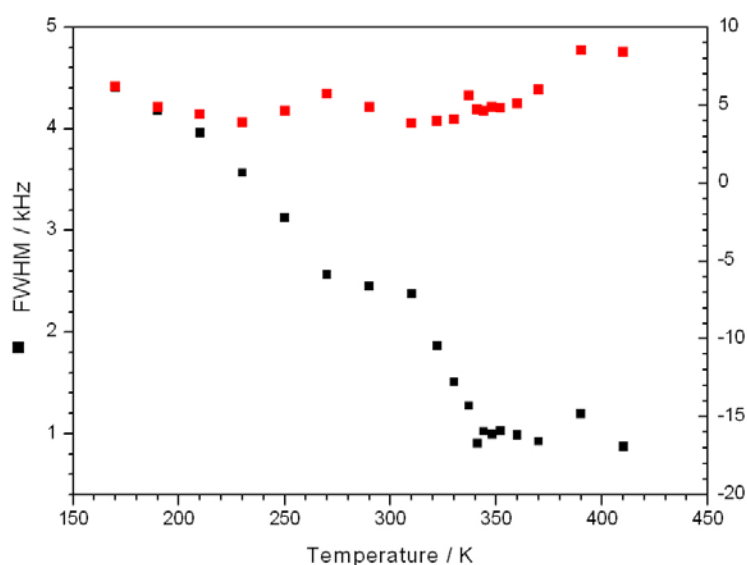


Figure S4. Linewidth (black squares) and chemical shift (red squares) of the ^6Li NMR signal in $^6\text{Li}_2\text{N}_2$. Herein, the linewidth is plotted as full width at half maximum (FWHM). An explanation of the still sizable linewidth in motional narrowing (at high temperature) could be that in Li_2N_2 the metallic character still contributes to the linewidth while in typical non-metallic Li-ion conductors this term can be neglected.

For ^7Li NMR measurements an analysis of linewidth and chemical shift was hindered due to the application of a self-built coil made of manganin wire, which contributes to linewidth and chemical shift of the observed ^7Li NMR signal. However the manganin wire helped to stabilize the probe at the much lower temperatures used in the ^7Li NMR experiments. The experimentally obtained chemical shift in the ^6Li NMR measurements (coil made of silver plated copper wire) was in the range of 4–6 ppm (see Figure S4). Thus a Knight shift of about 7 ppm is consistent with the NMR data taking into account a typical range for dielectric materials of -1 to -3 ppm. Deviations of the Knight shift calculated from relaxational data (Korringa formula) and direct measurements are not unusual.^[3]

Calculation of an averaged Li^+ Jump Length

The average jump length l for the estimation of the self-diffusion coefficient $D(T)$ of the lithium motion is calculated according to the crystal structure of Li_2N_2 (see Figure S5).^[1] Hereby, all distances between possible Li^+ jump sites including calculated structural voids are averaged (see Table S1) and result in an average jump length l of $2.25(1)$ Å.

Table S1. Distances Between Calculated Li^+ Jump Sites for one Unit-Cell According to Figure S5. E.s.d.'s of the Corresponding Distances are Neglected.

Li^+ jump sites	Distance / Å	Multiplicity
Li2–Void1	2.2186	4
Void1–Void2	1.8817	4
Li2–Li3	2.7086	2
Void2–Li3	2.3677	4
Li3–Void3	1.7548	4
Li3–Li3	2.7117	8
Void2–Li3	1.7548	8
Void3–Void4	1.8817	4
Li2–Li3	2.7086	8
Void4–Li2	2.2186	4
Li3–Void3	2.3677	8

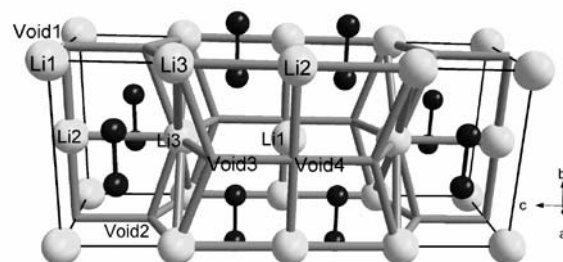


Figure S5. Crystal structure of Li_2N_2 (Li white, N black) illustrating the calculated possible Li^+ ion pathways (thick dark gray) according to the voids in the structure. Cell edges of the unit-cells are marked by black lines.

References

- [1] S.B. Schneider, R. Frankovsky, W. Schnick, *Angew. Chem.* **2012**, *124*, 1909; *Angew. Chem., Int. Ed.* **2012**, *51*, 1873.
- [2] S.B. Schneider, R. Frankovsky, W. Schnick, *Inorg. Chem.* **2012**, *51*, 2366.
- [3] J. Korrington, *Physica* **1950**, *16*, 601.

8.1.4 SUPPORTING INFORMATION FOR CHAPTER 4.2

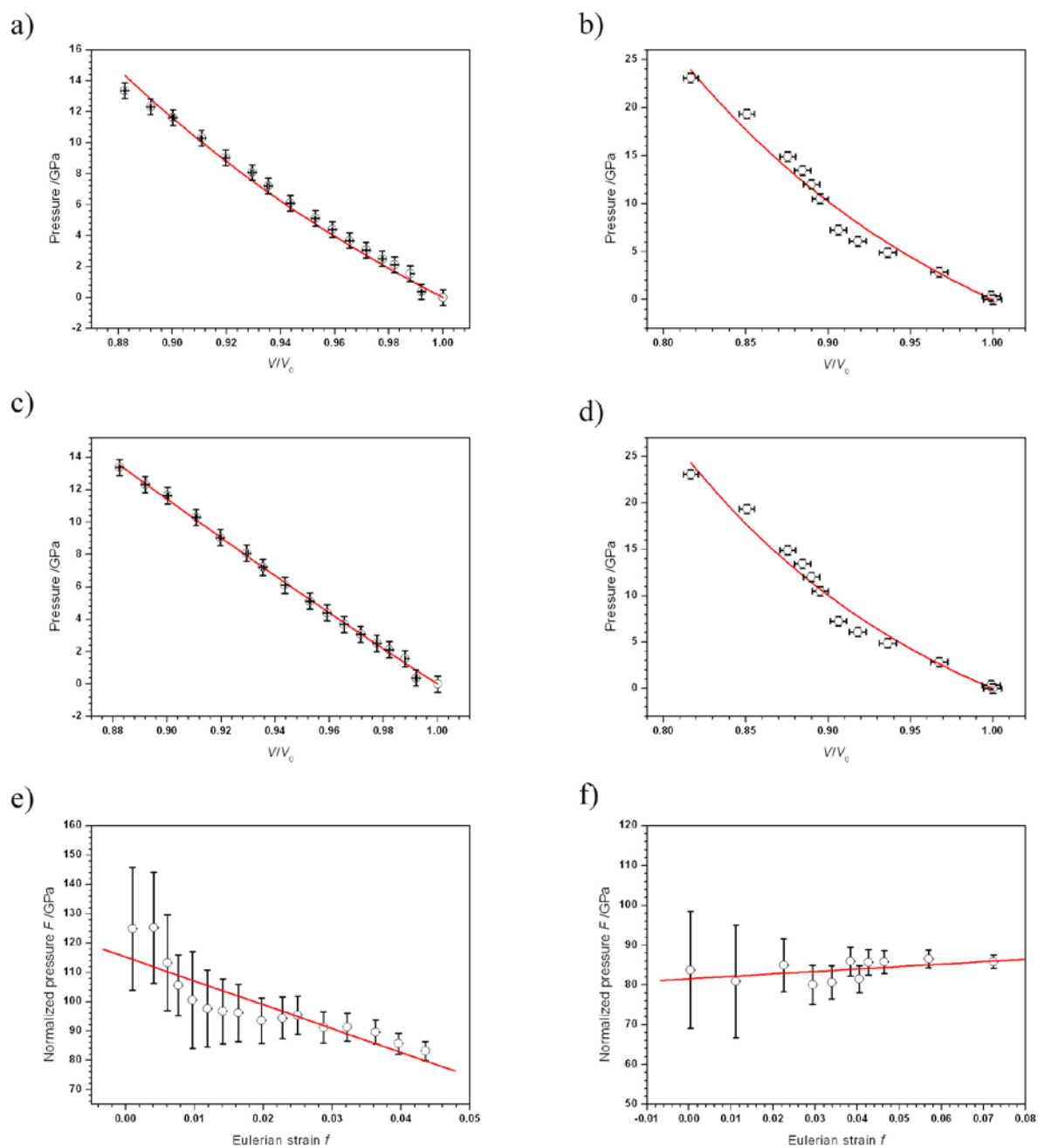
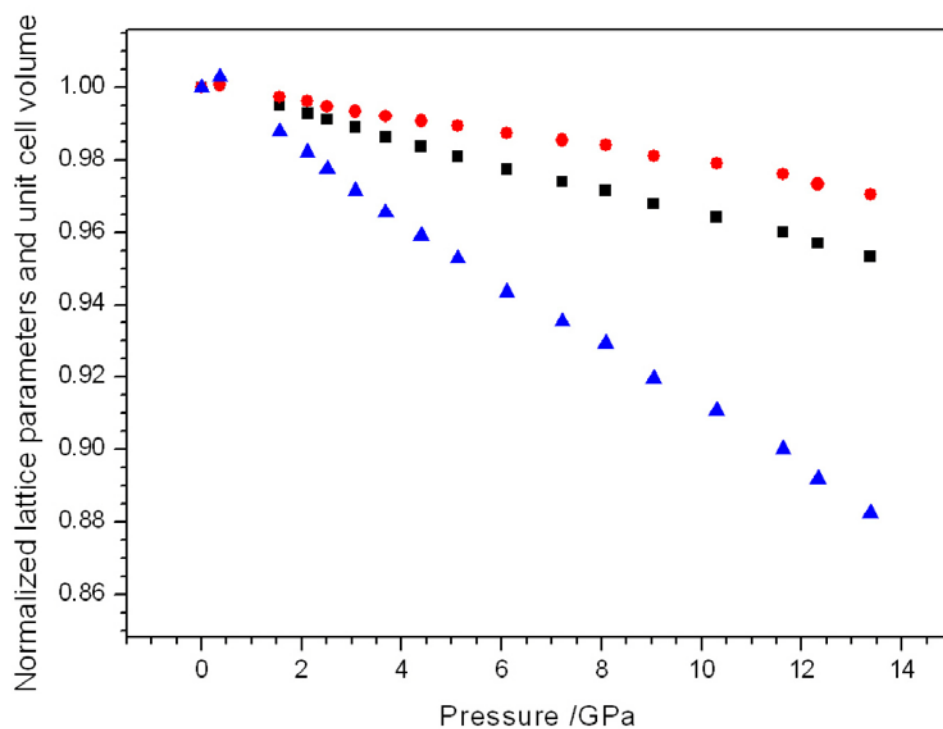


Figure S1. (a) and (b): second-order Birch-Murnaghan fits (red line) to the experimental p - V data of CaN₂ and SrN₂; (c) and (d): third-order Birch-Murnaghan fits (red line) to the experimental p - V data; e) and f): $F(f)$ -plots with linear fits (red line) to the applied values of the third-order BM-EoS. Left: CaN₂; right: SrN₂.

a)



b)

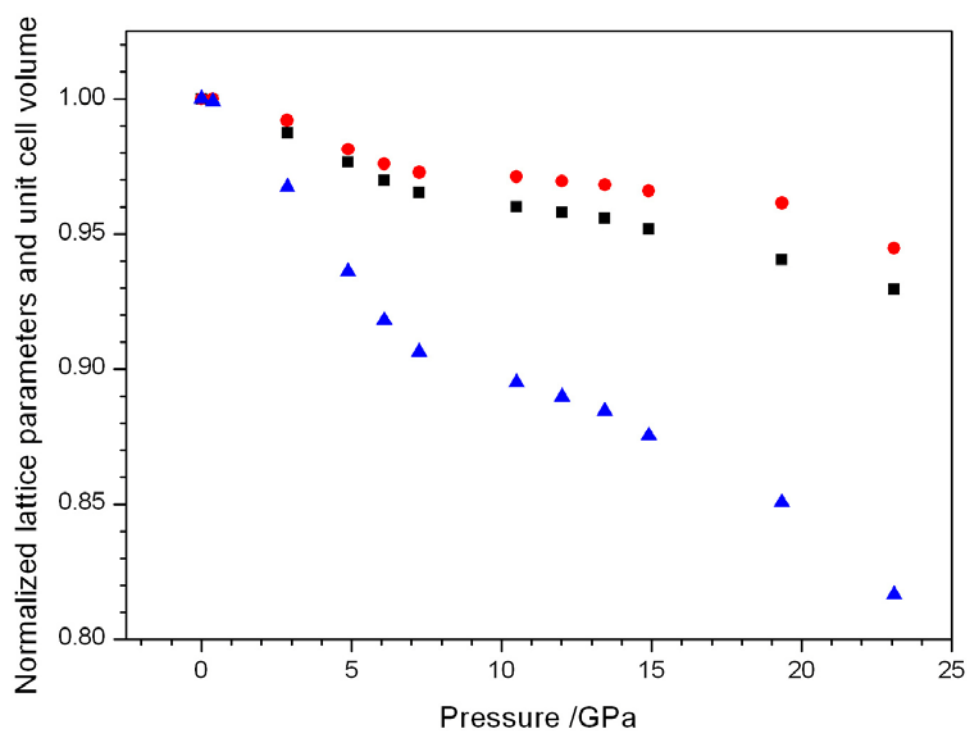


Figure S2. Evolution of normalized lattice parameters of CaN_2 (a) and SrN_2 (b) with pressure. The lattice parameters at zero pressure were taken from the Rietveld refinements of the powder X-ray pattern measured after synthesis with $\text{Cu } K_{\alpha 1}$ radiation; black: a , red: c , blue: V .

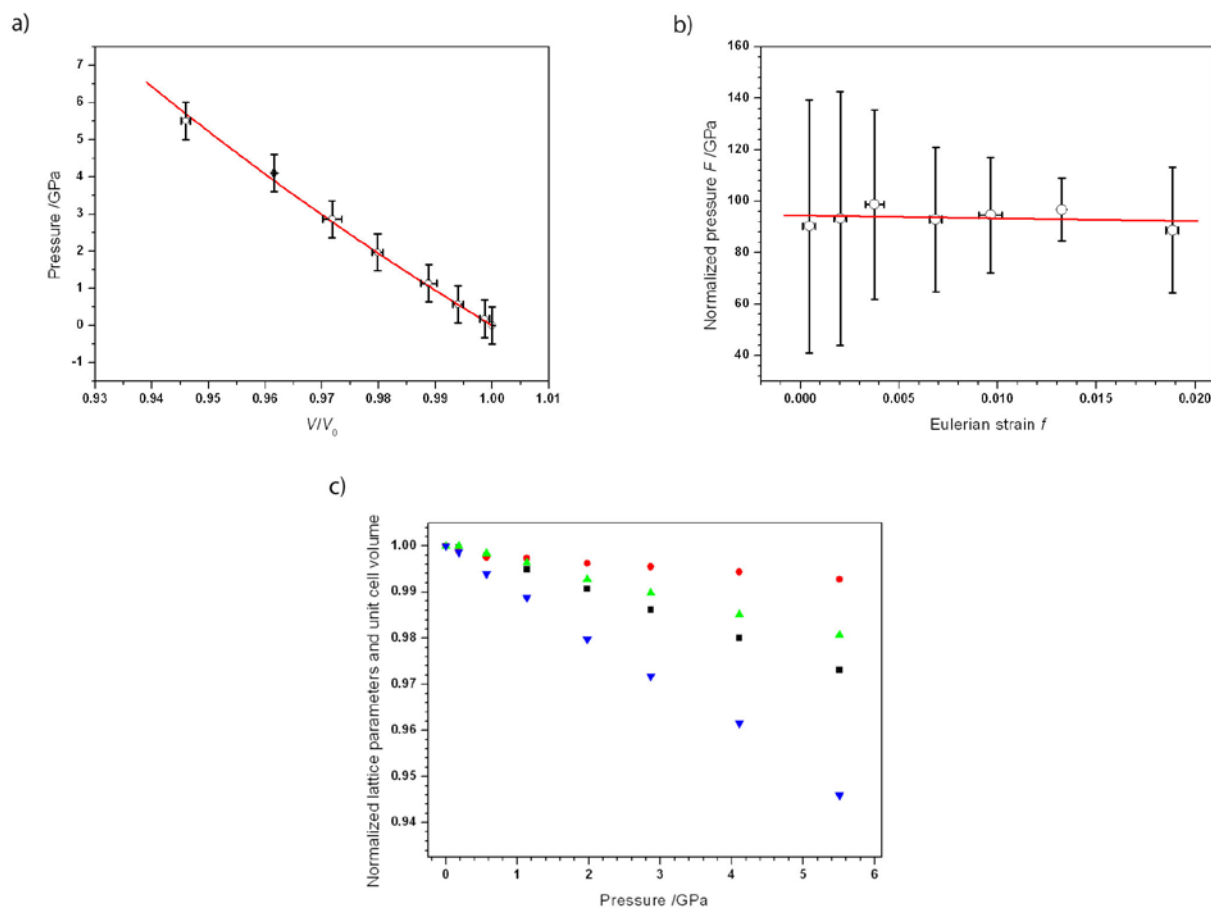


Figure S3. ; (a) third-order Birch-Murnaghan fit (red line) to the experimental p - V data of ambient Li_2N_2 ; (b) $F(f)$ -plot with linear fit (red line) to the applied values of the second-order BM-EoS; (c) Evolution of normalized lattice parameters with pressure. The lattice parameters at zero pressure were taken from the Rietveld refinements of the powder X-ray pattern measured after synthesis with $\text{Cu } K_{\alpha 1}$ radiation; black: a , red: b , green: c , blue: V

8.1.5 SUPPORTING INFORMATION FOR CHAPTER 5.1

Synthesis of Azides

Lithium azide was obtained by precipitation from its aqueous solution (Sigma-Aldrich, 20 wt% solution in water) by evaporation in vacuum. The product was dried over P_4O_{10} using a vacuum desiccator (24 h).

An aqueous solution of calcium azide was obtained from the reaction of $Ca(OH)_2$ with excess of NH_4N_3 (1:4) according to the procedure reported in literature.^[1] First $Ca(OH)_2$ (1.5 g, 20.1 mmol, Sigma-Aldrich, 99.995 %) is dissolved in 200 ml of water. Then an excess of NH_4N_3 (4.8 g, 80.5 mmol) is added generating aqueous $Ca(N_3)_2$, NH_3 and H_2O . Ammonia is boiled off and calcium azide is precipitated by evaporating the water. The obtained calcium azide is dried over $CaCl_2$ (Sigma-Aldrich, 99.99 %) using a vacuum desiccator (24 h).

NH_4N_3 was obtained by the metathesis reaction of NH_4NO_3 (3.99 g, 50 mmol, Sigma-Aldrich, 99.0 %) and NaN_3 (3.25 g, 50 mmol, Acros Organics, Geel, Belgium, 99 %) in a silica tube at elevated temperatures. By heating from room temperature to 473 K within 0.5 h, annealing for 12 h and cooling down again to room temperature within 6 h,^[2] NH_4N_3 was precipitated at the cold end of the silica tube separated from $NaNO_3$, which crystallized at the hot end during the reaction.

Each azide was analyzed by means of powder X-ray diffractometry (PXRD) and Fourier transform infrared spectroscopy (FTIR).

Appearance of $Li_2Ca_3[N_2]_3$ powder after HP/HT-experiment

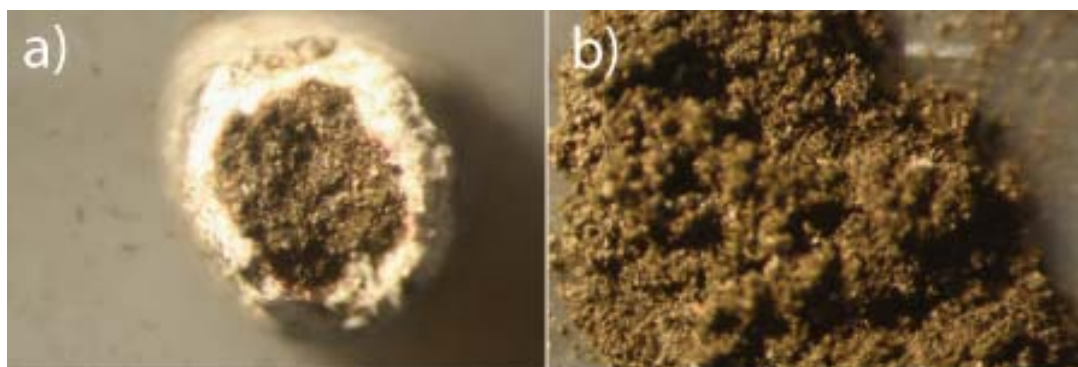


Figure S1. a) $Li_2Ca_3[N_2]_3$ (golden powder) surrounded by the white boron nitride h-BN crucible after HP/HT-experiment; b) isolated and ground $Li_2Ca_3[N_2]_3$.

Information about the data collection and selected crystallographic details of the Rietveld refinement of $\text{Li}_2\text{Ca}_3[\text{N}_2]_3$

Table S1. Information About the Data Collection and Selected Crystallographic Details of the Rietveld Refinement of $\text{Li}_2\text{Ca}_3[\text{N}_2]_3$.

Formula	$\text{Li}_2\text{Ca}_3[\text{N}_2]_3$
Synthesis Conditions	9 GPa @ 1023 K
fw /g·mol ⁻¹	218.16
space group	<i>Pmma</i> (no. 51)
cell parameters / Å	$a = 4.7747(1)$ $b = 13.9792(4)$ $c = 8.0718(4)$
$V / \text{Å}^3$	538.77(3)
Z / cell	4
$\rho_{\text{calc}} / \text{g}\cdot\text{cm}^{-3}$	2.6894(1)
$\mu_{\text{calc}} / \text{mm}^{-1}$	26.08(1)
Data Collection	
type of diffractometer	STOE Stadi P
geometry	Debye-Scherrer
radiation, monochromator	Cu $K_{\alpha 1}$ ($\lambda = 1.54056 \text{ \AA}$), Ge(111)
T / K	298(2)
detector	linear PSD ($\Delta 2\theta = 5^\circ$)
2θ range /°	5–100
number of observed reflections	345
Structure Analysis and Refinement	
method of refinement	fundamental parameter approach ^[3]
program package	TOPAS Academic ^[4]
atomic parameters	32
background function /parameters	shifted Chebyshev /16
R indices	$\text{GoF}(\chi^2) = 1.644$ $R_p = 0.06168$ $wR_p = 0.08109$

Temperature-dependent in situ X-Ray diffraction from 298 to 700 K

Figure S2 shows the high-temperature *in situ* X-ray diffraction patterns of $\text{Li}_2\text{Ca}_3[\text{N}_2]_3$ from room temperature to 700 K. At about 610 K $\text{Li}_2\text{Ca}_3[\text{N}_2]_3$ decomposes spontaneously. Thus no further reflections are obtained.

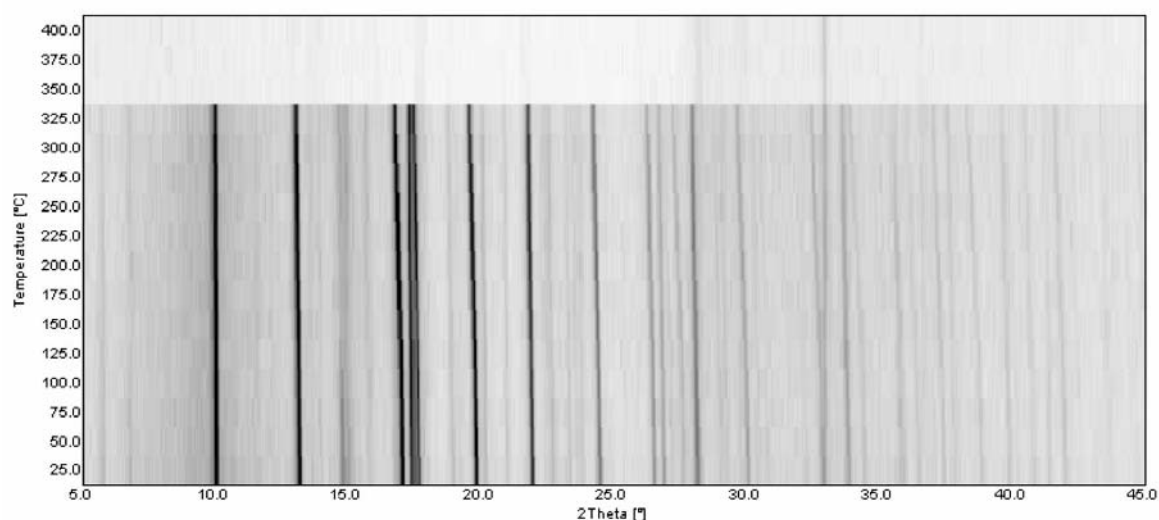


Figure S2. High-temperature *in situ* X-ray diffraction patterns of $\text{Li}_2\text{Ca}_3[\text{N}_2]_3$ (Mo $K_{\alpha 1}$ radiation (0.7093 Å)).

Electron Spin Resonance Spectroscopy

A) Further experimental details

Detail spectra of the narrow-line signal in the low- and high-temperature region were measured on spectrometer (a) at 26 dB microwave attenuation (0.5 mW microwave power) with a modulation amplitude of 0.1 mT peak-to-peak, a time constant of 20.48 ms, and a conversion time of 81.92 ms as well as at 20 dB microwave attenuation (2 mW microwave power) with a modulation amplitude of 0.5 mT peak-to-peak, a time constant of 10.24 ms, and a conversion time of 40.96 ms, respectively. The background corrected spectrum was obtained by subtracting the spectrum of the Ar filled capillary (50 scans) from the spectrum of the sample (50 scans) and the subtracting a third-order polynomial background fitted to the first and last 20 % of the spectrum (sweep width 25 mT, centered at $g = 2.0023$). The latter background subtraction removes the contribution of the broad-line signal in the measured range.

Overview spectra in the low-temperature region of both the broad-line and narrow-line signal were measured at all spectrometers, covering a temperature range between ambient temperature and 10 K in intervals of 20 K. A microwave attenuation of 14 dB (8 mW microwave power) was found not to lead to signal saturation of either the broad-line or narrow-line signal. Typically 5 scans were measured with a time constant of 10.24 ms and a conversion time of 40.84 ms in a range between 5 and 605 mT, except for spectrometer (c) where a range between 50 and 450 mT and digital smoothing with time constant of 50 ms were used.

Overview spectra in the high-temperature region of both the broad-line and narrow-line signal were measured on spectrometer (a) at a microwave attenuation of 14 dB (8 mW microwave power). Depending on signal intensity, either 10 or 40 scans were measured with a time constant of 10.24 ms and a conversion time of 40.84 ms in a range between 4 and 604 mT. Spectra were recorded at 300, 400, 500 and 525 K.

Mn^{2+} centers in magnesium oxide (Aldrich) were used as an intensity reference and TEMPOL (4-Hydroxy-2,2,6,6-tetramethylpiperidin-1-oxyl, Fluka) in deionized water or $\text{CuSO}_4 \cdot 5\text{H}_2\text{O}$ (Aldrich) were used as a concentration standard. Solid 2,2-Diphenyl-1-picrylhydrazyl (DPPH, Alexis Biochemicals) radical was used as standard ($g = 2.0037$). A quartz Mark tube capillary filled with argon was used as a background standard. Both the sample and background capillaries were placed in 1.5 mm Suprasil tubes (Wilmad), which were in turn placed in 3 mm fused quartz tubes.

Spectra measured over the whole range from 4 to 605 mT were analyzed by double integration of the broad line. The very small contribution of the double integral of the narrow line does not exceed other measurement and analysis errors and was neglected. Spectra measured on spectrometer (c) were analyzed by fitting a Voigt derivative line shape and a linear background contribution to the broad line, using home-written Matlab software. Temperature dependence of the sensitivity of spectrometer (a) was calibrated by measurements on the Mn:MgO sample. For analysis of the reference spectra, a Voigt derivative line with fixed Gaussian character of -0.3 and variable amplitude, width, and offset was fitted to the high-field line of the Mn^{2+} sextet, using Bruker Xepr software. The negative Gaussian character may be unphysical, but provided better fits than a purely Lorentzian line. Integral intensity of the absorption spectrum up to a constant factor was computed as the product of amplitude and square width of the derivative absorption signal. Spectra of the

concentration standard Tempol and $\text{CuSO}_4 \cdot 5\text{H}_2\text{O}$ were analyzed by double integration with Xepr.

B) Temperature-dependence of ESR signals from 10 to 525 K

The ESR spectra of $\text{Li}_2\text{Ca}_3[\text{N}_2]_3$ consist of a broad-line component that corresponds to the overwhelming fraction of the observed paramagnetic species and a narrow-line component that corresponds to traces of paramagnetic species of the order of magnitude as it is also found in BaN_2 .

At all temperatures the spectrum of the sample consists of an asymmetric, structured, narrow line with a width of approximately 4.3 mT and of a nearly symmetric, unstructured, broad line with a width of approximately 80 mT. The two lines have comparable amplitude in the usual absorption derivative representation of CW ESR spectra at all temperatures (see Figure S3), which means that the ratio of the numbers of spins contribution to the broad and narrow line, respectively, is about 350:1. The g -value at the zero crossing of the narrow-line spectrum is 2.0052 ± 0.0001 (see Figure 12 in publication); this corresponds to the maximum of the absorption spectrum. The broad line has a similar g -value however, because of the width and of uncertainties of background correction the uncertainty of this g -value is ten times larger. At low temperatures the shape of the broad line changes. At first sight this change is a line narrowing, however, broad wings of the line do persist down to a temperature of 10 K. At $g \sim 4.3$ we observe a background signal (data not shown) that could be traced back to the 1.5 mm Suprasil tube. Therefore, spectra are displayed and analyzed only at fields above 160 mT. Summarizing, the narrow-line component irreversibly changes line width and line shape during a temperature cycle between 300 and 525 K. The broad-line component narrows on decreasing temperature from 300 to 10 K and it broadens on increasing temperature from 300 to 525 K.

Throughout the temperature range between 10 and 525 K intensity of the ESR-signals in $\text{Li}_2\text{Ca}_3[\text{N}_2]_3$ corresponds to only a minor fraction of the N_2 species.

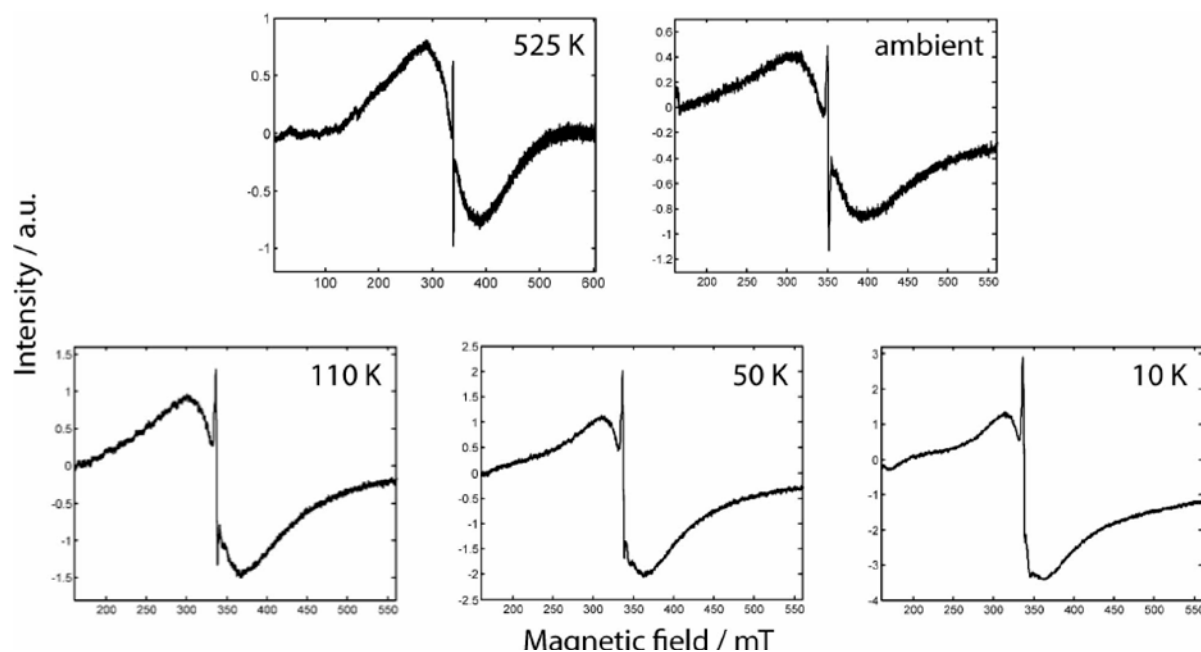


Figure S3. Overview ESR spectra of $\text{Li}_2\text{Ca}_3[\text{N}_2]_3$ at different temperatures after background correction.

Unit-Cell Metrics

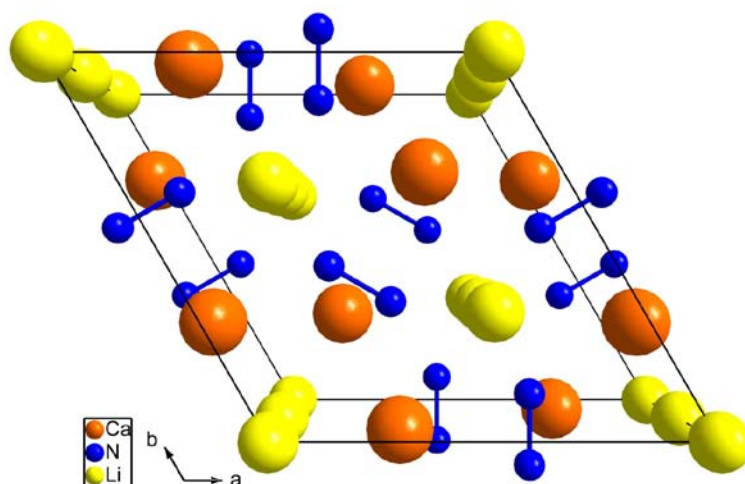


Figure S4. Indexing resulted in a unit-cell with hexagonal metrics and $a = 8.0707(7)$ and $c = 4.7630(7)$ Å. The as-depicted structural model was obtained upon structure solution and Rietveld refinement of the PXRD data. “ LiCaN_2 ” crystallizes in $P6_3/mcm$ (no. 193) with $a = 8.0726(2)$ and $c = 4.7755(1)$ Å. The crystallographic data for corresponding atoms are: Li1 at $2b$, Li2 at $4d$, Ca1 at $6g$ with $x = 0.7040(1)$, and N1 at $12j$ with $x = 0.3503(5)$ and $y = 0.4474(5)$.

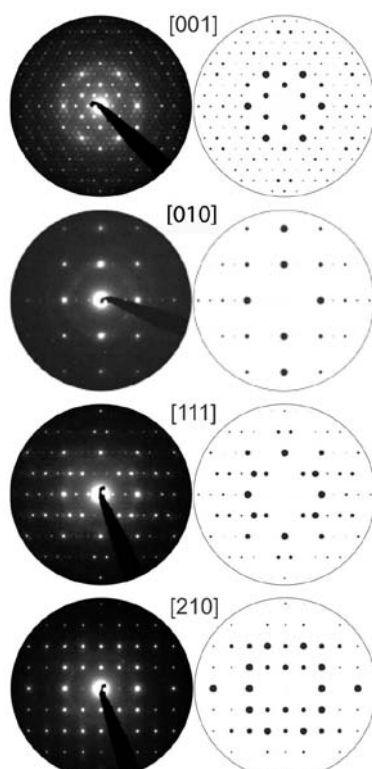


Figure S5. Experimental (black) and simulated (white) SAED patterns of various zone axes for hexagonal “LiCaN₂”.

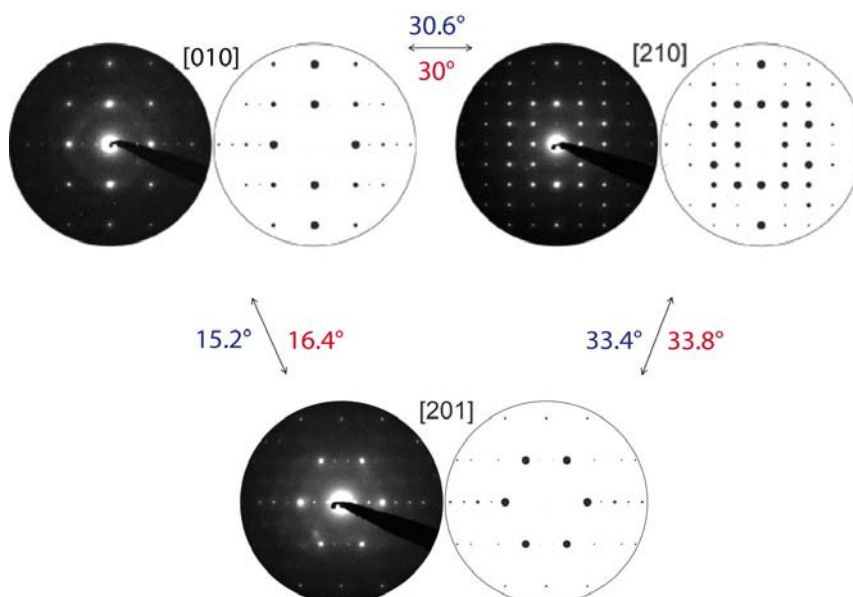


Figure S6. Experimental (black) and simulated (white) SAED patterns of the corresponding zone axes of hexagonal “LiCaN₂”. Experimental tilt angles (blue) between zone axes match calculated ones (red).

Transformation of Lattice Parameters

Transformation of the lattice parameters of the hexagonal starting model ($a = 8.06$, and $c = 4.76$ Å) into the orthorhombic C -centered unit-cell are deduced according to the transformation

$$\begin{bmatrix} \mathbf{a} \\ \mathbf{b} \\ \mathbf{c} \end{bmatrix}_{orthC} = P \begin{bmatrix} \mathbf{a} \\ \mathbf{b} \\ \mathbf{c} \end{bmatrix}_{hex} \quad (1)$$

with $P = \begin{bmatrix} 2 & 1 & 0 \\ 0 & 1 & 0 \\ 0 & 0 & 1 \end{bmatrix}$. The final orthorhombic P -centered lattice parameters ($a = 4.76$,

$b = 13.96$, and $c = 8.06$ Å) are obtained by the further transformation according to

$$\begin{bmatrix} \mathbf{a} \\ \mathbf{b} \\ \mathbf{c} \end{bmatrix}_{orthP} = \begin{bmatrix} 0 & 0 & 1 \\ 1 & 0 & 0 \\ 0 & 1 & 0 \end{bmatrix} \begin{bmatrix} \mathbf{a} \\ \mathbf{b} \\ \mathbf{c} \end{bmatrix}_{orthC} \quad (2)$$

Transformation of Zone Axes

The corresponding zone axes of the obtained C -centered intermediate as well as of the final P -centered orthorhombic threefold twin are deduced referring to the *International Tables for Crystallography: Volume A*. According to the transformation

$$\begin{bmatrix} \mathbf{u} \\ \mathbf{v} \\ \mathbf{w} \end{bmatrix}_{orthC} = Q \begin{bmatrix} \mathbf{u} \\ \mathbf{v} \\ \mathbf{w} \end{bmatrix}_{hex} \quad (3)$$

with $Q = P^{-1} = \begin{bmatrix} \frac{1}{2} & -\frac{1}{2} & 0 \\ 0 & 1 & 0 \\ 0 & 0 & 1 \end{bmatrix}$, the zone axes of the C -centered orthorhombic model are

obtained. A second transformation referring to

$$\begin{bmatrix} \mathbf{u} \\ \mathbf{v} \\ \mathbf{w} \end{bmatrix}_{orthP} = \begin{bmatrix} 0 & 0 & 1 \\ 1 & 0 & 0 \\ 0 & 1 & 0 \end{bmatrix} \begin{bmatrix} \mathbf{u} \\ \mathbf{v} \\ \mathbf{w} \end{bmatrix}_{orthC} \quad (4)$$

finally results in the zone axes for the model in space group *Pmma* (no. 51). In Table S2 corresponding related zone axes are listed.

Table S2. Relation Between Transformed Hexagonal, Orthorhombic *C*-Centered and *P*-Centered Zone Axes.

Hexagonal zone axes (<i>P6₃/mcm</i> , no. 193)	<i>C</i> -centered orthorhombic zone axes (<i>Cmcm</i> , no. 63)	<i>P</i> -centered orthorhombic zone axes (<i>Pmma</i> , no. 51)
[100]	[100]	[010]
[010]	[-120]	[0-12]
[001]	[001]	[100]
[210]	[120]	[012]
[111]	[011]	[101]

To confirm the orthorhombic unit-cell metrics in space group *Pmma* (no. 51), diffraction patterns of the former hexagonal model are transformed first into orthorhombic *C*-centered (*Cmcm*) and then into *P*-centered (*Pmma*) nomination. As-obtained simulated patterns are finally compared to experimental diffraction patterns of the corresponding zone axes and are still in good agreement with each other (see Figure S7) supporting the symmetry reduction to an orthorhombic 3-fold twin.

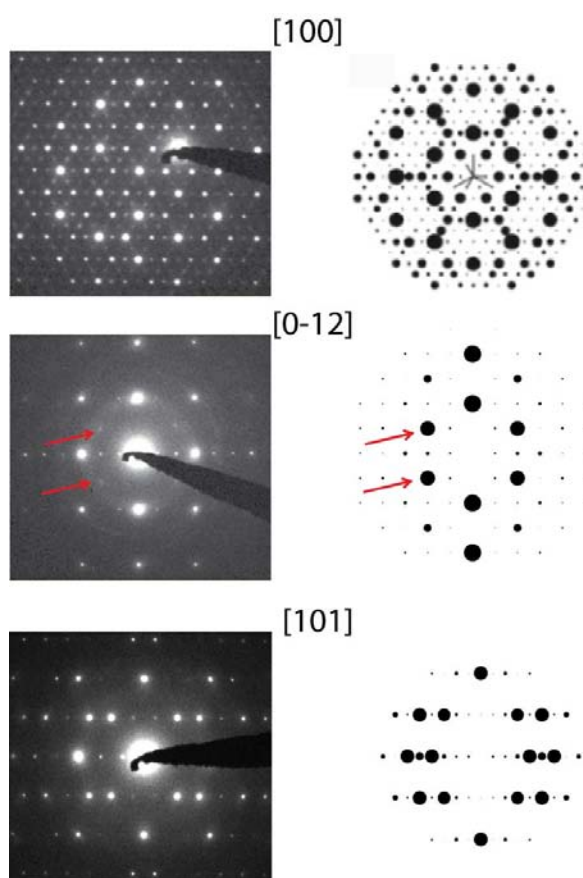


Figure S7. Experimental (black) and simulated (white) SAED patterns of various zone axes for orthorhombic “LiCaN₂” in space group *Pmma* (no. 51).

Elemental Analysis

Energy dispersive X-ray spectroscopy (EDX) confirmed the presence of only calcium and nitrogen/oxygen as lithium can not be detected. Oxygen is supposed to originate from hydrolysis of $\text{Li}_2\text{Ca}_3[\text{N}_2]_3$ due to the transfer of the sample holder into the microscope. EDX spectra were obtained with a SM-6500F scanning electron microscope (JEOL, Germany). A quantitative analysis of lithium, calcium, nitrogen and oxygen under inert conditions by the Mikroanalytisches Labor Pascher (Remagen, Germany) resulted in Li 7.0, Ca 49.4, N 35.9 and O 3.2 mass%. EDX measurements of non-hydrolyzed crystallites could be obtained by transmission electron microscopy. Hereby, an averaged ratio of Ca:N of about 1:1.8 besides only traces of oxygen was obtained (measured atomic%: Ca 32.8, N 64.1 and O 3.0; expected ideal atomic% without lithium: Ca 33.33, N 66.67 and O 0.0). TEM-EDX measurements are in good agreement with obtained results of quantitative analysis, the latter one resulting an Li:Ca:N ration of about 0.8:1:2.1 if the presence of oxygen is excluded. Note that if the mass percentages of the individual atoms Li, Ca, N and O are added, 100 % are not reached. This is due to the fact that only the corresponding elements have been investigated. However, other heavier elements are not present as TEM-EDX does only result in Ca, N and only traces of O. Therefore, within the fact that the HP/HT-product is always affected by an unknown (red) side phase and due to the fact the experiments are done in boron nitride crucibles, the residual mass is supposed to be constituted of e.g. boron originating from oxo- or nitridoborate formation (see FTIR section).

The presence of hydrogen was excluded by ^1H solid-state magic-angle spinning nuclear magnetic resonance spectroscopy (MAS-NMR) as no distinct signal was obtained upon measurements (data not shown).

Concluding, the initial hexagonal and/or orthorhombic models of “ LiCaN_2 ” concerning the Li:Ca ratio as elemental analysis has proven that the true crystal structure has to be a lithium deficient one.

Improving the Structural Model**Table S3.** Atomic Coordinates for $\text{Li}_2\text{Ca}_3[\text{N}_2]_3$ for the Fully Relaxed Structural Model (at Zero External Pressure), Obtained from Density-Functional Theory as Described in the Article. Computed Cell Parameters: $a = 4.9269 \text{ \AA}$; $b = 14.3732 \text{ \AA}$; $c = 7.9656 \text{ \AA}$.

atom (Wyckoff) ^a	atom ^b	transformation of coordinates	x	y	z
Li1 (4g)	Li41	$\frac{1}{2}, y, 0$	$\frac{1}{2}$	0.351	0
	Li42	$\frac{1}{2}, y, 0$	$\frac{1}{2}$	0.649	0
	Li43	$0, y, 0$	0	0.351	0
	Li44	$0, y, 0$	0	0.649	0
Li2 (4h)	Li37	$\frac{1}{2}, y, \frac{1}{2}$	$\frac{1}{2}$	0.851	$\frac{1}{2}$
	Li38	$0, y, \frac{1}{2}$	0	0.851	$\frac{1}{2}$
	Li39	$\frac{1}{2}, y, \frac{1}{2}$	$\frac{1}{2}$	0.149	$\frac{1}{2}$
	Li40	$0, y, \frac{1}{2}$	0	0.149	$\frac{1}{2}$
Ca1 (2e)	Ca28	$\frac{1}{4}, 0, z$	$\frac{1}{4}$	0	0.6927
	Ca33	$\frac{3}{4}, 0, z$	$\frac{3}{4}$	0	0.3073
Ca2 (2f)	Ca27	$\frac{3}{4}, \frac{1}{2}, z$	$\frac{3}{4}$	$\frac{1}{2}$	0.8074
	Ca34	$\frac{1}{4}, \frac{1}{2}, z$	$\frac{1}{4}$	$\frac{1}{2}$	0.1926
Ca3 (4k)	Ca25	$\frac{3}{4}, y, z$	$\frac{3}{4}$	0.1653	0.8455
	Ca26	$\frac{3}{4}, y, z$	$\frac{3}{4}$	0.8347	0.8455
	Ca35	$\frac{1}{4}, y, z$	$\frac{1}{4}$	0.8347	0.1545
	Ca36	$\frac{1}{4}, y, z$	$\frac{1}{4}$	0.1653	0.1545
Ca4 (4k)	Ca29	$\frac{1}{4}, y, z$	$\frac{1}{4}$	0.3347	0.6546
	Ca30	$\frac{1}{4}, y, z$	$\frac{1}{4}$	0.6653	0.6546
	Ca31	$\frac{3}{4}, y, z$	$\frac{3}{4}$	0.6653	0.3454
	Ca32	$\frac{3}{4}, y, z$	$\frac{3}{4}$	0.3347	0.3454
N1 (4k)	N7	$\frac{1}{4}, y, z$	$\frac{1}{4}$	0.1702	0.6984
	N8	$\frac{1}{4}, y, z$	$\frac{1}{4}$	0.8298	0.6984
	N17	$\frac{3}{4}, y, z$	$\frac{3}{4}$	0.8298	0.3016
	N18	$\frac{3}{4}, y, z$	$\frac{3}{4}$	0.1702	0.3016
N2 (4k)	N5	$\frac{3}{4}, y, z$	$\frac{3}{4}$	0.3298	0.8016
	N6	$\frac{3}{4}, y, z$	$\frac{3}{4}$	0.6702	0.8016
	N19	$\frac{1}{4}, y, z$	$\frac{1}{4}$	0.3298	0.1984
	N20	$\frac{1}{4}, y, z$	$\frac{1}{4}$	0.6702	0.1984
N3 (4k)	N11	$\frac{3}{4}, y, z$	$\frac{3}{4}$	0.9543	0.612
	N12	$\frac{3}{4}, y, z$	$\frac{3}{4}$	0.0457	0.612
	N13	$\frac{1}{4}, y, z$	$\frac{1}{4}$	0.0457	0.388
	N14	$\frac{1}{4}, y, z$	$\frac{1}{4}$	0.9543	0.388
N4 (4k)	N1	$\frac{1}{4}, y, z$	$\frac{1}{4}$	0.4543	0.89
	N2	$\frac{1}{4}, y, z$	$\frac{1}{4}$	0.5457	0.89
	N23	$\frac{3}{4}, y, z$	$\frac{3}{4}$	0.5457	0.11
	N24	$\frac{3}{4}, y, z$	$\frac{3}{4}$	0.4543	0.11
N5 (4k)	N9	$\frac{3}{4}, y, z$	$\frac{3}{4}$	0.3201	0.638
	N10	$\frac{3}{4}, y, z$	$\frac{3}{4}$	0.6799	0.638
	N15	$\frac{1}{4}, y, z$	$\frac{1}{4}$	0.6799	0.362
	N16	$\frac{1}{4}, y, z$	$\frac{1}{4}$	0.3201	0.362
N6 (4k)	N3	$\frac{1}{4}, y, z$	$\frac{1}{4}$	0.8202	0.8616
	N4	$\frac{1}{4}, y, z$	$\frac{1}{4}$	0.1798	0.8616
	N21	$\frac{3}{4}, y, z$	$\frac{3}{4}$	0.1798	0.1384
	N22	$\frac{3}{4}, y, z$	$\frac{3}{4}$	0.8202	0.1384

^aRelated to the refined model in *Pmma* (no. 51) according to Table 1; ^bNew atomic site labels as obtained from program output in *P1* (no. 1).

Table S4. Atomic Coordinates for $\text{Li}_2\text{Ca}_3[\text{N}_2]_3$ Calculated at a Simulated Pressure of Approx. 9 GPa. Computed Cell Parameters: $a = 4.6177 \text{ \AA}$; $b = 13.6960 \text{ \AA}$; $c = 7.8911 \text{ \AA}$.

atom (Wyckoff) ^a	atom ^b	transformation of coordinates	x	y	z
Li1 (4g)	Li41	$\frac{1}{2}, y, 0$	$\frac{1}{2}$	0.333	0
	Li42	$\frac{1}{2}, y, 0$	$\frac{1}{2}$	0.667	0
	Li43	$0, y, 0$	0	0.333	0
	Li44	$0, y, 0$	0	0.667	0
Li2 (4h)	Li37	$\frac{1}{2}, y, \frac{1}{2}$	$\frac{1}{2}$	0.833	$\frac{1}{2}$
	Li38	$0, y, \frac{1}{2}$	0	0.833	$\frac{1}{2}$
	Li39	$\frac{1}{2}, y, \frac{1}{2}$	$\frac{1}{2}$	0.167	$\frac{1}{2}$
	Li40	$0, y, \frac{1}{2}$	0	0.167	$\frac{1}{2}$
Ca1 (2e)	Ca28	$\frac{1}{4}, 0, z$	$\frac{1}{4}$	0	0.6888
	Ca33	$\frac{3}{4}, 0, z$	$\frac{3}{4}$	0	0.3112
Ca2 (2f)	Ca27	$\frac{3}{4}, \frac{1}{2}, z$	$\frac{3}{4}$	$\frac{1}{2}$	0.8124
	Ca34	$\frac{1}{4}, \frac{1}{2}, z$	$\frac{1}{4}$	$\frac{1}{2}$	0.1876
Ca3 (4k)	Ca25	$\frac{3}{4}, y, z$	$\frac{3}{4}$	0.1569	0.8440
	Ca26	$\frac{3}{4}, y, z$	$\frac{3}{4}$	0.8431	0.8440
	Ca35	$\frac{1}{4}, y, z$	$\frac{1}{4}$	0.8431	0.1560
	Ca36	$\frac{1}{4}, y, z$	$\frac{1}{4}$	0.1569	0.1560
Ca4 (4k)	Ca29	$\frac{1}{4}, y, z$	$\frac{1}{4}$	0.3441	0.6568
	Ca30	$\frac{1}{4}, y, z$	$\frac{1}{4}$	0.6559	0.6568
	Ca31	$\frac{3}{4}, y, z$	$\frac{3}{4}$	0.6559	0.3432
	Ca32	$\frac{3}{4}, y, z$	$\frac{3}{4}$	0.3441	0.3432
N1 (4k)	N7	$\frac{1}{4}, y, z$	$\frac{1}{4}$	0.1752	0.7246
	N8	$\frac{1}{4}, y, z$	$\frac{1}{4}$	0.8248	0.7246
	N17	$\frac{3}{4}, y, z$	$\frac{3}{4}$	0.8248	0.2754
	N18	$\frac{3}{4}, y, z$	$\frac{3}{4}$	0.1752	0.2754
N2 (4k)	N5	$\frac{3}{4}, y, z$	$\frac{3}{4}$	0.3262	0.7711
	N6	$\frac{3}{4}, y, z$	$\frac{3}{4}$	0.6738	0.7711
	N19	$\frac{1}{4}, y, z$	$\frac{1}{4}$	0.3262	0.2289
	N20	$\frac{1}{4}, y, z$	$\frac{1}{4}$	0.6738	0.2289
N3 (4k)	N11	$\frac{3}{4}, y, z$	$\frac{3}{4}$	0.9527	0.606
	N12	$\frac{3}{4}, y, z$	$\frac{3}{4}$	0.0473	0.606
	N13	$\frac{1}{4}, y, z$	$\frac{1}{4}$	0.0473	0.394
	N14	$\frac{1}{4}, y, z$	$\frac{1}{4}$	0.9527	0.394
N4 (4k)	N1	$\frac{1}{4}, y, z$	$\frac{1}{4}$	0.4525	0.89
	N2	$\frac{1}{4}, y, z$	$\frac{1}{4}$	0.5475	0.89
	N23	$\frac{3}{4}, y, z$	$\frac{3}{4}$	0.5475	0.11
	N24	$\frac{3}{4}, y, z$	$\frac{3}{4}$	0.4525	0.11
N5 (4k)	N9	$\frac{3}{4}, y, z$	$\frac{3}{4}$	0.2800	0.627
	N10	$\frac{3}{4}, y, z$	$\frac{3}{4}$	0.7200	0.627
	N15	$\frac{1}{4}, y, z$	$\frac{1}{4}$	0.7200	0.373
	N16	$\frac{1}{4}, y, z$	$\frac{1}{4}$	0.2800	0.373
N6 (4k)	N3	$\frac{1}{4}, y, z$	$\frac{1}{4}$	0.7830	0.8725
	N4	$\frac{1}{4}, y, z$	$\frac{1}{4}$	0.2170	0.8725
	N21	$\frac{3}{4}, y, z$	$\frac{3}{4}$	0.2170	0.1275
	N22	$\frac{3}{4}, y, z$	$\frac{3}{4}$	0.7830	0.1275

^aRelated to the refined model in *Pmma* (no. 51) according to Table 1; ^bNew atomic site labels as obtained from calculation in *P1* (no. 1).

Description of the Crystal Structure

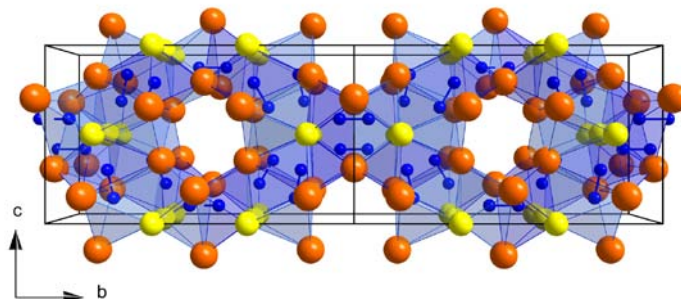


Figure S8. Coordination of the $[\text{N}_2]^{2-}$ ions in $\text{Li}_2\text{Ca}_3[\text{N}_2]_3$ (*Pmma*, no. 51); Li yellow, Ca orange, N blue. Each crystallographically independent nitrogen site is coordinated by two Li and four Ca atoms.

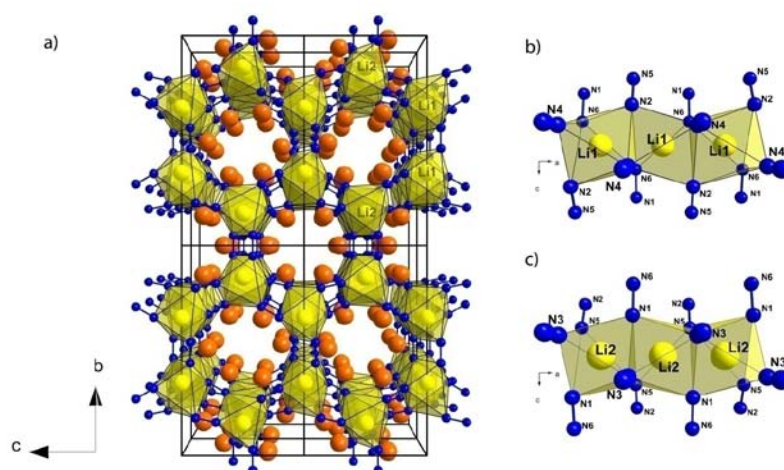


Figure S9. Coordination of the two independent lithium sites in $\text{Li}_2\text{Ca}_3[\text{N}_2]_3$ (*Pmma*, no. 51); Li yellow, Ca orange, N blue. The refined Li–Li distances match with reported values in literature.

Due to the voids in the crystal structure of $\text{Li}_2\text{Ca}_3[\text{N}_2]_3$, the calcium ions are not reliably coordinated if the Ca–X ($X = \text{Li}, \text{N}$) distance is set to a minimum of 2.9 \AA (see Figure S9). Hereby, each Ca^{2+} is coordinated by three *side-on* bound and two axial $[\text{N}_2]^{2-}$ ions in an *end-on* manner, which results in a coordination number of 8. The as-obtained Ca–N distances are also compared to the sum of their ionic radii. Eight-fold coordinated Ca^{2+} exhibits an averaged radius of 1.12 \AA .⁵ Thus again the Ca–N distances correspond well with their ionic sum. Increasing the coordination sphere to a maximum of about 3.8 \AA , then each calcium ion

is coordinated by 4 diazenide $[\text{N}_2]^{2-}$ units in *side-on* mode and four additional lithium atoms, resulting in a coordination number of 14.

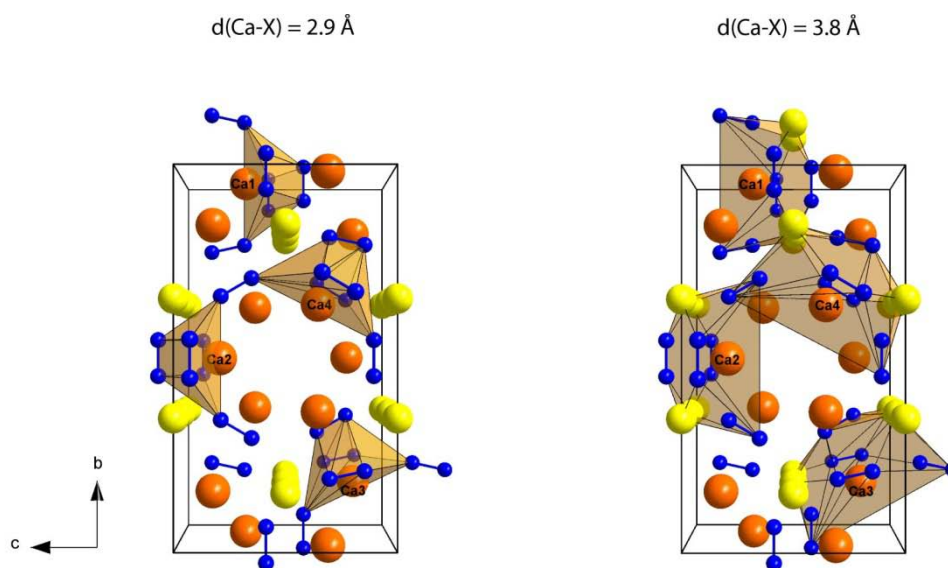


Figure S10. Coordination of the calcium sites in $\text{Li}_2\text{Ca}_3[\text{N}_2]_3$; Li yellow, Ca orange, N blue. The search for coordination polyhedra up to maximum Ca–X distance (X = Li, N) of 2.9 \AA results in solely anion-coordinated calcium ions. Thereby, the calcium ions are coordinated by three $[\text{N}_2]^{2-}$ in *side-on* manner and two axial *end-on* coordinated nitrogen dumbbells. If the Ca–X distance is further increased, the coordination of the calcium ions changes significantly. Up to a maximum Ca–X distance of 3.8 \AA each calcium ion is coordinated by four diazenide units in *side-on* mode and four additional lithium atoms, resulting in an coordination number of 14 (or $5(x2) + 4$).

Table S5. Refined Interatomic Distances in $\text{Li}_2\text{Ca}_3[\text{N}_2]_3$ (*Pmma*, no. 51).

atom pair	distance / Å	atom pair	distance / Å
Li1–Li1	2.387(1)	Ca1–Ca3	3.324(7)
Li2–Li2	2.387(1)	Ca1–Ca1	3.97(1)
Li1–N2	2.063(9)	Ca1–Ca3	4.28(1)
Li1–N4	2.015(6)	Ca1–Ca3	4.75(1)
Li1–N6	2.03(9)	Ca1–Ca1	4.7747(1)
Li2–N3	2.63(3)	Ca1–Ca4	4.997(7)
Li2–N1	2.0226(3)	Ca1–Ca1	5.45(1)
Li2–N5	2.063(9)	Ca2–Ca4	3.356(7)
Ca1–Li2	2.92(3)	Ca2–Ca2	3.95(2)
Ca1–Li2	4.46(2)	Ca2–Ca4	4.19(1)
Ca1–Li1	5.55(2)	Ca2–Ca2	4.7747(1)
Ca2–Li1	2.9(2)	Ca2–Ca4	4.83(2)
Ca2–Li1	4.46(1)	Ca2–Ca3	4.974(7)
Ca2–Li2	5.57(4)	Ca2–Ca2	5.47(2)
Ca3–Li2	2.964(9)	Ca3–Ca1	3.324(7)
Ca3–Li1	3.33(2)	Ca3–Ca3	3.57(1)
Ca3–Li2	4.493(6)	Ca3–Ca3	4.04(1)
Ca3–Li1	4.74(2)	Ca3–Ca4	4.086(9)
Ca3–Li2	5.11(3)	Ca3–Ca1	4.28(1)
Ca3–Li2	5.494(9)	Ca3–Ca1	4.75(1)
Ca4–Li1	3.063(9)	Ca3–Ca3	4.7747(1)
Ca4–Li2	3.32(4)	Ca3–Ca4	4.92(1)
Ca4–Li1	4.559(6)	Ca3–Ca2	4.974(7)
Ca4–Li2	4.73(3)	Ca3–Ca4	5.09(1)
Ca4–Li1	5.16(2)	Ca3–Ca3	5.39(1)
Ca4–Li1	5.391(9)	Ca3–Ca3	5.92(1)
Ca1–N3	2.409(3)	Ca4–Ca2	3.356(8)
Ca1–N1	2.47(2)	Ca4–Ca4	3.412(9)
Ca1–N3	2.63(1)	Ca4–Ca4	4.01(1)
Ca2–N2	2.31(1)	Ca4–Ca3	4.086(9)
Ca2–N4	2.4(2)	Ca4–Ca2	4.19(1)
Ca2–N4	2.62(8)	Ca4–Ca4	4.7747(1)
Ca3–N3	2.34(3)	Ca4–Ca2	4.83(2)
Ca3–N5	2.45(1)	Ca4–Ca3	4.92(1)
Ca3–N6	2.511(6)	Ca4–Ca1	4.997(7)
Ca3–N6	2.51(1)	Ca4–Ca3	5.09(1)
Ca3–N1	2.65(6)	Ca4–Ca4	5.267(9)
Ca3–N2	2.67(1)		
Ca4–N4	2.5(2)		
Ca4–N1	2.55(2)		
Ca4–N5	2.583(5)		
Ca4–N5	2.67(2)		

Calculation of Averaged Void-Diameter

To obtain the final void-diameter, the radius of $\text{Ca}^{2+}_{\text{CN}=8}$ (1.12 \AA)^[5] has to be subtracted twice from the averaged distance of adverse located Ca^{2+} ions (5.385 \AA) resulting in 3.15 \AA in diameter for the actual size of the cavities.

Table S6. Refined Distances in Ca–Ca Pairs in $\text{Li}_2\text{Ca}_3[\text{N}_2]_3$ Necessary to Calculate the Averaged Ca–Ca Distance.

atom pair	distance / \AA
2xCa1–Ca1	5.45(1)
1xCa2–Ca2	5.47(2)
4xCa3–Ca3	5.39(1)
2xCa4–Ca4	5.267(9)
averaged value = 5.385 \AA	

Fourier Transform Infrared Spectroscopy

To relate the observed features to the corresponding nitrogen dumbbells, the Wyckoff sites of each nitrogen atom as well as their pairing in combination with the N–N bond lengths have to be taken into account. Each nitrogen atom in $\text{Li}_2\text{Ca}_3[\text{N}_2]_3$ occupies the same site at $4k$ (see Table 1), but due to the pairing of nitrogen atoms the occurrence of corresponding nitrogen dumbbells differs (see Table 2 and Figure 7). Hereby, the pairs of $\text{N}_1\text{--}\text{N}_6$ and $\text{N}_2\text{--}\text{N}_5$ appear twice often than $\text{N}_3\text{--}\text{N}_3$ and $\text{N}_4\text{--}\text{N}_4$, implying an idealized intensity ratio of observed features of 2:2:1:1, respectively. As already mentioned, the feature at 800 cm^{-1} is not attributed to the N–N stretching vibrations of the diazenide ions. The remaining three visible features in the low-energy region show slight differences in intensity, which might be related to the frequency of occurring N–N-pairs in $\text{Li}_2\text{Ca}_3[\text{N}_2]_3$. The two more intense features at 1260 and 1100 cm^{-1} indicate shorter N–N bond lengths, which is in good agreement with the crystallographic data, as the two more frequent $\text{N}_1\text{--}\text{N}_6$ - and $\text{N}_2\text{--}\text{N}_5$ -pairs exhibit the shortest bond lengths (see Table 2). The less intense feature at 1020 cm^{-1} is therefore attributed to one of the longer and less frequent N–N-pairs. The missing feature for the fourth N–N stretching vibration might be covered by the broad appearance of the two-peak feature of 1100 and 1020 cm^{-1} , especially if compared to the very sharp signal at 1260 cm^{-1} .

Magnetic and Electric Conductivity Measurements

As the molar susceptibility slightly increases at decreasing temperatures starting at about 50 K, we plotted the product $\chi_{\text{mol}}T$ versus T . Hereby, truly temperature-independent behavior is observed if the corresponding run of the curve linearly decreases with decreasing temperature (see Figure S11). To check the presence of ferromagnetic impurities, we also plotted the field-dependence of μ/μ_{B} at different temperatures (see Figure S12). As no hysteresis is observed, no ferromagnetic impurities have been present during measurement.

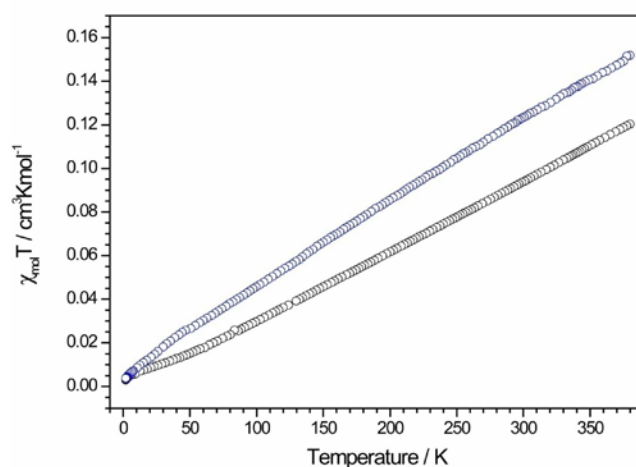


Figure S11. Temperature-dependence of the product $\chi_{\text{mol}}T$. $\chi_{\text{mol}}T$ increases linearly indicative for temperature-independent, metallic behavior. Blue: susceptibility measured at 0.01 T; black at 1T.

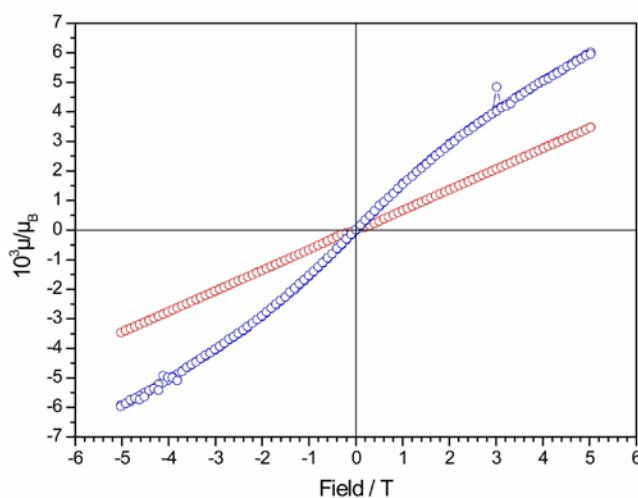


Figure S12. Field-dependence of μ/μ_{B} . As no hysteresis is observed, no ferromagnetic impurities are present in the sample chamber. Blue: magnetization measured at 1.8 K; red at 300 K.

References

- [1] H.D. Fair, R.F. Walker, *Energetic Materials Vol. 1: Physics and Chemistry of the Inorganic Azides*; Plenum Press: New York, **1977**.
- [2] W.J. Frierson, *Inorg. Synth.* **1946**, 8, 136.
- [3] J. Bergmann, R. Kleeberg, A. Haase, B. Breidenstein, *Mater. Sci. Forum* **2000**, 303, 347.
- [4] A.A. Coelho, *TOPAS-Academic*, Version 4.1; Coelho Software: Brisbane, **2007**.
- [5] R.D. Shannon, *Acta Crystallogr., Sect. A* **1976**, 32, 751.

8.2 LIST OF PUBLICATIONS

Basic results compiled in this thesis were published in scientific journals according to the below-mentioned list. As the scope of the thesis was the synthesis and characterization of novel diazenides, publications beyond this scope are not explicitly listed in prior chapters and are here referred to as *not part of this thesis*. Talks and posters presentations at scientific conferences as well as workshop participations are summarized separately.

6. **Electronic and Ionic Conductivity in Alkaline Earth Diazenides $M_{\text{AE}}\text{N}_2$ ($M_{\text{AE}} = \text{Ca, Sr, Ba}$) and in Li_2N_2**

Sebastian B. Schneider, Martin Mangstl, Gina M. Friederichs, Rainer Frankovsky, Jörn Schmedt auf der Günne, Wolfgang Schnick

Chem. Mater. **2013**, 25, 4149; DOI: 10.1021/cm4011629

For this publication, writing the manuscript main part, literature screening, synthesis of the samples, image editing, interpretation of electric conductivity data, topological analysis of Li_2N_2 , and calculation of self-diffusion coefficients was done by Sebastian B. Schneider. ^6Li and ^7Li NMR data acquisition was performed by both, Sebastian B. Schneider and Martin Mangstl, whereas the analysis of NMR data was done in close collaboration of Sebastian B. Schneider, Martin Mangstl and Jörn Schmedt auf der Günne. Gina M. Friederichs and Rainer Frankovsky performed the conductivity measurements. Each author also revised the manuscript.

5. **High-Pressure Synthesis and Characterization of $\text{Li}_2\text{Ca}_3[\text{N}_2]_3$ – An Uncommon Metallic Diazenide with $[\text{N}_2]^{2-}$ Ions**

Sebastian B. Schneider, Markus Seibald, Volker L. Deringer, Ralf P. Stoffel, Rainer Frankovsky, Gina M. Friederichs, Henryk Laqua, Viola Duppel, Gunnar Jeschke, Richard Dronskowski, Wolfgang Schnick

J. Am. Chem. Soc. **2013**, 135, 16668; DOI: 10.1021/ja408816t

For this contribution, writing the main part, synthesis of the sample, literature screening, PXRD investigations, analysis of FTIR data, unit-cell and atom-coordinates transformation due to symmetry reduction, image editing, and interpretation of

magnetic and electric conductivity measurements was performed by Sebastian B. Schneider. In close collaboration, SAED patterns of $\text{Li}_2\text{Ca}_3[\text{N}_2]_3$ were analyzed by Markus Seibald, including the identification of a 3-fold twin by rotation instead of hexagonal metrics, simulation of SAED patterns, and identification of zone axes for the final structural model in space group $Pm\bar{m}a$. TEM investigations and parts of the data analysis were carried out by Viola Duppel. Gina M. Friederichs and Rainer Frankovsky measured magnetic and electric conductivity data. ESR investigations and analyses were accomplished by Henryk Laqua and Gunnar Jeschke. All theoretical investigations and analysis, including the creation of figures, were done by the group of Richard Dronskowski (Volker Deringer, Ralf P. Stoffel). All authors also revised the manuscript.

4. **Materials Properties of Ultra-Incompressible Re_2P**

Sebastian B. Schneider, Dominik Baumann, Ashkan Salamat, Zuzana Konôpková, Wolfgang Morgenroth, Hanns-Peter Liermann, Marcus Schwarz, Lkhamsuren Bayarjargal, Alexandra Friedrich, Björn Winkler, Wolfgang Schnick
Chem. Mater. **2012**, *24*, 3240; DOI: 10.1021/cm3016885 (not part of this thesis)

For this article, writing the main part, image editing, synthesis of the sample, literature screening, analyses of high-pressure PXRD data, determination of bulk moduli, interpretation of magnetic and electric conductivity measurements, as well as analysis of thermal expansion coefficients were carried out by Sebastian B. Schneider. Measurements and analyses of Vickers hardness as well as chemical analysis were performed by Marcus Schwarz. In close collaboration, Sebastian B. Schneider, Dominik Baumann, Ashkan Salamat, Zuzana Konôpková, Wolfgang Morgenroth, Hanns-Peter Liermann, Lkhamsuren Bayarjargal, and Alexandra Friedrich loaded the diamond-anvil cells with samples, pressure transmitting media and standards for pressure determination upon in situ HP-investigations. All theoretical investigations were performed by Björn Winkler. All authors also revised the manuscript.

3. **Reversible High-Pressure Phase Transition in LaN**

Sebastian B. Schneider, Dominik Baumann, Ashkan Salamat, Wolfgang Schnick
J. Appl. Phys. **2012**, *111*, 093503; DOI: 10.1063/1.4709392 (not part of this thesis)

For this contribution, writing the main part, image editing, literature screening, as well as the determination of bulk moduli of ambient LaN and its high-pressure polymorph were performed by Sebastian B. Schneider. Both, Sebastian B. Schneider and Dominik Baumann, measured and analyzed high-pressure PXRD data, including the identification of the high-pressure polymorph. Sebastian B. Schneider, Dominik Baumann, and Ashkan Salamat, loaded the diamond-anvil cells with samples, pressure transmitting media and standards for pressure determination. All authors also revised the manuscript.

2. **High-Pressure Synthesis and Characterization of the Alkali Diazenide Li_2N_2**

Sebastian B. Schneider, Rainer Frankovsky, Wolfgang Schnick

Angew. Chem. **2012**, *124*, 1909; DOI: 10.1002/ange.201108252

Angew. Chem., Int. Ed. **2012**, *51*, 1873; DOI: 10.1002/anie.201108252

For this article, writing the main part, image editing, literature screening, synthesis of the sample, PXRD investigations, analysis of FTIR data, as well as the interpretation of theoretical results were carried out by Sebastian B. Schneider. The theoretical investigations themselves were performed by Rainer Frankovsky. All authors also revised the manuscript.

1. **Synthesis of Alkaline Earth Diazenides $\text{M}_{\text{AE}}\text{N}_2$ ($\text{M}_{\text{AE}} = \text{Ca}, \text{Sr}, \text{Ba}$) by Controlled Thermal Decomposition of Azides under High Pressure**

Sebastian B. Schneider, Rainer Frankovsky, Wolfgang Schnick

Inorg. Chem. **2012**, *51*, 2366; DOI: 10.1021/ic2023677

For this publication, writing the main part, image editing, literature screening, synthesis of the samples, PXRD investigations, analysis of FTIR data, as well as the interpretation of theoretical results were carried out by Sebastian B. Schneider. The theoretical investigations themselves were performed by Rainer Frankovsky. All authors also revised the manuscript.

8.3 CONFERENCES AND WORKSHOPS

8.3.1 CONFERENCES

High-pressure synthesis of novel N-based binary and multinary phases (oral presentation)

Sebastian B. Schneider, Dominik Baumann, Wolfgang Schnick

High-Pressure Synthesis of Novel (Oxo-)Nitridosilicates, (Oxo-)Nitridophosphates and Related Binary (poster presentation)

Sebastian B. Schneider, Dominik Baumann, Wolfgang Schnick

5th Berichtskolloquium of the DFG Priority Program 1236 „Strukturen und Eigenschaften von Kristallen bei extrem hohen Drücken und Temperaturen“ 2012, Bad Salzschlirf, Germany

Neue Diazenide...und noch mehr? (oral presentation)

Sebastian B. Schneider, Wolfgang Schnick

Hirschegg-Seminar on Solid State Chemistry 2012, Hirschegg, Austria

HP/HT-Synthesis of Novel Nitrogen-Related Materials (oral presentation)

Sebastian B. Schneider, Wolfgang Schnick

HP/HT-Synthesis of Nitride Materials (poster presentation)

Sebastian B. Schneider, Florian Pucher, Dominik Baumann, Stefan Sedlmaier, Rebecca Römer, Friedrich Karau, Wolfgang Schnick

4th Berichtskolloquium of the DFG Priority Program 1236 „Strukturen und Eigenschaften von Kristallen bei extrem hohen Drücken und Temperaturen“ 2011, Hünfeld, Germany.

8.3.2 WORKSHOPS

5th International Workshop **Spinel Nitrides and Related Materials**

2010, Rüdesheim, Germany

Hercules Specialised Course 12 (HSC 12) **Synchrotron Radiation and Neutron for Extreme Conditions Studies**

2010, Grenoble, France

8.4 DEPOSITED CRYSTALLOGRAPHIC DATA

Crystallographic data were deposited with the Fachinformationszentrum Karlsruhe, Germany (fax: +49-7247-808-666, e-mail: crysdata@fiz-karlsruhe.de) and are available on quoting the respective CSD depository numbers.

CaN ₂	423721
SrN ₂	423722
BaN ₂	423723
Li ₂ N ₂	423831
HP-LaN	423936
Li ₂ Ca ₃ [N ₂] ₃	426449

8.5 CURRICULUM VITAE

Personal Information

Name	Sebastian Bernhard Schneider
Date of birth	04/06/1984
Place of birth	Munich, Germany
Nationality	German

Education

since 02/2010	Research assistant in the group of Prof. Dr. Wolfgang Schnick <i>Department of Chemistry, Ludwig-Maximilian University Munich</i> PhD thesis entitled: “Novel Contributions to the Solid-State Chemistry of Diazenides”
05/2009–11/2009	Master thesis (Inorganic Chemistry) <i>Ludwig-Maximilian University Munich (Prof. Dr. Wolfgang Schnick)</i> Master thesis entitled: “Binäre Erdalkali-Stickstoff-Verbindungen durch Hochdruck-Hochtemperatur-Synthesen”
10/2007–11/2009	Master of Science (Chemistry) <i>Ludwig-Maximilian University Munich, Germany</i>
05/2007–09/2007	Bachelor thesis (Inorganic Chemistry) <i>Ludwig-Maximilian University Munich (Prof. Dr. Peter Klüfers)</i> Bachelor thesis entitled: “Polyolato-Komplexe mit Palladium(II): Umsetzungen im neutralen Milieu sowie Aufklärung komplexer Gleichgewichte mittels zweidimensionaler NMR-Spektroskopie“
10/2004–09/2007	Bachelor of Science (Chemistry and Biochemistry) <i>Ludwig-Maximilian University Munich, Germany</i>
09/2003–07/2004	Civilian service <i>Feierwerk e.V., Munich, Germany</i>
09/1994–06/2003	Allgemeine Hochschulreife, Abitur <i>Gymnasium Fürstenried-West, Munich, Germany</i>
09/1990–07/1994	Elementary school <i>Grundschule Forstenrieder Allee, Munich, Germany</i>